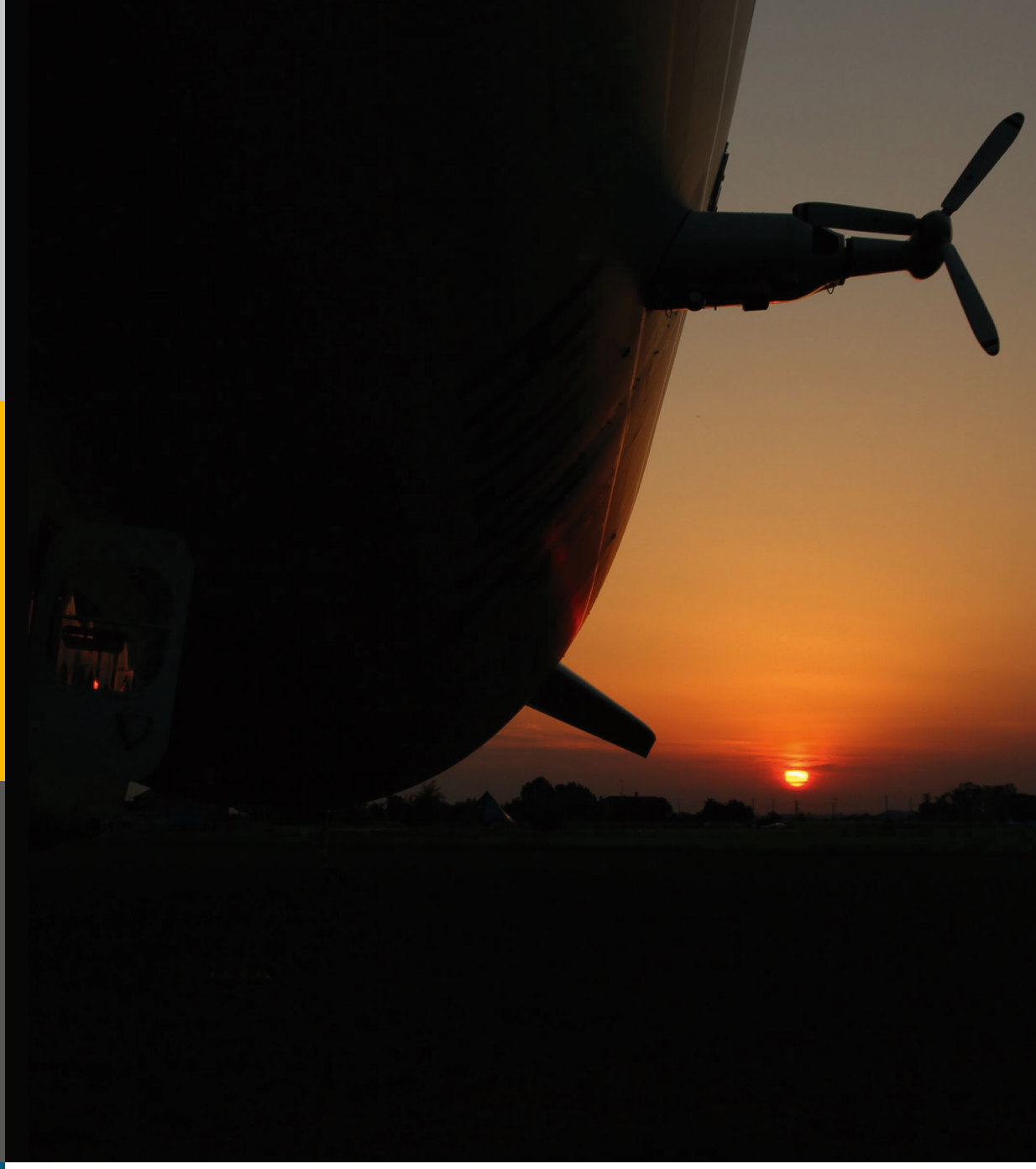

Airborne VOC measurements on board the Zeppelin NT during the PEGASOS campaigns in 2012 deploying the improved Fast-GC-MSD System

Julia Elisabeth Jäger

JÜLICH
FORSCHUNGSZENTRUM

Member of the Helmholtz Association

Schriften des Forschungszentrums Jülich
Reihe Energie & Umwelt / Energy & Environment Band / Volume 205

Forschungszentrum Jülich GmbH
Institute for Energy and Climate Research (IEK)
Troposphere (IEK-8)

Airborne VOC measurements on board the Zeppelin NT during the PEGASOS campaigns in 2012 deploying the improved Fast-GC-MSD System

Julia Elisabeth Jäger

Schriften des Forschungszentrums Jülich
Reihe Energie & Umwelt / Energy & Environment Band / Volume 205

ISSN 1866-1793 ISBN 978-3-89336-936-2

Bibliographic information published by the Deutsche Nationalbibliothek.
The Deutsche Nationalbibliothek lists this publication in the Deutsche Nationalbibliografie; detailed bibliographic data are available in the Internet at http://dnb.d-nb.de.

Publisher and Distributor: Forschungszentrum Jülich GmbH
Zentralbibliothek
52425 Jülich
Tel: +49 2461 61-5368
Fax: +49 2461 61-6103
Email: zb-publikation@fz-juelich.de
www.fz-juelich.de/zb

Cover Design: Grafische Medien, Forschungszentrum Jülich GmbH

Printer: Grafische Medien, Forschungszentrum Jülich GmbH

Schriften des Forschungszentrums Jülich
Reihe Energie & Umwelt / Energy & Environment, Band / Volume 205

D 38 (Diss., Köln, Univ., 2013)

ISSN 1866-1793
ISBN 978-3-89336-936-2

The complete volume is freely available on the Internet on the Jülicher Open Access Server (JUWEL) at www.fz-juelich.de/zb/juwel

Zusammenfassung

Die Klasse der flüchtigen organischen Verbindungen (VOCs) umfasst schätzungsweise 10^4-10^6 verschiedene Substanzen. Diese werden auf der Erdoberfläche von einer Vielzahl biogener und anthropogener Quellen emittiert und durch verschiedene Prozesse wieder aus der Atmosphäre entfernt. Hauptsächlich ist dafür die Oxidation mit anschließender trockener Deposition aber auch das Auswaschen durch Regen verantwortlich. Da jedoch die meisten der primär emittierten VOCs nicht polar sind, weisen sie eine geringe Wasserlöslichkeit auf. Durch Oxidation wird die Polarität und somit Wasserlöslichkeit erhöht. Das wichtigste photochemische Oxidationsmittel für VOCs in der Atmosphäre ist das OH-Radikal. Die Oxidation von VOCs erfolgt in mehreren Schritten bis sie entweder deponiert oder schließlich zu Kohlendioxid oxidiert werden. Der Nachteil des VOC-Oxidationsprozesses in Anwesenheit von Stickstoffmonoxid ist die Produktion von signifikanten Mengen Ozon und ist somit ein enormes Gesundheitsrisiko.

Der größte Teil der VOC-Oxidation findet im unteren Bereich der Atmosphäre statt. Allerdings wurde der Höhenbereich von 100 bis 1000 m bisher wenig untersucht. Daher liefern die schnellen VOC-Messungen mittels GC-MS an Bord des Zeppelin NT während den PEAGSOS-Kampagnen in den Niederlanden und in Italien im Jahr 2012 wichtige neue Erkenntnisse über die VOC-Verteilung. Um das GC-MS-System (HGC) an Bord des Zeppelins einsetzen zu können musste es, sowohl um die Messgenauigkeit und die Stabilität zu verbessern als auch um den Luftfahrtanforderungen gerecht zu werden, angepasst werden. Mit dem modifizierten HGC können nun VOCs von C4 bis C10 sowie oxygenierte VOCs (OVOCs) mit einer Nachweisgrenze von unter 10 ppt analysiert werden.

Die analysierten VOCs in beiden Teilen der Kampagne zeigten geringe VOC-Konzentrationen mit Werten unter 5 ppb. Besonders die Mischungsverhältnisse der primär emittierten VOCs waren mit mittleren Werten unter 200 ppt sehr niedrig. Höhere mittlere Konzentrationen bis zu 5 ppb konnten für die OVOCs beobachtet werden. Dabei waren Methanol, Ethanol, Aceton, Acetaldehyd und Formaldehyd die OVOCs mit den höchsten Konzentrationen mit Ausnahme von Formaldehyd.

Die mit einem unabhängigen gemessene OH-Reaktivität (k_{OH}) war niedrig und stimmte mit der aus den einzelnen Spurengasmessungen berechneten OH-Reaktivität weitgehend überein. In den Niederlanden betrug die Differenz 1.0±1.4 s^{-1} bei einer mittleren gemessen OH-Reaktivität von 6.13±1.23 s^{-1} und in Italien 0.1±2.2 s^{-1} bei einer gemessenen OH-Reaktivität von 3.8±1.4 s^{-1}.

Diese Ergebnisse zeigten, dass in beiden Teilen der Kampagne die analysierte Luft im Höhenbereich von 100 m 1000 m nicht sehr stark von primär emittierten Spurengasen belastet

war. Die Analyse ergab, dass die OVOCs mit einem Beitrag von 30 % in den Niederlanden und 40 % in Italien an der OH-Reaktivität die wichtigste OH-Senke waren. Die Quellen von OVOCs in der Atmosphäre sind vielfältig und reichen von primären Emissionen bis zur photochemischen Produktion. Berechnungen ergaben, dass die gemessenen OVOCs nicht vollständig aus der photochemischen Produktion stammen können, sondern dass ein Teil primär emittiert oder transportiert sein muss. Primär emittierte Alkohole konnten zum Beispiel in der Abluftfahne der Region um Mannheim/Ludwigshafen festgestellt werden. Die am häufigsten vorkommenden OVOCs weisen OH-Lebensdauern im Bereich zwischen Stunden und Tagen auf und können deshalb weit verbreitet werden. Aus diesem Grund haben die OVOCs sowohl regionale als auch globale Bedeutung und Auswirkungen.

Abstract

Volatile organic compounds (VOCs) comprise a large number of different species, estimated to 10^4-10^6. They are emitted on the Earth's surface from a variety of biogenic and anthropogenic sources. VOCs are removed by multiple pathways from the atmosphere, by oxidation and finally by dry or wet deposition. Most primary emitted VOCs are non-polar and therefore have a low solubility in water. Oxidation facilitates efficient VOC removal by wet deposition. In the atmosphere the main photochemical VOC oxidation agent is the OH radical. As a consequence the polarity of the VOCs is increased and they can be removed faster. The oxidation of VOCs proceeds in several steps until the VOCs are deposited or are eventually oxidized to carbon dioxide. A downside of the VOCs oxidation process lies in the production of significant amounts ozone if nitrogen oxide is present which is a serious health hazard.

Most of the VOC oxidation takes place in lower part of the atmosphere between the altitudes of 100 to 1000 m, which is only sparsely analyzed. Therefore, fast VOCs measurements by GC-MSD on board the Zeppelin NT offered new important insights in the distribution of VOCs. The measurements were performed within the PEAGSOS campaigns in the Netherlands and in Italy in 2012. For the implementation of the GC-MSD system (HCG) on board the Zeppelin it was reconstructed to enhance its performance and to meet aviation requirements. The system was optimized to measure VOCs ranging from C4 to C10 as well as oxygenated VOCs (OVOCs) with a detection limit below 10 ppt.

The analyzed VOCs for both parts of the campaigns showed low mean concentration below 5 ppb for all VOCs. Especially, the mixing ratios of the primary emitted VOCs were very low with mean values lower than 200 ppt. Higher concentrations could be observed for the OVOCs with mean concentrations up to 5 ppb. The most abundant OVOCs apart from formaldehyde were methanol, ethanol, acetone and acetaldehyde.

The total measured OH (k_{OH}) reactivity showed low values and the comparison to the calculated OH reactivity from the individual trace gas measurements revealed only very small differences due to unmeasured trace gases. In the Netherlands the mean difference was 1.0±1.4 s^{-1} at a mean measured with a mean of 6.13±1.23 s^{-1} and in Italy 0.1±2.2 s^{-1} at a measured total OH reactivity of 3.8±1.4 s^{-1}.

These results showed that the sampled air in the height range 100m -1000m was not very polluted from primary emitted trace gasses for both parts of the campaign. The analysis revealed that the OVOCs were the major OH sinks by contributing 30 % in the Netherlands and 40 % in Italy to the total OH reactivity. The sources of OVOCs are manifold ranging from primary emissions to photochemical productions. Calculations revealed that the measured OVOCs did not entirely originate from photochemical production; a significant

amount originated from primary emissions and advected OVOCs. Primary emitted alcohols were analyzed at one instance in the plume of the Mannheim/Ludwigshafen region. As the most abundant OVOCs have OH lifetimes ranging between hours and days they are widely distributed and thus have regional to global effects on the air quality and thus climate.

Table of Contents

1. Introduction

1.1 What is the air we breathe?

The Earth's atmosphere has fascinated scientists for centuries. Already, in 1676 John Mayow discovered that the ambient air consists of two components. He named them 'air' and 'fire-air'. As the methods of analysis developed, this general distinction was confuted between the years of 1743 and 1794 by Lavoisier, Cavendish, Rutherford, and Priestly. Their research discovered, that the atmosphere is made up predominantly by nitrogen (N_2), oxygen (O_2), water (H_2O), and carbon dioxide (CO_2) (Seinfeld and Pandis, 2006). Today, the precise composition of the dry atmosphere is well defined, containing 78 % of N_2, 21 % of O_2, and 1 % of argon. The degree to which water vapor is present in the atmosphere significantly varies between 1-3 %, depending on the evaporation and precipitation, altitude, and temperature. These main components, constituting the atmosphere and their relative proportion is the same around the globe and has not changed significantly over the last million years (Finlayson-Pitts and Pitts Jr, 1999; Jacob, 1999; Seinfeld and Pandis, 2006)

Next to these main components, less than 1 % of the ambient air is made up of thousands of trace gases. The most abundant ones are carbon dioxide, neon, helium, methane, krypton, hydrogen, ozone (O_3), nitrogen oxides (NO_x), and the group of volatile organic compounds (VOCs) with the greatest number and variety of species. The trace gas concentrations are very low and in the range of parts per trillion by volume (pptv) to parts per million by volume (ppmv). Despite their seemingly insignificant fraction within the atmosphere, trace gases are significantly impacting life on earth. Whether it is smog, the ozone formation close to ground, acid rain or the destruction of the ozone layer, all of them are caused by trace gases (IPCC, 2007). Thus, trace gases play a crucial role in the Earth's radiative balance and chemical properties, which have changed rapidly and dramatically during the last two centuries. Particularly, concentrations of CO_2 and CH_4 in the atmosphere have increased significantly (Finlayson-Pitts and Pitts Jr, 1999; Seinfeld and Pandis, 2006). New insights on the impact of these changes on life on Earth have led to an increased research focus on trace gases in the past decades. Especially, the large group of volatile organic compounds (VOCs) has been the subject of strongly growing interest as they play a large role the atmosphere with effects of air quality and climate. VOCs is the collective name for substances that contain carbon atoms and are gaseous at room temperature (25 °C). The abundance of VOCs ranges from parts per million (ppm) to parts per trillion (ppt). Often VOCs are also named NMVOCs (non-methane volatile organic compounds). This notation indicates that methane is excluded because it differs from the other VOCs by its slow reaction with OH and the resulting high concentrations. Also, CO and CO_2 are not regarded as VOC. A vast variety of VOCs is present in the atmosphere. Today, the number of VOCs is estimated to 10^4 - 10^5 different

species. Most of them have a very small mixing ratio, hence their importance for the atmospheric chemistry can be regarded as minor (Goldstein and Galbally, 2007). First research on VOCs dates back to the year 1950. This research was limited to two VOC species, namely methane and formaldehyde (Glueckauf, 1951). The problems with smog in larger cities stimulated the research in the field of VOCs (Haagen-Smit, 1952).

Research has shown that VOCs are mostly emitted at the ground from multiple sources which are foremost of biogenic or anthropogenic. Once emitted, VOCs are trapped in the troposphere, which extends from the Earth's surface to the tropopause above and is the lowest part of the atmosphere. The height of the troposphere is season and latitude dependent and ranges from 8 to 15 km (McIlveen, 1992). In general, the troposphere is characterized by a relative rapid vertical mixing and decreasing temperature. Above the tropopause the temperature rises again. This temperature inversion within the troposphere functions as a transport barrier for most trace gases to rise further into the stratosphere (Atkinson, 2000; Finlayson-Pitts and Pitts Jr, 1999; Seinfeld and Pandis, 2006).

If there would not be an effective removal process for VOCs, the concentrations would increase significantly on Earth which would make life impossible. Polar VOCs are removed from the atmosphere by dry and wet deposition (see Figure 1.1), whereas the wet deposition by rain is dominating (Koppmann, 2008). But many VOCs from anthropogenic sources are non-polar and not water soluble and thus removed very slowly. Oxidation converts these VOCs into more polar and more water soluble species. Because of the high oxygen content of

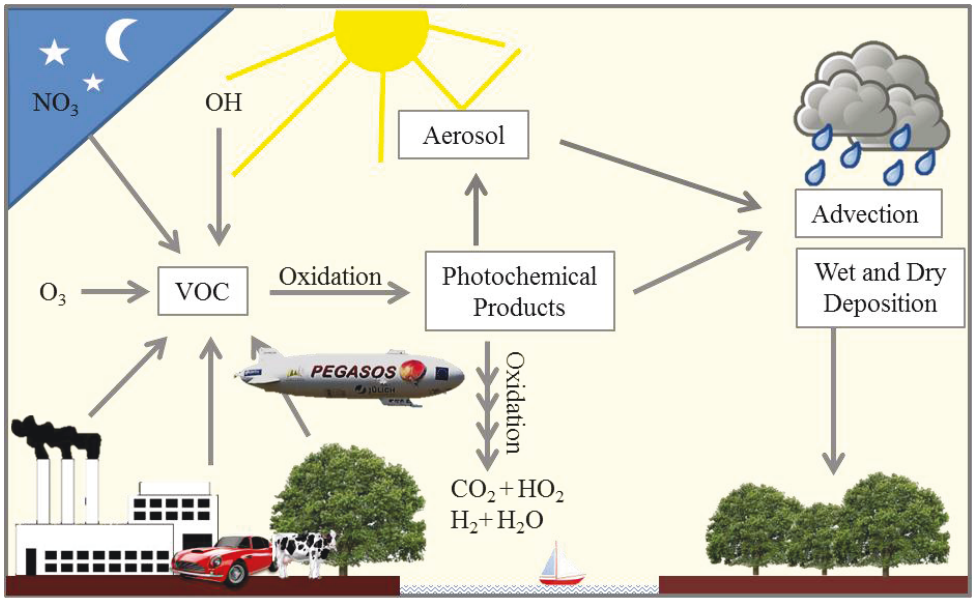

Figure 1.1: Various processes that determine the lifetime of VOCs in the atmosphere, ranging from oxidation, particle formation, advection and deposition (adapted from Koppmann (2008)).

the atmosphere the oxidation with oxygen is most likely. Yet, the high activation energies necessary for a direct reaction between the trace gases and the oxygen prevent the reaction at atmospheric conditions. Only in the 1970s the hydroxyl radical (OH radical) was discovered

as a reactant to oxidize traces gases. Levy (1972), showed that the OH radical is mainly formed from the ozone photolysis in the presence of water vapor. The review of Ehhalt (1999) showed that the OH radical is in fact the most important way to oxidize and therefore remove trace gases globally. Hence, it is referred to as "the cleaning detergent of the atmosphere". Due to its short lifetime it is only relevant for the trace gas oxidation during the day (Atkinson, 2000). The reaction of VOCs with OH, in the presence of NO, leads to the formation of O_3 especially close to the ground. Other oxidation pathways are initiated by direct photolysis by solar radiation at short wavelengths or reactions with O_3 and the nitrate radical (NO_3) at night. Once VOCs are oxidized, they can be further oxidized to CO_2 and water eventually, deposited (dry or wet) or transported by advection. Oxygenated volatile organic compounds (OVOC) also contribute to particle formation and growth. By all this VOCs have a significant impact on the air quality and climate.

In their large variety, VOCs play an important role as sources and sinks for radicals in the troposphere due to their structural variety and the degradation process. Thus, the VOC precursor can have an impact on the climate especially by its degradation products as O_3, organic nitrates, peroxy nitrates, aldehydes and ketones and the precursor for aerosols as shown in Figure 1.2.

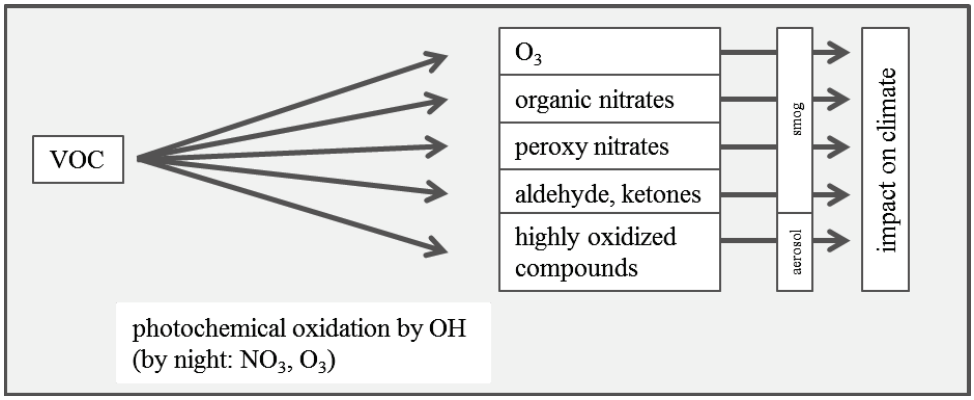

Figure 1.2: The impact of the VOCs to the climate.

The importance of VOCs depends on the relative distributions in the atmosphere and therefore on their concentrations. But also their removal time is of great importance, which is often dependent on the reaction rate with OH. In past field campaigns VOC in the lower troposphere have mostly been measured from ground based platforms or towers. Measurements from balloons or airplanes are very limited (Ammann et al., 2004; Apel et al., 2003; Arnold et al., 1986; Atkinson and Arey, 2003; Greenberg et al., 2003; Kuhn et al., 2007; Singh et al., 2001; Zimmerman et al., 1988). Consequentially, comprehensive VOC measurements with a high spatial and time resolution in the lower troposphere where steep trace gas gradients are expected are very limited. However, it is in this part of the troposphere where most of the VOC degradation chemistry takes place. Therefore, accurate fast time resolved VOC measurements together with other species such as CO, NO_x, and O_3 as well as the OH reactivity, encompassing different altitudes would essentially improve the understanding of the VOC distribution and their degradation in the lower troposphere.

This work contributes to existing research on VOCs by utilizing the Zeppelin NT as a measuring platform to explore the altitude range between 100 to 1000 m. The Zeppelin NT is an ideal measuring platform, allowing for a great payload of 1 t which is necessary to install the measuring equipment. The flight characteristics of the Zeppelin NT, especially its low velocity make it a perfect tool to probe the lower troposphere. A fast GC-MSD system (Gas Chromatography coupled with Mass Spectrometry) has been developed to measure VOCs on board the Zeppelin. The data reveal new insights on the distribution of VOCs in the lower troposphere, specifically the distribution of oxygenated VOCs which are mainly formed in VOC oxidation processes.

The measurements on board the Zeppelin were conducted within the European project PEGASOS where 26 project partners from 15 different countries all over Europe participated in order to gather a better understanding of the chemical and physical processes as well as their relevance for the changing climate in order to support the development of advanced politics to mitigate climate change and improve air quality (Pandis, 2010). This work contributes to this project by determining the VOC distributions vertically and horizontally across different biomes in Europe, from the Mediterranean in Italy to the mid-latitudes in the Netherlands. VOCs are very important OH sinks and as they also contribute significantly to the formation of O_3 and particles the measurements of VOCs are inevitable to learn more about their relevance for the air quality and therefore also their role for the climate change.

1.2 Sources of VOCs in the troposphere

The sources of VOCs in the atmosphere are almost always associated with life and can be found over remote oceans, rural areas as well as urban environments. VOCs are emitted from a wide variety of biogenic and anthropogenic processes ranging from foliage emissions to fossil-fuel consumption by humans.

Globally, the biogenic VOC (BVOC) emissions exceed those from the anthropogenic processes. Especially, large quantities of isoprene and monoterpenes are emitted in the tropics (Guenther et al., 1995; Guenther et al., 2006). The global source strength of BVOCs in the atmosphere is estimated to range between 312 and 1062 Tg C/year. Isoprene is the BVOC with the largest contribution, its total emission strength ranges from 250 to 750 Tg C/year (Wiedinmyer et al., 2004).

On a global scale, the emissions of anthropogenic VOC (AVOC), such as alkanes, alkenes and aromatics, are much smaller compared to the biogenic VOCs, with global emission estimates of 103 Tg C/year (Kansal, 2009). But on a regional scale AVOCs can make up the greatest fraction, especially in urban areas. A large source of anthropogenic VOCs is the production, storage and combustion of fossil fuels. Another significant source of anthropogenic VOCs is the production and use of paints and solvents (de Gouw and Warneke, 2007).

Biomass burning is also a large source of VOCs worldwide and can either occur naturally by forest fires or anthropogenically, when forests are cleared for agricultural land or agricultural waste is burnt. Globally, emissions by anthropogenically caused fires are dominating (Crutzen and Andreae, 1990). Through biomass burning large quantities of oxygenated VOCs, nitriles (HCH, CH_3CN), and aromatics (benzene, toluene) are released into the atmosphere (Andreae et al., 2001; Friedli et al., 2001).

The analysis of the oxygenated VOCs (OVOCs) has come into the focus of research in the last years. Because of analytical difficulties (Vairavamurthy et al., 1992), OVOCs have not been measured on routine basis (Apel et al., 2008). Already in the late 1960s Cavanagh et al. (1969) discovered the great abundance of OVOCs by measuring acetone, acetaldehyde, methanol, and ethanol at Point Barrow in Alaska. But only in the mid 80's the analysis of alcohols, aldehydes, and ketones was further advanced. Instrumental developments were especially driven by the analysis of the biogenically emitted 2-methyl-3-buten-2-ol (MBO) and the main isoprene degradation products methacrolein (MACR) and methyl vinyl ketone (MVK) (Apel et al., 2002; Goldan et al., 1993; Montzka et al., 1993; Yokouchi, 1994). Ground based measurements in rural regions and the marine free troposphere showed that the sum of the oxygenated VOCs exceeds the sum of the non-oxygenated VOCs. It was found that formaldehyde and acetaldehyde are the most abundant aldehydes, methanol and ethanol the most abundant alcohols and acetone the most abundant ketone (Goldan et al., 1995; Helmig and Greenberg, 1994; Leibrock and Slemr, 1997; Riemer et al., 1998; Snider and Dawson, 1985). The same was also observed for airborne studies above the Atlantic, Pacific and Canada between altitudes the of 0.5 and 12 km (Apel et al., 2003; Arnold et al., 1986; Singh et al., 2001; Singh et al., 1995; Singh et al., 1994). The measured concentrations are highly variable, but the studies have shown that methanol is the most abundant VOC after methane. The concentrations in the continental boundary layer range between 1 and 10 ppb and in the remote troposphere between 0.1 and 1 ppb (Heikes et al., 2002; Singh et al., 2000; Singh et al., 1995).

The sources of OVOCs in the atmosphere are manifold and controversially discussed. Sources are ranging from primary biogenic and anthropogenic emissions to biomass burning. But OVOCs can also be formed photochemically from both, AVOCs and BVOCs. This is shown for the most abundant OVOCs in Table 1.1. Overall, acetone and methanol have a large biogenic source, whereas ethanol is mostly emitted from anthropogenic processes. Formaldehyde and acetaldehyde are predominantly produced in the photochemical VOC degradation process as elaborated in Chapter 1.2.2. The global emission strengths of the OVOCs show a great variation for some compounds with a difference of a factor of 2 to 7 (see Table below). This shows that the global emission strengths of OVOCs still suffer from great uncertainties and further research is necessary to fully comprehend the sources that cause these high concentrations in the atmosphere.

Table 1.1: Sources of oxygenated VOCs (OVOCs) from biogenic and anthropogenic primary sources and secondary formed OVOCs from the photochemical VOC degradation. The estimations of the mean global source strength are mentioned below.

OVOC	**Biogenic source [Tg yr^{-1}]**	**Anthropogenic Source [Tg yr^{-1}]**	**Biomass burning /Oceanic [Tg yr^{-1}]**	**VOC oxidation [Tg yr^{-1}]**	**Literature**
Formaldehyde	Emissions from holm oak and pine **1.5**	Car exhaust (especially alcohol based fuels) **0 - 2**	Biomass burning **5 - 13**	Photochemical degradation of VOCs **10^3**	(Altshuller, 1993; Carlier et al., 1986; Gabele, 1990; Kesselmeier et al., 1997; Singh et al., 2000; Williams et al., 1990; Wittrock et al., 2006)
Acetaldehyde	Emissions from hayfields, Ponderosa pine and mixed hardwood Biomass burning **20 - 50**	Combustions of biofuel **0 - 1**	Biomass burning **3 - 11** Oceanic **75 - 175**	Intermediate oxidation product in the degradation process of higher alkanes, (predominantly ethane) **15 - 45**	(Finlayson-Pitts and Pitts Jr, 1999; Holzinger et al., 1999; Karl et al., 2001; Karl et al., 2003; Riemer et al., 1998; Schade and Goldstein, 2001; Singh et al., 2004a; Singh and Zimmerman, 1992)
Methanol	Emissions from hayfields and Ponderosa pine **28 - 280**	Solvent in the chemical industry and vehicle exhaust **2 - 11**	Biomass burning **2 - 32** Oceanic **0 - 80**	Disproportionation of methyl peroxy radicals **12 - 38**	(Galbally and Kirstine, 2002; Heikes et al., 2002; Jacob et al., 2005; Karl et al., 2001; Palmer et al., 2003; Riemer et al., 1998; Schade and Goldstein, 2001; Singh et al., 2001)
Ethanol	Emissions from Norway spruce and Ponderosa pine **4 - 8**	Solvent in the chemical industry and fuel and fuel additive **2**	Biomass burning **1 - 3** Oceanic **0 - 1**	Secondary product from the oxidation of hydrocarbons that generate $C_2H_5O_2$ radicals, e.g. ethane **1 - 3**	(Grabmer et al., 2006; Kelsey, 1996; Lamanna and Goldstein, 1999; Nguyen et al., 2001; Singh et al., 2004a)
Acetone	Emissions from mixed hardwood, Ponderosa pine and Norway spruce **10 - 75**	Solvent in the chemical industry **1 - 3**	Biomass burning **3 - 11** Oceanic **21 - 33**	Product of the oxidation of branched hydrocarbons and monoterpenes **19 - 39**	(Grabmer et al., 2006; Karl et al., 2003; Schade and Goldstein, 2001; Singh et al., 2000; Singh et al., 2004a)

1.2.1 Sinks of VOCs

The major sinks of VOCs in the atmosphere are reactions with the hydroxyl radical (OH), ozone (O_3), the nitrate radical (NO_3), and deposition processes. Deposition can either occur on surfaces such as vegetation or aerosols (dry deposition) or in rain (wet deposition). Thus, the lifetimes of VOCs vary between minutes and years depending on the respective rate coefficients of the reactions with OH, O_3, and NO_3 as well as the respective deposition velocities.

Overall, the predominant VOCs removal process is the reaction with the hydroxyl radical. The most significant OH sources in the troposphere are photolysis of O_3 and nitrous acid (HONO) where globally during daytime the ozone photolysis represents the largest source. Ozone can be photolyzed at a wavelength lower than 335 nm and excited oxygen atoms $\left(O(^1D)\right)$ are formed as shown in Equation 1.1. These excited oxygen atoms can be deactivated in collisions with air molecules such as nitrogen or oxygen by forming ground state oxygen atoms $\left(O(^3P)\right)$ (see Equation 1.2). $O(^3P)$-atoms can react further with oxygen forming ozone (see Equation 1.3).

$$O_3 + h\nu \rightarrow O(^1D) + O_2 \qquad (\lambda \leq 335\ \text{nm}) \qquad 1.1$$

$$O(^1D) + M \rightarrow O(^3P) + M \qquad (M = N_2, O_2) \qquad 1.2$$

$$O(^3P) + O_2 + M \rightarrow O_3 + M \qquad (M = N_2, O_2) \qquad 1.3$$

But the $O(^1D)$ atoms can also react with water forming two OH radicals as shown in Equation 1.4.

$$O(^1D) + H_2O \rightarrow 2\ OH \qquad 1.4$$

Therefore, the OH production is dependent on the short-wave radiation and on the water content of the atmosphere. Especially, in the lower troposphere, where the VOC concentration is the highest, high humidity levels are present. But overall, the radiation is the limiting factor to this reaction in the troposphere, depending on the diurnal and seasonal and the ozone layer that filters short-wave light.

At 298 K and a relative humidity (RH) of 50 %, approximately 0.2 OH radicals are formed per $O(^1D)$ atoms (Atkinson, 2000), resulting in a globally averaged OH concentration of $0.94 \pm 0.13 \times 10^6$ cm^{-3} (Prinn et al., 2001). This is considerably low in comparison to the concentrations of VOCs. A characteristic behavior for the OH radical is that it does not react with the main components of the atmosphere such as N_2, O_2, and H_2O. In the degradation process of VOCs, OH radicals are recycled efficiently if NO is present. This process is described in more detail in the following for the example of the degradation (see Equations 1.5 - 1.10) of methane in the presence of nitric oxide (NO) (Atkinson, 2000).

In the case of methane the OH radical abstracts one hydrogen atom. A fast recombination with molecular oxygen (O_2) leads to the formation of the methylperoxy radical (CH_3O_2) (see Equation 1.5). In the presence of NO the methylperoxy radical can react further, producing a methoxy radical (CH_3O) and nitrogen dioxide (NO_2) (see Equation 1.6). A further hydrogen

atom is abstracted from CH_3O by molecular oxygen, yielding formaldehyde ($HCHO$) a stable oxygenated VOC and a hydroperoxy radical (HO_2) as shown in Equation 1.7. The resulting HO_2 can react with NO; leading to the production of one OH and another NO_2 molecule (see Equation 1.8). Both NO_2 molecules formed can be photolyzed producing atomic oxygen atoms and NO radicals (see Equation 1.9). In the presence of air molecules as N_2 and O_2, the atomic oxygen atoms can react rapidly with oxygen forming O_3 (see Equation 1.10). Consequently, in the presence of OH and NO, one methane molecule is oxidized to one formaldehyde molecule (see Equation 1.11) and one water molecule. Two ozone molecules are formed in the NO channel as a byproduct (Ehhalt, 1999). But HO_2 can also react with RO_2 without the formation of O_3.

$$CH_4 + OH + O_2 \rightarrow CH_3O_2 + H_2O \quad 1.5$$

$$CH_3O_2 + NO \rightarrow CH_3O + NO_2 \quad 1.6$$

$$CH_3O + O_2 \rightarrow HCHO + HO_2 \quad 1.7$$

$$HO_2 + NO \rightarrow OH + NO_2 \quad 1.8$$

$$2(NO_2 + h\nu \rightarrow NO + O) \qquad (\lambda \leq 398\ \text{nm}) \quad 1.9$$

$$2\,(O + O_2 + M \rightarrow O_3 + M) \qquad (M = N_2, O_2) \quad 1.10$$

Net reaction:

$$CH_4 + 4\,O_2 \rightarrow HCHO + 2\,O_3 + H_2O \quad 1.11$$

The resulting formaldehyde can be degraded further with OH, forming carbon monoxide and HO_2 (see Equation 1.12). However, the lifetime of formaldehyde is also determined by the photolysis by light with a wavelength lower than 330 nm. The photolysis can occur via two channels. First, the molecular channel leading to the production of CO and hydrogen (see Equation 1.13) and second the radical channel leading to CO and two HO_2 molecules (see Equation 1.14). The produced CO in all three reaction pathways is further degraded by OH to CO_2 and hydrogen (see Equation 1.15).

$$HCHO + OH + O_2 \rightarrow CO + HO_2 + H_2O \quad 1.12$$

$$HCHO + h\nu \rightarrow CO + H_2 \qquad (\lambda < 360\ \text{nm}) \quad 1.13$$

$$HCHO + 2\,O_2 + h\nu \rightarrow CO + 2HO_2 \qquad (\lambda < 340\ \text{nm}) \quad 1.14$$

$$CO + OH \rightarrow CO_2 + H \quad 1.15$$

$$H + O_2 \rightarrow HO_2 \quad 1.16$$

$$HO_2 + NO \rightarrow OH \quad 1.17$$

The radical degradation of VOCs with OH in the presences of nitric oxide (NO) leads to the formation of intermediate radicals such as peroxy radicals (RO_2) and alkoxy radicals (RO). These radicals can form stable products as formaldehyde and other oxygenated VOCs (OVOCs). In this process HO_2 radicals are produced which can recycle to OH in the reaction with NO forming also NO_2 (see Equation 1.17). NO_2 is photolyzed forming oxygen atoms that

react further with O_2 forming ozone. The process of VOC degradation with OH is summarized in Figure 1.3. Notably, in the case of a reaction of RO_2 with HO_2, or a recombination of two RO_2, radicals are lost.

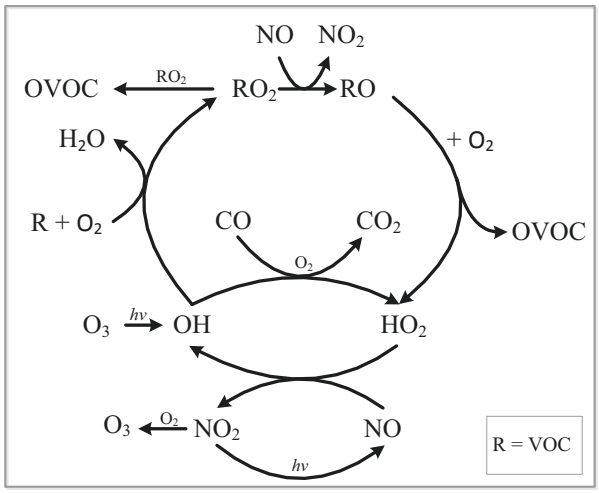

Figure 1.3: Schematic of the degradation of saturated hydrocarbons with OH in the presence of nitric oxide (NO). VOCs (RH) react with OH forming peroxy radicals (RO_2). These can react with NO forming alkoxy radicals (RO) or recombine with another RO forming an oxygenated VOC (OVOC). RO reacts further forming the hydroperoxy radical (HO_2) and an OVOC. HO_2 can react with NO recycling OH. But also NO_2 is produced which reacts further forming ozone.

During the day the main VOC sink is the reaction with OH. Contrary, at night, when there is no photolysis of O_3 forming OH, other atmospheric oxidants such as the nitrate radical (NO_3) and O_3 gain in importance. NO_3 can abstract H-atoms like OH, preferably from aldehyde groups, or add to double bonds of unsaturated compounds, forming multifunctional organic nitrates.

The reaction with O_3 is only relevant for unsaturated VOC. In this case O_3 can add to the double bond as illustrated for ethene below (branching ratios taken from Atkinson et al. (1997)). The ozonolysis of ethene leads to the formation of formaldehyde and an excited Criegee biradical (see Equation 1.18). The excited Criegee biradical can react further along three possible pathways. First, the reaction with an air molecule yields a stabilized Criegee biradical (see Equation 1.19) which can react further. Second, the excited Criegee biradical reacts to CO and water as shown in Equation 1.18, third, to HCO and OH (see Equation 1.21). Finally it can react to CO_2 and H_2 as shown in Equation 1.22. The branching ratios are 0.37, 0.38, 0.12 and 0.13 respectively.

$$C_2H_4 + O_3 \rightarrow HCHO + HCHOO^* \quad 1.18$$

$$HCHOO^* + M \rightarrow HCHOO + M \quad 37\ \% \quad 1.19$$

$$HCHOO^* \rightarrow CO + H_2O \quad 38\ \% \quad 1.20$$

$$HCHOO^* \rightarrow HCO + OH \quad 12\ \% \quad 1.21$$

$$HCHOO^* \rightarrow CO_2 + H_2 \quad 13\ \% \quad 1.22$$

1.2.2 OH reactivity

Together with inorganic trace gases, such as CO, NO, and NO_2, VOCs are important OH sinks. The OH radical is short-lived, with an average lifetime shorter than 1 s (Lou et al., 2010). Thus the OH concentration in the atmosphere can be assumed to be in steady-state and therefore determined by the production (P_{OH}) and destruction (D_{OH}) term of OH (see Equation 1.23).

$$\frac{d[OH]}{dt} = P_{OH} - D_{OH} = P_{OH} - k_{OH}[OH] \approx 0 \quad 1.23$$

The main contributions to the OH production term are the photolysis of O_3 (see Equation 1.1-1.4) and the recycling of HO_2 (see Equation 1.8). The destruction rate is dependent on k_{OH} and the OH concentration itself. The k_{OH} is also denoted as the total OH reactivity and equivalent to the reciprocal of the OH lifetime (τ_{OH}) (see Equation 1.24). The term k_{OH+Xi} describes the respective reaction rate constant for the reaction of one component x_i with OH, which is multiplied by $[x_i]$, the concentration component x_i in order to consider the contribution of x_i to k_{OH}. The sum of the contributions of the individual substances is denoted as the total OH reactivity.

$$k_{OH} = \sum k_{OH+xi} \times [x_i] = \frac{1}{\tau_{OH}} \quad 1.24$$

Large uncertainties in interpretation and modeling of atmospheric observations can result from incomplete measurements of the single trace gases. Measurements must be complete and accurate. The analysis of the relatively few important inorganic compounds (NO, NO_2, CO, O_3) has become more accurate in the last years, but measurements of VOCs are still challenging. The measurements are difficult due to the large variety of VOCs (10^4-10^6 different species) which leads to great uncertainties in the quantification because in most field campaigns only a limited number of VOCs of less than 100 species are analyzed (Goldstein and Galbally, 2007).

Newly developed methods for direct measurements of the total OH reactivity, have been ground-breaking and facilitate to constrain the completeness of trace gas measurements that determine the lifetime of OH, especially VOCs. There are different measurement aproaches. First, the OH reactivity is measured as the reciprocal of the OH lifetime. In this aproach artifically generated OH radicals are produced in a flowtube in the presence of ambient air to monitor the OH loss rate (decay) and the OH lifetime is calculated from the measured OH decay due to the reaction of the radicals with trace gases in the airflow. OH is injected into the flowtube either by laser flash photolysis of ozone (Lou et al., 2010; Sadanaga et al., 2004) or by a moveable OH injector (Ingham et al., 2009; Kovacs and Brune, 2001). Second, the OH reactivity can be measured directly utilizing the Comparative Reactivity Method (CRM). This measurement technique is based on the competitive reaction of a selected reactant that is not present in the atmosphere and reactants from the ambient air with artificially produced OH (Sinha et al., 2008).

The total OH reactivity can also be calculated as shown in Equation 1.24 from the sum of single trace gas concentrations denoted as (k_{OH}^{calc}) in the following. The calculated OH

reactivity can be compared to the measured OH reactivity to determine the integrity and completeness of the individual measurements. For the comparison the term of the missing OH reactivity (k_{OH}^{miss}) is introduced and calculated as outlined in Equation 1.25.

$$k_{OH}^{miss} = k_{OH}^{meas} - k_{OH}^{calc} \quad 1.25$$

Previous studies have shown that the measured OH reactivity varies between values of 4 s^{-1} in an airplane study above the Pacific Ocean (Mao et al., 2009) and 200 s^{-1} in Mexico City (Shirley et al., 2006) (see Table 1.2). Significant gaps between the measured and the calculated OH reactivity have been reported which is due to unmeasured VOCs which can differ from region to region. Nölscher et al. (2012) reported an unexplained fraction of up to 89 % in the boreal forest in Finland, resulting from non-measured biogenic emissions. On the contrary, in the study by Ren et al. (2006b) in Whiteface-Mountain, USA, the measured OH reactivity could be understood completely. In anthropogenic regimes the OH reactivity could be fully explained in a campaign in New York (Ren et al., 2003). But, a study in Tokyo reports a missing reactivity of 50 % due to primary anthropogenic sources and photochemically produced oxygenated VOCs (Chatani et al., 2009). Thus, there are different findings regarding the missing reactivity across different regimes. Consistently, in all cases of where missing reactivity was found, the VOC measurements of biogenic compounds such as sesquiterpenes and unmeasured oxygenated VOCs were assumed to be incomplete.

Table 1.2: The OH reactivity measured with the missing fraction, the measured species and the hypothesis for the missing fraction.

Literature	Site	Condition	k_{OH}^{meas} [s^{-1}]	k_{OH}^{miss} [s^{-1}]	Measured species [a]	Hypothesis
Di Carlo et al. (2004) PROPHET, Jul – Aug 2000	Michigan, USA	Rural mixed forest	1-12	2.6 ±1.0 (mean)	I A Iso O F	Unmeasured temperature dependent monoterpenes
Ren et al. (2006b) PMTACS Jul – Aug 2002	Whiteface-Mountain, USA	Rural forest	4-10	-	I A Iso O	No significant missing reactivity
Sinha et al. (2008) GABRIEL August 2005	Brownsberg, Surinam	Tropical forest	53 (mean)	[b]	Iso O	Unmeasured biogenic compounds
Lou et al. (2010) PRIDE-PRD2006 July 2006	PRD, China	Rural, Subtropics	20 - 50	10-25	I A Iso	Photochemically produced unmeasured OVOCs
Nölscher et al. (2012) HUMPPA-COPEC July – Aug 2010	Hyytiälä, Finland	Boreal forest	7-23	5 -21	I A Iso M O	Unmeasured biogenic compounds
Edwards et al. (2013) OP3 April 2008	Borneo	Tropical rainforest	29±8.5 (mean noon)	18.9	I A Iso M O	Photochemically produced OVOCs

Literature	Site	Condition	k_{OH}^{meas} [s^{-1}]	k_{OH}^{miss} [s^{-1}]	Measured species [a]	Hypothesis
Mao et al. (2010) TEXAQS2000 Aug - Sep 2000	Houston, USA	Urban region	5-10	-	I Iso O F	No significant missing reactivity
Kovacs and Brune (2001) SOS June-July 1999	Nashville, USA	Urban	11.3 ± 4.8 (mean)	3.8 ± 2.0 (mean)	I A Iso O F	Short-lived VOCs
Ren et al. (2003) June – August 2001	New York, USA	Megacity	15-25	-	I Iso O F	No significant missing reactivity
Shirley et al. (2006) MILAGRO April 2003	Mexico City, Mexico	Megacity	10-200	[b]	[b]	[b]
Yoshino et al. (2006) 2003/2004	Tokyo, Japan	Megacity	18-27	0.9-8.1	I A Iso M O F	Photochemically produced OVOCs
Ren et al. (2006a) PMTACTS Jan - Feb 2004	New York, USA	Megacity	10-100	2-10	I A F	Primary emitted OVOCs (aldehyde, ketone)
Sinha et al. (2008) August 2005	Mainz, Germany	Urban	10.4 (mean)	[b]	[b]	[b]
Mao et al. (2010) Aug - Sep 2006	Houston, USA	Urban region	10-24	-	I Iso O F M	No significant missing reactivity
Chatani et al. (2009) August 2007	Tokyo, Japan	Megacity	15-55	8.5 (mean)	I A Iso M O F	Primary anthrop. sources and produced OVOCs
Mao et al. (2009) INTEX-B April - May 2006	Pacific ocean	Marine air (Airborne)	4 ± 1.0 (mean)	2.4 ± 0.6 (mean)	I A O F	Photochemically produced OVOCs
This study PEGASOS May - July 2012	Netherlands, Italy	Zeppelin measurements	5.7 (NL) 3.7 (IT) (mean)	0.9 (NL) 0.3 (IT) (mean)	I A Iso M O F	No significant missing reactivity

[a] Measured species used to calculate (k_{OH}^{calc}): I = CO, NO_x, O_3 etc, A = alkanes, alkenes, aromatics (excluding isoprene), Iso = isoprene, M = monoterpenes, O = oxygenated VOCs excluding formaldehyde, F = formaldehyde. [b] Not reported.

The results shown in the table above indicate that there are still very high uncertainties in the determination of all trace gases which are main OH sinks. This leads to large uncertainties in the atmospheric research which makes forecasts of OH and the formation of secondary pollutants as O_3, OVOCs and SOA difficult. Thus, more VOC measurements together with k_{OH} measurements would provide more insight on the integrity of VOC measurements. This would provide more knowledge of the distribution of the main OH sinks.

1.3 Measurements of VOCs

In the past, VOCs have predominantly been measured by gas chromatography (GC). In this approach VOC compounds are separated on a chromatographic column based on their chemical and physical properties (McNair and Miller, 2009). However, concentrations of most atmospheric VOCs are too low for a direct gas chromatographic analysis. In order to measure VOCs in the ppt-range, they have to be pre-concentrated as outlined in Chapter 1.3.1 prior to the separation on the GC column (see Figure 1.4, upper panel). The separated VOC species are subsequently analyzed by a detector (see Figure 1.4, lower panel), where they appear as chromatographic peaks. The GC column and detector are chosen depending on the respective target analytes. In recent research systems equipped with a pre-focusing step have been increasingly utilized (see Figure 1.4, middle panel). In this procedure the target molecules are trapped on a micro-trap which can be heated up rapidly for a fast injection of the analytes onto the GC column. Results show narrower chromatographic peaks and an improved resolution of the more volatile VOCs (Helmig, 1999; Korytár et al., 2002; Leclercq and Cramers, 1985).

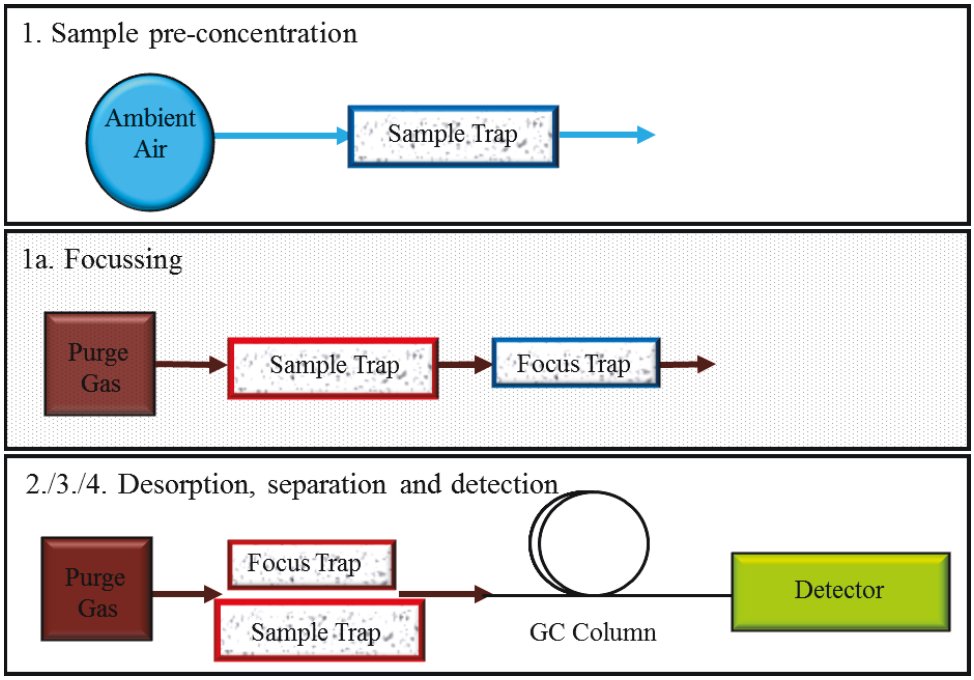

Figure 1.4: The GC analysis of VOCs with the pre-concentration. (1.) Adsorption (top panel) and the desorption (2.), separation (3.), and detection step (4.) (bottom panel). Some systems are equipped with a micro-trap prior the GC column (1a.) for an improved resolution (middle panel).

1.3.1 Preconcentration techniques

Depending on the experimental design, the air can be sampled offline or online. For offline analysis the air samples are collected in glass or metal containers (Bottenheim and Shepherd, 1995; Donoso et al., 1996; Rudolph et al., 1986) or on adsorbent cartridges (Plass-Dülmer et

al., 1998) in the field and measured in the laboratory. This method does not require elaborate instrumentation on the field site. However, when samples have to be stored for longer periods before they are analyzed, artifacts may be formed Therefore, online GC instruments are being used predominantly, if possible (Helmig, 1999).

For online GC systems, there are two different pre-concentrating techniques which are predominantly utilized. First, the cryogenic sampling on glass beads (Koppmann et al., 1992) or empty liners and second, the enrichment onto carbon based adsorbents at ambient temperatures which dates back to the 1960's. The key advantages of the cryogenic sampling are low desorption temperatures, which ensure that measurements are less affected from artifacts (Apel et al., 2003; Goldstein et al., 1995; Greenberg et al., 1996; Koppmann et al., 1995). Carbon based adsorbents have to be chosen with care to prevent contamination by artifacts, especially when sampling ambient O_3 (Ciccioli et al., 1986; Helmig and Vierling, 1995).

1.3.2 Separation and detection

For the GC separation, the sample is partitioned between two phases. First, the stationary phase which is a glass column (GC column) with coated walls. This coating is a microscopic layer of a liquid or a polymer. Second, the mobile phase or carrier gas is usually an inert gas such as helium or nitrogen. The analytes are separated from one another based on their relative vapor pressures and affinities for the stationary bed. To increase the analysis time the column can be heated. The heating reduces the interaction of the analytes with the stationary phase (Hübschmann, 1996; McNair and Miller, 2009). There is a large variety of GC columns which are used today depending on the target compounds and range from packed columns to liquid stationary phase columns. Recently, methods to analyze VOCs have integrated the multidimensional or comprehensive GC analysis (GC x GC) to increase the analysis spectrum of VOCs (Goldstein and Galbally, 2007).

The choice of column as well as the coupling to different detectors is application-specific. Flame ionization (FID) and mass spectrometry (MSD) are predominately used to detect light hydrocarbons. For halogenated compounds the electron capture detector (ECD) is the detection method of choice (Helmig, 1999).

1.3.3 New improvements in the VOC analytics

Recently, there has been an increasing demand for higher sample throughput and thus a better time resolution in VOC measurements. Especially, airborne measurements require a better time resolution. Thus, new techniques to analyze VOCs, such as the chemical ionization mass spectrometry (CIMS) (Arnold et al., 1986; Mohler et al., 1993) and the proton-transfer-reaction mass spectrometry (PTR-MS) (Lindinger et al., 1998; Wisthaler et al., 2001), were developed. Both techniques do not require a preconcentration step enabling the analysis of temperature-labile compounds which would otherwise not survive the preconcentration and chromatography of the GC analysis. Moreover, these methods allow for a good time

resolution (1 s – 1 min) and relatively good sensitivity. However, the specificity of these methods is lower compared to the GC, as the compounds are detected at once and not separated prior to detection. Thus, structural isomeric species, such as the monoterpenes, are not distinguishable with a PTR-MS (Grabmer et al., 2004; Hayward et al., 2004).

Another alternative for a better time resolution with a good specificity are the newly developed Fast-GC systems. Whilst, the analysis time with GC was in the range of hours in the early 90s, GCs have been consistently improved resulting in a better time resolution. George (2001) showed that time resolution below 30 min could be achieved by adjusting each part of the system (the preconcentration, the separation, and the detection) according to the respective target compounds.

The time required for a GC separation depends on the resolution to be achieved, the selectivity of the method and the sensitivity of the detector. The fastest analysis time is achieved by reducing the method to the lowest acceptable resolution, with the highest selectivity and sensitivity (Apel et al., 2003; Korytár et al., 2002). For a better resolution and a broadening of the target spectra, the separation was revolutionized by implementing fused silica columns. Moreover, shorter GC columns which a smaller diameter ($\leq$ 0.1 mm ID) can be used to shorten the analysis time without reducing the resolution (Leclercq and Cramers, 1985). Also, a faster heating rate and the increase of the carrier gas velocity can be used to reduce the time needed for a chromatogram. Moreover, carrier gases with low molecular weight, such as hydrogen, decrease the analysis time even further. Yet, for safety reasons, helium remains the most frequently used carrier gas. In conclusion, the method allows for more rapid desorption times, a lower baseline disturbance and a better sensitivity for early eluting analytes (Grob and Barry, 2004).

A loss in chromatographic resolution can be compensated by coupling the GC to a MSD. This allows for the measurement of co-elution components that still can be separated by their different masses or different fragmentation patterns. The improvement of the electron multipliers and the mass filter designs has led to an improvement of the detector sensitivity of MSDs. The operation of the MSD in the selective ion monitoring mode (SIM) leads to an additional increasing sensitivity of the target compounds, as only specific mass to charge (m/z) ratios are detected at a longer time (George, 2001; Korytár et al., 2002). An alternative is the implementation of time-of-flight (TOF) analyzers for a faster analysis with more spectra per second than a quadrupol MSD (George, 2001; Grob and Barry, 2004; van Deursen et al., 2000)

The preconcentration now becomes a time limiting step and needs to be optimized for the target compounds and the application by choosing the ideal preconcentration method. The utilization of two individual preconcentration systems, working asynchronously reduces the analysis time drastically (George, 2001).

In the year 2005 there was the motivation to build a fast-GC-MSD at the Forschungszentrum, Jülich, Germany to measure VOCs on board the German research aircraft HALO (High Altitude LOng range). Dr. R. Wegener (Forschungszentrum, Jülich, Germany) together with D. Bremer, B. Rose and W. Waltke (GERSTEL GmbH & Co.KG, Mühlheim, Germany)

made the conception planning. But the instrument was then build by Gerstel and delivered in October 2008 to the Forschungszentrum, Jülich, Germany.

1.4 The PEGASOS project

The Pan-European-Gas-AeroSOl-climate interaction Study (PEGASOS) is a European project including 26 partners that are the leading research groups with state of the art observational and modeling tools from 12 European- and 3 associated countries. The research interests of the PEGASOS project are twofold. Firstly, the project is set up to quantify the magnitude of regional and global responses of atmospheric processes to the changing climate. Secondly, the aim is to identify pollution reduction strategies and policies to improve air quality while limiting their impact on climate change (Pandis, 2010). These tasks are addressed in 18 different work packages (WP) that are assigned to four different themes: first the emissions and exchange processes (Theme I, WP 1-5), second, atmospheric processes (Theme II, WP 6-9), third, links between air pollution and climate change (Theme III, WP 10-13), and fourth integration with policy (Theme IV, WP 14-17). WP 18 comprised the overall coordination and management (Pandis, 2010).

This study is part of the WP 7 in theme II, making use of the Zeppelin NT as a platform for field experiments to explore the photo-oxidation of mixtures of anthropogenic and biogenic VOCs, to improve the understanding of the corresponding mechanisms. Here, the focus is predominantly on the HOx cycle, the formation of photo-oxidants, and the formation and aging of secondary organic aerosol (SOA). The Zeppelin NT provides the opportunity to explore the planetary boundary layer (PBL) dynamics, the vertical and spatial distribution of trace gases and aerosols across different biomes, reaching from the Mediterranean in Italy to the boreal forests in Finland (Pandis, 2010).

1.5 Focus of this work

This study utilized the Zeppelin NT as a suitable measurement platform to analyze the distribution of VOCs across different biomes, emission patterns and height ranges (100 to 1000 m). It contributes to research on atmospheric chemistry by exploring the distribution of VOCs in the lower part of the troposphere. This part of the troposphere has been subject in previous tower-, balloon- or airplane studies (Ammann et al., 2004; Apel et al., 2003; Arnold et al., 1986; Greenberg et al., 2003; Kuhn et al., 2007; Singh et al., 2001; Zimmerman et al., 1988). The focus of this study is especially on the spatially highly resolved analysis of oxygenated VOCs in line with the non-oxygenated VOCs over the central and southern part of Europe. Finally, this research compares the calculated OH reactivity of the single trace gas measurements to the total OH reactivity across different regions.

In chapter 2 the benefits of the Zeppelin NT as a measurement platform for atmospheric research is outlined. Furthermore the redesign measures taken to enable the utilization the Fast-GC system on board the Zeppelin are delineated. This redesign of the Fast-GC system

was necessary, as it was originally designed for the deployment on the German research aircraft HALO.

Chapter 3 presents the observations of the VOC measurements on board the Zeppelin NT during the two PEGAOS campaigns in the Netherland and Italy. The measurements in the Netherlands and in Italy are described, along with the analysis of the VOC distribution across Europe reaching from Rotterdam in the Netherlands to Bologna in Italy. Furthermore, the vertical VOC distribution of the atmosphere is analyzed with a particular focus on the different layers which is further elaborated upon in Chapter 4.3.

In Chapter 4 the total OH reactivity measured is compared to the total OH reactivity calculated from the single trace gas measurements (as outlined in Chapter 1.2.3; Equation 1.24). This comparison enables the analysis of the integrity of the VOC measurements, with respect to the OH reactivity. Moreover, the composition of the measured OH reactivity and thus the major OH sinks can be determined for the Netherlands and Italy, across Europe, and across different height profiles.

2. Experimental section

2.1 Zeppelin NT as a measuring platform for atmospheric research

Previous research on the chemical degradation of VOCs in the troposphere has utilized towers, balloons or airplanes (Ammann et al., 2004; Apel et al., 2003; Arnold et al., 1986; Greenberg et al., 2003; Kuhn et al., 2007; Singh et al., 2001; Zimmerman et al., 1988). Unfortunately, these approaches do not enable detailed measurements between the altitude of 100 and 1000 meters, where most of the VOC degradation occurs.

Specifically, this study utilizes the Zeppelin NT as a measuring platform to investigate the troposphere (Hofzumahaus and Holland, 2006; Hofzumahaus et al., 2006; Hofzumahaus et al., 2009b). In 2012 two PEGASOS campaigns were performed in the Netherlands and in Italy. The Zeppelin NT was deployed for another PEGASOS campaign in 2013 measuring in Sweden and Finland. The main advantages of utilizing the Zeppelin NT as a measuring platform are twofold. First, the Zeppelin NT can fly at a low velocity with low vibrations which is ideal for the performance of the measuring equipment on board. The travelling speed is between 0 and 115 km/h. Its skeletal carbon structure is covered by a hull of a multilayer laminate that makes it a semi rigid airship. The hull is inflated with helium and together with the attached propellers it gives the Zeppelin NT the required uplift. The gondola with the cockpit is attached to the carbon structure as well as the two side engines and the aft engine with the propellers. The engines provide electricity which can be used to operate the instrumentation. The Zeppelin NT has a total length of 75 m and a height of 17.40 m. It can carry a payload of 1 t which is sufficient for the scientific equipment necessary to probe the atmosphere. Depending on the weather conditions and the payload the Zeppelin NT can fly up to 24 hours. Second, the Zeppelin NT can fly in altitudes between 100 and 2600 m. The maximum flight altitude is determined by the payload, the amount of helium and the ambient temperature. Especially, the low flight altitude offers substantial new opportunities to advance research on the VOC distribution inside the boundary layer by realizing unique flight patterns.

The main limitation of the Zeppelin NT as a measuring platform derives from its weather dependency. Contrary to airplanes, the Zeppelin NT is flown by sight and not by instrumentation. Accordingly, there are strict air regulations which restrict the Zeppelin NT to flights at VFR (Visual Flight Rules) conditions. Moreover, the Zeppelin NT can fly at wind speeds larger than 15 kn (28 km/h) but then it is difficult for the start and landing maneuvers on the mast. This makes the exact scheduling of the flights difficult and flexibility is needed.

2.2 Equipment on board the Zeppelin NT

Instruments can be placed at two different positions on board the Zeppelin NT (see Figure 2.1). Primarily, instrumentation can be installed in the gondola onto the seat rails of the passenger seats and secondarily, on the top platform. The top platform is only installed for scientific purposes.

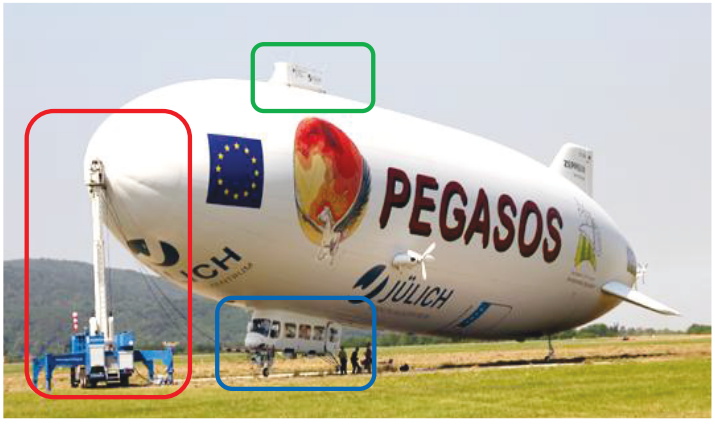

Figure 2.1: Zeppelin NT on the ground attached to the mast truck (red), the top platform (green) and the gondola (blue).

The airship is equipped with two different kinds of instruments: first, those that are mounted permanently on board the airship. And second, instruments that are installed depending on the research question inside the gondola. There are three different cabin layouts (CL) as seen in Figure 2.2. First, CL-8 to analyze the photochemistry of trace gases. Second, CL-5 to investigate of the distribution of secondary organic aerosol and finally, CL-9 is implemented to study the nucleation process of aerosols (see Figure 2.2).

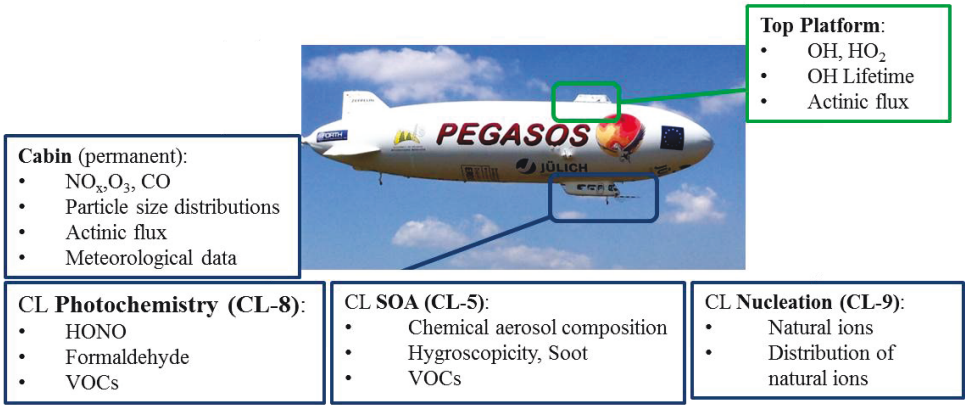

Figure 2.2: The Zeppelin NT with the top platform (green) and gondola (blue), including the division into permanent instrumentation and the three cabin layouts (CL) and all the measured species.

2.2.1 Permanent equipment

The gondola permanently houses five different instruments: first, the LDA Rack, measuring inflight aviation data and meteorological parameters as temperature, pressure, humidity and wind speed, second, the NO_x Rack that analyses NO, NO_2, O_3 and third, the COD instrument measuring the CO distribution. Fourth, the CPN-Rack measuring particle size distributions and fifth, a spectral radiometer measuring the actinic flux density (see Figure 2.2).

The top platform is equipped with instruments for the measurements of the HO_x radical concentration (OH and HO_2), utilizing Laser Induced Fluorescence (LIF) as well as the OH lifetime instrument. This setup is ideal for measurements of radicals because they are not influenced by the hull of the Zeppelin. This would be the case if the radical instruments were installed in the gondola. Next to the radical measurements a spectral radiometer is also installed in the top platform measuring the actinic flux density.

2.2.2 Cabin layout Photochemistry (CL-8)

In addition to the permanently mounted instruments, three additional instruments are installed in the photochemistry layout (see Figure 2.3). First, the HGC rack measuring VOCs by GC-MSD, second, the LOPAP instrument analyzing nitrous acid (HONO) by long path absorption (Häseler et al., 2009), and third, the FFL instrument analyzing formaldehyde by the LIF technique (Hottle et al., 2009).

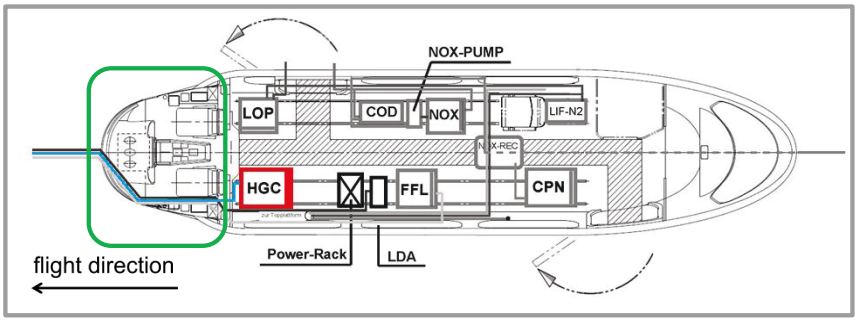

Figure 2.3: Outline of the Gondola for CL-8, with cockpit (green) and the HGC marked in red with the sampling line (blue) leading to the nose boom.

2.2.3 Cabin layout SOA (CL-5)

The SOA package is equipped besides the permanent equipment with three additional instruments. First, the HGC rack measuring VOCs , second, the AMS rack, this Aerosol Mass Spectrometer analyzes the chemical composition of aerosols (Rubach, 2013), and third, the PSI rack to measure the hygroscopicity of aerosols and to analyze soot with an aethalometer (Hansen et al., 1984).

2.2.4 Cabin layout Nucleation (CL-9)

The nucleation layout is equipped without the HGC, but with two additional instruments to the permanent equipment. First, the NAIS instrument, a spectrometer for the measurement of cluster ion and nanometer aerosol size distributions (Mirme and Mirme, 2011), and second, the API-TOF analyzing naturally charged ions and clusters (Junninen et al., 2010) in addition to the permanent instrumentation.

An overview of the instruments on board the Zeppelin with affiliations and responsible persons is given in Table 2.1 as within this dissertation only the VOC data was measured (excluding HCHO) by the HGC. All other used data were taken from the instruments listed below.

Table 2.1: Overview of the instrumentation with the measured species, responsible persons and the affiliation.

CL	**Rack**	**Name**	**Measured Species**	**Responsible Person**	**Affiliation**
Permanent	NO_X	Nitrogen oxides	NO, NO_2, O_3	F. Rohrer, K. Lu	FZJ
			Actinic Flux	B. Bohn, I. Lohse	FZJ
	COD	CO Detector	CO	F. Rohrer, K. Lu	FZJ
	CPN	Condensation Particle Counter new	Particle Size Distribution	R. Tillmann	FZJ
	LDA	Luftschiff Daten Aufzeichnung	Meteorological parameters	F. Holland (FZJ)	ZLT, FZJ
	Top Platform		OH, HO_2	M. Bachner, S. Broch, H. Fuchs, S. Gomm, F. Holland, A. Hofzumahaus	FZJ
			OH Lifetime		
			Actinic Flux	B. Bohn, I. Lohse	
CL-8	HGC	HALO-GC	VOCs	J. Jäger, R. Wegener	FZJ
	LOPAP	LOng-Path-Absorption Photometer	HONO	R. Häseler, L. Xi	FZJ
	FFL	Formaldehyde via Fiber Laser induced fluorescence	Formaldehyde	J. Kaiser, F. Keutsch, G. Wolfe	UWI
CL-5	HGC	HALO-GC	VOCs	J. Jäger, R. Wegener	FZJ
	AMS	Aerosol Mass Spectrometer	Chemical composition of aerosols	F. Rubach	FZJ
	PSI	Paul Scherer Institut	Hygroscopicity of aerosols and soot	B. Rosati	PSI

CL	Rack	Name	Measured Species	Responsible Person	Affiliation
CL-9	NAIS	Neutral cluster and Air Ion Spectrometer	Cluster ion and nanometer aerosol size distributions	S. Mirme, H. Manninen	EST, UHEL
	API-TOF	Atmospheric Pressure Inlet Time of Flight Mass Spectrometer	naturally charged ions and clusters	M. Ehn	UHEL

FZJ = Forschungszentrum Jülich, IEK-8, Germany, ZLT = Zeppelin Luftschifftechnik, Friedrichshafen, Germany, UWI = University of Wisconsin–Madison, USA, PSI = Paul Scherrer Institute, Villingen, Switzerland, UHEL = University of Helsinki, Finland, EST = University of Tartu, Estonia

Since, the focus of this dissertation is on the measurements of the VOCs and the comparison of the results to the measured OH reactivity, the functionality the OH lifetime instrument and the HGC will be described in further detail in the following.

2.3 Measurement of the total OH reactivity

The total OH reactivity is measured directly as the reciprocal chemical OH lifetime. Artificial OH is produced in an 80 cm long flow tube with an inner diameter of 40 mm by a frequency quadrupled Nd:YAG laser (see Figure 2.4). The flow tube is flushed with a laminar ambient air flow with a resulting velocity of 20 L/min. The pulsed laser beam passes longitudinally through the flow tube and photolyses ambient ozone which leads to the production of OH radicals. The produced OH reacts with reactive components of the ambient air (CO, NO_x, VOCs etc.) and the OH is consumed (Lou et al., 2010). The OH decay is monitored in the OH detection cell by laser induced fluorescence (LIF) (Holland et al., 2003). Air from the flow tube is continuously sampled through a nozzle into an OH detection cell. The OH radicals in

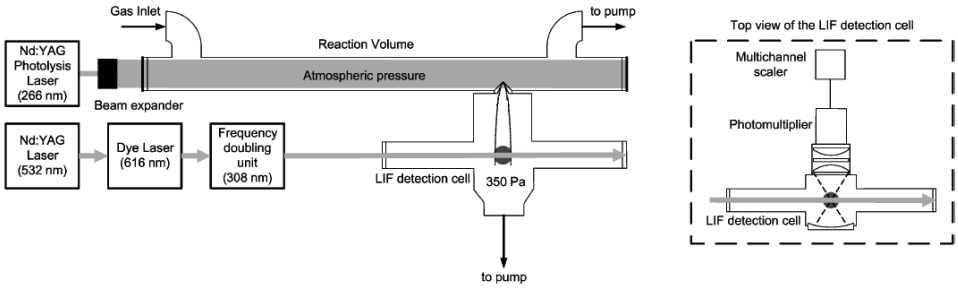

Figure 2.4: Setup of the instrument measuring the total OH reactivity with the photolysis laser (Nd:Yag) which produces the OH radical in the flow tube flushed with ambient air and the OH detection cell operated with the LIF technique. (Adapted from Nehr et al., 2011)

the emerging gas beam are excited by a pulsed laser beam with a wavelength of 308 nm. Subsequently, the re-emitted fluorescence photons are detected by a multi-channel plate (MCP). The OH reactivity of the sampled air in the flow tube is then calculated from the measured OH decay which follows a pseudo-first order kinetic. The signal is stored in time bins of 1 ms width over a time period of 1 s. The signal is averaged, so that the OH lifetime instrument has a time resolution between 1-3 min.

The uncertainty of the measured total OH reactivity depends on the precision and accuracy of the OH lifetime instrument. The precision is determined by the fit error of the OH decays and is between 4-10 % (1 σ). Zero decays are caused by the wall losses of OH as observed in clean synthetic air (99.9999 %, Linde Gas, München, Germany) enriched with water vapor (1 %) and ozone (50 ppb). For this PEGASOS campaign the zero decay was estimated to be (1.3 ± 0.25) s^{-1} and was subtracted from the ambient measurements. The accuracy of this measurement technique was tested and estimated to be lower than 10 % (Hofzumahaus et al., 2009a; Lou et al., 2010). Thus, the resulting accuracy has a value of (± 0.25 s^{-1} + 0.1 x k_{OH}) (Gomm, manuscript in preparation). The linearity of the system is good until a value of 60 s^{-1}.

2.4 Set-up of the HGC instrument

2.4.1 General overview of the instrument

The HGC instrument measures VOCs and is part of the CL-8 and CL-5. It is build up out of five core components (see Figure 2.5), a gas chromatograph (GC) with a mass spectrometer (1), the electronic enclosure (2), the cooling assembly (3) as well as two gas cylinders (4) filled with helium and gas standard installed on the top of the rack. For the system control and data acquisition the instrument is equipped with a laptop (5).

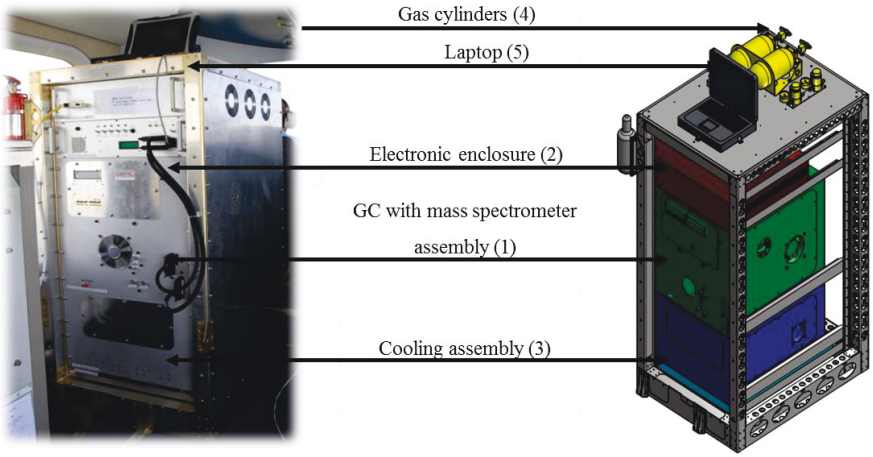

Figure 2.5: The instrument on board the Zeppelin NT consisting out of the GC with the mass spectrometer unit, the electronic enclosure, the cooling assembly, the gas cylinders and the laptop.

The following chapter firstly outlines the general functionality of the instrument to illustrate the measuring principle and secondly, describes the construction and implementation of parts one to five (above) to measure VOCs on board the Zeppelin NT.

2.4.2 General functionality of the HGC instrument

The HGC consists of a GC-MS system with an upstream preconcentration unit as outlined in Chapter 1.3.3. To increase the sample throughput and thus the time resolution, the instrument is unique with its tandem set-up. It consists of two adsorption units and two GC units (see Figure 2.6). Both GC columns are connected to the same mass spectrometer. The adsorption units and the chromatographic units are operated in an interlaced manner. Therefore, the mass spectrometer is only detecting the analytes of one channel at a time.

The measurement procedure can be subdivided into four phases: adsorption, desorption, separation and detection. In the following, these four phases will be explained for Channel 1. Channel 2 is operated identically, but in an interlaced manner.

In phase 1 the ambient air is collected at the inlet (see Figure 2.6) and the containing particles are segregated at the upstream filter. VOCs measurements are negatively biased by ozone (Ciccioli et al., 1986) and humidity (Helmig and Vierling, 1995) in the sampled air. An ozone destructor and a water trap (WT) are introduced to deplete the ozone and segregate the humidity. The containing VOCs are then pre-concentrated on a coal-based adsorbents inside the sample trap (ST).

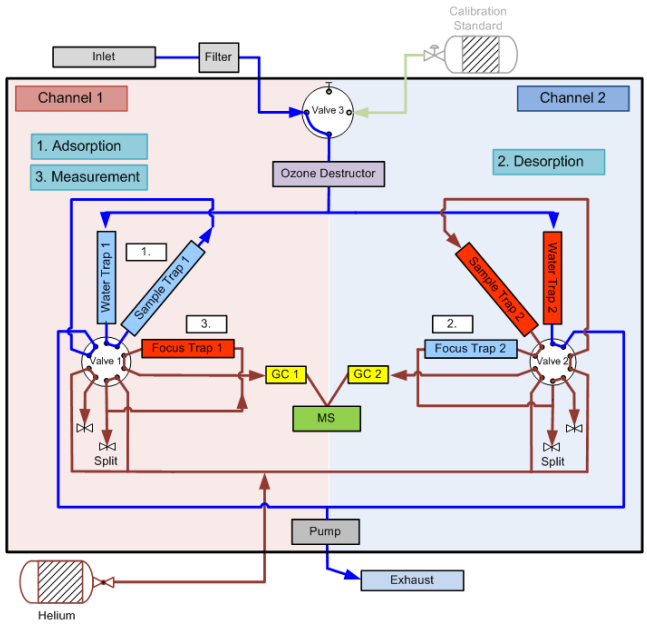

Figure 2.6: Operation of the instrument with the two identical channels operating in an interlaced manner towards one mass spectrometer (MSD). The measurement is divided into three phases, the adsorption (1.) where the sample trap enriches the VOC concentration, the desorption (2.) where the sample is transferred onto a focus trap for focusing before it is transferred onto the GC column for the measurement (3.) and detected with the mass spectrometer. All ambient airflows are color-coded in blue and the helium flows in brown.

The valve is then switched for desorption (phase 2). Subsequently, the ST is heated and the analytes are transferred by the purge gas onto a focus trap (FT). The FT is used for re-focusing before the analytes are injected onto the GC column. To accelerate the desorption process the split flow is enlarged and the flow rate over the trap can be increased. There is an overflow behind the FT that can be regulated by a mass flow controller. At this time the WT is heated and flushed with a part of the sampling flow to evaporate the collected water.

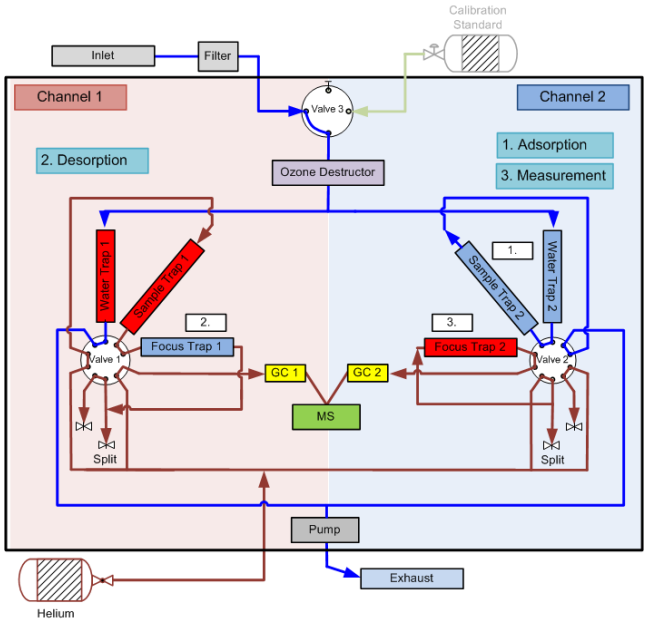

Figure 2.7: The two channels after the switching of the valves, channel 1 is in the desorption phase and channel 2 in the adsorption and measurement phase.

The valve is subsequently switched again for the measurement (phase 3) and the FT heats up (see Figure 2.7). The collected sample is then injected into the GC column for separation of the analytes. The separation is based on the chemical and physical properties of the analytes (McNair and Miller, 2009). Now, the separated analytes can be detected by the mass spectrometer (phase 4).

The method of the instrument is designed in a way that every 3 minutes both, valve 1 and 2 are switched simultaneously and the measuring mode changes. This leads to a time resolution of 3 minutes, but every sample needs a total of 9 minutes from the sampling until the detection. Valve 3 is only switched for the purpose of calibration as explained in Chapter 2.6.1.

2.4.3 Implementation of the HGC on the Zeppelin NT

The conception planning of the GC-MS system to measure VOCs on board the new scientific DLR aircraft HALO (High Altitude LOng range) began in 2005 by Dr. R. Wegener from the Forschungszentrum, Jülich, Germany together with D. Bremer, B. Rose and W. Waltke from GERSTEL GmbH & Co.KG, Mühlheim, Germany, giving it its name HGC (HALO Gas Chromatograph). The instrument was then built by GERSTEL GmbH & Co.KG in the following years and delivered in 2008 to the Forschungszentrum, Jülich. There, the instrument was modified by A. K. Wenk in order to implement it on the mobile laboratory van (Vito). Within this work, the existing GC-MS system in the HALO setup as shown in Figure 2.8 on the left was modified to meet the Zeppelin requirements, to broaden the substance spectra and to enhance the measurement stability as elaborated in the following.

First, to implement the instrument on board the Zeppelin, the previously utilized HALO rack was changed to the ZLT - rack with the dimensions of 1266.65 (25 HU) x 604.00 x 784 mm (see Figure 2.8). Second, it was necessary to reduce the weight of the instrument to meet the weight specifications of the Zeppelin. The new Zeppelin conform instrument weight was reduced by 17 kg from 145 kg to 128 kg. Third, the entire concept of the instrument was changed to an entirely modular system. Due to flight regulations every part of the instrument needs to be mounted to resist a force of 3G- in every direction. To simplify the calculation of the statics, the concept of 19'' crash containments was introduced. They were designed in order to hold up every single part of the instrument and were themselves attached to the rack to resist a force of 3G-force in every direction. Hence, the originally stacked HALO design, with single parts mounted separately onto two different ground plates, was altered into a Zeppelin specific design consisting of disjoint crash containments (see Figure 2.8). This new, separate design enables the repair of potential malfunctions at relative ease. Every enclosure can be separately removed and reinstalled, rather disassembling the entire instrument to access to bottom parts of the instrument.

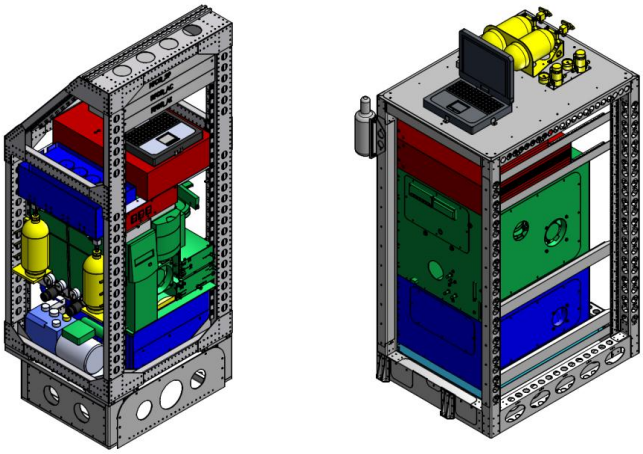

Figure 2.8: HGC HALO airplane setup (left side) and the setup for the Zeppelin PEGASOS campaign (right side) with the electronics (red), the mass spectrometer assembly (green), the cooling unit (blue), the gas cylinders (yellow) and the impounding basin in (turquois).

Finally, the gas flow of the system was changed to increase the number of analyzed substances. This is further elaborated in Chapter 2.4.3.4. Additionally, the electronic unit was modified resulting in a more stable operation of the instrument. All 3D Inventor illustrations in the following were taken either from the original Gerstel Model or the modified Model for the Zeppelin instrument by Dr. R. Wegener and J. Jäger.

2.4.3.1 Reconstruction of the GC- and mass spectrometer assembly

The GC- and mass spectrometer assembly is the center of the instrument as all of the above elaborated processes are taking place in this enclosure. With a total weight of 46 kg it is also the heaviest part of the instrument.

Figure 2.9 shows the system consisting of two custom-made adsorption units manufactured by GERSTEL GmbH & Co.KG, Mühlheim, Germany, two MACH GC columns (DB624, 20 m x 0.18 mm x 1.9 µm, Agilent, Santa Clara, USA) and one mass spectrometer detector (MSD 5975C, Agilent, Santa Clara, USA). For the depletion of ambient ozone in the sample flow a custom-made ozone destructor is added to the assembly.

The mass spectrometer unit consists of an aluminum body housing the ion source and the quadrupol, the electronic box and the turbo pump. To produce the fore vacuum for the turbo pump and to sample ambient air, two membrane pumps are introduced into the assembly.

Furthermore, the GC- and mass spectrometer assembly is equipped with two pneumatic assemblies that control the sampling flow as well as helium purge flow.

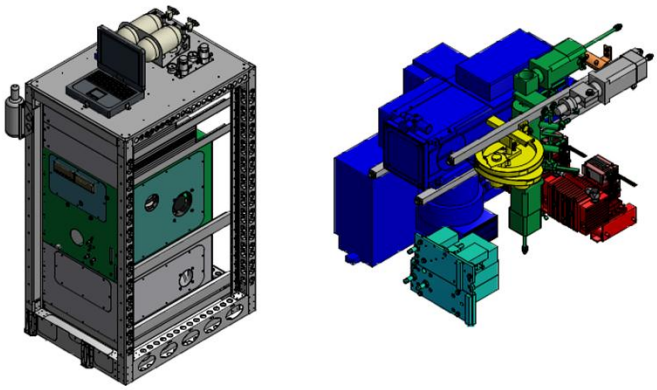

Figure 2.9: Outside view of the GC- and mass spectrometer assembly (left) and on the right a detailed view of the adsorption unit (green), the GC columns (yellow) and the mass spectrometer unit (blue), the pumps (red), pneumatic assemblies (light blue) and the ozone destructor (orange).

2.4.3.2 The ozone destructor of the HGC

Large concentrations of ambient ozone falsify the VOCs measurements during the sampling process as it reacts with some VOCs. The ambient ozone can be thermally depleted by heating the sampling flow (Hellén et al., 2012). The ozone destructor as shown in Figure 2.10 consists of an aluminum body that houses a capillary (Silcosteel® 42.5 cm x 0.25 mm (ID), Restek, Bellefonte, USA). The aluminum body is heated to 120 °C by a heating cartridge (hotrod® 6.5x30 50 W 24 A, Hotset, Lüdenscheid, Germany) which is controlled by a temperature sensor. The aluminum body is insulated with a knitted fabric out of stainless steel and Kevlar® fiber (50 % each). The ozone destructor is attached to the back panel of the enclosure by a thermally decoupled fixing bracket. The decoupling is realized by a Kapton® polyimide film (3M, St. Paul/Minnesota, USA) that is introduced onto the contact surfaces.

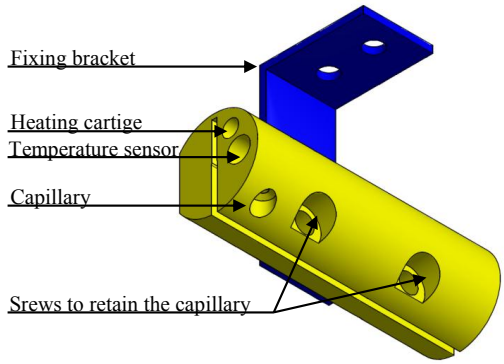

Figure 2.10: The Ozone destructor including the aluminum body (yellow), with the slit where the capillary is inserted and the holes for the heating cartridge and the temperature sensor as well as the thermally decupled fixing bracket (blue).

2.4.3.3 The adsorption unit of the HGC

The center of the adsorption unit (as shown in Figure 2.11) comprises of two valves (EDX3C10UWE, VICI, Houston, Texas, USA) one for each channel, with a valcon E medium temperature rotor. Each valve is equipped with a microelectric actuator for operation. They are connected by an aluminum body that is heated to 220 °C to ensure that the rotor material is lubricant. Previously, valcon T rotors with sulfinert coating were deployed, but at temperatures above 250 °C the rotor adhered to the body of the valve. By exchanging the rotor material, this risk could be extenuated. The barbell shaped unit consisting of the two valves and the actuators could not fit the height of unit. To reduce the height a right angle drive (RAD, VICI, Houston, Texas, USA) is introduced between the valve and the actuator in channel 1.

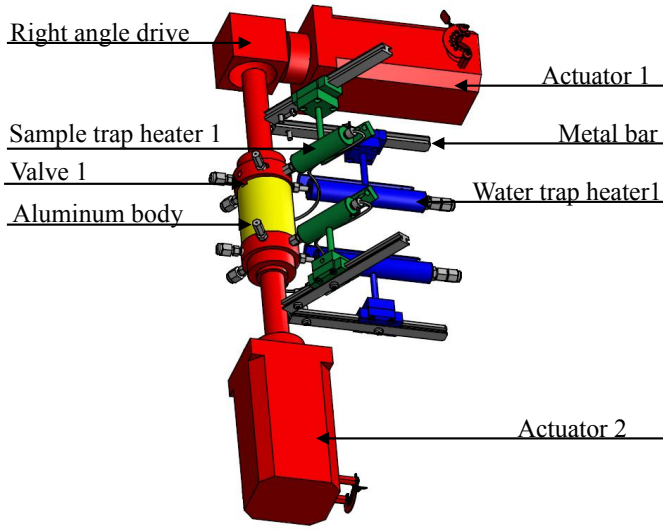

Figure 2.11: The adsorption unit with the two valves (red) connected to an actuator. The valves are connected by a heated aluminum block (yellow), the water trap heater (blue) is mounted adjacent to the sample trap heater (green) in both channels. The setup in channel 1 is the upper part and channel 2 the lower part.

The adjacent ports of the valves are connected to one water trap heater (WTH) and one sample trap heater (STH) for each channel. Both trap heaters are identically designed (GERSTEL GmbH & Co.KG, Mühlheim, Germany) and can be heated ohmically and cooled rapidly by a cooled ethanol/water (50/50 v/v) mixture coming from the cooling assembly which is elaborated in Chapter 5.3.3 (see Figure 2.12).

The trap heaters are mounted with a miniature guiding carriage onto a metal bar and anchored with a screw. The only difference between the trap heaters is their lengths. The longer WTH has a length of 7.8 cm and the STH one of 4.4 mm.

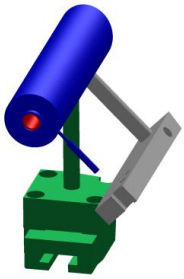

Figure 2.12: The design of the sample- and water- trap heater with the central heating (red), the outside hollow casing for cooling (blue) and the miniature guiding carriage (green) for attaching the trap heater. The gray part is securing the capillaries for the cooling and the cables for the heating.

The hollow inside of the WTH is lined with a Silcosteel® coated tube where the humidity of the ambient air is segregated. It can be removed through heating them after the sampling process. The STH houses a glasliner (60 mm x 3 mm (AD), 1.8 mm (ID), GERSTEL GmbH & Co.KG, Mühlheim, Germany) filled with carbon adsorbents (see Chapter 2.5.4).

The focus trap heater (FTH) (52 x 2.3 x 10 mm GERSTEL GmbH & Co.KG, Mühlheim, Germany) is mounted adjacent to the STH (see Figure 2.13). The FTH can be heated rapidly to desorb the containing analytes. In contrast to the WTH and STH the FTH has no active cooling but due to its low mass this is not a disadvantage. Inside the FTH there is a Prosteel® capillary (30 cm x 0.70 mm (AD) 0.53 mm (ID), GERSTEL GmbH & Co.KG, Mühlheim, Germany) filled with a carbon based adsorbents.

Figure 2.13: The focus trap heater with the aluminum handle (gray) where the cables are attached and the inserted capillary (brown).

2.4.3.4 Improvement of the gas flow for the new HGC

The gas flow of the instrument is improved from the previous airplane setup to a setup which enables the analysis of a broader substance spectrum. Especially, substances with a high boiling point like limonene, benzaldehyde, and indane can now be analyzed. This new setup manifests itself through modifications in the desorption process of the focus trap as shown in Figure 2.14. In the previous setup the focus trap was adsorbed and desorbed in the same direction which led to substantial losses of substances with a high boiling point, as they had to pass all the way through the adsorbent to reach the column. This was compensated by utilizing a weaker adsorbent. Therefore, the substances with a low boiling point, like acetaldehyde and methanol, were not retained and therefore lost.

The new setup is optimized by reversing the direction in the gas flow for the desorption process of the focus trap, leading to 16 new substances that can now be analyzed. This is achieved by exchanging the Valco-6-port-valve (C6UWT) to a 10-port-valve (C10UWE). In the previous 6-port-valve cycle, the focus trap is positioned directly in front of the GC column and all the analytes have to pass through the entire trap (see Figure 2.14). With the 10-port system a new phase has been added and the sample is conveyed from the ST onto the FT in the one direction. After switching the valve to the measuring phase the FT is desorbed in the opposite direction onto the GC column.

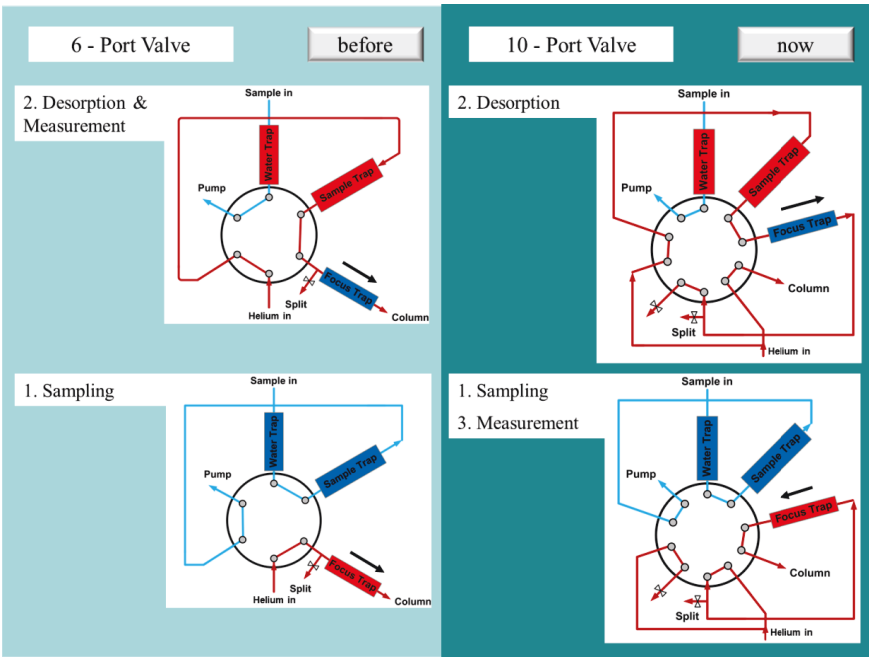

Figure 2.14: The gas flow of the instrument in the previous (6-port-valve) and present (10-port-valve) setup encompassing the sampling, desorption and measurement phase.

2.4.3.5 The GC columns of the HGC

The HGC utilizes Modular Accelerated Column Heater (MACH) GC columns that are characterized by a low thermal mass. The heating wire and the temperature sensor are wrapped around the column and are well isolated. Hence, the column can be heated and cooled very fast. The columns are separately housed in a cage (see Figure 2.15). Each cage has a ventilator attached that conveys cold air from the cooling assembly to cool the column independently after each analysis.

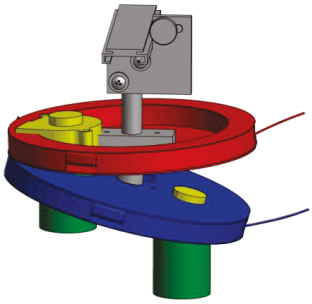

Figure 2.15: The GC columns are housed in two GC column cages channel 1 in red and channel 2 in blue. Both cages are equipped with ventilators (yellow) and tubing (green) for the conveyance of cooled air from the cooling assembly.

2.4.3.6 The mass spectrometer of the HGC

The Agilent mass spectrometer comprises an aluminum analyzer chamber that houses the ion source and the quadrupol with an attached turbo pump (see Figure 2.16). For flight regulations a turbo pump is considered to be a major risk, as it consists of sets of small blades that radiate from the central shaft. At normal operation the shaft spins at 90,000 rpm (Agilent, 10.04 2013). Because of the momentum it can cause excessive damage in case of a malfunction. Consequently, it is important to secure the attachment of the turbo pump to the analyzer chamber.

The Agilent 5975C mass spectrometer is delivered with four screws and claw grips clamping the turbo pump (TMH 262, Pfeiffer Vacuum GmbH, Asslar, Germany) to the aluminum body of the analyzer chamber. For stationary purposes of the instrument this is sufficient, but as the instrument is not operated stationary, four additionally holes needed to be introduced into the aluminum body as proposed by the manufacturer Pfeiffer (Pfeiffer, 10.04 2013). The aluminum body of the quadrupol is attached to the enclosure by two traversal aluminum bars. Consequently, the new holes could not be arranged symmetrically around the opening, so for extra security reasons six holes were introduced as seen in Figure 2.16.

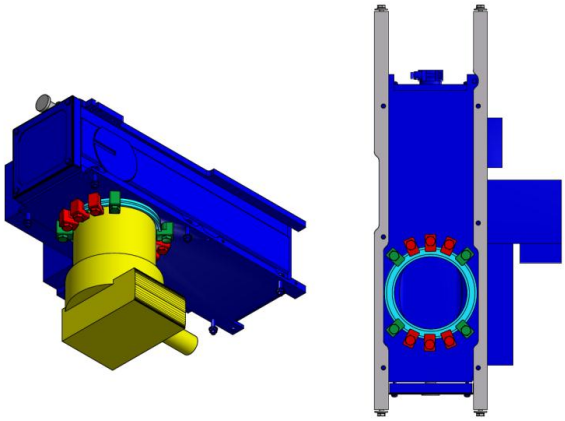

Figure 2.16: Quadrupol with the turbo pump (yellow) attached to the body of the analyzer chamber (blue) with 10 screws and brackets, four of the holes are original (green) and six are new (red). The two traversal aluminum bars are indicated in gray.

The fastening of the turbo pump is not only dependent on the amount of screws but also on the strength of the aluminum body. The chemical analysis of the body shows that the material of the quadrupol is Aluminum EN AW 6060 T 66. The tensile strength of this material is 215 N/mm^2 which is sufficient for attaching the turbo pump.

To secure the screws in the aluminum body inserts (HELICOIL®, Böllhoff GmbH & Co. KG, Bielefeld, Germany) are introduced. For this reason the drilling depth needs to be at least 12.5 mm. The material of the aluminum body of the MSD 5975C only has a material thickness of 13 mm, which made the drilling impossible. However, the material of the predecessor model, the 5975B, has a thickness of 14 mm which is sufficient for the holes.

Subsequently, the body of the 5975B is prepared with six additionally holes and all the components of the 5975C are installed without any further complications. The screws fastening the turbo pump are attached clockwise with a tightening torque in three steps (3, 10 and 16±1 Nm) according to the Pfeiffer manual.

2.4.3.7 The pump system of the HGC

The vacuum inside the mass spectrometer (MSD) can only be maintained by the turbo pump in addition to a foreline pump. In the original setup the MSD is equipped with a rotary vane pump (DUO 2.5, Pfeiffer Vacuum GmbH, Asslar, Germany). The main disadvantages of the standard MSD foreline pump are its weight of 11.2 kg and the possible leakage of oil. In addition to a foreline pump, an additional pump to sample the ambient air is needed. In order to save weight, two membrane pumps (N813.3 ANDCB, KNF Neuberger GmbH, Freiburg, Germany), with a weight of 2.3 kg each, are installed. They are arranged to facilitate the fore vacuum and enable the sampling flow (see Figure 2.17). The sampling flow is controlled by a valve that is introduced before the sampling unit.

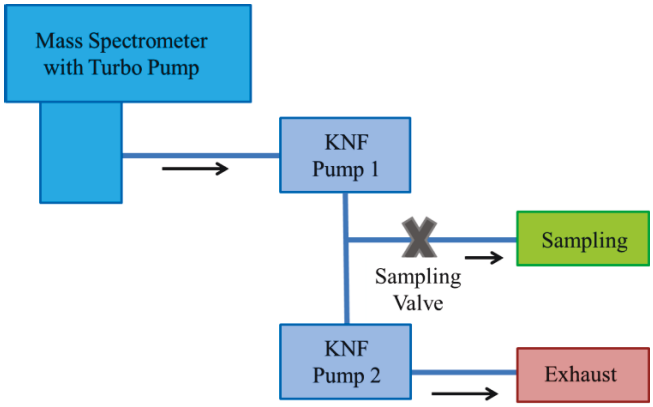

Figure 2.17: Assembly of the turbo pump and the two KNF pumps in order to provide vacuum for the MSD and for the sampling flow.

2.4.4 The cooling assembly of the HGC

The cooling assembly is equipped with two compressors (CU-85, Dometic WAECO International, Louisville, USA) one lamellar evaporator (VD-03, Dometic WAECO International, Louisville, USA), and one custom made tube evaporator (GERSTEL GmbH & Co.KG, Mühlheim, Germany). One compressor forms a closed cycle with the lamellar evaporator and the other connects to the tube evaporator (see Figure 2.18 and Figure 2.19).

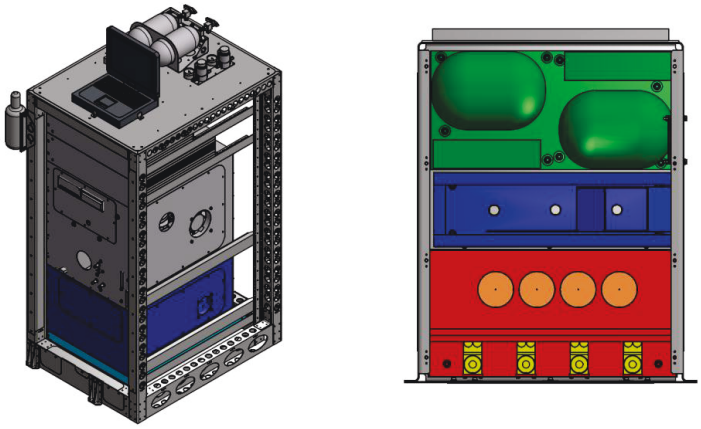

Figure 2.18 The cooling assembly is situated in the lower part of the instrument (in blue; illustration on the left). It houses the two compressors (green), the lamellar evaporator producing cold air to cool the GC columns (blue) and the tube evaporator (red) with the four reservoirs (orange) and the liquid pumps (yellow) to cool the traps subsequent to the sampling process. The impounding basin (turquois) is situated underneath the cooling assembly.

Both compressors cool the containing refrigerant R134A (1,1,1,2-Tetrafluorethan). In the first case this is transported to the lamellar evaporator (see Figure 2.19). The lamellar evaporator cooles air which is then transported to the mass spectrometer assembly by the fans in order to cool the GC columns after each analysis separately. The second compressor is connected to the tube evaporator that cools the cooling liquid (Ethanol/Water 50 /50 v/v) to -10 °C. This cold liquid is pumped from the four independent reservoirs, by four liquid pumps, (NF 130, KNF Neuberger GmbH, Freiburg, Germany) through small capillaries to the mass

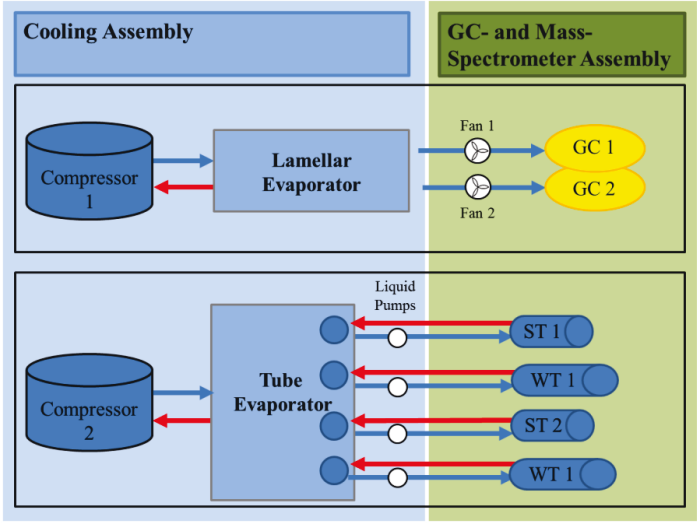

Figure 2.19: The connection of the compressor 1 to the lamellar evaporator supplying the GC columns with cold air through fans. And compressor 2 connected to the tube evaporator providing cold fluid to cool the sample (ST) as well as the water traps (WT), one for each channel.

spectrometer assembly, cooling the water- and sample traps after the desorption process. Quick Connectors (Swagelok, Solon, USA) are introduced to separate the capillaries if the enclosures are removed from the rack. To keep the thermal loss as low as possible the tubing for the cooled air as well as the small capillaries are insulated with the unburnable insulation material (Jehier, Chemillé, France).

Underneath the cooling assembly an impounding basin is installed to hold back the condensed water of the lamellar evaporator as well as possible leakage of the cooling fluids.

2.4.5 The electronic enclosure of the HGC

The electronic enclosure of the HGC is situated in the upper part of the instrument (see Figure 2.20) and was originally designed for 230 VAC. However, to operate most of the components of the HGC, it is necessary to transform the 230 VAC to 28 VDC in the electronic enclosure. As the generator of the Zeppelin only provides 28 VDC it is more efficient to redesign the electronic enclosure to operate at 28 VDC. This saves 4 kg of weight.

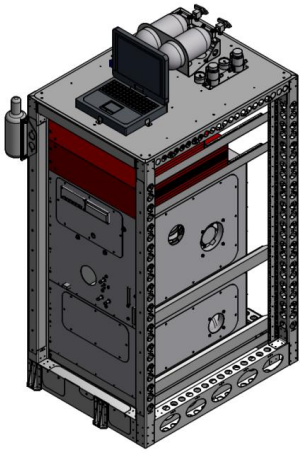

Figure 2.20: The HGC rack with the converter enclosure (red) above the electronic enclosure (dark red).

The commercially available mass spectrometer and the laptop (CF-19GAXAE, Panasonic, Kadoma, Japan) are operated at 230 VAC, so that a converter is integrated to provide 230 VAC to the instrument. It is situated in the converter enclosure.

2.4.6 Gas cylinder unit

The gas cylinder unit consists of a bend aluminum plate that is mounted on the top plate of the rack (see Figure 2.21). Two gas cylinders (ALT 838, SCI Worthington Cylinder Corporation, Columbus, USA) can be inserted through the large hole and secured with a buckle on the other side. The pressure regulators are mounted to the right of the gas cylinders. One gas cylinder is filled with the carrier gas helium and the other with a calibration standard.

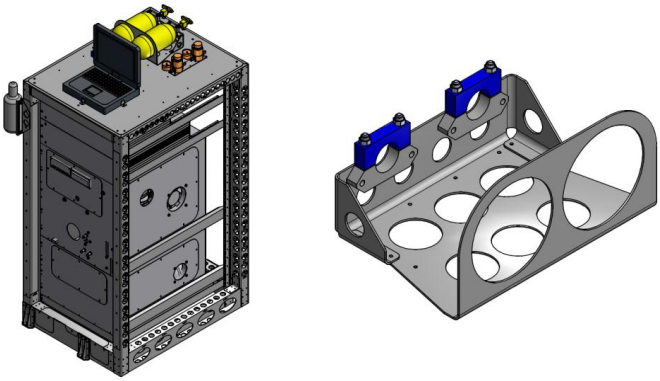

Figure 2.21: The gas cylinder unit is mounted on the rack (right) with the pressure regulators (orange) containing the two gas cylinders (yellow). Close up of the gas cylinder bracket with the buckles (blue) to secure the cylinders.

2.5 Measuring method and the characterization of the HGC

In the following details of the measuring method that has been utilized to measure VOCs on board the Zeppelin NT during the PEGASOS campaign 2012 are outlined including the sampling setup, the influence of humidity and ozone on the analysis of VOCs, the adsorption parameters of the HGC as well as the subsequent separation by the GC column, detection with mass spectrometer and the data analysis.

2.5.1 Sampling setup

The inlet for the ambient air is mounted at the nose boom of the Zeppelin next to the inlet for the FFL instrument and the humidity, temperature and pressure sensors of the LDA rack which is mounted in the gondola (see Figure 2.22). The PFA inlet line has a length of 5 m (6 mm (AD), 4 mm (ID), Bohlender GmbH, Grünsfeld, Germany) and enters the Zeppelin in the front underneath the pilot seat. The inlet line is equipped with an omnipore PTFE filter (Ø 47 mm, 0.45 µm, Merck KGaA, Darmstadt, Germany) to avoid congestion in the tubing caused by aerosols or dust particles in the ambient air. The filter was replaced weekly.

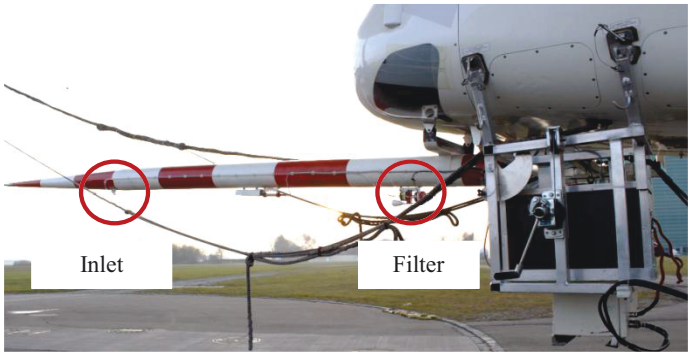

Figure 2.22: The Zeppelin nose boom with the inlet line and the filter bracket with the 0.45 µm filter.

The influence of filters on the VOC measurements was investigated in a laboratory experiment prior the campaign. Measurements of a VOC gas standard were made with and without filters. In this experiment two different filters with a pore size of 5 and 0.45 µm were tested.

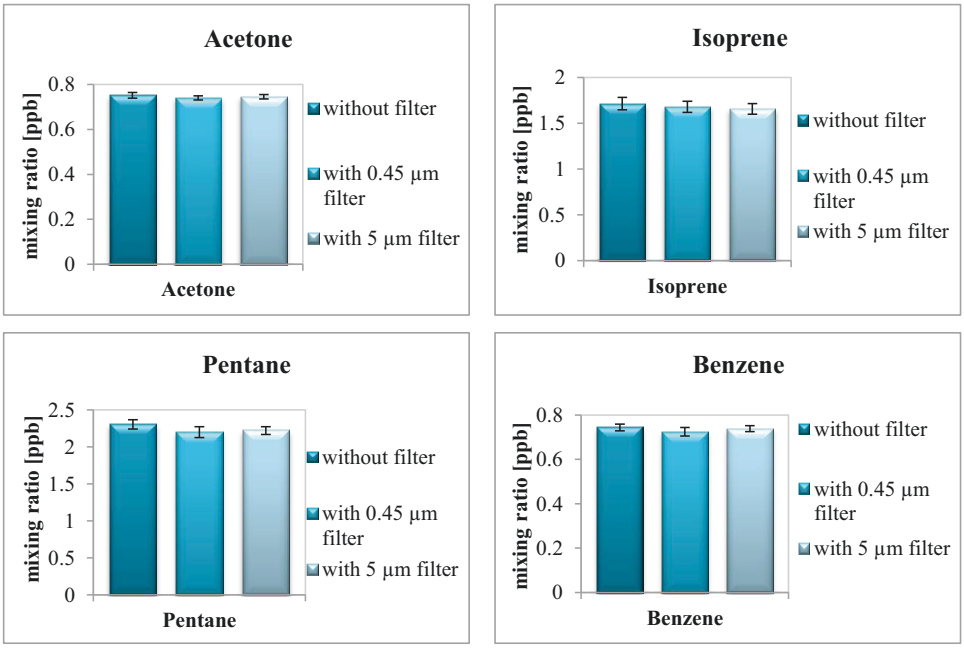

Figure 2.23: Measurements testing the implementation of a particle filter in the sampling line.

When comparing the three experimental set-ups (1) 0.45 µm filter, (2) 5 µm filter (3) no filter, the results show no significant differential effects of the filter conditions on the concentration of the VOC. As examples, the findings for acetone, isoprene, pentane and benzene are shown in Figure 2.23. The calculated relative standard deviation between the three different measurement setups is below 5 % for all measures substances. Hence, it can be inferred that the filter does not have a negative effect onto the VOC measurements.

2.4.3 Sampling flow

The HGC samples 100 mL of ambient air per minute. After passing through the ozone destructor the flow is split between the two channels. 50 mL/min pass through the sample trap on channel 1 (see Figure 2.6) and the other 50 mL/min are utilized to flush the water trap of channel 2 in the desorption process. This overflow also reduces the residence time of the analytes in the sampling line to 36 seconds. Consequently, in the sampling period of 3 minute a total of 150 mL of ambient air is sampled onto the sample trap. At higher altitudes the ambient pressure is lower compared to laboratory experiments on the ground. Therefore, it needs to be ensured that the sampling flow rate of 50 mL/min can be also realized at lower ambient pressures. This was tested in a laboratory pre-experiment. In 6 sequential steps, the upstream pressure was continuously lowered from 1013 to 521 mbar. During this process the absorption volume flow rate was constantly monitored.

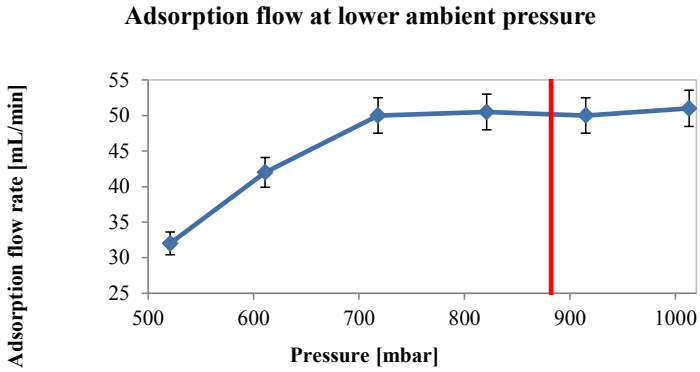

Figure 2.27: The dependency of the sampling flow of the upstream pressure (blue). The campaign minimum of 882 mbar is indicated in red.

The pre-study shows that the sampling flow remains constant at 50 ml/min for upstream pressures higher than 700 mbar (see Figure 2.27). Only at an upstream pressure of 611 mbar the sampling flow lowers to 42 mL/min. This suffices for the Zeppelin measurements since the lowest pressure encountered during the campaign is 882 mbar.

2.5.2 Influence of ozone

High ambient ozone concentrations can lead to the formation of artifacts by the oxidation of VOCs during the sampling process (Ciccioli et al., 1986). Therefore, an ozone destructor is introduced. To test the efficiency of the ozone destructor, laboratory experiments with different ozone concentrations were conducted. Measurements were carried out with a starting ozone concentration of 88 ppb and 218 ppb of ozone in synthetic air. Notably, this lower bound value of 88 ppb was higher than the mean concentration of 64 ppb measured during the PEGASOS campaign. It was chosen to be comparable to previous observations by Altshuller

and Lefohn (1996). The chosen upper bound concentration of 218 ppb was well above (45%) the maximum concentration observed during the campaign.

The experiments were conducted in a two-step procedure. First, the ozone was produced utilizing a Pen-Ray® mercury lamp (99-0055-01, UVP, Upland, USA) in a flow of synthetic air. The ozone concentration of 88 ppb for the first experiment and 218 ppb for the second experiment were determined by an O_3 Analyzer (U.V. Photometric O_3 Analyzer, Thermo Environmental Instruments Inc., Waltham, USA). At this point the ozone destructor was held constant at 25 °C. Subsequently, the ozone destructor was heated from 25 °C to 120 °C and the ozone concentrations were re-measured. Due to the experimental setup a flow rate of 644 mL through the ozone destructor had to be applied in the test experiment. This is more than a factor of 6 higher than the flow rate in the real measuring setup. Analyses between the two ozone experiments found that the initial lower bound concentration level of 88 ppb was completely depleted by the ozone destructor. For the second experiment the upper-bound concentration of ozone of 218 ppb was reduced by 76 % to 52 ppb (see Figure 2.24).

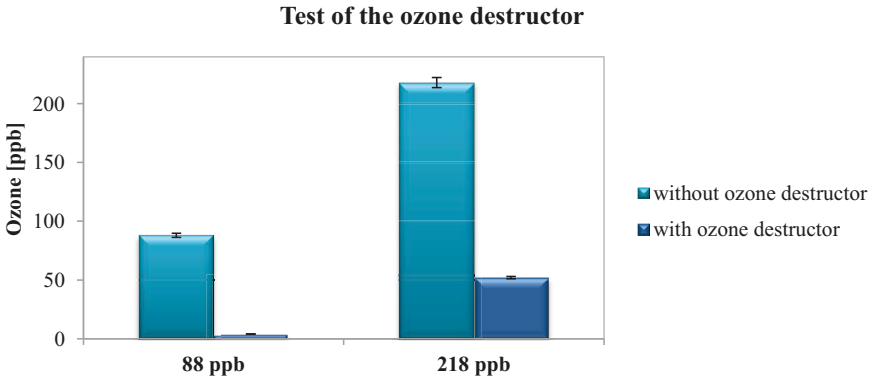

Figure 2.24: Evaluation of the ozone experiment to test the sufficiency of the ozone destructor.

The pre-test study verifies the capability of the ozone destructor to remove the ambient ozone. Throughout the PEGASOS campaign, the mean ozone concentration for the ambient ozone was 64 ppb, with no values exceeding 150 ppb.

Prior to entering the ozone destructor, the ambient air flows through the sample line. Thus, it was also necessary to analyse the effect the ozone may have on the analytes before they enter the ozone destructor. The synthetic air was enriched with two different ozone concentrations This ozone enriched air was mixed to the calibration standard in a mixing chamber. Therefore, an ozone concentration of 75 ppb and 135 ppb were reached. To determine the influence of ozone during the residence time in the sample line, the measurements with the ozone enriched synthetic air were compared to air samples without the addion of ozone.

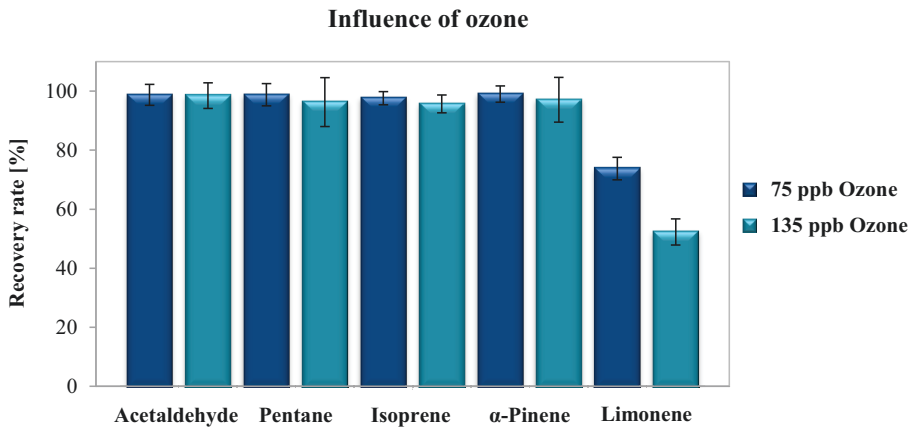

Figure 2.25: The recovery rates of the analytes after the supplement of 75 and 135 ppb of ozone compared to the measurement without ozone.

Overall, the results show that neither at 75 ppb, nor at 135 ppb the ozone significantly reduces the concentrations of the VOCs during the sampling process for all measured VOCs (shown for acetaldehyde, pentane, isoprene and α-pinene in Figure 2.25). Only for limonene there is a significant reductive effect by 27 % at 75 ppb and 48 % at 135 ppb of ozone.

The reduction of limonene during the sampling process may occur due to a number of reasons. Generally, the degradation can be explained by the reaction with ozone during the residence time in the inlet line. Based on the ozone rate constant with ozone it is to be expected that limonene is degraded about 2.5 times faster than α-pinene, but if limonene is depleated that strongly, α-pinene should also be affected by the ozone. An explanations for the astounding reduction of limonene may be heterogeneous reactions on the walls of the inlet line, inside the instrument or a conversion of terpenes inside the adsorption tube caused by active surfaces (see Chapter 2.6.4.1). Particularly, the conversion of terpenes in the instrument that leads to the redistribution of terpenes towards the more stable species as α-pinene could be observed. Therefore, it is plausible that both, α-pinene and limonene are degraded by the ozone in the inlet line, but this remains unobservable for α-pinene, as it is artificially produced from limonene in the adsorption tube.

2.5.3 Influence of humidity

In the atmosphere there is a mean total water content of 1-3 %, but this varies with height and temperature (Atkinson, 2000; Gleick, 1996). During the sampling, water can also be collected on the sample trap, where it can reduce the sampling efficiency of analytes. After desorption, high levels of humidity can also reduce the separation capacity of the GC column and reduce the sensitivity of the mass spectrometric detector (Helmig and Vierling, 1995). The effect of humidity on the measurements is especially high for substances with high volatility (Betz et

al., 1989). The incorporated water in the ambient air needs to be segregated and therefore a water trap (WT) is introduced into the sampling flow (see Chapter 2.3.2). The water trap consists of an empty Silcosteel® tube which is cooled to 10 °C to condense the ambient water. After the sampling process the water trap is heated to 120 °C to evaporate the water. In a laboratory experiment the measurements of the calibration standard with humidified and dry synthetic air were compared to test the efficiency of the WT.

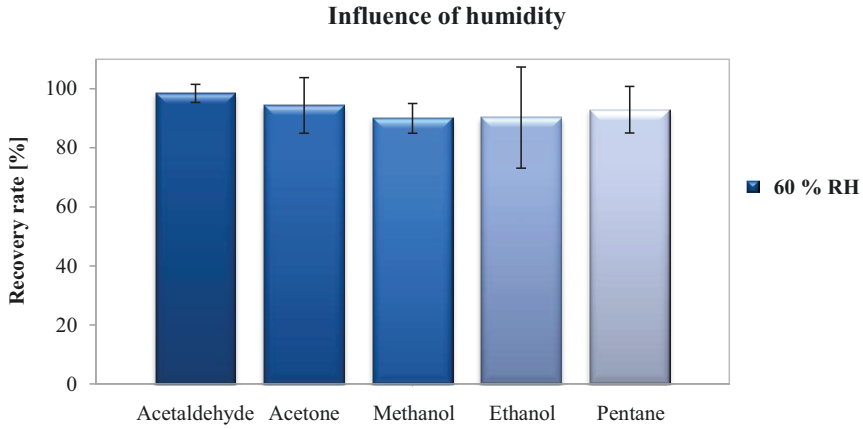

Figure 2.26: The recovery rate during measurements at 60 % relative humidity compared to measurements in dry air measurements with 60 % relative humidity (RH) compared to measurements without the supplement of humidity (dry air).

The analysis shows that the recovery rate is on average 94 % (see Figure 2.26) with a minimum loss of 1.5 % for acetaldehyde and a maximum loss of 10 % for methanol. The humidity has the largest effect on methanol, which needs to be taken into account when interpreting the data. Importantly, the chosen 60 % RH is well above the 52 % RH mean humidity during the campaign. Therefore, it is unlikely that the study's results are significantly affected by humidity during the adsorption process.

2.5.4 Carbon based adsorbents

The sample trap (ST) and the focus trap (FT) are filled with carbon based adsorbents. The glass liner of the ST (GERSTEL GmbH & Co.KG, Mühlheim, Germany) is filled with three different adsorbents (Supelco, Bellefonte, Pennsylvania, USA), also referred to as 3-bed-adsorbent. The adsorbents were arranged in the order of increasing sampling capacity, with the weakest at the trap inlet. First, Carbotrap C 20/40 mash (20.8 mg) is implemented, followed by Carbotrap B 20/40 mash (14 mg) and Carbosieve SIII (15.5 mg) (see Figure 2.27). Carbotrap C is deployed to adsorb the low volatile VOCs, Carbotrap B for the VOCs with a medium volatility and the strongest adsorbent Carbosieve for the highly volatile substances. To prevent the different adsorbents from mixing, custom made trap packing discs from Quartz Fiber Filters (AQFA04700, Ø 2 mm, Merck Millipore, Billerica, USA) are introduced. At the side of the glass tube facing the valve, the adsorbents are immobilized by an indentation in the glass liner and at the other side by a salinized glass wool stopper.

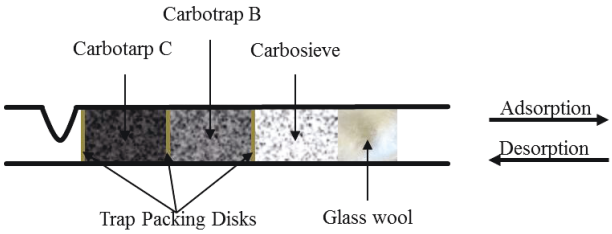

Figure 2.27: The glass liner inside the sample trap filled with a 3-bed adsorbent.

The focus trap (FT) is deployed downstream of the ST to reduce the physical dispersion of the sample, resulting in a more consistent and sharper injection and sharper chromatographic peaks (Johnson, 2011). To retain the analytes, the sulfinert capillary of the FT (30 cm long, 0.74 mm (AD), 0.53 mm (ID), GERSTEL GmbH & Co.KG, Mühlheim, Germany) is filled with Carbopack X (20/40 mash) adsorbent and immobilized by a silanized glass wool (198009, CS-Chromatographie GmbH, Langerwehe, Germany) and two dents in the metal capillary (see Figure 2.28).

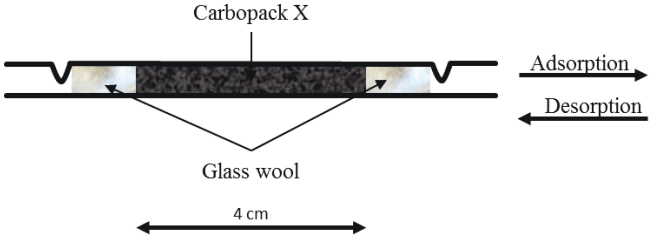

Figure 2.28: The capillary of the focus trap with the Carbopack X material and the glass wool.

For the desorption process in the sample and the focus trap the flow direction is reversed in the order that compounds with a higher boiling point never come into contact with the strongest absorbent for the ST or the sparsely occupied adsorbent of the FT, from which they would be difficult to desorb.

Besides the cryogenic trapping approach (Wang et al., 1999), using carbon based adsorbents is a well-established method to sample VOCs. However, VOC measurements using carbon based adsorbents suffer from memory effects and the formation of artifacts leading to biases. These memory effects describe the incomplete desorption of the analytes from the adsorbents, which leads to potential inaccuracies in subsequent measurements. Such effects are determined by the physical properties of each analyte and therefore the adhesive strength towards the adsorption material (Konrad, 2000). The Carbotrap, B and C, and Carbosieve SIII adsorbers are most resistant to degradation artifacts (Helmig and Greenberg, 1994). In order to prevent potential measurement inaccuracies, the application of the adsorption material and the desorption temperature were optimized to minimize the memory effect for all the calibrated substances in the concentration range that is expected for the PEGASOS campaign. Extensive

measurements were conducted to optimize the sample trap and focus trap temperatures and the adsorbents in order to minimize the memory effect of the system.

As a consequence the VOCs are adsorbed at a temperature of 30 °C on the ST to reduce the influence of water that has not been segregated on the WT (Helmig and Vierling, 1995). After a sampling time of 3 min the ST is heated in 0.3 min to 225 °C and the sample is desorbed for 0.8 min (see Figure 2.29). Then the ST is cooled by liquid cooling. For the adsorption process the FT is kept at a constant temperature of 35 °C and for the desorption process it is heated rapidly within 0.15 min to 225 °C. The temperature is then maintained for a further 0.6 min (see Figure 2.29). The system is operated at a constant split of 2 mL/min after the focus trap. To increase the desorption velocity from the sample trap, the gas flow is accelerated considerably by opening the split to 20 mL/min.

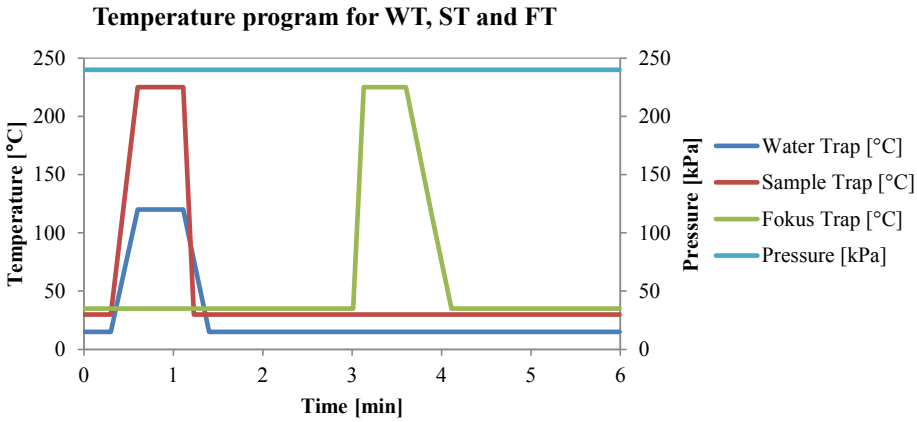

Figure 2.29: Temperature program of the sample trap (ST) and the focus trap (FT).

To determine the remaining memory effect, measurements with calibration gas were conducted and subsequently the system was switched to blank measurements with synthetic air. Consequentially, the memory effect was calculated from the amount of analytes that remained in the consecutive blank measurement.

Table 2.2: The memory effect of the analyzed substances showing the concentration in the standard, the blank concentration and the calculated memory effect.

	Standard measurement [ppb]	**Blank measurement [ppb]**	**Memory effect [%]**
Acetaldahyde	12.94	0.58	4.50
Acetone	1.48	0.08	5.54
Benzene	1.24	0.04	2.88
Ethanol	1.84	0.13	6.94
Isoprene	2.15	0.46	2.16
Methacrolein	1.83	0.02	1.30
Methanol	4.93	0.31	6.30
Methyl vinyl ketone	2.63	0.06	2.14
Pentane	3.69	0.09	2.54

The measurements showed that the mean memory effect is very low and for all the analyzed analytes is 6.94% (typical examples shown in Table 2.2). The resulting variation is still large ranging from 1.3 % for methacrolein to 7 % for methanol. This is caused by the diversity of the analyzed substances which makes it difficult to account for every substance. For all the calibrated substances the calculated memory effects are shown in Table 2.5.

2.5.5 Separation and detection

After the preconcentration and the focusing the substances are transferred to the GC column for separation. The HGC houses two GC columns (DB624, 20 m x 0.18 mm x 1.9 µm, Agilent, Santa Clara, USA), one for each channel. This is a mid-polar column with a bonded phase of methyl-phenyl-cyanopropyl-polysiloxane. The column has a good thermal stability and a low sensitivity to humidity.

Once the sample is transferred from the FT on the GC column, the temperature is kept constant at 35 °C for 0.3 min, then ramped with a heating rate of 120 °C/min to 220 °C and held isothermal for 1.4 min as seen in Figure 2.30. The system is operated at a constant pressure of 240 kPa which leads to a flow rate of 1.45 mL/min at 35 °C and 0.96 mL/min at 220 °C.

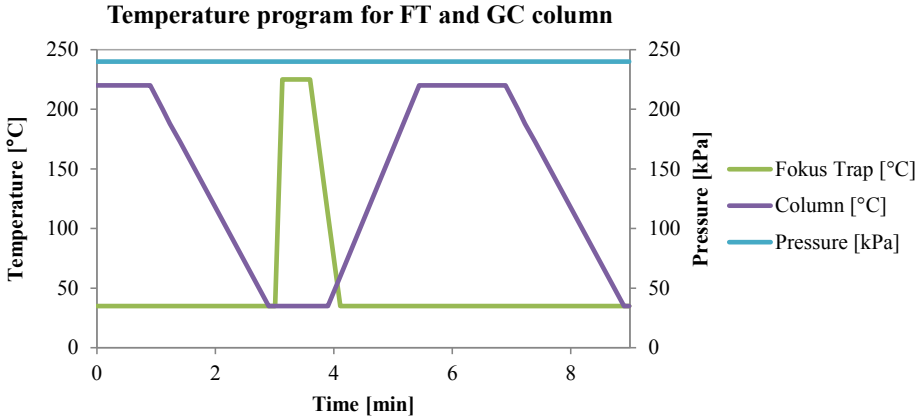

Figure 2.30: Temperature program of the adsorption unit and the GC including the head pressure exemplarily for one channel.

The separated analytes are detected by a mass spectrometer detector with Electron Ionization (EI). The MSD is operated in the Select Ion Monitoring (SIM) to lower the detection limit. In this mode only pre-selected ions are detected and not an ion range like in the SCAN mode. The SCAN mode is utilized to detect the substances retention time and the most specific mass to charge ratios (m/z) (see Table 2.5 in Chapter 2.5.4). Subsequently, the SIM method is set up. SIM windows are introduced to reduce the number of m/z to a maximum number of 14 ions that are analyzed at a time. To account for potential retention time shifts the windows

are overlapping. Consequently, ions of substances at the end or the beginning of one window are measured in both windows as shown in Table 2.3.

Table 2.3: Overlapping SIM windows utilized during the detection with the mass spectrometer.

	time	Mass 1	Mass 2	Mass 3	Mass 4	Mass 5	Mass 6	Mass 7	Mass 8	Mass 9	Mass 10	Mass 11	Mass 12	Mass 13	Mass 14
SIM Window 1	0.00	19	29.1	31	35	42	45.1	47	54.1	56	58.1	68.1	71.1	72.1	101
SIM Window 2	0.46	29.1	31	35	38	45.1	47	54.1	56.1	58.1	59.1	71.1	72.1	86.1	
SIM Window 3	0.91	35	45.1	47	59.1	68.1	70.1	71.1	72.1	78.1	82.1	86.1	100	117.	
SIM Window 4	1.36	35	45.1	56.1	59.1	71.1	73.1	78.1	82.1	84.1	91.1	100	117.		

2.5.6 System control and data analysis

The system control of the adsorption unit and the GC are covered by the TDSG software (GERSTEL GmbH & Co.KG, Mühlheim, Germany) custom made for the HGC. After each GC run, the TDSG software starts the data acquisition of the mass spectrometer software, the ChemStation (Agilent, Santa Clara, USA) that acquires the chromatograms.

The data analysis was conducted, using the chromatograms which were acquired during the PEGASOS campaign. Retention time shifts, caused by insufficient cooling during the measurement process at high ambient temperatures (see Figure 2.31), prohibited the utilization of the ChemStation software. Similarly, the MassHunter software (Agilent, Santa Clara, USA) for automated peak allocation and integration could not be used. Therefore, an IDL program (Interactive Data Language, ITT VIS, Boulder, USA) was used to correct for the time shifts in the acquired chromatograms. First, the most abundant substances, such as acetone, isoprene, CCl_4, benzene and toluene were identified and integrated for all chromatograms. These substances were selected based on their wide spread across the chromatogram. Secondly, the retention time shift was calculated utilizing the IDL program and a correction of the retention time and the signal intensity was applied to all chromatograms. Following these correctional steps, all substances in all chromatograms were integrated automatically using the MassHunter software, leaving only minor corrections to the integration procedure. The integral with the dimension counts derived were thereafter used to calculate the individual mixing ratios.

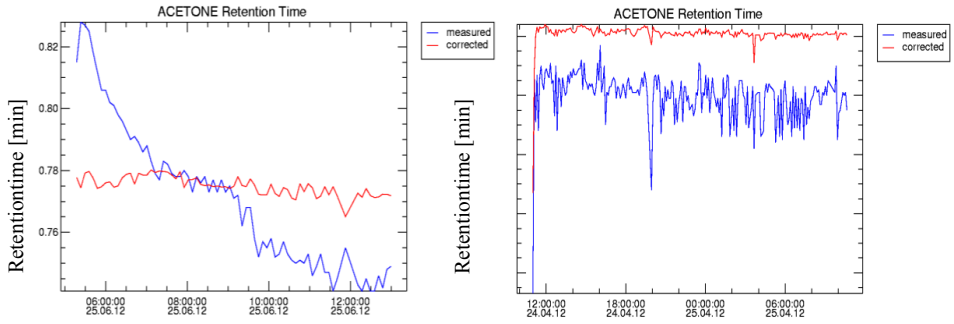

Measurement in the Zeppelin NT at 35 °C ambient temperature

Measurement in the air- conditioned Container

Figure 2.31: The measured and corrected retention time for acetone for a measurement day on board the Zeppelin at high ambient temperatures with a high retention time shift (left) and in an air conditioned environment with a low retention time shift (right).

2.6 Calibration of the HGC

The instrument was calibrated before the campaign with a 4 step calibration for all measured substances (see Table 2.5) with two different certified gas standards from Apel - Riemer (Environmental Inc., Denver CO, USA). One standard (Apel 7) for the calibration of non-oxygenated substances containing 75 different VOC components in the concentration range of 0.2 – 10 ppb (delivery date 20.05.2009) and a second standard (Apel 8) for the calibration of oxygenated substances with higher concentrations of 30 - 1000 ppb (delivery data 20.09.2009) were utilized. The gas standards were diluted with synthetic air (99.9999 %, Linde Gas, München, Germany) in a mixing chamber. The mixing chamber is coated with silcosteel® and heated to 50 °C with a total volume of 1.2 L. This calibration was the basis for the calculation of the measured probes. Beside the ambient air measurements, blank measurements with synthetic air were also conducted.

2.6.1 Sensitivity shift of the MSD

The key advantage of the mass spectrometer detector is the separate detection of different analytes simultaneously on different masses. Such performance cannot be achieved by for example the Flame Ionization Detection (FID). The measurement approach of the MSD eases the analysis of the peaks, which do not have to be baseline-separated but can be distinguished in the MSD by the different ionization masses. A disadvantage of the MSD is its sensitivity shift (Kitson et al., 1996). To ascertain a stability of measurements, the MSD was tuned daily using the standard spectra target tune with the internal standard of the mass spectrometer Perfluorotributylamine (PFTBA). This ensured that the ionization properties of the mass spectrometer were adjusted according to defined values for selected masses throughout the mass range. Thus, the sensitivity of the MSD was normalized to identical values every day.

Table 2.4: Relative intensity of PFTBA mass fragments as targeted by automated standard spectra tuning. The aimed intensity of the mass 69 was 500.000 counts.

Mass [m/z]	**Value [%]**
69	100
50	0.9
131	43
219	49
414	2.4
502	1.7

To quantify the offset to the calibration as a cause of the sensitivity shift of the MSD, a daily calibration with a self-produced standard (Zeppelin standard) was performed on board the Zeppelin. This Zeppelin standard contains a limited amount of substances (37 substances), at least one substance per measured ion in order to account for the sensitivity shift for each ion throughout the day. The Zeppelin standard was calibrated with the certified Apel - Riemer standard before the campaign.

For the calibration the valve 3 was switched and the gas cylinder and the Zeppelin standard was sampled (see Figure 2.32). As there is no possibility for dilution, the standard was prepared at expected ambient concentrations. During the PEGASOS campaigns, the Zeppelin standard was always measured before and after each flight to determine the sensitivity shift of the instrument throughout the day. For the first flights it was also deployed every two hours in between the measurements. The approach was improved due to consistent failures of valve 3. This valve did not switch back from the Zeppelin standard to the ambient air. And since for 5 flights it could be seen that the decrease of sensitivity was a linear function (see Figure 2.33) the calibration was reduced to before and time after each flight.

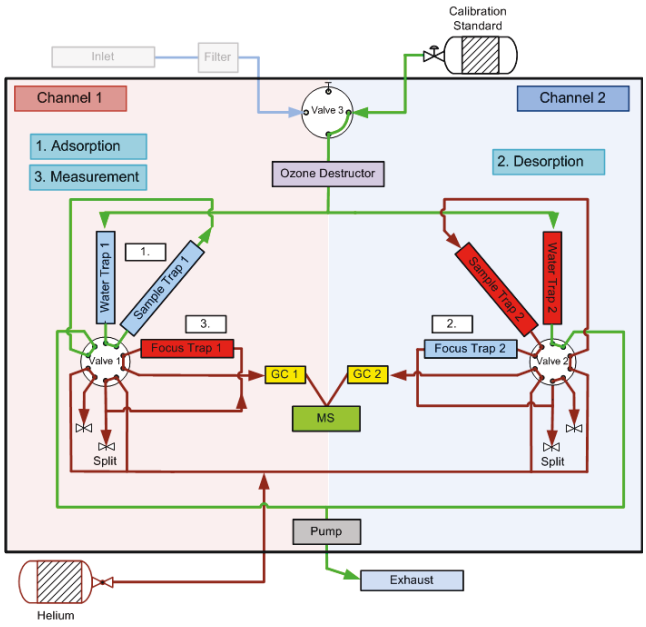

Figure 2.32: Operation of the instrument in the calibration mode.

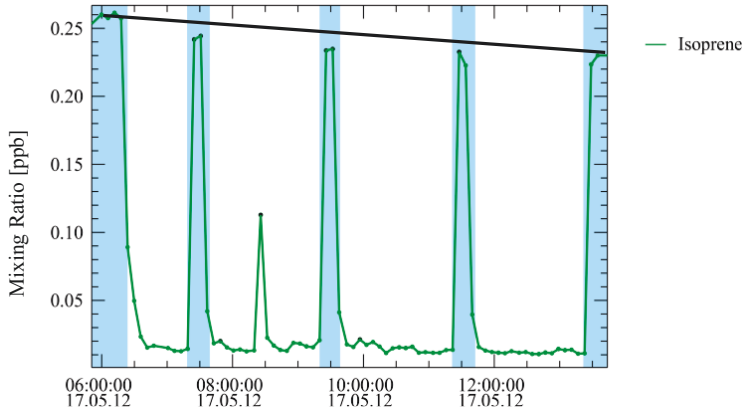

Figure 2.33: The linear decrease of the MSD sensitivity throughout one day as exemplarily shown for the calibration measurements (blue shaded) of isoprene.

A contamination of the ion source can lead to short time variations in the sensitivity of the mass spectrometer. CCl_4, a long lived trace gas with almost uniform distribution in the troposphere (Apel et al., 2003) was used to track short time variations in the sensitivity. The insensitivity of the ion 117 from CCl_4 remained constant during the Netherlands campaign. During the Italy campaign the CCl_4 signal showed variations in intensity (see Figure 2.34).

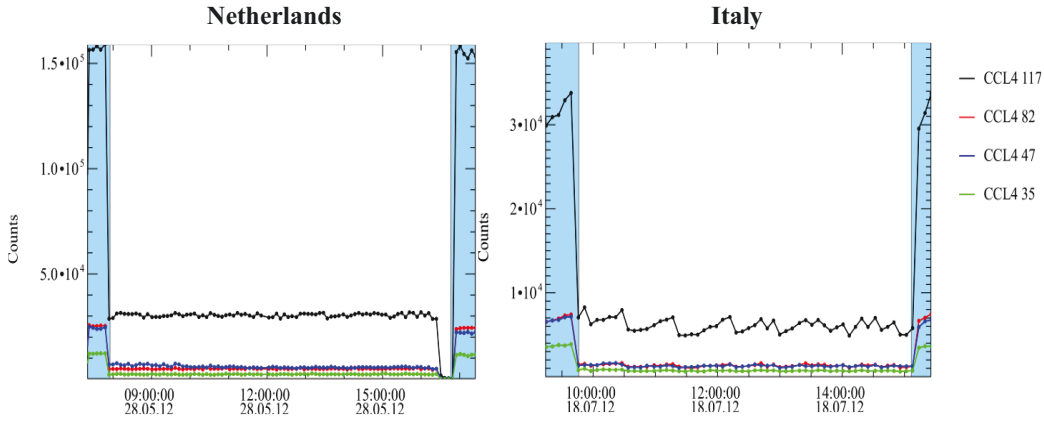

Figure 2.34: The intensity of the ion at m/z 117 of CCl4 in the Netherlands and in Italy. The measurements indicated in blue are calibration measurements.

This sensitivity shift can also be seen for all other trace gases. To account for these sensitivity shifts, the data collected during the Italian campaign was corrected by a factor f (see Equation 2.1) derived from the ratio of the counts of ambient CCl_4 measurements and the CCl_4 in the Zeppelin standard before the campaign and the ratio between the counts of CCl_4 in the ambient air and in the standard measurement at the day of analysis.

$$\frac{\text{counts } CCl_4 \text{ ambient at calibration (Jülich)}}{\text{counts } CCl_4 \text{ Zepelin STD at calibration (Jülich)}} = f \times \frac{\text{counts } CCl_4 \text{ ambient (daily calibration)}}{\text{counts } CCl_4 \text{ Zepelin STD (daily calibration)}} \qquad 2.1$$

2.6.2 Blank measurements

Blank measurements were conducted before and during the campaign utilizing synthetic air. These synthetic air blank measurements were included in the calibration. But as this is time consuming for a daily procedure the instrument blank was determined by measurements with no adsorption flow (see Figure 2.35). These blank with no adsorption values were accounted for each day separately when calculating the concentrations.

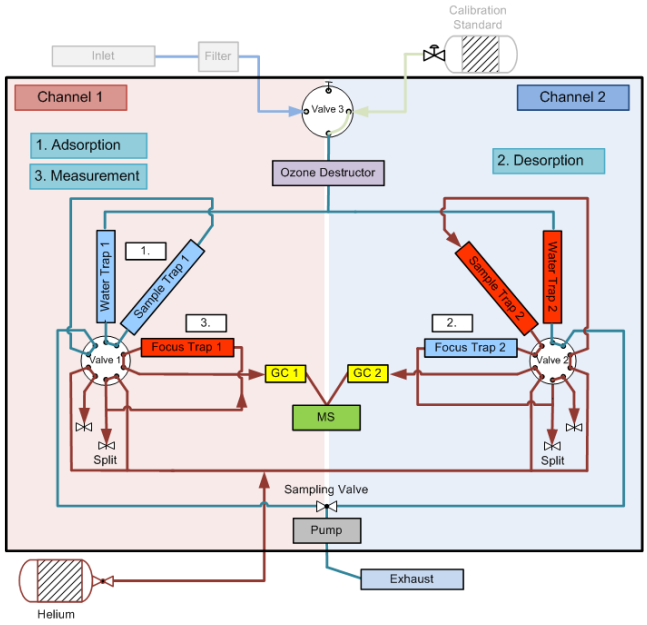

Figure 2.35 The operation of the instrument for internal blank measurements.

2.6.3 Calculation of mixing ratios

The calculation of the mixing ratio was realized by an IDL program that used the raw data and applied the calibration prior to the campaign. Subsequently, the determined blank values from the measurements without adsorption were subtracted and the correction factor derived from the Zeppelin standard measurements was applied. This correction factor compensates for the sensitivity shift of the MSD between the measurement and the calibration. For the data acquired during the Italy campaign the CCl_4 correction was additionally implemented. These calculations were done for each channel separately and the results merged to one dataset.

For most of the measurements Channel 1 and 2 agree well, as shown for pentane in Figure 2.36 in Section A and C, but in some minor cases there is a significant difference between both Channels (Section B) which manifests itself in this saw tooth structure between Channel 1 and 2. The cause for this phenomenon could not be found.

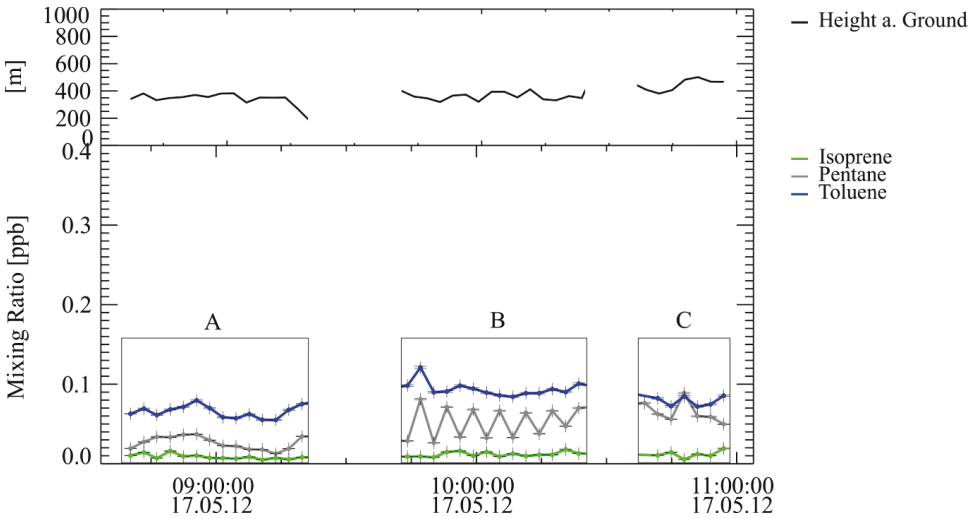

Figure 2.36: The merging of the two Channels with a good agreement shown in A and C and a poor agreement leading to a saw tooth structure in B shown for pentane.

2.6.4 Calibrated substances

The system was calibrated for the 49 substances as seen in Table 2.5. The table also shows the ion measured in the MSD, the obtained precision, the detection limit and the memory effect. The compounds are sorted due to their retention times.

Table 2.5: The 49 different VOC analytes that were analyzed during the PEGOSOS campaigns and their corresponding ions, precision, detection limit and memory effect.

Nr.	Substance	m/z	Precision [%]	Accuracy [%]	Detection limit [ppt]	Memory effect [%]
1	1-Butene	56.0	2.0	7.0	6.0	4.7
2	n-Butane	58.0	3.4	8.4	7.8	15.5
3	Acetaldehyde	42.0	7.4	12.4	3.6	4.5
4	Methanol	31.0	8.8	13.8	6.9	6.3
5	Isopentane	72.0	1.4	6.4	1.2	9.4
6	1-Pentene	70.0	0.4	5.4	3.1	29.1
7	n-Pentane	72.0	1.0	6.0	1.8	2.6
8	Ethanol	31.0	5.9	10.9	10.2	7.0
9	trans-Pentene	70.00	3.6	8.6	4.1	3.3
10	Isoprene	68.0	2.7	7.7	2.6	2.2

Nr.	Substance	m/z	Precision [%]	Accuracy [%]	Detection limit [ppt]	Memory effect [%]
11	cis-Pentene	70.0	3.7	8.7	2.3	29.8
12	Propanal	29.0	8.0	13.0	5.7	22.7
13	Acetone	58.0	3.4	8.4	1.6	5.5
14	2-Propanol	45.0	6.6	11.6	19.3	25.2
15	Acetonitrile	38.0	3.3	8.3	4.9	2.8
16	Methyl acetate	59.0	4.3	9.3	13.4	1.9
17	Cyclopentene	68.0	2.3	7.3	2.3	4.9
18	2;3-Dimethybutane	86.0	4.8	9.8	8.2	16.3
19	Cyclopentane	70.0	2.3	7.3	7.7	1.1
20	Methacrolein	70.0	4.5	9.5	6.2	1.3
21	n-Hexane	86.0	1.3	6.3	5.7	2.0
22	1-Propanol	59.0	5.9	10.9	5.6	14.0
23	Butanal	72.0	1.1	6.1	1.4	4.4
24	Methyl vinyl ketone	70.0	1.6	6.6	11.3	2.1
25	Ethyl acetate	70.0	4.7	9.7	14.2	3.7
26	Butanone	72.0	1.3	6.3	6.9	3.4
27	Cyclohexane	84.0	1.4	6.4	1.9	11.9
28	Benzene	78.0	1.1	6.1	1.4	2.9
29	Cyclohexene	82.0	1.4	6.4	12.5	11.0
30	n-Heptane	100.0	1.6	6.6	2.9	2.5
31	2,3-Dimethyl-2-pentene	98.0	1.2	6.2	7.7	19.9
32	Pentanal	44.0	5.2	10.2	4.7	3.3
33	Toluene	91.0	1.1	6.1	1.3	2.7
34	n-Octane	71.0	4.3	9.3	12.3	6.0
35	Hexanal	44.0	3.3	8.3	2.1	12.8
36	Ethylbenzene	91.0	1.1	6.1	4.2	6.4
37	*m/p*-Xylene	91.0	4.3	9.3	4.8	4.8
38	n-Nonane	71.0	1.5	6.5	12.7	14.9
39	*o*-Xylene	91.0	1.6	6.6	4.4	14.1
40	Styrene	104.0	7.7	12.7	2.7	34.2
41	Isopropylbenzene	120.0	1.2	6.2	1.0	7.5

Nr.	Substance	m/z	Precision [%]	Accuracy [%]	Detection limit [ppt]	Memory effect [%]
42	α-Pinene	93.0	2.3	7.3	4.4	26.7
43	Cyclohexanone	98.0	3.3	8.3	3.9	11.0
44	Myrcene	93.0	9.8	14.8	1.5	6.5
45	Propylbenzene	91.0	2.3	7.3	4.5	30.0
46	Mesitylene	71.00	4.1	9.1	1.4	9.6
47	Limonene	93.0	3.0	8.0	1.5	23.2
48	Benzaldehyde	106.0	5.3	10.3	5.5	19.5
49	Indane	117.0	2.6	7.6	1.9	16.0

In the concentration range between 0.5 and 2 ppb, the calculated precision from calibration measurements had a mean of 3.0 % for all calibrated substances. The accuracy of the system is dominated by the calibration standard which is delivered with an accuracy ± 5% for all substances. Consequently, the accuracy of the system lies between 6-15 %, depending on the respective precision of each analyte. For the calculation of the accuracy the uncertainty caused by ozone and humidity have not been taken into account. The linearity of the instrument is good for all calibrated substances within the concentration range (10 ppt - 10 ppb) that was expected for the Zeppelin measurements (see Figure 2.37).

The detection limit was calculated by the tripled signal to noise ratio method (Fleming et al., 1997). Overall, the instrument showed a detection limit in the lower ppt range with a mean mixing ratio of 5 ppt for all calibrated substances.

The memory effect describes the effect caused by the incomplete desorption of the analytes from the adsorbents which leads to potential overestimation in subsequent measurements (Konrad, 2000) (see Chapter 2.4.4.). The mean memory effect of the system for all calibrated VOCs is 7 %.

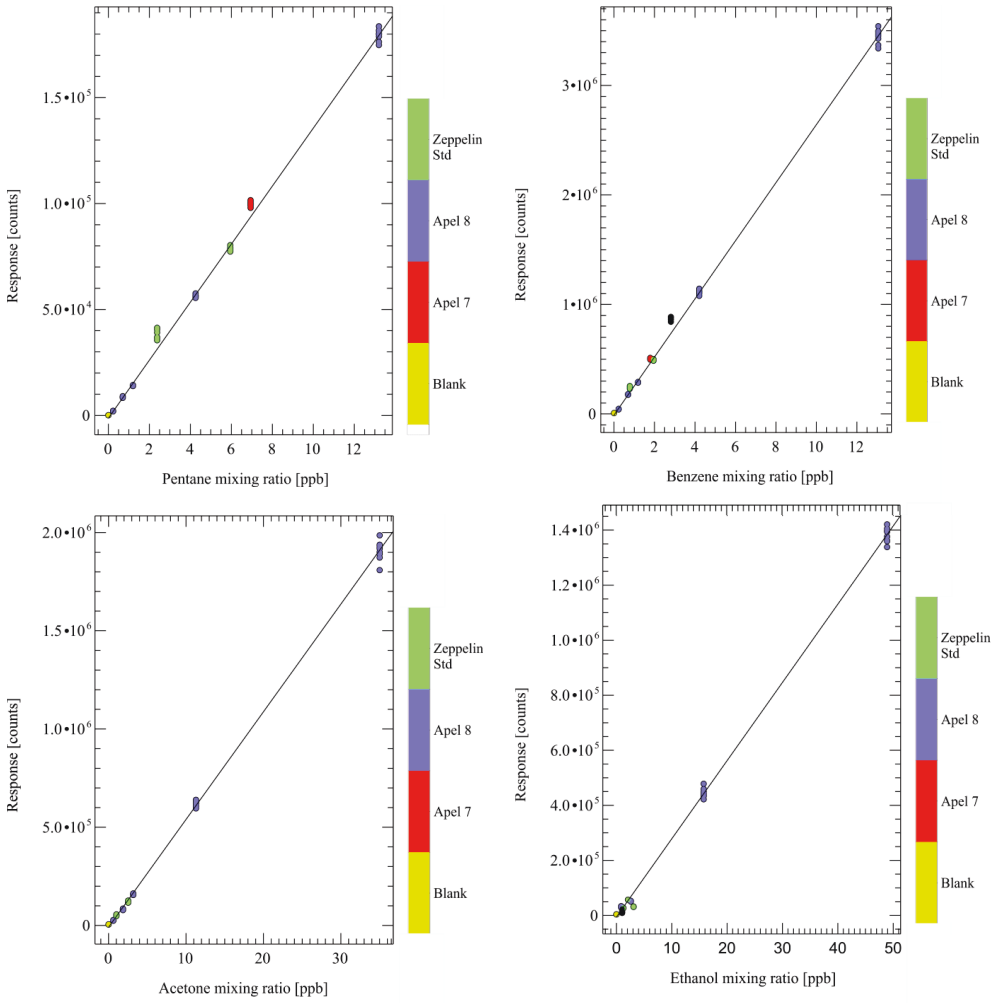

Figure 2.37: Calibration of pentane, benzene, acetone and ethanol for the calibration standards Apel 7, Apel 8 and the Zeppelin standard with the respective response in counts.

2.6.4.1 Limitations

All components must be volatilized to be analyzed by GC/MS. Thermally labile components can be affected and form artifacts due to high temperatures during the desorption process (Woolfenden, 1997). Within this work it could be observed that 2-methyl-3-buten-2-ol (MBO) was degraded as well as the group of terpenes. This was first not recognized because as the gas standard contained MBO, isoprene and 3 terpenes (α-pinene, β-pinene and limonene). Only in the individual analysis of each compound showed that there are degradation processes. A significant fraction of MBO is degraded to isoprene as seen in a large isoprene peak next to the MBO peak although there was no isoprene in the sample. The

same phenomenon could also be observed that for the more labile terpenes such as β-pinene. Here, peaks of more stable terpene species such as α-pinene, myrcene and limonene could be observed thus it can be concluded that the labile terpenes are converted to more stable species. Throughout all the analysis, α-pinene and myrcene showed the greatest stability of all terpenes. To reconstruct the true ambient monoterpene concentrations before the conversion the ratio between the three main terpene peaks (α-pinene, myrcene and limonene) in the Zeppelin standard measurements was analyzed throughout the campaign. The analysis showed that the ratio changed significantly throughout the 3 months. Thus, it is impossible to reconstruct the true ambient monoterpene concentrations.

Especially, the research of M. Kaminski led to hypothesis that the active surfaces particularly those of the adsorption tubes can induce conversion of thermally labile terpenes. He implemented liners that have been deactivated by silanization and could herewith prevent the degradation of MBO and terpenes. A similar process was reported by Rudich et al. (1995), who found that MBO is decomposed to isoprene, but by the light of a deuterium lamp. This reaction is catalyzed by the surface. This surface catalyzed conversion could not been avoided for the measurements of the PEGASOS campaigns in 2012 as the special liners were not accessible. Thus, the isoprene concentration may be overestimated and terpene concentrations may be higher. On the other hand the concentrations of isoprene were low during both parts of the campaigns. Also the trees in both the Netherlands and Italy emitted only very low concentrations of MBO. The concentrations of terpenes were in the lower ppt range (max. 25 ppt) which is just above the detection limit throughout the Netherland and Italy campaign. Consequently, the redistribution of terpenes has an only limited effect on their contribution to the OH reactivity.

The results of this dissertation are thus excluding estimations of MBO and terpenes. The degradation problem of VOCs by active parts in the liners can be solved by introducing adsorption liners that have been deactivated by silanization. The implementation during the PEGASOS Finland campaign in 2013 showed good results.

3. Observations

The HGC instrument which is described in the previous chapter has been deployed in the PEGASOS campaigns in 2012 to measure VOCs on board the Zeppelin NT. The north-bound campaign was in May 2012 the Netherlands and the south-bound campaign in Italy in June/July 2012.

3.1 Measurement sites

3.1.1 North campaign in the Netherlands

The north bound campaign was performed from May 17th until May 29th in the westerly part of the Netherlands close to the KNMI tower at the Cabauw supersite (52.0° N, 4.9° E). For the duration of the campaign the Zeppelin NT was stationed at the Rotterdam The Hague Airport.

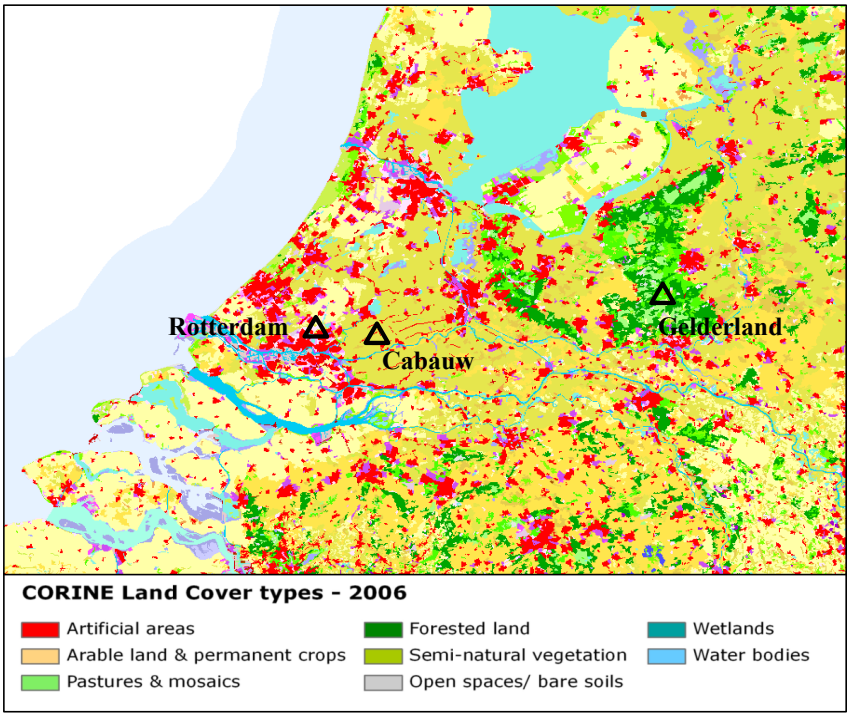

Figure 3.1: Land cover on the measuring sites in the Netherlands (European Environment Agency, June 2013) .

The city of Rotterdam is characterized by Europe's largest harbor with its refineries and the industrial surroundings as seen in Figure. 3.1. The road traffic is high with a large fraction of heavy duty vehicles (Keuken et al., 2011; van Ierland et al., 2000). The North Sea around Rotterdam is dominated by a large amount of container ships traveling or being at berth (Hulskotte and Denier van der Gon, 2010). The region around Cabauw is dominated by flat grassland with narrow ditches and livestock. Up to 200 m from the tower there are no obstacles (Beljaars and Holtslag, 1991). The Gelderland region is the largest forest area in the Netherlands and covered with conifer forest and deciduous forest with oaks and beeches. (European Environment Agency, June 2013).

3.1.2 South campaign in Italy

The south-bound campaign was performed from June 14th until July 19th in the south-eastern part of the Po Valley close to Bologna. During this time the Zeppelin NT was based 20 km east of Bologna at the Airfield Aviosuperficie di Ozzano 'Guglielmo Zamboni'. The Po Valley is regarded as a region with high levels of pollution due to the high population density, industrial activities, transport and agriculture (Zappoli et al., 1999). The southeastern sector of the Po Valley is dominated by cultivated plains without any characteristic plants (see Figure 3.2) (Pedrotti, 2004). Bologna (44.5° N, 11.3° E) is the largest city in this part of the Po Valley as an important transportation hub with its highways, railway and airport.

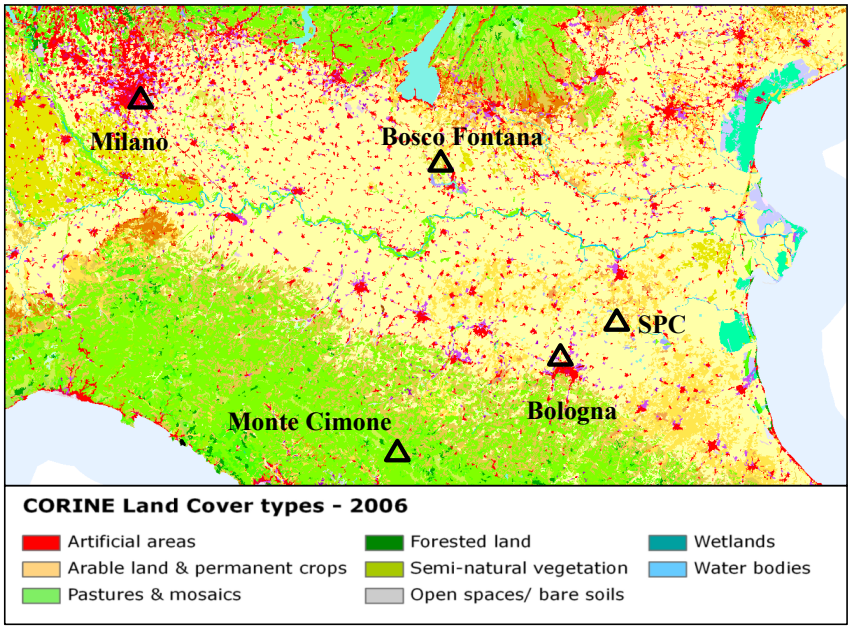

Figure 3.2: Land cover on the measuring sites in Italy (European Environment Agency, June 2013).

The supersite San Pietro Capofiume (SPC) (44.6° N, 11.6° E) is located in this flat rural area in between of agricultural fields and grassland (Cassardo et al., 2006; Decesari et al., 2001). In the southern direction the Po Valleys boarders the Apennines with the vegetation dominated by pine trees and robinias (EEA, 2013). One supersite was situated on the Monte Cimone (MTC) (44.2° N, 10.7° E) at the highest peak of the Apennines at 2165 m (Bonasoni et al., 2000).

3.2 Measurement flights and HGC data coverage

During both campaigns three different flight patterns were conducted. First, vertical profiles above supersites were flown to analyze the vertical structure of the troposphere. Here, the focus was mainly to probe the layering of the Planetary Boundary Layer (PBL). Especially, the evolvement of the stable Nocturnal Boundary Layer which is elaborated in Chapter 4.5 was of great interest. Second, transect flights were conducted to analyze different emission patterns as well as cross sections of landscape and over the North and Adrian Sea. Third, transfer flights to relocate the Zeppelin NT to the Dutch and Italian research base providing a cross section of the air above Southern and Western Europe.

3.2.1 Campaign in the Netherlands

During the north campaign 14 measurement flights with the HGC on board were performed. This includes six transfer flights, four vertical profile flights above the Cabauw supersite and two transects flights, one to the Gelderland and one flight above the North Sea (see Figure 3.3).

Figure 3.3: Flight tracks for all the flights obtained in the Netherlands, excluding the transfer flights, colored by the height above ground.

For 11 of 14 flights performed in the Netherlands the HGC had full data coverage (see Table 3.1). For flight number F011 only for half of the flight data were obtained and for two flights (F210 and F212) there is no data available. The reason for the data loss was the failure of a LAN cable at high ambient temperatures and a malfunction of the calibration valve. The flights in the tables below that consist of two flights have a petrol stop in between but were flown in the identical pattern above the same ground.

Table 3.1: Overview of the measurements flights made on the north-bound campaign in the Netherlands and the performance of the HGC instrument.

Date	Flight Number	Take off [UTC]	Landing [UTC]	Flight Route	Flight Pattern	CL	HGC Status
17/05	006/007	7:30	14:42	Friedrichshafen - Mainz	Transfer	8	Full Data
18/05	008/009	8:53	15:55	Mainz - Rotterdam	Transfer	8	Full Data
19/05	010	9:03	13:40	Cabauw	Vertical Profiles	8	No Data
21/05	011	8:05	14:15	Gelderland, Wageningen, Cabauw	Transects	5	Half Data
22/05	012	14:54	17:38	Cabauw	Vertical Profiles	5	No Data
24/05	013	9:01	12:28	Cabauw	Vertical Profiles	8	Full Data
24/05	014	12:48	15:16	North Sea	Transects	8	Full Data
27/05	015/016	2:35	9:01	Cabauw	Vertical Profiles (morning flight)	8	Full Data
28/05	017	9:12	14:12	Rotterdam - Mainz	Transfer	8	Full Data
29/05	018	7:27	12:02	Mainz Friedrichshafen	Transfer	8	Full Data

3.2.2 Italy campaign

During the course of the Italian campaign 30 measurement flights with CL-5 and CL-8 were performed including the eight transfer flights (see Figure 3.4). Eleven vertical profile flights were performed above the SPC and Bosco Fontana supersites as well as Argenta. Two flights were conducted partly over the Adrian Sea and nine transect flights to the bordering Apennine Mountains and above parts of Bologna. For 25 flights there is full VOC data coverage. For 3 flights (F022, F030 and F032) there is no data and for one flight (F29) only half the data was acquired (see Table 3.2). For the final transfer flight (F053) the instrument had to be

dismounted due to bad weather. The reason for the inability to collect data on the flights F022, F030 and F032 was again a LAN cable connection failure (same as in the Netherlands). During flight F022 the filaments of the mass spectrometer burnt out and had to be replaced.

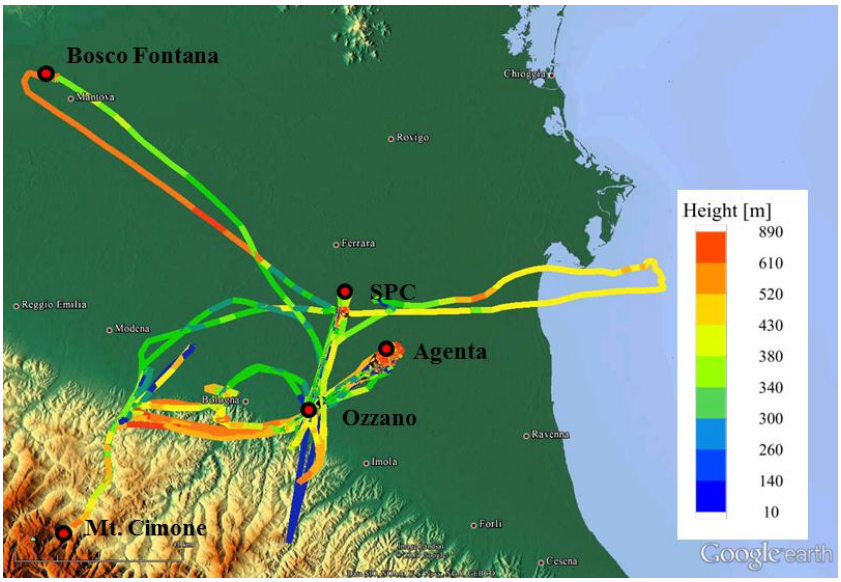

Figure 3.4: Flight tracks for all the flights obtained in Italy, excluding the transfer flights, colored by the height above ground.

Table 3.2: Overview of the Flights made on the south part of the 2012 campaign in the Netherlands and the performance of the HGC instrument.

Date	Flight Number	Take off [UTC]	Landing [UTC]	Flight Route	Flight Pattern	CL	HGC Status
14.06.	019	10:44	14:50	Friedrichshafen - Wels	Transfer	8	Full coverage
15.06.	020/021	5:27	15:40	Wels - Gorizia	Transfer	8	Full coverage
16.06.	022	10:09	16:14	Gorizia - Ozzano	Transfer	8	no Data
18.06.	023/024	2:50	9:39	SPC	Vertical Profiles	8	Full coverage
20.06.	027/028	4:30	12:30	SPC	Vertical Profiles	5	Full coverage
21.06.	029/030	3:53	10:17	SPC-Apennin	Transects	5	half Data
22.06.	031	4:00	8:28	Adria	Transects	5	Full coverage
24.06.	032	7:00	13:10	Adria	Transects	5	No Data
25.06.	033/034	6:07	12:16	Bologna - Valley	Transects	8	Full coverage

Date	Flight Number	Take off [UTC]	Landing [UTC]	Flight Route	Flight Pattern	CL	HGC Status
01.07.	039	4:40	10:06	Monte Cimone - Bologna	Transects	5	Full coverage
03.07.	040	3:50	9:37	Bosco Fontana	Vertical Profiles	5	Full coverage
04.07.	041	5:09	11:15	Monte Cimone - Bologna	Transects	5	Full coverage
05.07.	042/043	4:50	11:40	SPC	Vertical Profiles	8	Full coverage
07.07. morning)	044	6:00	10:05	Agenta	Vertical Profiles	8	Full coverage
07.07. (evening)	045	17:00	20:20	Agenta	Vertical Profiles	8	Full coverage
08.07.	046	6:00	10:15	Monte Cimone - Bologna	Transects	8	Full coverage
09.07.	047	6:06	10:35	Agenta	Vertical Profiles	8	Full coverage
10.07.	048	6:03	10:35	Monte Cimone - Bologna	Transects	8	Full coverage
12.07.	049	3:20	9:20	Agenta	Vertical Profiles	8	Full coverage
13.07.	050	6:00	8:12	Appenin-Ferrara	Transects	8	Full coverage
16.07.	051	9:37	15:25	Bologna - Gorizia	Transfer	8	Full coverage
17.07.	052	6:05	10:15	Gorizia - Graz	Transfer	8	Full coverage
18.07.	053	9:37	18:25	Graz - Wels	Transfer	8	Full coverage
19.07.	054	6:45	12:00	Wels – Friedrichshafen	Transfer	8	Not on board

3.2.3 Meteorology of both parts of the campaign

During the campaign in the Netherlands the mean temperature was 18 °C with a relative humidity (RH) of 74 % (see Table A.1 in the appendix). The averaged wind speed was 10 km/h, ranging between 8 and 13 km/h. The wind was coming predominantly from the north. The mean visibility was 8.9 km. During the measurement days there was no precipitation.

In the period of the campaign in Italy the mean temperature was 28 °C, reaching maximum temperatures of 36 °C on July 2nd and reaching daytime maximum temperatures between 26 °C and 36 °C (see Table A.2 in the appendix). The mean relative humidity was 46 %. The visibility had a value of 10 km. The averaged wind speed was 9 km/h. The wind was

predominantly coming from east, south-east and west. During the measurement days there was no precipitation or fog.

3.3 Overall VOC observations

The distribution for the most abundant VOC species is elaborated in the following. For the analysis the data obtained is divided into the data obtained in the Netherlands and in Italy. It needs to be taken into account that the number of observations was higher in Italy compared to the Netherlands as more flight hours were flown in Italy. The transfer flights have not been included into this analysis. The respective mean, median, standard deviation, minimum and maximum values of the discussed VOC species are shown in Table A.3 and A.4 in the appendix.

3.3.1 Anthropogenic VOCs

The mean concentration of the single measured anthropogenic VOC (AVOCs) was below a value of 200 ppt for both parts of the campaign with higher concentrations in the Netherlands compared to Italy.

3.3.1.1 Alkanes and alkenes compounds

The mean mixing ratios of all individual alkanes and alkenes were below 140 ppt for both parts of the campaign. The most abundant alkanes were isopentane and pentane with respective mean values of 124 ppt and 135 ppt in the Netherlands and 43 ppt and 80 ppt in Italy (see Figure 3.5). The most abundant alkene was 1-butene with a mean mixing ratio of 40 ppt in the Netherlands and 18 ppt in Italy.

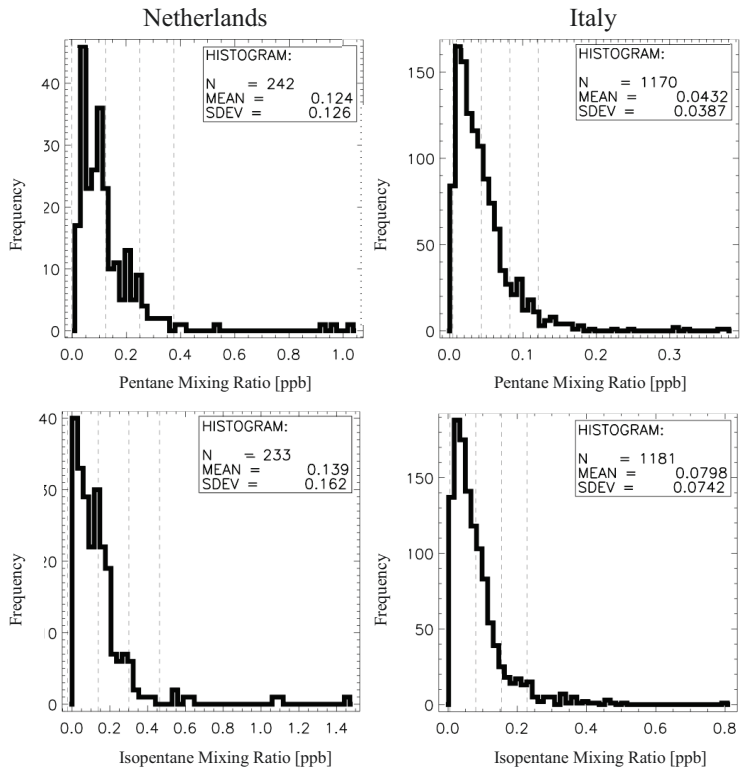

Figure 3.5: Histograms of mixing ratios of pentane and isopentane from the data obtained in the Netherlands and in Italy.

3.3.1.2 Aromatic compounds

The most abundant aromatics were toluene, m-xylene and benzene (see Figure 3.6). The mean mixing ratios in the Netherlands were 153 ppt, 79 ppt and 90 ppt, respectively, and 116 ppt, 35 ppt and 42 ppt in Italy. As for the alkanes and alkenes the mixing ratios of anthropogenic VOCs in the Netherlands exceeded the mixing ratios in Italy.

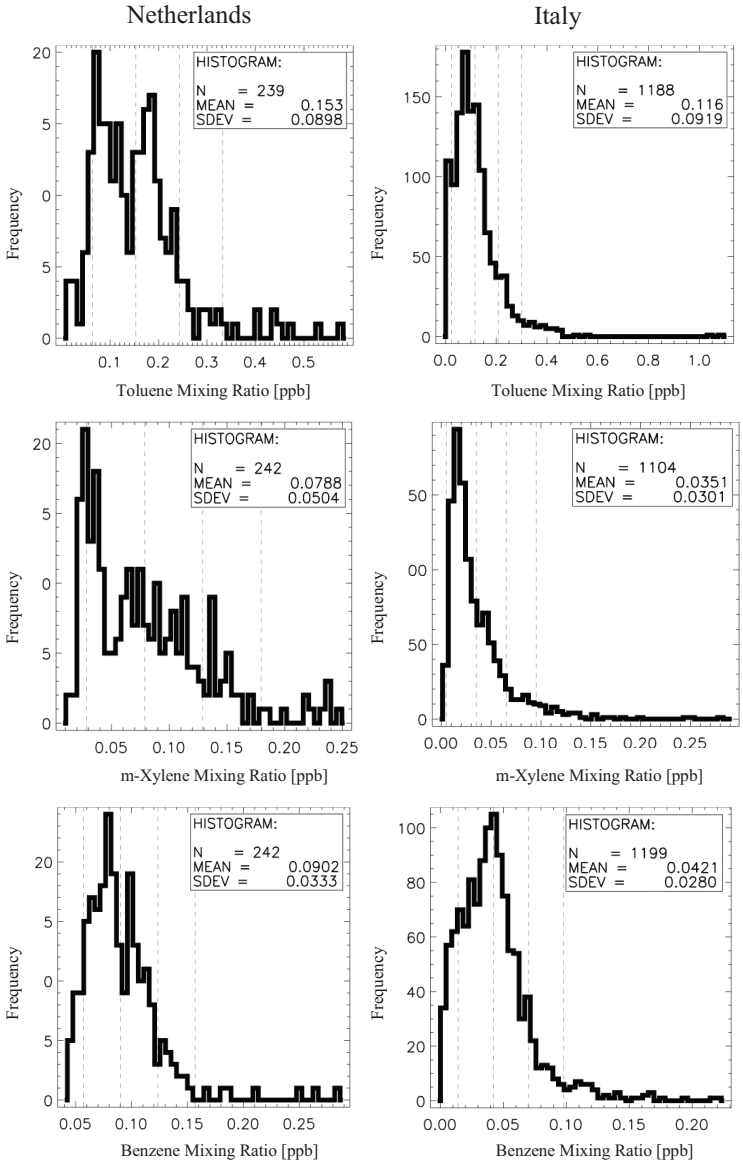

Figure 3.6: Histograms of the toluene, m-xylene and benzene mixing ratios from the data obtained in the Netherlands and in Italy.

3.3.2 Biogenic VOCs

The contribution of the biogenic VOCs (BVOCs) was limited to isoprene as the mean values of all monoterpenes were below their detection limit. The mean isoprene mixing ratio was lower in the Netherlands with a value of 43 ppt compared to a value of 130 ppt in Italy (see Figure 3.7).

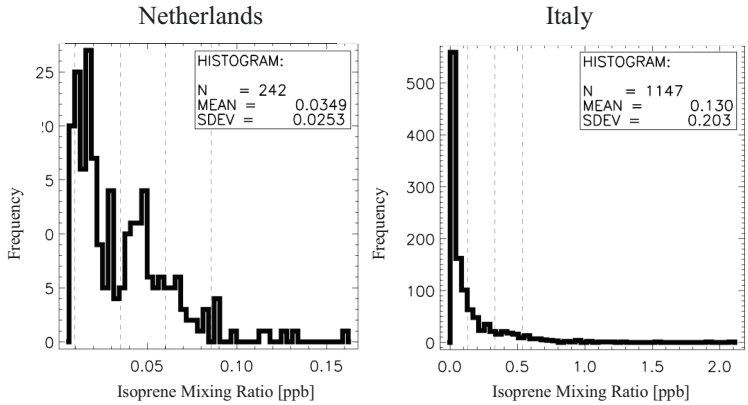

Figure 3.7: Histograms of the isoprene mixing ratios from the data obtained in the Netherlands and in Italy.

3.3.3 Oxygenated compounds

Compared to the concentrations of the anthropogenic and biogenic compounds, the oxygenated compounds (OVOCs) were more abundant with mean mixing ratios in the ppb range for both parts of the campaign.

3.3.3.1 Alcohol compounds

Methanol and ethanol were the most abundant alcohols with mean values of 4.9 ppb and 1.4 ppb, respectively, in the Netherlands and 2.5 ppb and 0.7 ppb in Italy (see Figure 3.8). The values in the Netherlands also exceeded the values in Italy. Other alcohols that were measured had mixing ratios below 80 ppt.

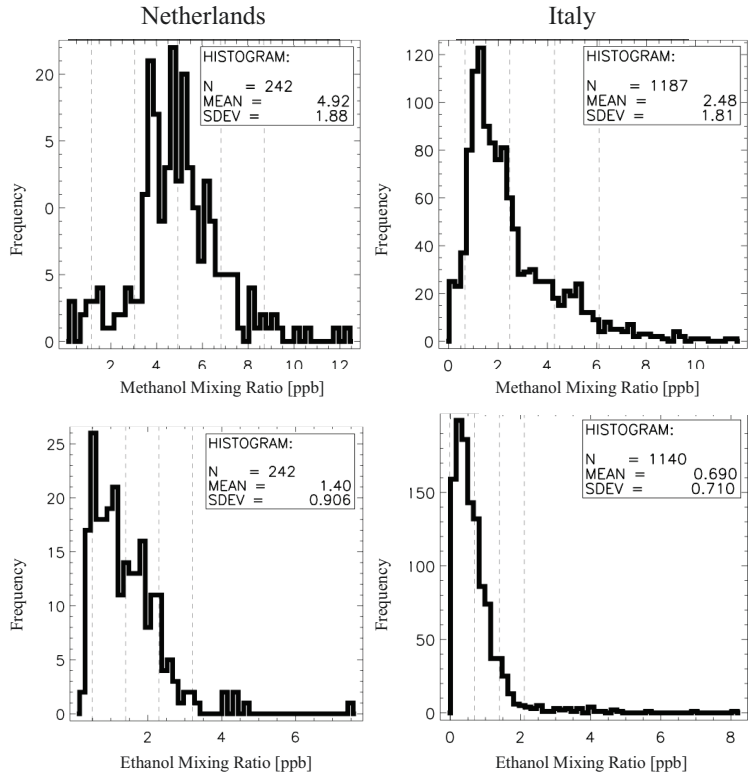

Figure 3.8: Histograms of the methanol and ethanol mixing ratios from the data obtained in the Netherlands and in Italy.

3.3.3.2 Aldehyde compounds

With a mean value of 1.0 ppb in the Netherlands and 1.4 ppb in Italy acetaldehyde was the most abundant aldehyde (see Figure 3.9). This was followed by propanal with a mean of 595 ppt in the Netherlands and 341 ppt in Italy. The other ketones play only a subordinate role with mixing ratios below 100 ppt.

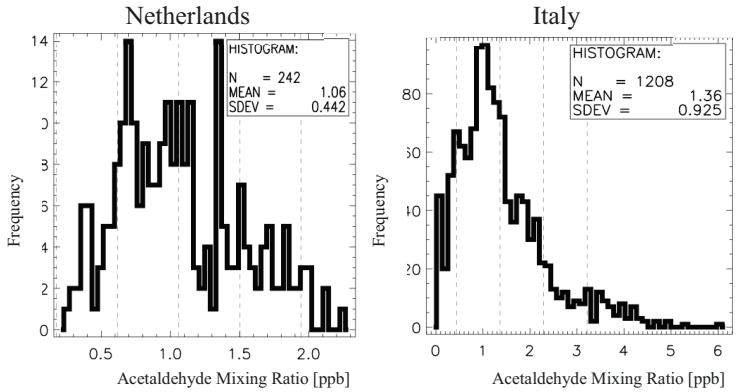

Figure 3.9: Histograms of the acetaldehyde mixing ratios from the data obtained in the Netherlands and in Italy.

3.3.3.3 Ketone compounds

Acetone was the most abundant ketone with a mean mixing ratio of 2.2 ppb in the Netherlands and 1.6 ppb in Italy (see Figure 3.10). Methyl ethyl ketone (MEK) and methyl vinyl ketone (MVK) showed lower mixing ratios with 661 ppt and 262 ppt respectively in the Netherlands and 324 ppt and 191 ppt in Italy.

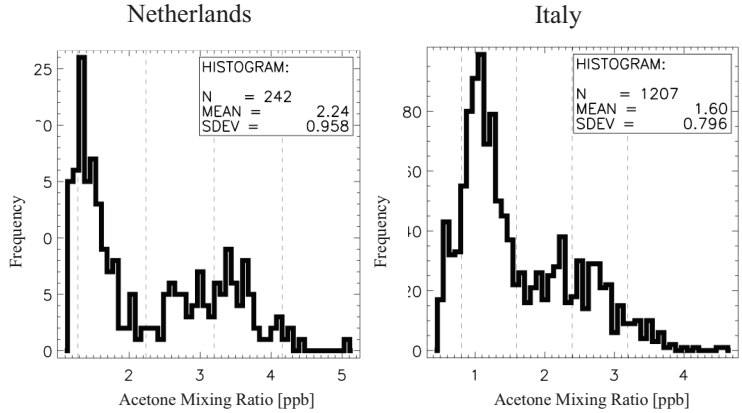

Figure 3.10: Histograms of the acetone mixing ratios from the data obtained in the in the Netherlands and in Italy.

3.3.4 Overall observation for both parts of the campaign

The VOC measurements showed overall low mixing ratios of anthropogenic and biogenic compounds for both parts of the campaign but higher values of oxygenated compounds. The mixing ratios of the AVOCs were higher in the Netherlands compared to Italy. But in Italy the

BOVOCs had higher mixing ratios compared to the Netherlands. This could not be found for the OVOCs as the mixing ratios of acetone, methanol and ethanol were higher in the Netherlands. But acetaldehyde showed higher values in Italy. A detailed analysis of the causes for these observations is given in Chapter 4.3.3.

3.4 Transfer flights

The Zeppelin NT is stationed in Friedrichshafen. To reach the measurement sites in the Netherlands and in Italy it had to be transferred. These measurements facilitated a good cross section of the VOC distribution of southern Europe. Both the transfer to Rotterdam and the transfer from Italy are elaborated in the following. The back transfer flights from the Netherlands and the transfer to Italy could not be evaluated due to missing data

The transfer flights (F006-009) from Friedrichshafen to Rotterdam were flown in two consecutive flight days with an overnight stop in Mainz-Finthen with CL-8 (see Figure 3.11).

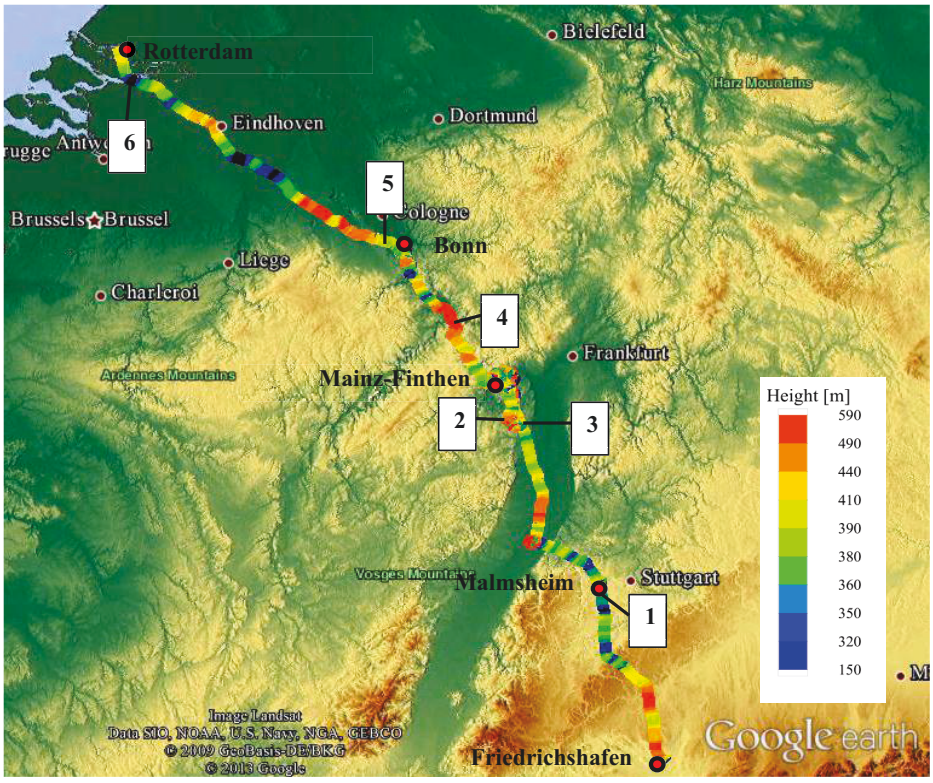

Figure 3.11: Flight track of the transfer flights F006-009 from Friedrichshafen to Rotterdam on May 17th and 18th 2012 with an overnight stop in Mainz-Finthen and refuel stops in Malmsheim and Bonn. The flight track is color coded by the height above ground. The numbers represent the points in the flight track corresponding to the points in the time series (Figure 3.16 - 3.19) where there is a change in the VOC pattern.

The Zeppelin started on the May 17th at 7:30 UTC in Friedrichshafen and landed in Mainz-Finthen at 14:42 UTC. The flight was interrupted for a refuel stop at 9:23 UTC in Malmsheim. On May 18th the Zeppelin started at 8:53 UTC in Mainz-Finthen and landed at 15:55 UTC in Rotterdam with a refuel stop in Bonn at 11:56 UTC. For both flight legs the average traveling height was 402 m Above Ground Level (AGL) with a mean air temperature of 10 °C and a RH of 59 %. The wind speeds were low with 10.8 km/h on the flight to Mainz-Finthen. The wind was coming from the south-east. The wind speeds were higher on the flight to Rotterdam with 21.6 km/h. The wind was coming from the south-east for the first part of the flight until Bonn. Then the wind turned to the south in between Bonn and Roermond before coming from the south-west above the Netherlands.

On the transfer flights to the Netherlands the VOC measurements were interrupted by inflight calibration measurements. This is the reason for the gaps in the data shown in the following. The primary emitted VOCs of the entire transfer flight from Friedrichshafen to Rotterdam were mainly AVOCs (see Figures 3.12 and 3.15). The isoprene mixing ratio was below 34 ppt for the entire flight. The AVOC mixing ratios in the first part of the Flight 006/007 as indicated by pentane and toluene were low (see Figure 3.16). Only after the refuel stop in Malmsheim indicated at point 1 the AVOCs mixing ratios increased as seen in the toluene time series. But in this section the pentane showed a saw tooth structure which is elaborated in Chapter 2.6.3 which disappears again just before point 2. The highest concentrations were observed shortly before reaching Mainz-Finthen (point 2) indicated by high toluene and pentane values.

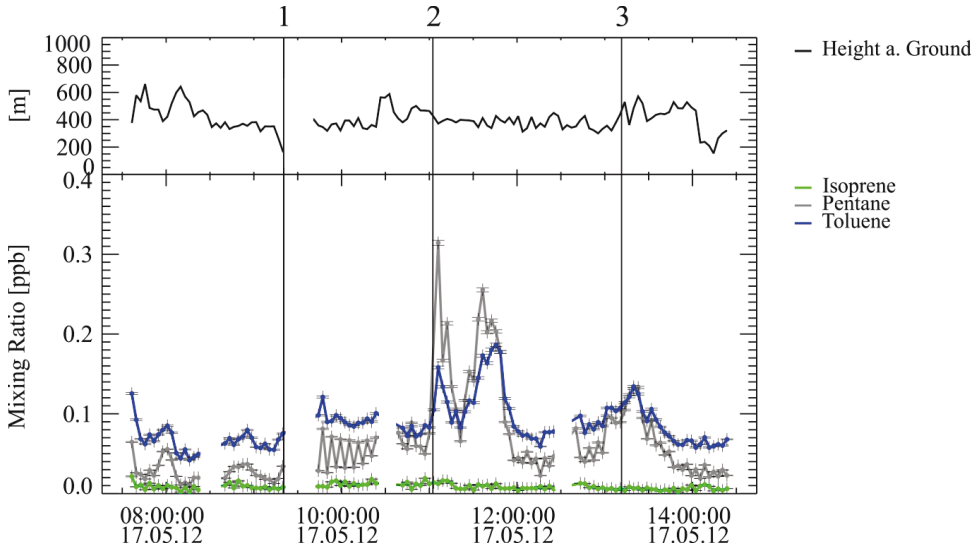

Figure 3.12: The time series of the transfer flight F006/007 from Friedrichshafen to Mainz-Finthen for isoprene, pentane and toluene. The numbers correspond to the points in the flight track indicated in Figure 3.11 and the time is in UTC.

The mixing ratios of the OVOCs displayed only little variation in the first transfer flight to Mainz-Finthen (see Figures 3.13). But just after the start in Friedrichshafen, acetaldehyde showed higher values, especially at higher altitudes with a maximum of 2.5 ppb. The methanol mixing ratios were lower in the first part of the flight. In line with the high concentrations of AVOCs at point 2, methanol also showed higher values with a maximum of 1.6 ppb at the same time. This was also seen a second time at point 3. Acetone and acetaldehyde showed no increase at these two points.

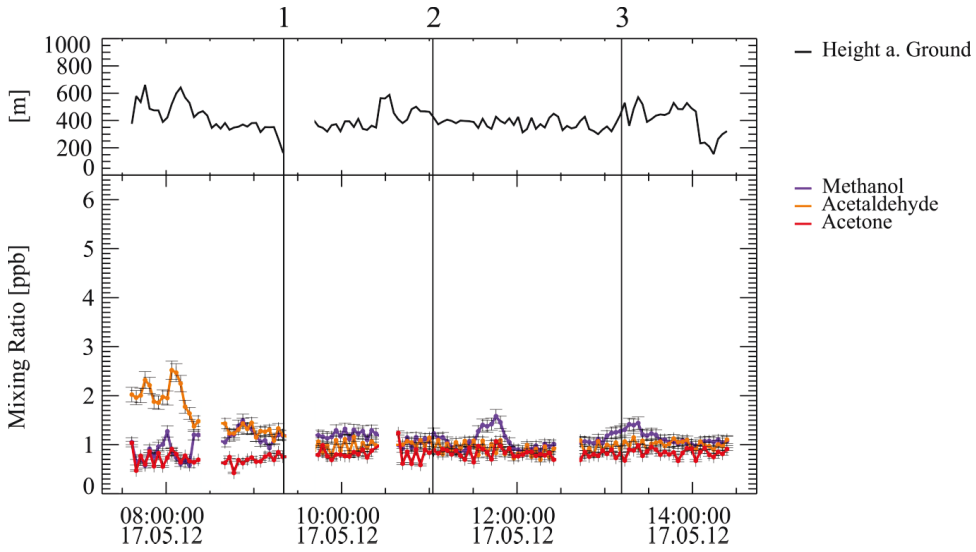

Figure 3.13: The time series of the transfer flight F006/007 from Friedrichshafen to Mainz-Finthen for methanol, acetaldehyde and acetone. The numbers correspond to the points indicated in the flight track in Figure 3.11 and the time is in UTC.

The first part of the second north transfer flight (F008/009) was dominated by high concentrations of AVOCs with a maximum of pentane of 368 ppt at point 4 (see Figure 3.14). The values of pentane and toluene lowered down until the refuel stop at 11:56 UTC in Bonn. After the refuel stop they both increased slightly and the concentrations lowered down to values below 100 ppt. Toluene and pentane increased very steeply close to Rotterdam at point 6 with maximum values of 363 ppt and 234 ppt respectively.

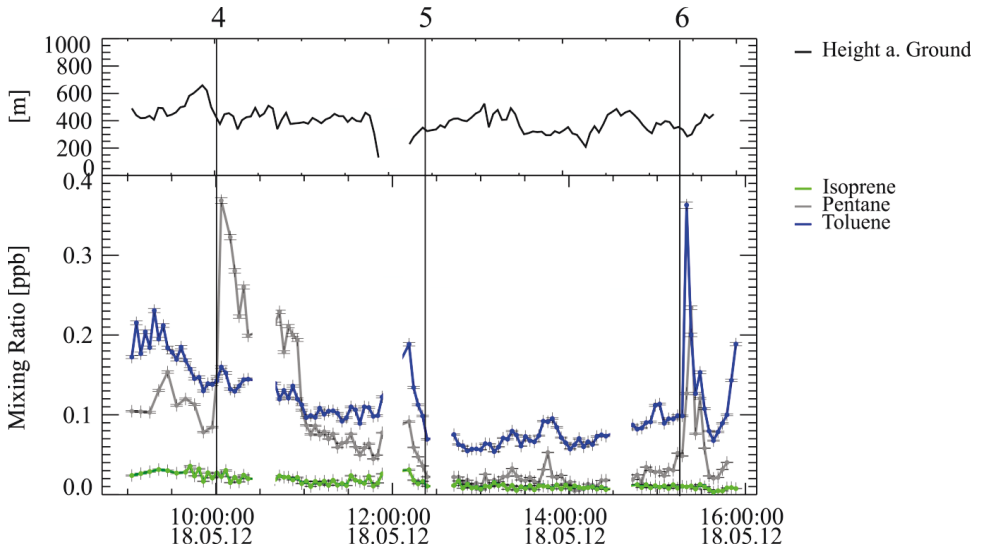

Figure 3.14: The time series of the transfer flight F008/008 from Mainz-Finthen to Rotterdam for isoprene, pentane and toluene. The numbers correspond to the points in the flight track indicated in Figure 3.11 and the time is in UTC.

The OVOCs concentration of the second flight (F008/009) showed higher values compared to the first transfer flight (see Figure 3.15). Especially, the methanol concentration was higher with a maximum of 4.7 ppb. At point 5 the methanol concentration decreased drastically to a value of 2.6 ppb. This was also the same point where the pentane and toluene concentrations decreased. Acetaldehyde again showed higher values in the beginning of the flight that lowered fast with only little variation. For all the OVOCs there was no significant increase in the concentration at point 6 close to Rotterdam. Methanol, acetaldehyde and acetone show this saw tooth structure especially until point 5. This structure vanishes for methanol and acetaldehyde, but not for acetone.

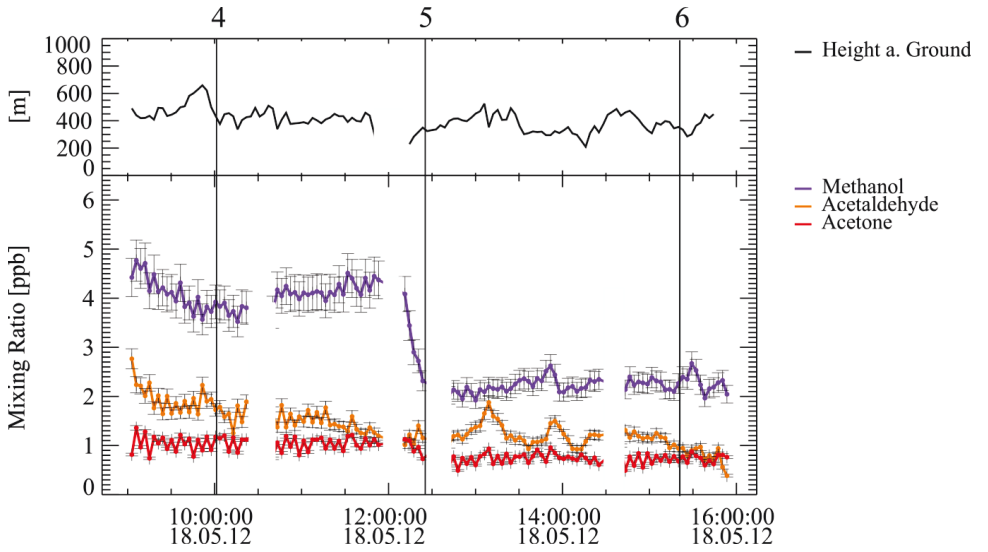

Figure 3.15: The time series of the transfer flight F008/008 from Mainz-Finthen to Rotterdam for methanol, acetaldehyde and acetone. The numbers correspond to the points in the flight track indicated in Figure 3.11 and the time is in UTC.

3.4.1 South transfer flights

The south transfer flights (F051-054) from Bologna to Friedrichshafen were performed in four flight days with overnight stops in Gorizia, Graz and Wels with CL-8. For the flight from Graz to Wels the LDA rack failed and there is no height information. For the last flight from Wels to Friedrichshafen the HGC rack was dismounted due to bad weather. Therefore, only the flight route from Bologna to Graz is discussed in the following. On July 16th 2012 at 9:37 UTC the Zeppelin started in Ozzano and landed at 15:25 UTC in Gorizia (see Figure 3.16). From Gorizia the flight was continued at 6:05 UTC on July 17th 2012 and the Zeppelin landed at 10:15 UTC in Graz.

The mean traveling height above ground was 385 m for both flight legs with an average ambient air temperature of 19 °C and a relative humidity of 45 %. The wind speeds were low with 4.7 km/h on the flight from Ozzano to Gorizia coming from the north-east. For the second flight to Graz the wind speed was 10 km/h coming from the east.

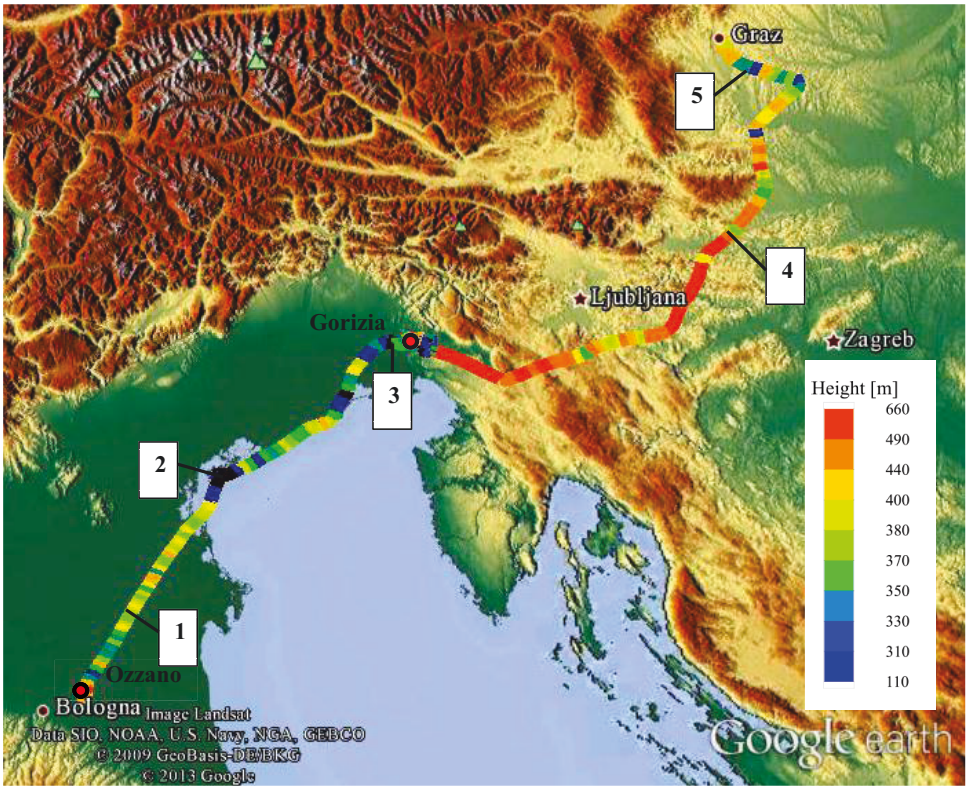

Figure 3.16: Flight track of the transfer flights F051/052 from Ozzano to Graz on July 16th and 16th 2012 with an overnight stop in Gorizia. The flight track is color coded by the height above ground. The numbers represent the points in the flight track corresponding to the points in the time series (Figure 3.21 -3.24) where there is a change in the VOC pattern.

The AVOC mixing ratios of the first south transfer flight from Ozzano to Gorizia showed low mixing ratios which were below 80 ppt (see Figure 3.17). The isoprene mixing ratios were also very low in the beginning of the flight and at point 2 above Venice the values increased slightly. Only at point 3 where the Zeppelin circled above Gorizia the isoprene concentrations enlarged to a maximum value of 161 ppt.

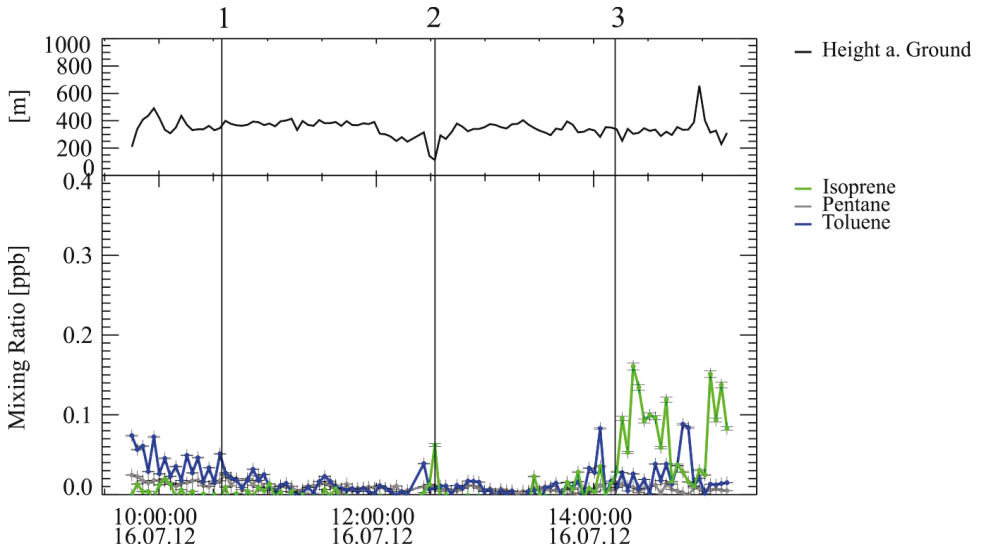

Figure 3.17: The time series of the transfer flight F051 from Ozzano to Gorizia for isoprene, pentane and toluene. The numbers correspond to the points in the flight track indicated in Figure 3.16 and the time is in UTC.

The mixing ratio of acetone showed only little variation throughout the entire flight (see Figure 3.18). The methanol concentration was also relatively constant with little variation around point 2 in Venice and a peak close to Gorizia.

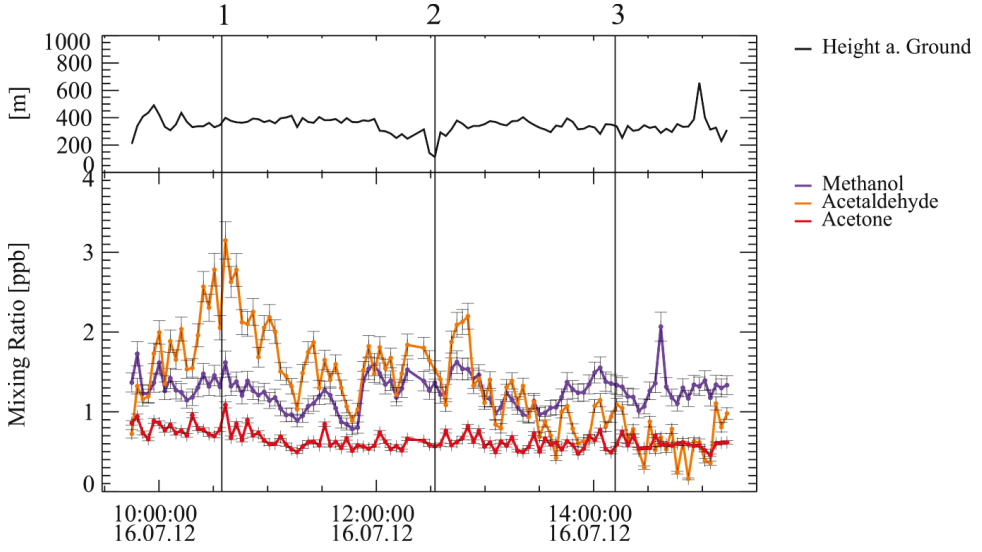

Figure 3.18: The time series of the transfer flight F051 from Ozzano to Gorizia for methanol, acetaldehyde and acetone. The numbers correspond to the points in the flight track indicated in Figure 3.16 and the time is in UTC.

The acetaldehyde mixing ratios were lower in the first part of the flight and increased to a maximum of 3.3 ppb at point 1. Coming closer to Gorizia the concentrations dropped to values below 1 ppb. The concentrations of OVOCs were comparable to the north transfer with the exception of methanol which had higher values.

Compared to the first south transfer flight the AVOC concentrations were higher on the second transfer flight from Gorizia to Graz showing also variability but no peaks (see Figure 3.19). There was only a steep pentane peak with a maximum of 365 ppt at point 4, but toluene showed no increase. The isoprene mixing ratios were also lower compared to the previous south transfer flight with values below 80 ppt and low variation.

Throughout the entire flight the methanol and acetone mixing ratios showed only little change (see Figure 3.20). The methanol concentrations varied between 1.11 and 2.13 ppb whereas the acetone values varied between 0.89 and 2.47 ppb. The acetaldehyde values showed a great variation between values of 3.3 ppb and 1.1 ppb for the first part of the flight and after point 4 the value lowered to 1.5 ppb. At the end of the flight close to Graz at point 5 there was an increase to 2.8 ppb. This was also the same time when methanol increased to a value of 2.1 ppb.

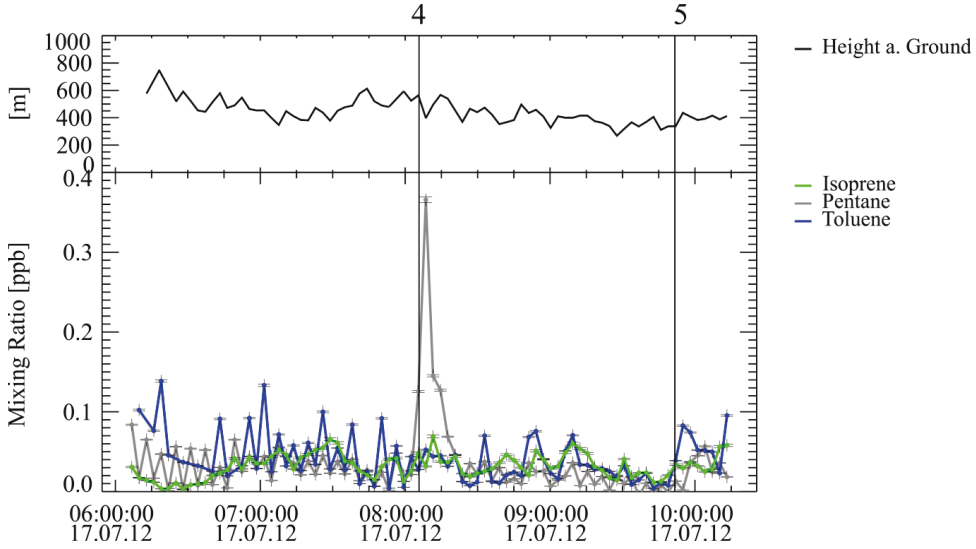

Figure 3.19: The time series of the transfer flight F052 from Gorizia to Graz for isoprene, pentane and toluene. The numbers correspond to the points in the flight track indicated in Figure 3.16 and the time is in UTC.

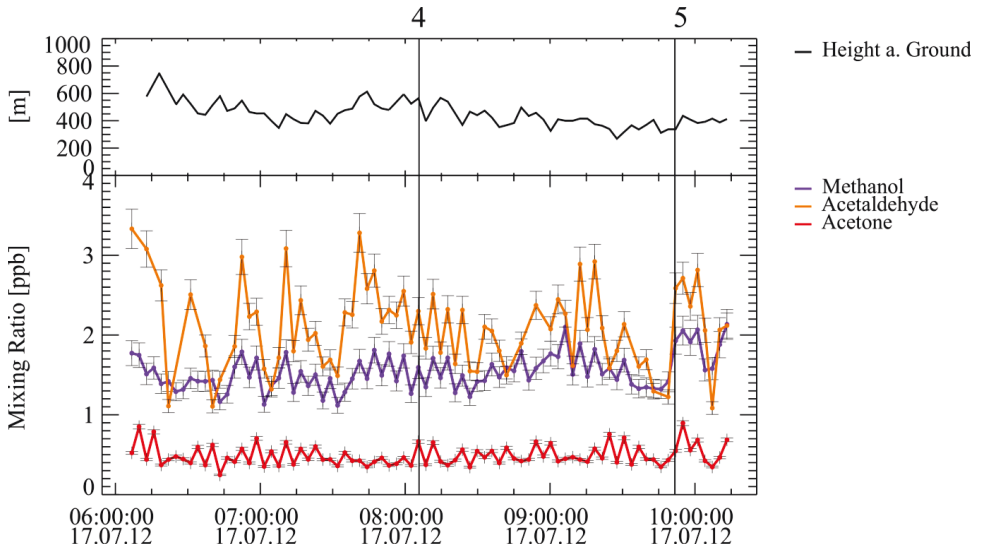

Figure 3.20: The time series of the transfer flight F052 from Gorizia to Graz for methanol, acetaldehyde and acetone. The numbers correspond to the points in the flight track indicated in Figure 3.16 and the time is in UTC.

3.5 Vertical profiles

Vertical profile flights were implemented to analyze the vertical structure of the atmosphere. The focus of these flights was to probe the vertical structure of the PBL, especially the evolvement of the nocturnal boundary layer into the mixed layer which is elaborated in Chapter 4.5. All vertical profile flights in the Netherlands and in Italy were flown above supersites of PEGASOS project partners. For the vertical profile flights the Zeppelin was flying in circles with a diameter of larger than 1 km to prevent sampling the Zeppelin exhaust. The circles were flown at different heights that depended on air regulations and the maximum possible flight altitude of the Zeppelin and therefore varied between 75 and 900 m (AGL). The residence time on each level was between 5 and 20 min, depending on the time resolution of the instruments on board.

During the campaign 15 different vertical profiles were flown with varying residence time at each height. Generally, it could be observed that the mixing ratios at the lower height were higher compared to the mixing ratios at the higher height. Here, also the concentrations of the OVOCs exceeded the concentrations of the AVOCs and BVOCs. In the following the observations of the VOC concentrations for vertical profile flight F023/024 are shown as this flight is representative for all the other vertical profile flights.

3.5.1 Vertical profile flight F023/024

The vertical profile flight F023/024 was performed on the 18th of June 2012 north-east of the Italian supersite SPC with CL-8. The Zeppelin started at 3:20 UTC at Ozzano airport and landed at 9:20 UTC. The flight was intermitted by a refuel stop at 6:55 UTC. During the flight 7 vertical profiles were flown between the two altitudes of 74 and 890 m (AGL) (see Figure 3.21). Each vertical profile had an average duration of 50 min. The residence time on each level was 20 min with a 5 min ascent and descent time. In the following the vertical profile time series is divided into 7 flight sections (FS) which include a vertical ascent and descent.

The vertical profile flights F023/024 were performed on a clear sky day with no precipitation and a relative humidity of 37 %. The average ambient temperature for the entire flight was 23 °C, ranging between 20.5 and 27.5 °C. The wind speeds were low with 7 km/h. The wind was coming from the south-easterly direction. The entire flight was divided into 7 flight sections (FS) which are elaborated in detail in the following.

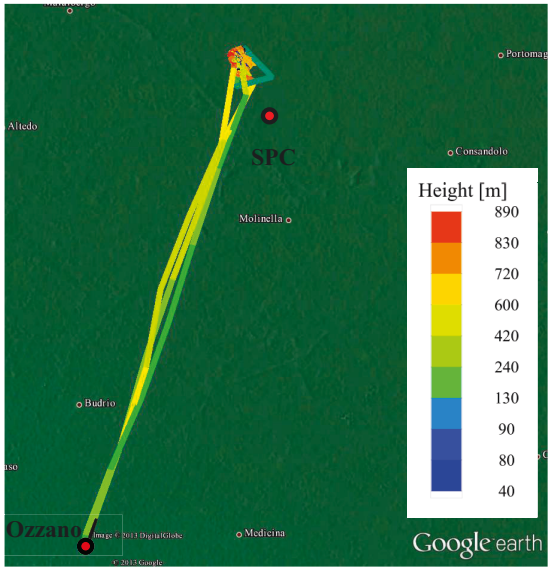

Figure 3.21: Flight track of the vertical profile flight F023/024 near SPC on June 18th 2012. The flight track is color coded by the height above ground.

Anthropogenic and biogenic VOCs, as exemplarily shown by toluene, pentane and isoprene in Figure 3.22 showed a clear height dependency with higher values at lower heights. Isoprene concentrations above the detection limit were only analyzed from FS no. 5 onwards on the contrary toluene and pentane were present in every FS. The first FS at the lower height was dominated by high AVOC mixing ratios as seen in the high toluene concentration of 356 ppt and a pentane concentration of 167 ppt. In the following three flight sections the concentrations of both, toluene and isoprene, decreased. After the third FS the pentane mixing ratio showed no significant height dependency anymore. At higher heights the concentrations of toluene and pentane stayed constant and the isoprene concentrations were below 10 ppt.

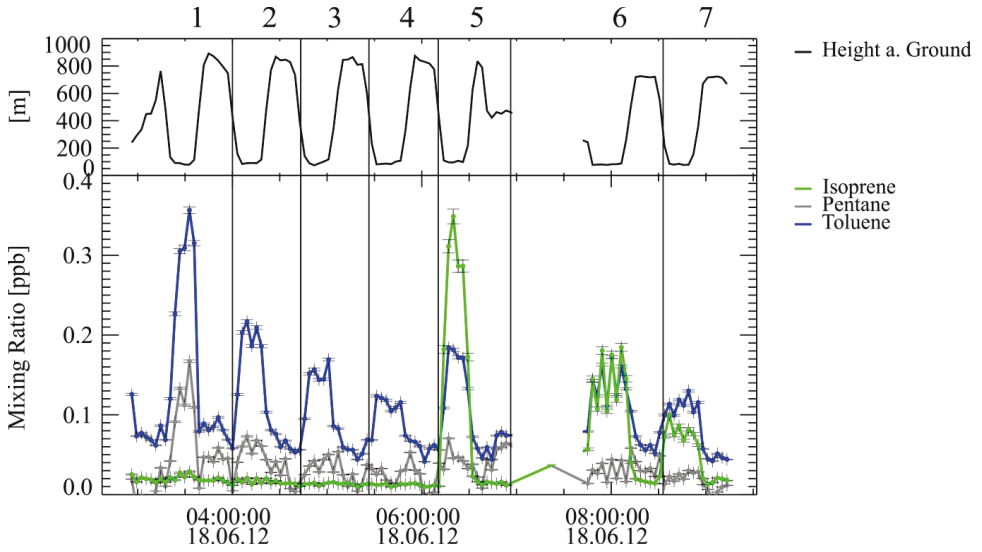

Figure 3.22: The time series of the vertical profile flight F023/024 above the supersite SPC for isoprene, pentane and toluene. The time is given in UTC.

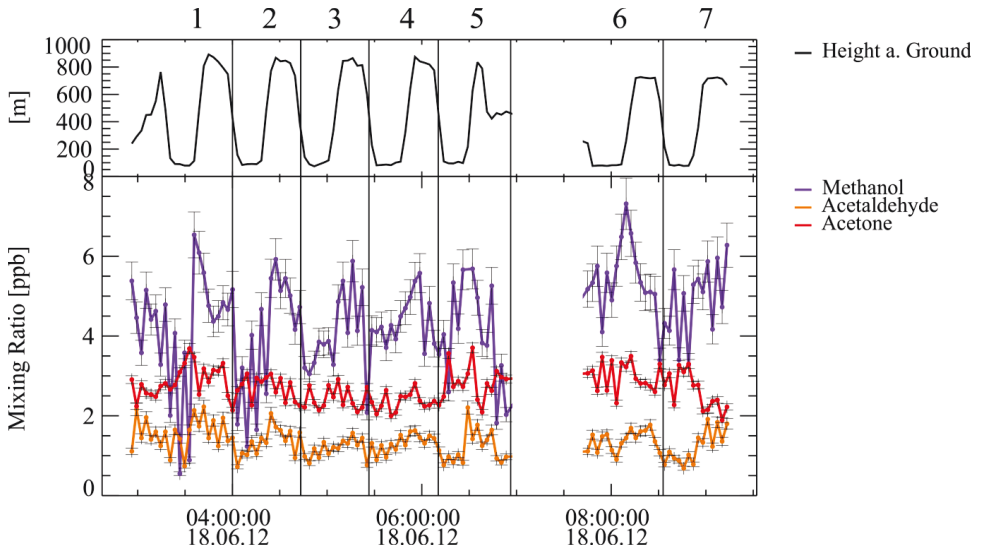

Figure 3.23: The time series of the vertical profile flight F023/024 above the supersite SPC for methanol, acetaldehyde and acetone. The time is given in UTC.

The concentrations of acetaldehyde and acetone showed no pronounced height dependency as for the AVOCs and BVOCs (see Figure 3.23). The mixing ratios of acetone varied between 1.88 and 3.7 ppb whereas acetaldehyde showed lower mixing ratios between 0.68 and 2.2 ppb. The methanol time series differed from the others OVOCs because of some height dependency with higher values at higher heights in FSs 1-4. This slight height dependency disappeared in the following FS.

To demonstrate the difference between the different heights for the different flight sections the vertical profiles are shown for toluene and isoprene in Figure 3.24 for the FS 1, 3, 5, and 7. The ascent and descent could not be analyzed in detail as the time resolution of the HGC was too slow for the fast ascent and descent. For toluene the concentrations were higher closer to the ground for all 4 flight sections and lower at the higher altitudes. In FS7 the difference between the lower height and higher height is the lowest of all profiles. The isoprene concentration was below the detection limit on both heights in FS1 and FS2. Only in FS5 the isoprene concentration rose to a value of 0.3 ppb close to the ground, but not at the higher level. In FS7 the isoprene concentrations were lower at the lower height compared to FS5 but slightly higher isoprene concentrations could be measured on the higher height.

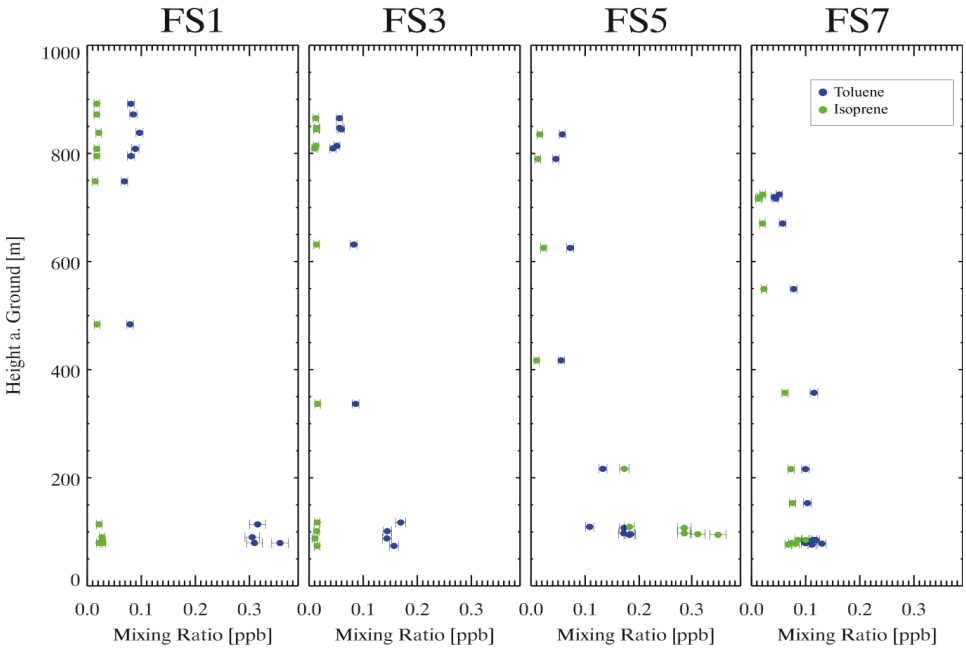

Figure 3.24: Height profiles for FS 1,3,5 and 7 for the vertical profile flight F023/024 above the supersite SPC for isoprene and toluene.

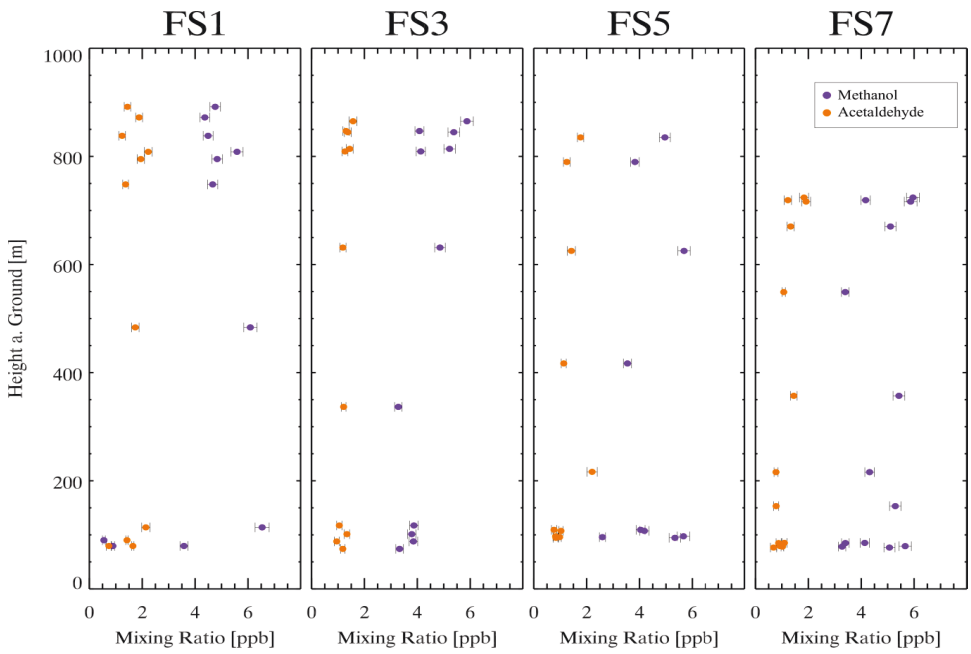

Figure 3.25: Height profiles for FS 1, 3, 5 and 7 for the vertical profile flight F023/024 above the supersite SPC for methanol and acetaldehyde.

Methanol as shown in the vertical profiles in Figure 3.25 showed only in FS1 and 2 a slight inverse height dependency, with lower values at lower heights and higher values at higher heights. But this vanished in FS5 and 7. But the data points show a high scattering. On the contrary the acetaldehyde values show no clear height dependency, but only an overall scattering.

4. Discussion

4.1 The OH reactivity

The removal of most atmospheric trace gases from the atmosphere is initiated by reactions with the hydroxyl radicals (Ehhalt, 1999). The quantification of the OH radical as well as their sources and sinks is necessary to fully comprehend the atmospheric removal processes of trace gases as elaborated in Chapter 1.2.3. Since, the measurement of inorganic species has been well developed over the past decades, the accurate quantification of NO_x, CO and ozone has become possible. However, due to their large variety, research on VOCs suffers from great uncertainties (Goldstein and Galbally, 2007). The measurement of the OH reactivity as the reciprocal of the OH lifetime utilizing the newly developed OH lifetime instrument offers a new way to constrain the total sum of reactive trace gases that react with OH. Previous studies have shown that there can be a significant missing reactivity due to unmeasured species as shown in Table 1.2 in different environments.

The k_{OH}^{calc} in this study was calculated from the measured concentrations of VOCs, HCHO, NO_x, CO, HO_2, HONO and O_3 and their respective rate constants (see Table A.3 in the appendix) as shown in Equation 1.24 in Chapter 1.2.2. Pressure and temperature dependent rate constants were calculated using the respective temperature and pressure values measured at the nose boom (LDA). Data gaps due to different cabin layouts or instrumental failure are corrected for by implementing the campaign median. The methane and hydrogen concentrations were not determined during this campaign. But as they contribute significantly to the total OH reactivity they were set to constant values: 1774 ppb for methane (IPCC, 2007) and 500 ppb for the hydrogen (Grant et al., 2010).

The contributions to the calculated OH reactivity can be subdivided into two major parts: the contribution of inorganic components (k_{OH}(inorg)) and of VOCs (k_{OH}(VOC)). The OH reactivity of the inorganic compounds (k_{OH}(inorg)) was calculated from the contributions of seven different substances, namely NO_2, CO, NO, O_3, HONO, HO_2 and H_2 (see Table 4.1). The k_{OH}(VOC) was calculated from the OH reactivity of 49 different VOCs measured by the HGC, HCHO measured by the FFL and CH_4 which was set to a constant value. To simplify the graphical presentation, the k_{OH}(VOC) was divided into three different classes. The total OH reactivity of the VOC containing one or more oxygen atoms like aldehydes, alcohols, ketones and esters were designated as k_{OH}(OVOC). The total OH reactivity of anthropogenic VOC, e.g. alkanes, alkenes and aromatics was designated k_{OH}(AVOC) and the total OH reactivity of VOC with a biogenic source pooled as k_{OH}(BVOC). Isoprene degradation products as methacrolein (MACR) and methyl vinyl ketone (MVK) are regarded as OVOCs.

Table 4.1: Definition of the calculated k_{OH} for the different classes of trace gases.

Class	Species
k_{OH}(inorg)	NO_2, CO, NO, O_3, HONO, HO_2 H_2 [a)]
k_{OH}(VOC)	all VOC species including CH_4 [a)]
k_{OH}(OVOC)	aldehydes, alcohols, ketones and esters
k_{OH}(AVOC)	alkanes, alkenes (excluding BVOCs) and aromatics
k_{OH}(BVOC)	isoprene, terpenes

[a)] Assumed to be constant: H_2 (500 ppb), CH_4 (1.774 ppm) values taken from Grant et al., 2010 and IPCC, 2007.

4.2 Discussion of errors and uncertainties of the measured and calculated OH reactivity

4.2.1 Random and systematic errors

The uncertainty of the measured total OH reactivity is elaborated in Chapter 2.3.

The uncertainty of the calculated total OH reactivity is dependent on the random and systematic errors, defined as the precision and accuracy of each single measurement [x_i] (see Table 4.2), as well as errors of the respective rate constants. The random error is defined by the statistical error of the single measurements specified by the precision. The error of the rate constant and the accuracy of the measurements are regarded as systematic errors. In the calculation of the errors the possible measurement errors in the temperature and pressure for rate constants and concentrations, were not taken into account as they are negligible small considering the other errors terms.

Table 4.2 The utilized values for the precision and accuracy to determine the random and systematic errors of k_{OH}^{calc}.

Species	Precision (1 σ)	Accuracy (1 σ)	Reference
GC-Data	See Table 2.4	See Chapter 2.5.3	
NO	10 ppt	5 %	Personal communication F. Rohrer
NO_2	30 ppt	7.5 %	Personal communication F. Rohrer
CO	5 ppb	5 %	Personal communication F. Rohrer
O_3	1 ppb	2 %	Personal communication F. Rohrer
HCHO	50 – 600 ppt (3 σ)	15 % + 40 ppt	Personal communication J. Kaiser

The random error of the calculated k_{OH} is determined by the Gaussian error propagation for the measurement of each substance. This results in a median of 4.9 %. The maximum random error observed during the campaign has a value of 21.9 % for the calculated OH reactivity.

For simplification, only the most abundant species making the largest contributions to the k_{OH}^{calc} as acetaldehyde, methanol, ethanol, acetone, isoprene, toluene, formaldehyde, CO, NO, NO_2 and O_3 and their respective error of the rate constant (see Table 4.3) were included into the calculations of the systematic error. Thus, the calculated systematic error has a maximum value of 42 % for all obtained measurements with a median of 13.5 %.

Table 4.3: The error of the rate constants for 298 K.

Specie	Error of the rate constant for 298 K [%]	Source
Acetaldehyde	6	IUPAC (May 2009) [a)]
Methanol	8	IUPAC, (August 2007) [a)]
Ethanol	6	IUPAC, (June 2009) [a)]
Acetone	8	IUPAC, (December 2007) [a)]
Isoprene	6	IUPAC, (May 2009) [a)]
Toluene	10	IUPAC, (July 2008) [a)]
HCHO	8	Atkinson et al. (2006)
CO	10	Atkinson et al. (2006)
NO	20	Evaluation No. 15, JPL Publication 06-2
NO_2	30	Evaluation No. 15, JPL Publication 06-2
O_3	20	Evaluation No. 15, JPL Publication 06-2

[a)] The values were taken from the datasheet published on http://www.iupac-kinetic.ch.cam.ac.uk. The date indicates when the datasheet was last evaluated

4.2.1 Influence of temperature on the calculated total OH reactivity

There is a difference between the temperature and pressure in the flow tube of the OH lifetime measurement cell ($T_{LIF,}$ p_{LIF}) and the ambient temperature ($T_{a,}$ p_a) measured at the nose boom of the Zeppelin. Throughout the campaigns in 2012 the pressure difference was insignificant compared to the temperature with maximum difference between both the T_{LIF} and T_a of 10.5 K. When comparing k_{OH}^{calc} and k_{OH}^{meas} to calculate the k_{OH}^{miss} it is important to take this temperature difference into account. As shown by Lou et al. (2010) the difference in temperature can lead to considerably lower values of -0.5 %/K due to lower number densities in the flow tube and the temperature dependence of k_{OH}.

For most of the flights the temperature difference is low as seen in Figure 4.1, but for some flights there was a large temperature difference between ambient and the measurement cell and together with a high OH reactivity the difference reached a maximum of -0.5 s^{-1}. To compensate for these differences the calculated total OH reactivity was calculated using the parameters of the measurement cell.

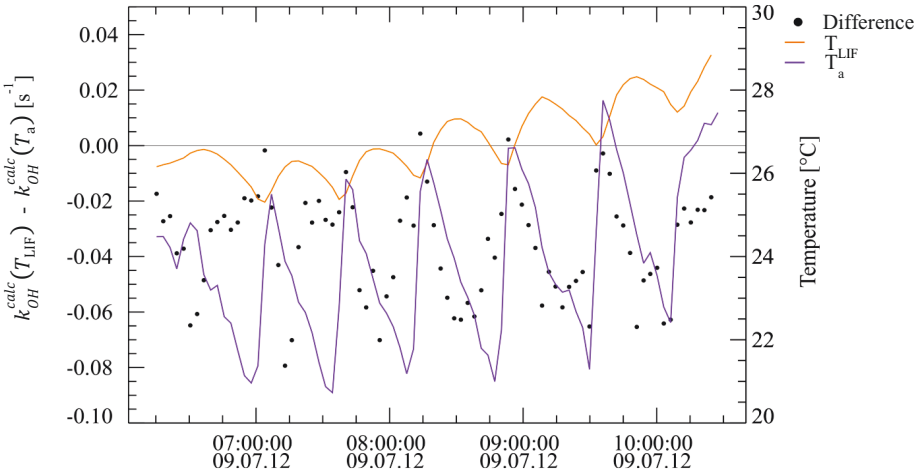

Figure 4.1: Difference between $k_{\mathrm{OH}}^{\mathrm{calc}}$(LIF) calculated with the temperature measured in the flow tube of the OH lifetime instrument (LIF) and $k_{\mathrm{OH}}^{\mathrm{calc}}$ (LDA) calculated with the ambient temperature measured at the nose boom (LDA) for flight F047.

4.3 Overview of the total OH reactivity during the PEGASOS campaign

Prior to analyzing the individual flight patterns the total OH reactivity in the Netherlands and in Northern Italy is compared. For that, the complete set of data measured during the Netherlands and Italy flights excluding the transfer flight was analyzed respectively. This also provides an overview over the attained data. Note, that these aggregated results should only be interpreted with the caveat that different flight patterns, altitudes and layers were probed in each region. Moreover, the aggregation only includes 5 flights in the Netherlands but 20 flights in Italy. In the final dataset all measurement data were synchronized to the GC data. In total, there were 185 observations in the Netherlands and 1464 observations in Italy.

In the following the focus will be on the comparison of the data obtained in the Netherlands and Italy data. Thereafter, the transfer flights and the vertical profile flights will be discussed focusing on the analysis of the evolvement of the nocturnal boundary layer and morning mixing layer.

4.3.1 Observations of the measured and calculated OH reactivity

In general, the OH reactivity measured by the OH lifetime instrument was low for the entire campaign with a median of 4.3 s^{-1} for all the obtained data compared to other studies as outlined in Table 1.2. The total OH reactivity in the Netherlands with a median of 5.7 s^{-1} was larger than in Italy with a median value of 3.7 s^{-1} The variation of the $k_{\mathrm{OH}}^{\mathrm{meas}}$ in the Netherlands and Italy was low as shown in the box and whisker plot in Figure 4.2. The upper

and lower whiskers show the 5 and 95 percentiles of the data. The 25 and 75 percentiles are indicated by the upper and lower band of the box. The line dividing the box indicates the median. This description applies to all the following boxplots.

Comparing the calculated OH reactivity in the Netherlands to Italy data it is evident that the median of the campaign in the Netherlands (5.3 s^{-1}) was well above the median in Italy (3.4 s^{-1}). The variation of the data in the Netherlands was larger in comparison with the Italian data which is indicated by the larger box and the larger whisker range. This is in good agreement to the measured OH reactivity which also showed higher values in the Netherlands (see Figure 4.2). The analysis of the individual contributions to the calculated OH reactivity is elaborated in Chapter 4.3.2.

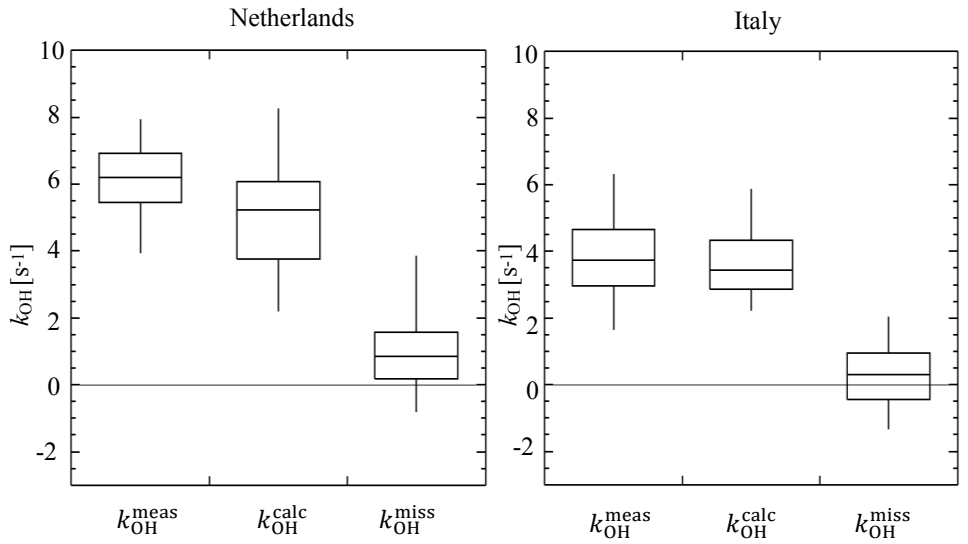

Figure 4.2: The measured and calculated OH reactivity and their corresponding missing reactivity for the campaign in the Netherlands and in Italy without the transfer flights. The bottom and top of the box show the 25th and 75th percentiles with the band inside the box showing the median. The ends of the whiskers represent 5th and 95th percentiles of the data.

The calculated missing reactivity for both parts of the campaign is small. The median for the Netherlands is 0.9 s^{-1} and 0.3 s^{-1} for Italy as shown in Figure 4.2. The variations are larger in the Netherlands compared to the data from Italy as indicated by the larger box and whisker range.

When considering the random and systematic errors for both the measured and calculated OH reactivity for the data obtained in Italy the missing reactivity is not significantly different from zero. Thus, it can be concluded that the OH reactivity calculated from the single measurements represents the measured OH reactivity well. For the data obtained in the Netherlands this is also valid for some of the data points, but there are data points represented by the upper whisker which indicate that there is also in spite of the systematic and random errors a missing reactivity. Thus, there is a significant gap between the measured and

calculated OH reactivity due to unmeasured trace gases. To identify the cause for the missing reactivity, which could originate from unmeasured trace gases from anthropogenic, and biogenic primary emissions, the missing reactivity was correlated to NO_x, toluene and isoprene. Furthermore, correlations between the missing reactivity and height and temperature were examined using the complete dataset. No significant correlation for all the applied parameters was found as r^2 values of the correlations were below 0.2. The identification of the cause of the missing reactivity was analyzed for individual flights, especially the vertical profile flights which is elaborated in Chapter 4.5.4.

4.3.2 Observations of the individual contributions to the OH reactivity

When comparing the individual contributions to the k_{OH}^{calc} of the data obtained in the Netherlands and Italy it becomes evident that the k_{OH}(VOC) was the largest subclass making up 44 % of the total k_{OH}^{calc} in the Netherlands and 61 % in Italy as displayed in Figure 4.3. Notable is that the k_{OH}(OVOC) was the largest class within the k_{OH}(VOC) with a share of 30 % in the Netherlands and 40 % in Italy and therefore of great importance. The other fraction of k_{OH}^{calc} was composed of the inorganic components which were slightly higher in the Netherlands (40 %) compared to Italy (37 %). The k_{OH}(missing) made up a larger fraction in the Netherlands with 16 %. Thus, it is higher compared to Italy with 2 % of the total OH reactivity.

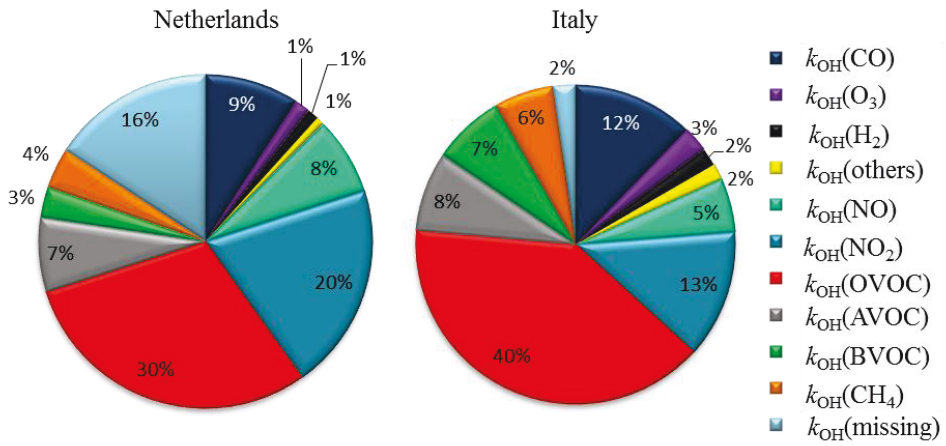

Figure 4.3: Mean k_{OH} contribution for each compound class to the k_{OH}^{calc} including the missing reactivity for both parts of the campaign. k_{OH}(others) contains the combined contributions of HONO and HO_2.

Yet, when comparing the absolute values of k_{OH}(VOC) and k_{OH}(inorg), there was no significant difference between the k_{OH}(VOC) in the Netherlands and Italy (see Figure 4.3). The difference observed in Figure 4.2 is caused by the k_{OH}(inorg), since the fraction of

k_{OH}(inorg) was lower in Italy compared to the Netherlands. Considering the single contributions of the k_{OH}(VOC), the class of the k_{OH}(OVOC) clearly made up the largest fraction in both parts of the campaign (see Figure 4.4). With 68 %, their fraction in Netherlands was slightly larger compared to Italy with 65 %. The contributions of k_{OH}(AVOC), k_{OH}(BVOC) and k_{OH}(CH_4) were below 17 %. The class of k_{OH}(AVOC) made up a slightly higher contribution in the Netherlands (16.4 %) compared to Italy (13.2 %). The k_{OH}(BVOC) on the other side shows a higher contribution in Italy (11.9 %) compared to the Netherlands (6.7 %) and was dominated by isoprene. The contribution of k_{OH}(CH_4) was the lowest with 8.9 % for the Netherlands and 9.8 % in Italy. The explicit analysis for the different VOC classes with median, mean, SD, maximum and minimum is shown in Table A.6 and A.7 in the appendix.

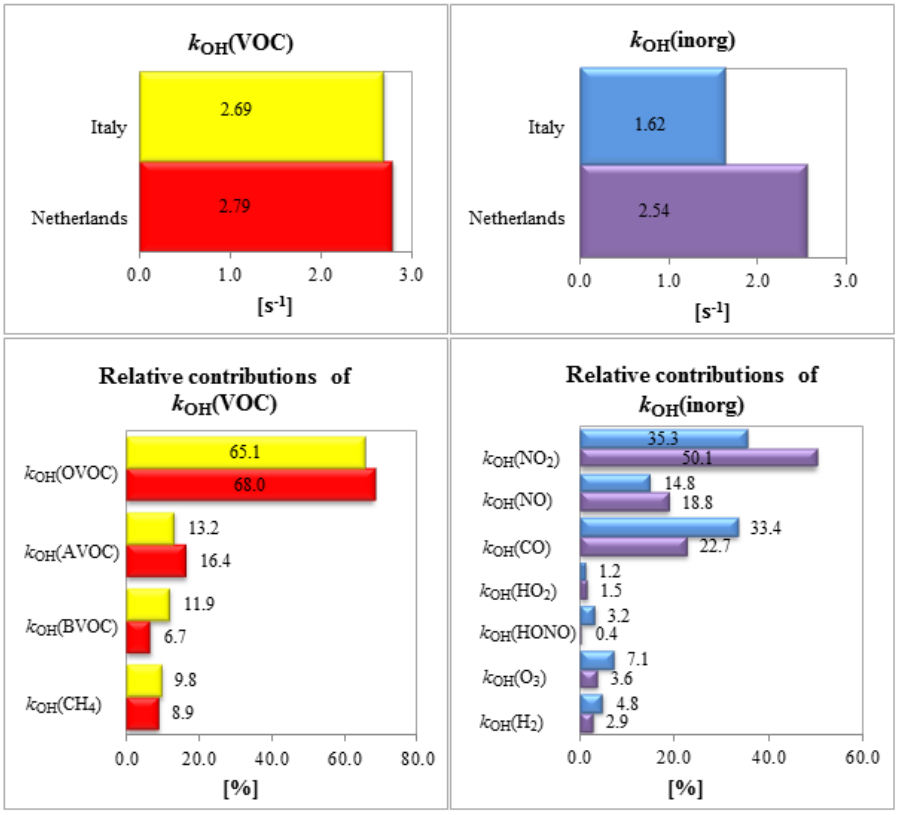

Figure 4.4: Mean values for the calculated k_{OH} values for the Netherlands and Italy campaign separated in k_{OH}(inorg) and k_{OH}(VOC) with the respective individual components. The values of k_{OH}(inorg) and k_{OH}(VOC) are in the dimension of s^{-1} the contributions of each species are in %.

The three main contributors to k_{OH}(inorg) were NO_2, CO and NO. The other species as O_3, HONO, HO_2 and H_2 constituted only minor contributions which was less than 8 %. NO_2 contributed most both in the Netherlands and Italy, but the share is higher in the Netherlands.

This was also the case for NO. On the contrary the contribution of CO was larger in Italy (33.4 %) compared to the Netherlands (22.7 %) although the absolute value was nearly identical with 0.58 s^{-1} in the Netherlands and 0.54 s^{-1} in Italy.

4.3.3 Discussion of the observations of the individual contributions to the OH reactivity

When comparing the measured OH reactivity of this study with a mean of 5.7 s^{-1} in the Netherlands and 3.7 s^{-1} to previous research in Table 1.2 in Chapter 1.2.3 it is evident that the OH reactivity. The sampled air was comparable to the airborne measurements of Mao et al. (2009) above the Pacific Ocean with a mean OH reactivity of 4 s^{-1} analyzing the outflow from Asia. All other studies were performed close to anthropogenic and biogenic sources. There the measured OH reactivity was higher and reached values up to 200 s^{-1}.

The analysis of the single contributions to the calculated OH reactivity shows that the sampled air in both the Netherlands and Italy is dominated by the high value of k_{OH}(OVOC) which shows only little variation. Together with CH_4 and H_2 the OVOCs make up a high fraction of the global background OH reactivity. The importance of OVOCs and the comparison to other studies is elaborated in Chapter 4.3.4.

The other contributions of the primary emitted constituents show local variation. Measurements in the Netherlands display higher contents of primary emissions from anthropogenic origin as shown by the higher share of k_{OH}(AVOC), $k_{OH}(NO_2)$ and k_{OH}(NO) compared to the measurements in Italy. But the biogenic share was higher in Italy compared to the Netherlands. The higher concentrations of anthropogenic emissions in the Netherlands compared to Italy can be explained by the different land use pattern as elaborated in Chapter 3.1. The measurement site in Rotterdam was closer to the large harbor emitting high concentrations of anthropogenic trace gases. High benzene, xylene and toluene concentrations have been reported from ground based measurements in Rotterdam by Guicherit and Schulting (1985). Also other studies as from Keuken et al. (2009) report that other anthropogenic traces as NO_x show higher values in the west of Rotterdam. In this study the NO_x values in the Netherlands also exceed the values in Italy. In Italy the observations seem to contradict previous studies stating that the Po Valley is rich in anthropogenic trace gases (Zappoli et al., 1999). However, only the upper Po Valley close to the cities of Milan and Torino is highly industrialized emitting higher concentrations of anthropogenic trace gases. But the region around Bologna is dominated by cultivated plains. When analyzing the wind directions for the course of the campaign in Italy the wind direction was predominantly from the east, south-east and west (see Chapter 3.2.4). Therefore, the wind was never coming from this polluted region, but from the Adrian Sea, Apennine Mountains and the Tyrrhenian Sea with low primary anthropogenic sources.

The observations also show that the missing reactivity is higher with a mean of 1.4 s^{-1} in the Netherlands compared to Italy with 0.1 s^{-1}. As the anthropogenic OH reactivity had higher values in the Netherlands as well as the missing reactivity it is likely that the missing OH

reactivity may be caused from unmeasured VOCs from an anthropogenic origin. This is further discussed in Chapter 4.5.4. Another possibility for the high missing reactivity in the Netherlands could be the unmeasured ammonia. Ammonia is of great importance in the Netherlands as the emissions are among the highest in the world (Bouwman, 1997). It originates from agricultural sources mainly from the excrement of livestock. The mean annual concentrations of ammonia in the Netherlands are within the range of 2 - 23 $\mu g/m^3$ on the ground (Van Der Eerden et al., 1998). Still, the resulting contribution to the k_{OH} can only reach a maximum value of 0.13 s^{-1} close to the ground. This contribution to the OH reactivity would be too low, in order to significantly increase the calculated OH reactivity in the Netherlands. The contribution of ammonia to the OH reactivity would be very small for the Zeppelin measurements as the measurements were conducted above 100 m (AGL).

4.3.4 Observations of the contribution of the OVOCs to the OH reactivity

Previous research has often neglected the importance of the oxygenated VOCs due to missing techniques to measure them regularly during field campaigns (Apel et al., 2008). However, in the research of the last decade it has become evident that a large number of OVOCs are present in the global troposphere (Singh et al., 2001; Wisthaler et al., 2002). The global carbon flux from OVOCs is estimated to 150 - 500 Tg C yr^{-1} (Singh et al., 2004b). The importance of OVOCs as OH sink is due to their abundant existence rather than their fast reaction with OH (Lewis et al., 2005). OVOCs, especially carbonyl compounds, as acetaldehyde are photolytical precursors of radicals as well as important precursors to peroxyacetyl nitrate (PAN). PAN can then be thermally decomposed and form NO_2 and acetylperoxy radicals. Both influence the oxidizing capacity and the ozone formation potential of the atmosphere (Lloyd, 1979; Singh and Hanst, 1981). OVOCs also contribute significantly to the organic carbon in aerosols by heterogeneous reactions on particles (Li et al., 2001) as well as by forming SOA (Kanakidou et al., 2005).

The sources of OVOCs in the atmosphere are manifold and due to a lack of observations highly uncertain (Singh et al., 2004a) thus the studies conducted show large discrepancies. Yet, OVOCs originate from primary anthropogenic and biogenic sources or are generated in the VOC degradation process in numerous reactions as elaborated in Chapter 1.2.1. When combining the OVOCs as a class, although a fraction is from primary sources, this study shows that OVOCs are the most abundant VOC species for the different parts of Europe analyzed in this study, well exceeding the concentrations of alkanes, alkenes, aromatics and terpenes (see Chapter 3.3). Furthermore, when considering the entire OH reactivity, OVOCs constitute the largest fraction of it (30 % in the Netherlands and 40 % in Italy, see Figure 4.3). This is astounding as there are large differences between the Netherlands and Italy in geography, climate and weather. But all measurement flights were not conducted directly in the source regions (Mega city, forest or industrial centers) where higher k_{OH} values with a lower OVOC fraction would have been measured.

Analyzing the individual contributions to the k_{OH}(OVOC) it becomes evident that the substance class of aldehydes made up the largest contributions with 76 % in the Netherlands and 86 % in Italy (see Figure 4.5). The k_{OH}(alcohol) and k_{OH}(ketone) constitute only a share less than 16 %. The contribution k_{OH}(ester) was very small and therefore not included in the figure.

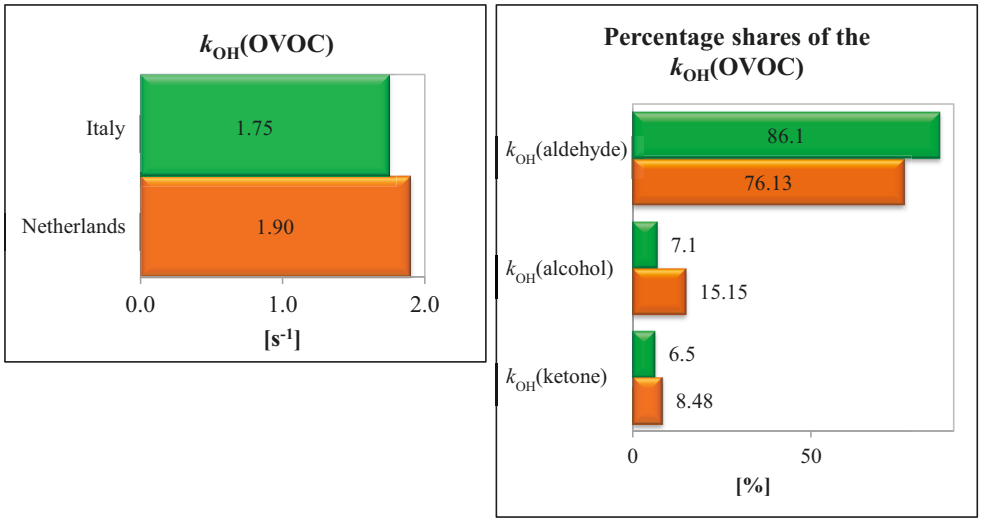

Figure 4.5: Mean values for the calculated k_{OH}(OVOC) values for the Netherlands and Italy campaign and the relative contributions of the individual components. The values of k_{OH}(OVOC) are in the dimension of s^{-1} and the contributions of each species are in %.

Within the class of aldehydes, formaldehyde and acetaldehyde constituted the largest fraction of the total OH reactivity in both, the Netherlands and Italy (see Figure 4.6). But in the Netherlands the mean contributions from HCHO and acetaldehyde were lower compared to Italy. Propanal also constituted a significant portion, however it was lower in the Netherlands as well as the contribution of k_{OH}(others). k_{OH}(others) comprises the sum of small contributions from various aldehydes. Considering the k_{OH}(alcohol), ethanol and methanol make up the largest contributions with higher values in the Netherlands compared to Italy. The k_{OH}(others) of the alcohols was also larger in the Netherlands than in Italy. The k_{OH}(ketone) was generally very small and dominated by MVK which was also larger in the Netherlands compared to Italy. The contribution of slightly MACR was lower as the measured concentrations were lower. But as the contributions of the other aldehydes was so high is falls under k_{OH}(others) of the aldehydes.

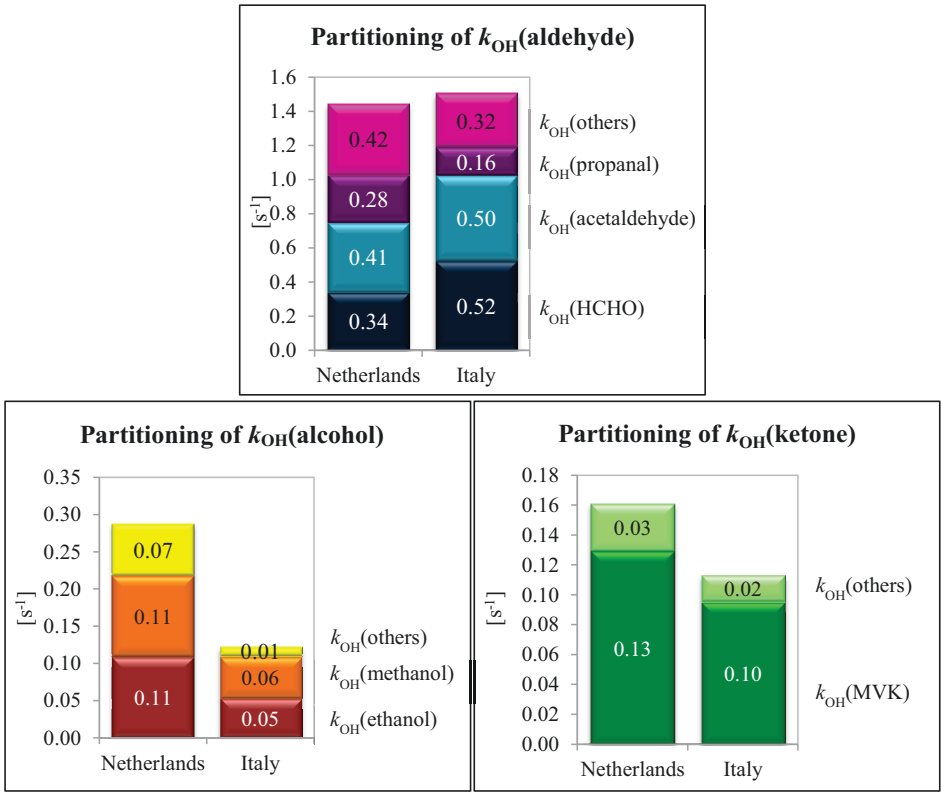

Figure 4.6: The partitioning of k_{OH}(aldehyde), k_{OH}(alcohol) and k_{OH}(ketone) into the contributions of the species with the largest contributions.

4.3.5 Discussion of the contribution of the OVOCs to the OH reactivity

OVOCs have many sources in the atmosphere. They are emitted directly or produced by photochemical degradation processes from AVOCs and BVOCs. But they can also be transported directly or their precursors. Thus, it is impossible with the current data set to elucidate the exact sources of the OVOCs. Only 3D transport models or the analysis of isotopes could offer more insight. But the obtained data reveals indication for potential sources. When analyzing the observations especially of the alcohols the values in the Netherlands exceed the values in Italy significantly. Both alcohols have a primary anthropogenic source and in line with the observations of the total k_{OH}^{calc} showing the sampled air in the Netherlands was affected by higher concentrations of primary emissions as seen by the contributions of NO_x and AVOCs, it can be assumed that parts of the methanol and ethanol were coming from a primary anthropogenic sources. In Italy the majorities of flights were performed above rural areas with low industrial use and therefore lower contributions of anthropogenic primary emissions. But here also methanol and ethanol together with higher contributions of secondary oxidation products as acetaldehyde and HCHO could be analyzed.

Still it is impossible with the current data set to distinguish between OVOCs from primary and secondary sources they are still taken as a group in the following.

Comparing the obtained results to recent studies on the reactivity of OVOCs in different regimes as summarized in Table 4.4, the OVOC contributions range from 3 %, in the urban area of Tokyo in winter, to 80 % in the clean marine air at Mace Head in Ireland. The OVOC fractions obtained in this work would be in between the clean marine air and urban polluted air with an OVOC fraction of 30 % in the Netherlands and 40 % in Italy.

When considering these studies the missing reactivity has been taken into account when calculating the OVOC fraction. But the missing reactivity could also comprise OVOCs. Especially, in the studies of Mao et al. (2009) with a missing fraction 40 % and the measurements of Chatani et al. (2009) in the urban Tokyo with their high missing reactivity of 56 % the reported OVOC fraction could be higher. Thus, the OVOC ratio could be even larger. In this study the missing fraction was very low with 16 % in the Netherlands and 2 % in Italy. Especially, for the data obtained in Italy this missing fraction is small and can be neglected.

Directly in the source regions where the concentrations of primary emitted AVOCs and BVOCs lower OVOC contributions are expected. But, outside this source region, the air is aged and the primary emitted AVOCs and BVOCs have been processed, thus lower AVOC and BVOC contributions but higher OVOC contributions would be expected. But, this problem is even more complex as OVOCs can also be emitted directly.

Table 4.4 The OVOC contributions to the total OH reactivity in recent ground based and airborne field campaigns. For all studies the missing reactivity has been taken into account when calculating the OVOCs fraction.

Publication	**k_{OH}^{meas} [s^{-1}] (mean)**	**k_{OH}^{miss} [s^{-1}]**	**OVOC fraction of k_{OH}^{calc} [%]**	**Observation site**	**Origin of air**	**Measured OVOC species**
Sadanaga et al. (2004)	18	5.3	18	Tokyo, 2003	Urban polluted air	Acetaldehyde, Acetone, Formaldehyde, Methanol, Ethanol
Lewis et al. (2005)	Not measured	-	80[b)]	Mace Head, Ireland	Clean marine air	Acetone, Methanol, Acetaldehyde
Yoshino et al. (2006)	27 18 20 21	8.1 0.9 6 6.3	15 (summer) 7 (winter) 9 (spring) 8 (autumn)	Urban area of Tokyo	Urban polluted air	Formaldehyde, Acetaldehyde, Acetone, Methanol

Publication	k_{OH}^{meas} [s^{-1}] (mean)	k_{OH}^{miss} [s^{-1}]	OVOC fraction of k_{OH}^{calc} [%]	Observation site	Origin of air	Measured OVOC species
Mao et al. (2009)	4 ± 1.0	2.4±0.6	< 20	Airborne measurements between 1-12 km from Alaska and Hawaii analyzing the Asian pollution outflow over the Pacific Ocean	Marine air	Acetaldehyde, Propanal, Acetone, MEK, Methanol, Ethanol
Chatani et al. (2009)	15-55	8.5	13 Incl.	Tokyo 2007	Urban polluted air	Acetaldehyde, Acetone, Formaldehyde, Methanol
Mao et al. (2010)	5-10	[a]	24	Houston 2000	Urban polluted air	Acetaldehyde, Acetone, Formaldehyde, Methanol
	18-33	[a]	14	New York 2001		
	13-30	[a]	14	Houston 2006		
This study	6.1±1.2 3.8±1.4	1.0±1.4 0.1±2.1	30 (NL) 40 (Italy)	Airborne measurements between 100 - 800 m above Rotterdam area and south-eastern Po valley	Clean processed air with a low contributions of primary emissions	Acetaldehyde, Formaldehyde, Methanol, Ethanol, Propanal MVK, etc. see Chapter 2.5.4.

[a] Measured and calculated OH reactivity agree well within measurement and calculated uncertainties. [b] No total OH reactivity measurement.

4.4 A cross-section of the OH reactivity of western and southern Europe

In addition to the comprehensive analysis of the OH reactivity for the regions close to Rotterdam in the Netherlands and Bologna in Italy, the transfer flights to these destinations from and to Friedrichshafen provide insights into the cross section of the OH reactivity over the middle and southern part of Europe. In the following, the transfer flight from Friedrichshafen to the Netherlands and the return flight from Italy will be analyzed in detail. The other transfer flights could not be analyzed as the data set is not complete for the back transfer from Rotterdam and the transfer to Italy.

First, an overview of each transfer flight is discussed. Thereafter, selected flight sections are analyzed in detail. In order to do so, each transfer flight is divided into several sections. The data points within these consecutive sections are characterized by similar OH reactivity contributions of the inorganic compounds (k_{OH}(inorg)) and VOCs (k_{OH}(VOC)).

4.4.1 North transfer flight

The transfer flight from Friedrichshafen to Rotterdam was performed on the 17th and 18th of May 2012 and divided into two flight legs. The first flight leg (F006/007) started in Friedrichshafen and ended in Mainz-Finthen with a refuel stop in Malmsheim. The second flight leg (F008/009) was from Mainz-Finthen to Rotterdam with a refuel stop in Bonn (see Figure 4.7). The mean travelling height for both flight legs was 400 m (AGL). The mean air temperature was 10 °C and there was no precipitation. The wind speed was low with 3 m/s from the south easterly directions for the first flight leg. For the second flight leg the wind speed was higher with a mean speed of 6 m/s coming from the south-east for the first sub section, between Mainz-Finthen and Bonn, then from the south for the sub-section from Bonn to Roermond. The wind direction turned to south-west during the flight over the Netherlands. The flight track in Figure 4.7 is color coded according to the calculated OH reactivity. For this calculation the ambient (LDA) temperature and pressure parameters were used. Several calibration measurements of the HGC were conducted during the transfer flight, marked black on the flight track in Figure 4.7. The k_{OH} measurements only covered a limited period of the whole flight and are shown in Figures A.1 and A.2 in the appendix.

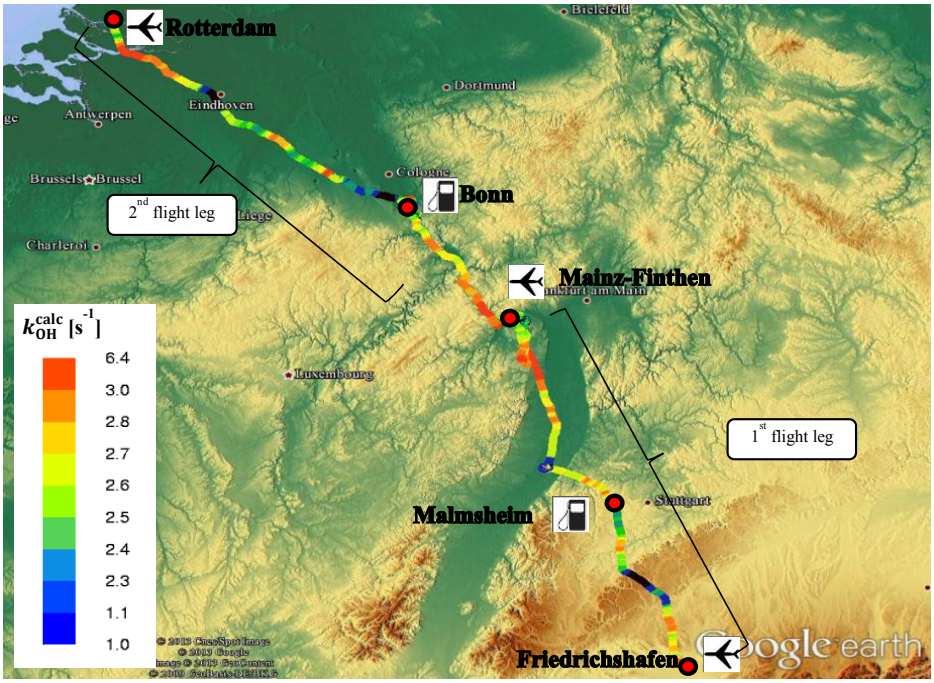

Figure 4.7: Transfer flight (F006-009 - CL-8) from Friedrichshafen to Rotterdam with an overnight stop in Mainz-Finthen and two refuel stops in Malmsheim and Bonn on May 17th and 18th 2012. The flight track is color coded according to the k_{OH}^{calc}. The sections of the flight track colored in black indicate calibration measurements of the HGC.

Overall, the OH reactivity was relatively low (see Table 1.2) for both transfer flight legs with a mean k_{OH}^{meas} value of 3.5 s^{-1} for the first and 3.4 s^{-1} for the second flight leg (see Table 4.5). A more detailed overview including the mean, standard deviation, maximum- and minimum

levels of reactivity is shown in Table A.6/A.7 in the appendix. The mean k_{OH}^{calc} value was 2.7 s^{-1} for the first and 3.4 s^{-1} for the second flight leg. The calculated missing reactivity was low with a mean value of 0.7 s^{-1} for the first and 0.6 s^{-1} for the second flight leg. Accounting for the random and systematic errors of the k_{OH}^{meas} and k_{OH}^{calc} measurements, as displayed in Figures A.3/A.4, the missing reactivity is not significant.

Table 4.5: Overview of the mean k_{OH}^{meas}, k_{OH}^{calc} and k_{OH}^{miss} values.

	k_{OH}^{meas} [s^{-1}]	SD [s^{-1}]	Accuracy [s^{-1}]	k_{OH}^{calc} [s^{-1}]	SD [s^{-1}]	Accuracy [s^{-1}]	k_{OH}^{miss} [s^{-1}] [b]
1. leg	3.5	0.9	0.59	2.7 2.8 [a]	0.9 0.9 [a]	0.43 0.45 [a]	0.7 [a]
2. leg	3.3	0.6	0.58	3.4 2.7 [a]	0.6 0.8 [a]	0.48 0.35 [a]	0.6 [a]

[a] For the sections when k_{OH}^{meas} data is available.

When analyzing the mean contributions of the different species to the OH reactivity for both flight legs (see Figure 4.8), it becomes evident that NO_x and CO made up the largest contributions to the k_{OH}(inorg). Furthermore, k_{OH}(OVOC) makes up the largest fraction of the k_{OH}(VOC). The contributions of AVOC and BVOC were minor. Also in the part of the flight above the black forest the biogenic emissions were very small. Due to the low temperature and the high flight altitude the isoprene contribution was very small. The small contribution of terpenes is in line with previous studies by Jüttner (1988) which showed that the trees in the black forest only emit low concentrations of monoterpenes.

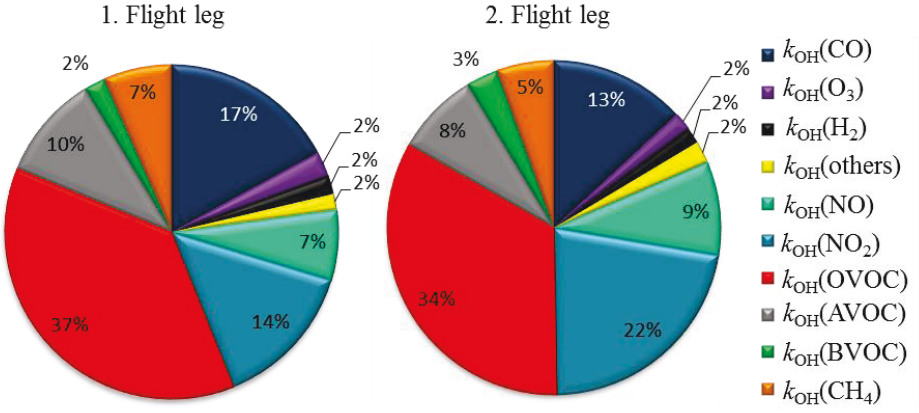

Figure 4.8: Mean k_{OH} contribution for each species to the k_{OH}^{calc} for both flight legs.

When comparing both flight legs, the contribution of NO_x was lower in the first leg compared to the second leg. Equally, the contributions of k_{OH}(AVOC) and k_{OH}(CO) increased from the first- to the second leg. An explanation for these differences may be the different land use patterns of the regions which were probed. Particularly, during the first flight leg, which

covered parts of the black forest, less primary anthropogenic emissions but more OVOCs were measured. In comparison, during the second flight leg, larger contributions of primary anthropogenic emissions and less OVOCs were measured across the industrially developed regions of the upper Rhine valley and the highly populated Netherlands.

For Figure 4.8 the missing reactivity was neglected as the OH lifetime instrument only functioned for a limited time. These observations are in line with the observations of the VOC measurements as displayed in Chapter 3.4.1.

4.4.1.1 Analysis of the entire flight track

The entire flight track of the north transfer was then divided into 10 sections according to similarities in the single k_{OH} contributions as elaborated in Chapter 4.4.1.2. Despite the overall low OH reactivity, significant differences in the contributions to the OH reactivity can be observed along the flight track. Based on the contribution of NO_x to k_{OH}, flight sections can be grouped into 3 separate categories as shown in Table 4.6.

Table 4.6: Overview of the different categories.

Category	NOx Contribution [s^{-1}]	Color code
I	< 0.4	green
II	0.5 – 1	blue
III	> 1	red

The first category represents sections with low NO_x contribution to the total OH reactivity of < 0.4 s^{-1}. The second category represents flight sections with medium NO_x values between 0.5 and 1 s^{-1} and the third category summarizes sections with a NO_x contribution to the k_{OH} of 1 s^{-1} and more.

Table 4.7: Absolut mean values of the $k_{OH}(NO_x)$, k_{OH}^{calc}, k_{OH}(other), k_{OH}(AVOC), k_{OH}(BVOC), k_{OH}(OVOC) and the ratio k_{OH}(OVOC)/k_{OH}(VOC) for the 10 sections and the corresponding categories of the north transfer flights.

Category	Section	Mean $k_{OH}(NOx)$ [s^{-1}]	Mean k_{OH}^{calc} [s^{-1}]	Mean k_{OH}(other) [a)] [s^{-1}]	Mean k_{OH}(AVOC) [s^{-1}]	Mean k_{OH}(BVOC) [s^{-1}]	Mean k_{OH}(OVOC) [s^{-1}]	Ratio k_{OH}(OVOC)/ k_{OH}(VOC) [s^{-1}]
I	1	0.22	2.47	0.63	0.28	0.09	1.08	0.66
I	2	0.31	2.34	0.64	0.22	0.08	0.92	0.67
I	7	0.38	2.35	0.55	0.18	0.12	0.91	0.64
II	3	0.66	2.78	0.63	0.27	0.08	0.93	0.63
II	4	0.56	2.66	0.64	0.26	0.07	0.93	0.63
II	8	0.75	3.02	0.56	0.19	0.12	1.19	0.69
II	9	0.71	2.73	0.55	0.18	0.10	0.97	0.66

Category	Section	Mean $k_{OH}(NOx)$ [s^{-1}]	Mean k_{OH}^{calc} [s^{-1}]	Mean $k_{OH}(other)$ [a] [s^{-1}]	Mean $k_{OH}(AVOC)$ [s^{-1}]	Mean $k_{OH}(BVOC)$ [s^{-1}]	Mean $k_{OH}(OVOC)$ [s^{-1}]	Ratio $k_{OH}(OVOC)/k_{OH}(VOC)$ [s^{-1}]
III	5	1.54	3.91	0.63	0.34	0.06	1.14	0.65
III	6	2.01	5.09	0.76	0.43	0.17	1.52	0.65
III	10	1.42	3.37	0.58	0.33	0.06	0.78	0.56

[a] k_{OH}(other) includes the contributions of CO, O_3, HO_2 and HONO.

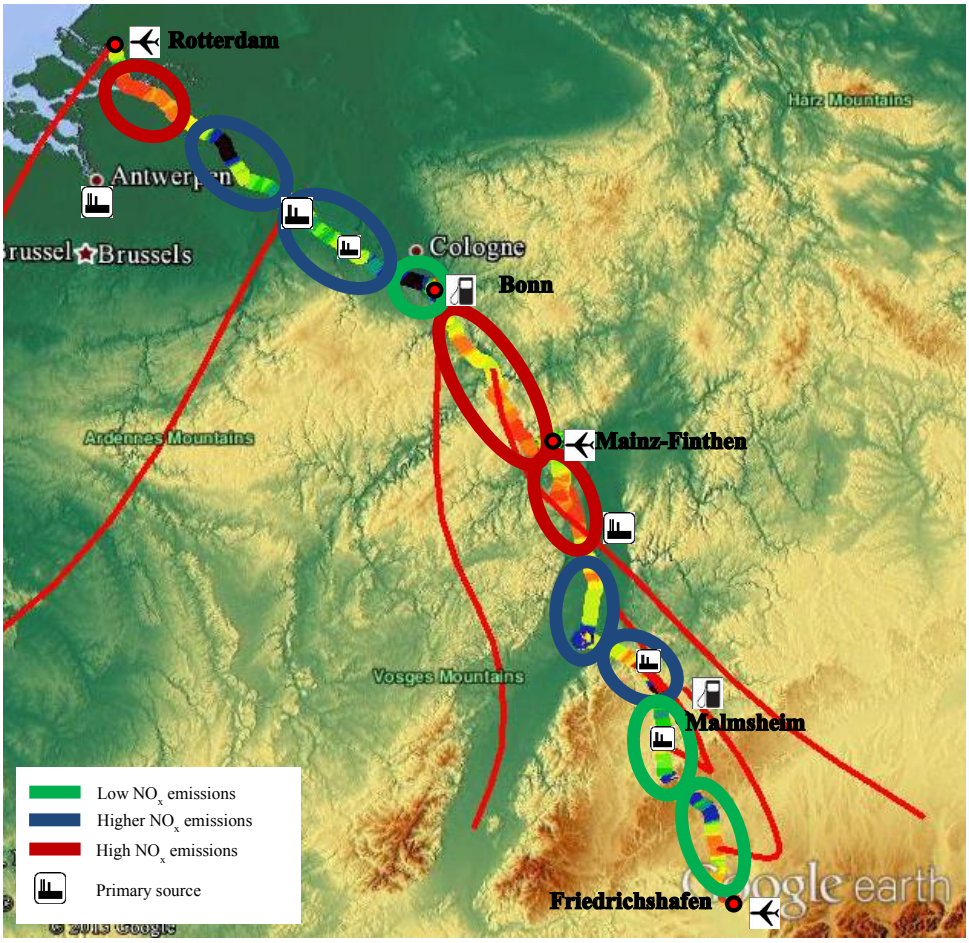

Figure 4.9: Analysis of the flight track grouped into three emission categories for the north transfer flight from Friedrichshafen to Rotterdam. The HYSPLIT back trajectories are shown as red lines.

The category I (marked green in Figure 4.11 and Table 4.7) indicates the parts along the flight track with very low NO_x contribution of below 0.38 s^{-1}. The mean k_{OH}^{calc} values in these regions were below 2.5 s^{-1}. The mean k_{OH}(AVOC) was low as well as the k_{OH}(BVOC). The k_{OH}(OVOC) values were high and above 0.9 s^{-1} and the ratio k_{OH}(OVOC)/k_{OH}(VOC) was constant at 0.65. This category could only be identified in the first flight track across the black forest and after the refuel stop in Bonn.

Second, the parts of flight track over areas that have larger NO_x emissions (marked blue in Figure 4.9 and Table 4.7) were grouped in category II. Here the $k_{OH}(NO_x)$ was larger as in category I and in the range of 0.5 and 1 s^{-1}. The overall k_{OH}^{calc} values were between 2.5 and 3 s^{-1} but the mean k_{OH}(AVOC) and k_{OH}(BVOC) values were comparable to category I. Also the k_{OH}(OVOC) showed an increase as well as the k_{OH}(OVOC)/k_{OH}(VOC) ratio. But within these areas some strong primary emission sources were identified, which were marked in by factory pictograms in Figure 4.9. This was not the case in in category I. Observations that fall under this category II were found along the A8 highway from Malmsheim to Karlsruhe and on the flight part from Bonn until Eindhoven.

All flight parts across regions with high NO_x emissions were grouped into the third category (marked red in Figure 4.9 and Table 4.7). In these areas the k_{OH}^{calc} values exceed values of 3 s^{-1}, reaching maximum mean values of 5 s^{-1}. There were two main regions that fall under this category: first the region north of Karlsruhe to Bonn and second, south-east of Rotterdam.

In the first region considered as category III, the higher k_{OH}^{calc} values derive from the higher NO_x and AVOCs. But there was also an increase in the k_{OH}(OVOC) to values above 1 s^{-1} mainly from alcohols (see Chapter 3.4.1). As with the OVOCs, NO_x and AVOCs also increased, it can be assumed that the measured OVOCs originate from primary sources. This primary source of OVOCs also causes the k_{OH}(OVOC)/k_{OH}(VOC) ratio to be comparable to the category I and II. This characteristic pattern can be seen on two consecutive flight days: firstly, south of Mainz-Finthen on the first flight leg and secondly north of Mainz-Finthen on the second flight leg. Also, the k_{OH}(OVOC)/k_{OH}(VOC) ratio has the same value for both days. The analysis of the HYSPLIT back trajectories (Rolph, 2013) enables the identification of sources. This indicates that this sampled plume was coming from the highly industrialized Mannheim/Ludwigshafen region with high solvent use (Ibrahim et al., 2010).

The higher k_{OH}^{calc} values in the second main region under category III, derived from higher NO_x and AVOC contributions. Here, there was no increase in the OVOC contributions as for the plume originating from the Mannheim/Ludwigshafen region. Thus, the k_{OH}(OVOC)/k_{OH}(VOC) ratio decreased to a value of 0.56. The analysis of the back trajectories showed that this plume came from Antwerp with its large harbor with high anthropogenic emissions (Dewulf et al., 1998).

4.4.1.2 Detailed analysis of the first 5 section of the north transfer

In the previous chapter the overall flight track was analyzed in terms of low, medium and high NO_x contributions to the calculated k_{OH}. This analysis was based on the sections shown in Figures 4.10/4.11 and Figures A.5- A.8. In the following the flight track between FN and Mainz is analyzed in more details to provide insights how specific sources contribute to the local k_{OH}. This part of the flight track included examples of all three categories mentioned in Chapter 4.4.1.1.

The k_{OH}^{calc} values in the 1st section were very low when compared to the overall measurements during the flight. All values were below 3 s^{-1} as shown in Figure 4.10 with the exception of

the first part close to Friedrichshafen (maximum values of 5.5 s^{-1}). Predominantly, OVOCs contributed to the k_{OH}^{calc} while NO_x made up a very small fraction of only 9 %. The air for flight section 1 comprised only a small fraction of primary anthropogenic emissions but a large fraction of OVOCs.

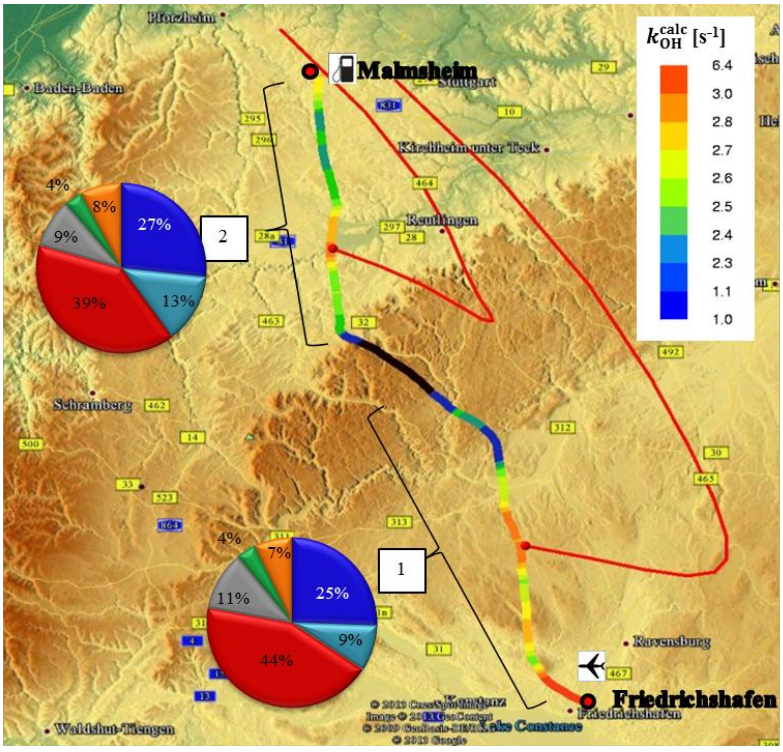

Figure 4.10: Flight from Friedrichshafen to the refuel stop in Malmsheim (F006) color coded by the total k_{OH}^{calc} divided into two sections. The red lines show the 12 h back trajectories for 400 m (AGL). The pie charts resemble the partitioning of k_{OH}^{calc}. Sections in dark blue represents kOH(others), which is the sum of $k_{OH}(CO)$, $k_{OH}(HO_2)$, $k_{OH}(HONO)$, $k_{OH}(O_3)$ and $k_{OH}(H_2)$, light blue $k_{OH}(NO_x)$, red k_{OH}(OVOC), gray k_{OH}(AVOC), green k_{OH}(BVOC) and orange $k_{OH}(CH_4)$.

The 2nd section was also characterized by low k_{OH}^{calc} values. The overall distribution amongst the different constituents had changed slightly to a higher $k_{OH}(NO_x)$ and a higher k_{OH}(OVOC) compared to the 1st section. This showed that the air consists of fresher anthropogenic emissions. The peak of the OH reactivity derived from larger contributions of OVOCs. Using the back trajectories these OVOCs may have come from the emissions by the cities Rottenburg, Reutlingen and Tübingen in the Neckar valley (see Figure 4.10).

The 3rd section covers the flight track above the A8 highway, showing a homogenous k_{OH}^{calc} pattern with little variation around the mean OH reactivity of 3 s^{-1} (see Figure 4.11). Notably, the $k_{OH}(NO_x)$ increases and the OVOC contribution to the OH reactivity was reduced when compared to the previous section. Based on this shift of contributions, combined with the information provided by the back trajectories, it is reasonable to conclude that the air masses

along the 3rd section were directly influenced by emissions from vehicles on the highway and/or the industrial emissions around Stuttgart.

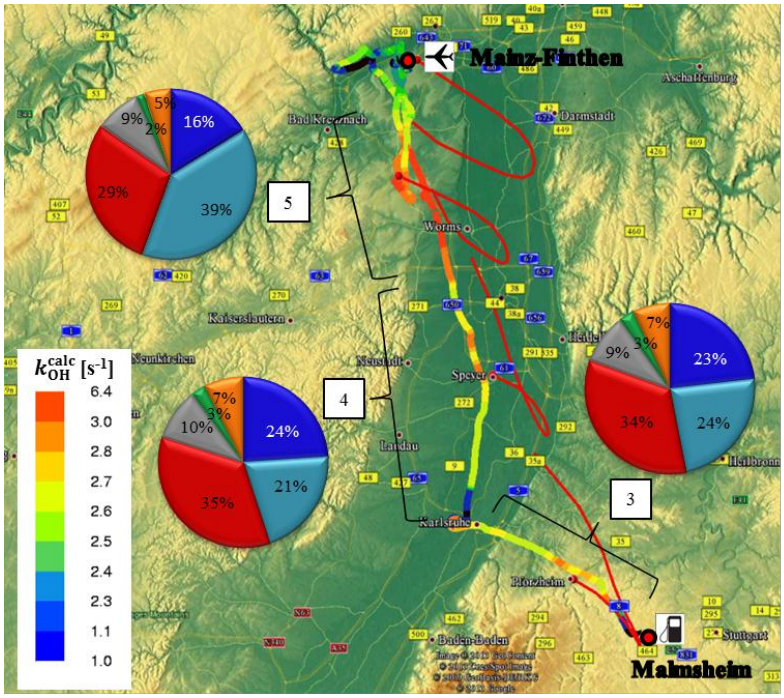

Figure 4.11: Flight track from Malmsheim to Mainz-Finthen (F007) color coded by the total k_{OH} divided into three sections. The red lines show the 12 h back trajectories for 400 m (AGL). The pie charts resemble the partitioning of k_{OH}^{calc}. Sections in dark blue resembles k_{OH}(others), which is the sum of k_{OH}(CO), k_{OH}(HO_2), k_{OH}(HONO), k_{OH}(O_3) and k_{OH}(H_2), light blue k_{OH}(NO_x), red k_{OH}(OVOC), gray k_{OH}(AVOC), green k_{OH}(BVOC) and orange k_{OH}(CH_4).

The 4th section hardly differed from the 3rd section. The NO_x ratio was lower and the OVOC and anthropogenic ratios were both 1% larger. This indicated that the sampled air was still anthropogenically dominated but with a different AVOC/NO_x ratio.

The 5th section showed the highest k_{OH}^{calc} values of this entire flight leg, well exceeding 5 s^{-1} (see Figure 4.13). The k_{OH}^{calc} was dominated by non VOC contributions, particularly by NO_x which made up 39 %. But, also the contributions of alkanes, aromatics, ethanol, and methanol were larger compared to the previous flight sections. These findings support the assumption of previous studies that a major proportion of alcohols are primarily emitted and not photochemically produced (see also Figure 3.13). The back trajectories showed that the air was coming from the highly industrialized Mannheim/Ludwigshafen region (Ibrahim et al., 2010). This sampled plume was very stable and was detected in a second flight loop more to the west 1.5 h later with slightly lower values.

The other flight sections not shown in detail indicate that the air from Mainz-Finthen to Rotterdam was also relatively clean. But in the region before Rotterdam higher k_{OH} values

could be measured due to higher NO_x contributions. The back trajectory analysis showed that the air originated from the highly industrialized region around Antwerp.

4.4.2 South transfer flight

The back transfer (F051/F052/F053/F054) from Italy was performed on four flight days between the 16th and 19th of July 2012 with overnight stops in Gorizia, Graz and Wels. Hence, the flight track was divided up into four flight legs (see Figure 4.12). In the following only the first two flight legs are discussed in depth. For the 3rd flight leg there is no altitude and k_{OH}^{meas} data as the LDA rack and the LIF system were malfunctioning during the flights. For the 4th section the HGC instrument had to be disassembled from the Zeppelin because of bad weather conditions.

The mean travelling height for both the first and the second flight leg of the south transfer was 385 m (AGL). During these two flights the mean ambient air temperature was 19.5 °C. The wind speed at departure in Bologna was 8 m/s. The wind was coming from the north-east during the first flight. For the second flight leg the wind speed was 7 m/s in Gorizia. The wind was coming from the east. The flight track in Figure 4.12 is color coded based on the calculated OH reactivity. A detailed overview including the respective contributions to the k_{OH}^{calc} across the entire two flight legs is shown in Figures A.9 and A.10 of the appendix.

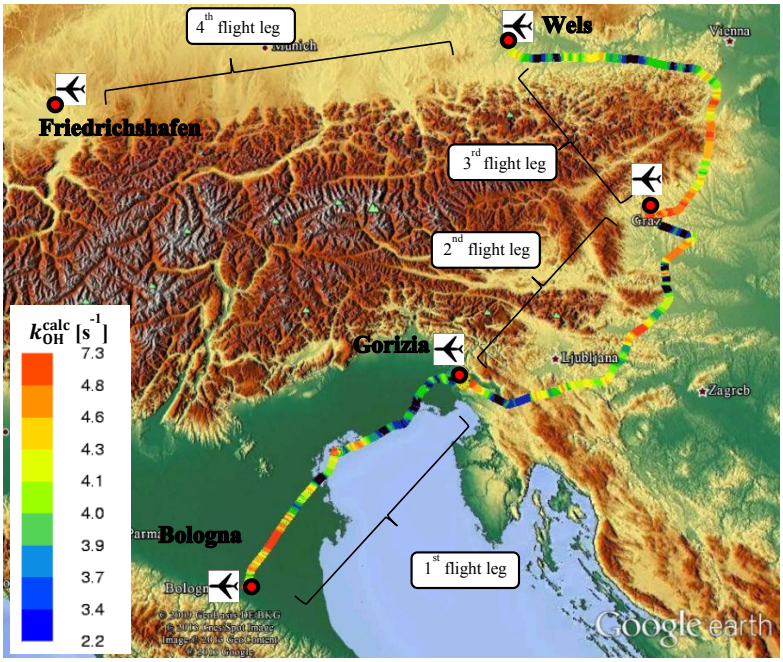

Figure 4.12: South transfer flight (F051/F052/F053/F054 - CL-8) from Bologna to Friedrichshafen with three overnight stops in Gorizia, Graz and Wels. The flight track is color coded by the total k_{OH}^{calc}.

The OH reactivity on the southbound transfer was lower compared to the northbound as the wind direction came predominantly from the north with its less industrialized regions as the Alps and Slovenia. Thus, the mean k_{OH}^{meas} value was 1.9 s^{-1} for the first and 2.4 s^{-1} for the second flight leg, as shown in Table 4.6. A more detailed analysis including the median, maximum and minimum can be found in Table A.6/A.7 of the appendix. For the calculation of the OH reactivity the HCHO values had to assumed be constant and were set to the campaign median, as there was no data obtained for these two flights. The resulting calculated overall OH reactivity had a mean value of 2.2 s^{-1} for the first and 2.4 s^{-1} for the second flight leg. The k_{OH}^{miss} is negative for both flight legs with a median value of -0.4 s^{-1} and -0.03 s^{-1}. Regarding the random (see Figures A.11/A.12.) and systematic errors of both the k_{OH}^{meas} and k_{OH}^{calc} the missing reactivity was not significant.

Table 4.8: Overview of the mean k_{OH}^{meas}, k_{OH}^{calc} and k_{OH}^{miss} values.

	k_{OH}^{meas} [s^{-1}]	SD [s^{-1}]	Accuracy [s^{-1}]	k_{OH}^{calc} [s^{-1}]	SD [s^{-1}]	Accuracy [s^{-1}]	k_{OH}^{miss} [s^{-1}] b)
1. leg	1.9	0.5	0.44	2.2	0.2	0.32	-0.3
2. leg	2.4	0.5	0.49	2.4	0.5	0.37	-0.03

When comparing the mean contributions to the k_{OH}^{calc} of the individual substances for both flight legs, again the k_{OH}(OVOC) contributed most to the total OH reactivity (see Figure 4.13). The k_{OH}(OVOC) fraction was with 49 % larger for the first flight leg than for the second with 46 %. The relative contribution of OVOCs to the total OH reactivity was highest measured during the whole campaign 2012. Other species were only of minor importance with exception of k_{OH}(CO) contributing 17 % for the first flight leg and 15 % for the second. The contributions of NO_x and AVOCs were smaller in the first leg compared to the second leg. These results demonstrate that the air masses in the first flight leg over the Adrian coastline were less influenced by primary anthropogenic sources than the second leg where the plumes of Zagreb and Graz have been probed. The missing reactivity was not included in Figure 4.13 as it was very low for both flight legs.

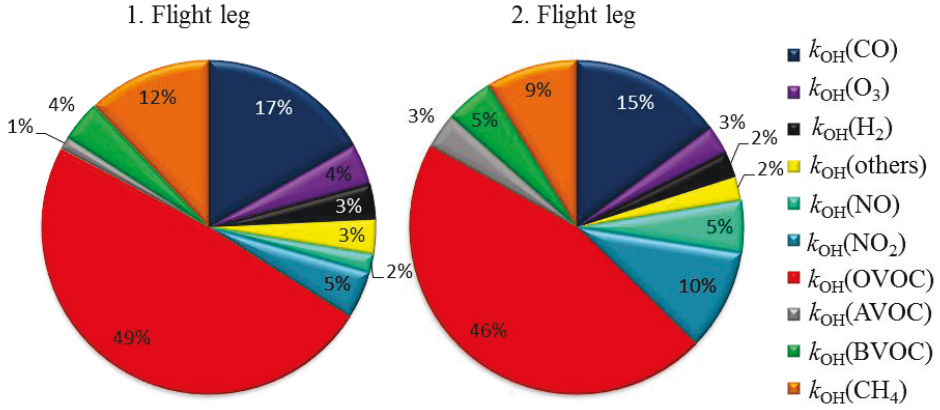

Figure 4.13: Mean k_{OH} contribution by the respective species to the k_{OH}^{calc} for each flight leg.

4.4.2.1 Analysis of the entire flight track

For the detailed analysis of south transfer the flight track was divided into 9 flight sections based on the individual k_{OH} contributions from each substance class which is elaborated in Chapter 4.4.2.2. The individual flight sections were categorized like for the north transfer into with low, higher and high NO_x contributions to the OH reactivity as seen in Table 4.6. In contrast to the north transfer the $k_{OH}(NO_x)$ did not exceed a value of 0.9 s^{-1} during the entire south transfer. Therefore, only category I and II were observed as shown in Figure 4.14 (marked green and blue). There were no strong direct primary anthropogenic sources on the flight route of the south transfer.

Category I can be applied for most parts of this flight track with two exceptions. The air sampled on the south transfer was characterized by an OH reactivity below 3 s^{-1} and very small primary contributions from NO_x as indicated in green in Figure 4.14 and Table 4.9. In these designated areas the absolute OVOC contribution was high, well exceeding values of 1 s^{-1} and relative contributions of 45 %. This indicates that the sampled air was processed with low contributions of primary anthropogenic contributions.

Table 4.9: Absolut mean values of the $k_{OH}(NO_x)$, k_{OH}^{calc}, k_{OH}(other), k_{OH}(AVOC), k_{OH}(BVOC), k_{OH}(OVOC) and the ratio k_{OH}(OVOC)/k_{OH}(VOC) for the 9 flight sections and the corresponding categories of the south transfer flights.

Category	Section	Mean $k_{OH}(NOx)$ [s^{-1}]	Mean k_{OH}^{calc} [s^{-1}]	Mean k_{OH}(other) [a)] [s^{-1}]	Mean k_{OH}(AVOC) [s^{-1}]	Mean k_{OH}(BVOC) [s^{-1}]	Mean k_{OH}(OVOC) [s^{-1}]	Ratio k_{OH}(OVOC)/ k_{OH}(VOC) [s^{-1}]
I	1	0.22	2.33	0.61	0.07	0.06	1.12	0.74
I	2	0.12	2.09	0.66	0.02	0.02	1.02	0.78
I	3	0.17	2.21	0.65	0.05	0.06	1.03	0.74
I	4	0.15	2.31	0.67	0.02	0.17	1.03	0.70
I	5	0.08	2.49	0.49	0.17	0.06	1.48	0.77
I	6	0.16	2.23	0.54	0.07	0.19	1.06	0.69
I	8	0.40	2.51	0.59	0.07	0.10	1.12	0.74
II	7	0.71	2.74	0.55	0.09	0.10	1.07	0.72
II	9	0.87	2.95	0.60	0.08	0.09	1.08	0.73

[a)] k_{OH}(other) includes the contributions of CO, O_3, HO_2 and HONO.

During the second flight leg of the south transfer two areas with higher NO_x emissions, such as in the range of 0.7 and 0.9 s^{-1} were probed. The air (marked in blue in Figure 4.14) showed a higher OH reactivity of above 2.5 s^{-1}. These plumes likely arose from cities like Zagreb and Graz as can be visualized by the back trajectories.

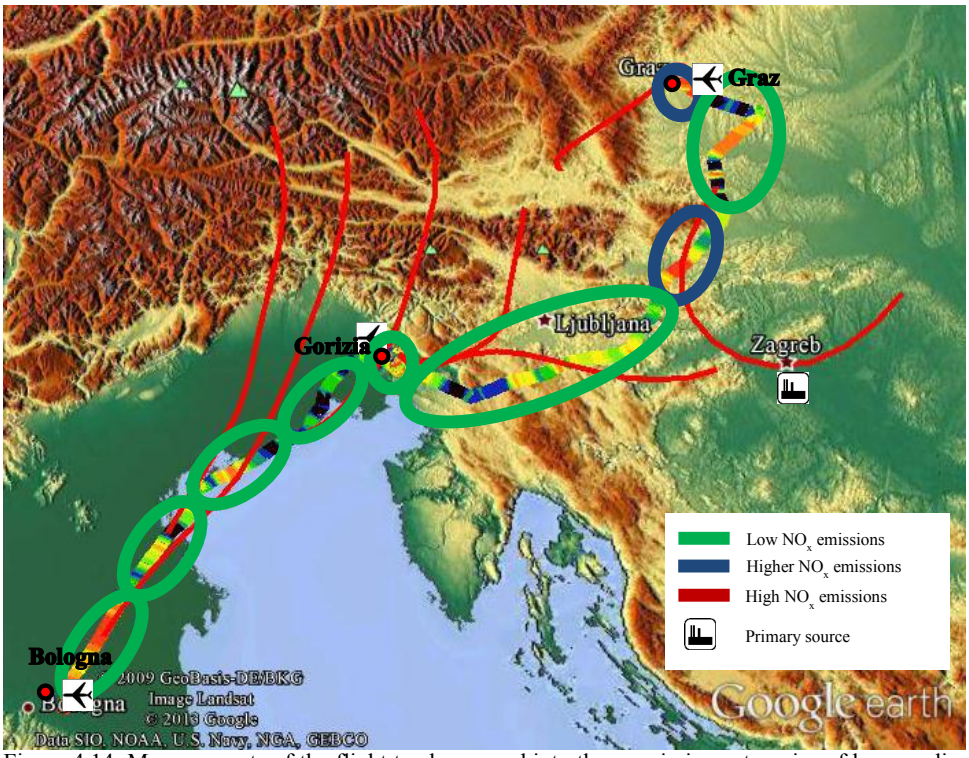

Figure 4.14: Measurements of the flight track grouped into three emission categories of low, medium and very high anthropogenic emissions for the first two flight legs of the south transfer flight from Bologna to Graz (F051/F052). The HYSPLIT back trajectories are shown as red lines.

4.4.2.2 Detailed analysis of the last 5 sections of the south transfer

The flight track of the south transfer was divided further into 9 sections based on the individual k_{OH} contributions. The sections 1-4 showed high OVOC and very low AVOC contributions (see Figure A.13 of the appendix). In the 4th section the BVOC contribution was slightly higher. However, sections 5-9 of the second flight leg show more variation and are discussed in the following.

In the 5th section of the transfer flight (F052) the OVOC share of the OH reactivity was high with 59 % as shown in Figure 4.15. The contributions of NO_x, AVOC and BVOC were small (2 % to 7 %). Other inorganic compounds as CO, HO_2, HONO, O_3 and H_2 (k_{OH}(others)), contributed the second largest part of the total OH reactivity with 20 %. In section 6 the pattern changed as the fraction of k_{OH}(others), $k_{OH}(NO_x)$ and k_{OH}(BVOC) increased at the cost of k_{OH}(OVOC). Compared to section 5 the k_{OH}^{calc} decreased to a value of 2.2 s^{-1}. These two sections covered rural parts of Slovenia with a low population density and hardly any industrial areas. The plume of the capital city Ljubljana, with a high degree of industrialization (Bizjak et al., 1999) was not detected as the wind was coming from the east.

The pattern changed again in section 7, with a significant increase of $k_{OH}(NO_x)$ to a fraction of 26 % at a k_{OH}^{calc} value of 2.7 s^{-1}. Here, the k_{OH}(OVOC) fraction decreased to below 40 %.

Following the back trajectories the source for these larger contributions of NO_x could be Zagreb. Zagreb has a population of 1.2 million and is the largest industrial area of Croatia. The industrial activities are dominated by the food-, chemical- and engineering industry (Acker et al., 2008; Bošnir et al., 2003). In the 8th section the k_{OH}^{calc} was lower with a value of 2.5 s^{-1}. Accordingly, the fraction of NO_x was reduced but still larger than in sections five and six. These air masses were still influenced by the plume arising from Zagreb. The 9th section, close to the city of Graz, showed the highest k_{OH}^{calc} values of this flight leg, with a mean of 3 s^{-1}. Here, also $k_{OH}(NO_x)$ constituted a large fraction of the OH reactivity. Graz is a city with 250 000 inhabitants and little industrial activity. But, as it is situated in a mountainous region pollution can reach high levels (Almbauer et al., 2000).

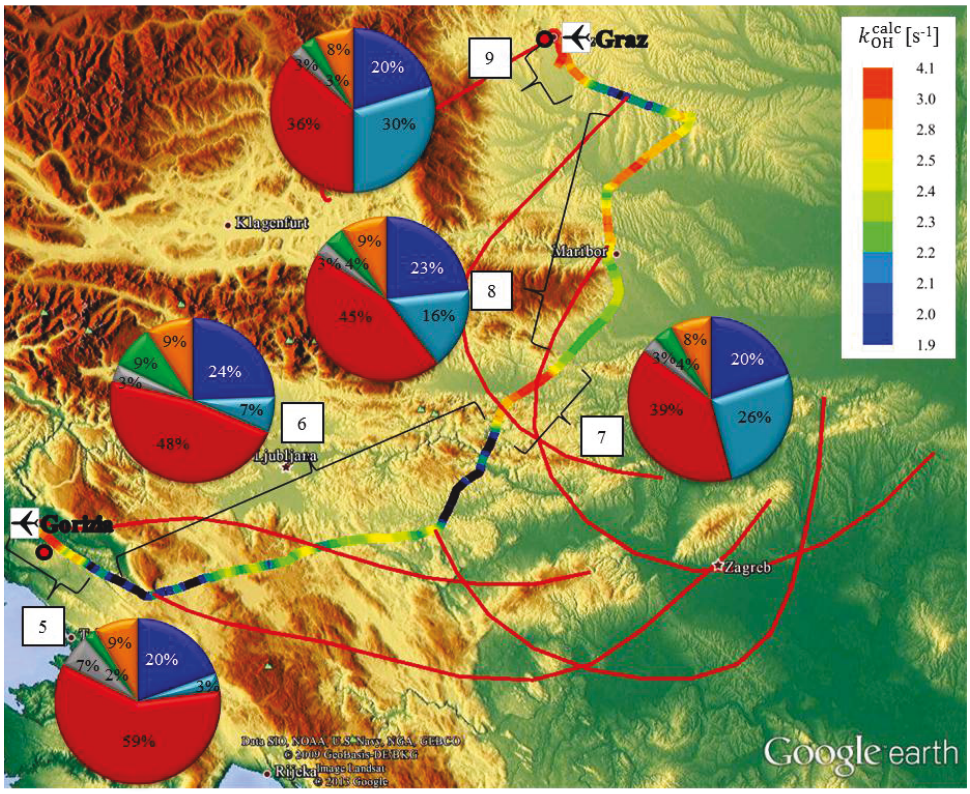

Figure 4.15: Flight from Gorizia to the Graz (F052) color coded by the total k_{OH}^{calc} divided into five sections. The red lines show the 12 h back trajectories for 400 m (AGL). The pie charts resemble the partitioning of k_{OH}^{calc}. Sections in dark blue resembles k_{OH}(others), which is the sum of k_{OH}(CO), $k_{OH}(HO_2)$, k_{OH}(HONO), $k_{OH}(O_3)$ and $k_{OH}(H_2)$, light blue $k_{OH}(NO_x)$, red k_{OH}(OVOC), gray k_{OH}(AVOC), green k_{OH}(BVOC) and orange $k_{OH}(CH_4)$.

4.4.3 Comparison of both transfer flight

When comparing both transfer flights it is evident that the mean OH reactivity was low for both flights compared to other studies as shown in Table 1.2. With a mean of 3.14 s^{-1} the k_{OH}^{calc}

value was higher on the entire north transfer compared to the south transfer with a value of 2.43 s^{-1}. The north transfer was dominated by overall higher NO_x values with a mean of 0.86 s^{-1} contributing with a share between 9 and 42 % to the OH reactivity. On the south transfer flight the NO_x contribution was lower with a mean of 0.32 s^{-1}. The contribution to the OH reactivity ranged from 3 to 30 %.

In line with the higher NO_x contribution the AVOC contribution showed also higher values on the north transfer with a mean of 0.27 s^{-1} compared to a value of 0.07 s^{-1} on the south transfer. The contributions of BVOCs were low for both transfers.

Next to the NO_x contribution the OVOC contribution was high for both transfer flight with a mean value of 1.04 s^{-1} for the north transfer and a value of 1.11 s^{-1} for the south transfer. On the north transfer the OVOC contribution to the k_{OH}^{calc} varied between 23 and 44 % and for the south transfer between 36 and 59 %. The mean value of the k_{OH}(OVOC)/k_{OH}(VOC) ratio was higher for the south transfer with 0.73 compared to the north transfer with 0.65. Whereas the OVOCs on the south transfer were predominantly from secondary sources, primary OVOC sources could be identified on the north transfer close to the Mannheim/Ludwigshafen region. The primarily emitted OVOCs were methanol and ethanol.

These results show that the north transfer was influenced more by higher concentrations of primary anthropogenic trace gases compared to the south transfer that was dominated by aged air masses and very low anthropogenic primary sources. Notably, this classification only holds for these specific weather conditions. This is only valid for these specific weather conditions, wind directions, flight heights and temperatures.

4.5 Analysis of the PBL layering - Vertical profiles

4.5.1 The layering of the troposphere

The troposphere is the lowest part of the atmosphere. The height is latitude and season dependent and varies between 8 km and 15 km above ground level (Seinfeld and Pandis, 2006). The planetary boundary layer (PBL) is the lowest part of the troposphere; it is where most of the chemical reactions and degradation processes of trace gases occur. Trace gases are emitted at the ground and processed as they rise in the atmosphere for instance by reaction with OH (see Chapter 1.2.2). As the PBL is directly influenced by the earth's surface and responds within an hour or less to surface forcing thus the PBL is of significant importance when studying trace gases (Graedel and Crutzen, 1993; Stull, 1988). Given the ideal conditions, four layers are formed within the PBL during the course of a day namely the surface layer (SL), the mixed layer (ML), the nocturnal boundary layer (NBL) and the residual layer (RL) (see Figure 4.16). These ideal conditions comprise a dry, horizontally flat surface, clear sky conditions and low winds.

After sunset fast radiative cooling begins on the surface and a stable nocturnal boundary layer (NBL) is formed. This process starts from the ground and as only layers close to the ground are affected by the radiative cooling the NBL reaches a maximum height of 400 m above

ground level (AGL). Typical for the NBL is its stable stratification due to low winds and no upward mixing. This causes all emissions from the ground to be trapped in this thin layer during night time, leading to elevated concentrations of trace gases (Stull, 1988; Velasco et al., 2008).

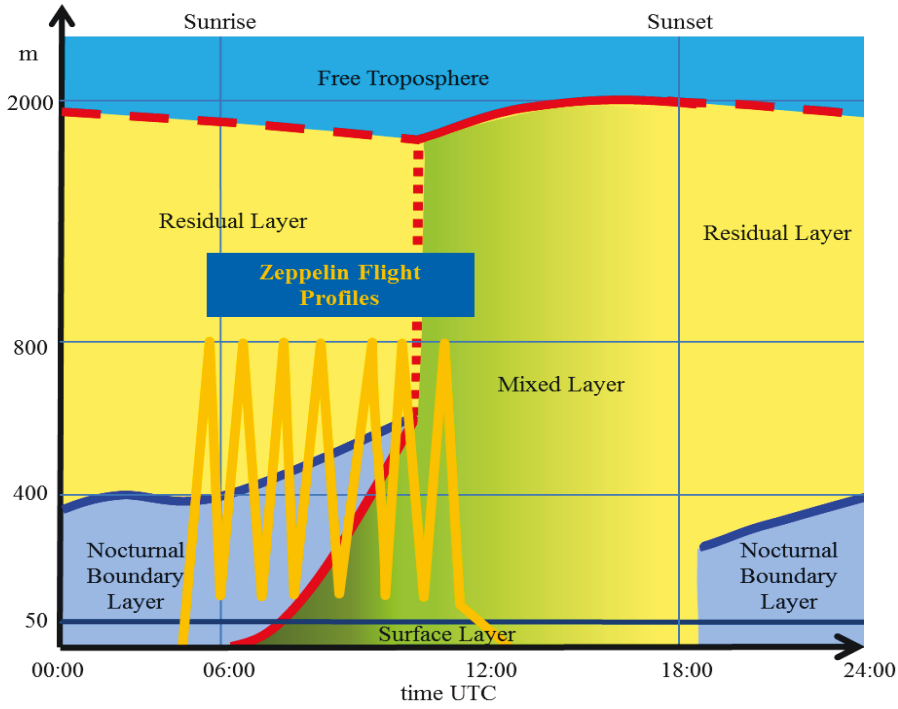

Figure 4.16: The evolvement of the nocturnal boundary layer (NBL) and the residual layer (RL) into the mixed layer (ML) after sunrise and the formation of the NBL and RL after sunset. The Zeppelin flight pattern to probe this evolvement is indicated in yellow (adapted from graphic by Franz Rohrer (Forschungszentrum Jülich)).

At night the residual layer (RL) is formed above the NBL. The RL exists between the heights of 400 and 2000 m (AGL) and is completely decoupled from the NBL. The NBL is characterized by a positive and the RL by a negative temperature gradient. The RL contains the processed air from the previous day with the same trace gas concentrations as only little oxidation or deposition take place. The oxidation is limited to O_3 and NO_3 as the OH concentrations are low. After sunrise, when the solar radiation is heating the earth's surface, a new layer called mixed layer (ML), is formed. First, the air from the NBL is assimilated followed by the air from the RL. Finally, both layers have been fully incorporated into this well mixed new layer. All day and night the well mixed surface layer (SL) is present with a maximum height of 50 m. Generally, it contains high concentrations of primary emissions.

The allocation of the different layers in the data obtained can be carried out by the calculation of the potential temperature θ. The potential temperature is a measure of the stability of the different layers as proposed by Stull (1988). Alternatively, Franz Rohrer proposes to use the

ozone (O_3) concentration within the air as indicator for the respective layer. This method is shown in Li et al. (manuscript in preparation). During the PEGASOS campaigns, the O_3 concentration in the RL was approximately 100 ppb and higher than in the NBL. This concentration was comparable to the value of the previous day as no dry deposition occurred. In the NBL the O_3 concentration was lower, with average values of 70 ppb. The ozone was removed during the night by dry deposition at the ground and titration with NO. When the ML was formed the O_3 concentration reached low values of 40 ppb as the air of the surface layer with a higher O_3 deposition rate is mixed in. Following, the approach of Franz Rohrer and Li et al. (manuscript in preparation) the respective layers are allocated based on the observed O_3 concentrations.

These previously described ideal conditions could be found in both the Netherlands and Italy during the Zeppelin flights. The NBL, the RL as well as the evolving ML were probed with vertical profile flight patterns. The surface layer could not be analyzed as the Zeppelin was not allowed to fly below 70 m (AGL). During the campaign 15 vertical profile flights have been conducted, probing the vertical distribution of trace gases and aerosols with a varying residence time at each height. Not all vertical profile flights accomplished a full coverage of all three previously elaborated layers. Due to a later take off time the NBL could not be probed in all flights as it had already been integrated into the ML.

4.5.2 Vertical profile flights

Illustratively, the results of the vertical profile flight (F023/024) conducted on the 18th of June 2012 with the photochemistry cabin layout (CL-8) are shown in Figure 4.17 as it is exemplary of all vertical profile flights. Similarly, to all other vertical profile flights the altitude of all 7 flight sections (FS) on flight F023/024 ranged between 100 and 800 m (AGL). The profile flight was flown above the San Pietro Capofiume (SPC) supersite and only interrupted by a refuel stop. It was a clear sky day with sunrise at 4:50 UTC. The mean ambient temperature measured at the nose boom was 23 °C and the wind speed was 7 km/h. The wind was coming from the north-east. This flight pattern was dominated by fast ascends and descends with a residence time of 20 minutes on each layer.

The assignment of the probed profiles to the layers allocated from the respective ozone concentrations is shown in Figure A.14 in the Appendix. The method was analyzed by Franz Rohrer and is shown in Li et al. (manuscript in preparation) as elaborated above. The highest O_3 concentrations are found in the RL, the lowest in the ML and the medium O_3 concentrations are observed in the NBL. During flight 023/024 all three layers (NBL, RL and ML) could be probed. The entire flight was subdivided into 7 FS. The first four FS the NBL was probed at lower levels and the RL at the higher levels. The measurements from the first FS clearly differed from the remaining FSs in their low O_3 concentration of 50 ppb and their elevated OH reactivity. Based on these data this layer would normally be classified as part of the ML. However, this layer only evolved later during the day and not this early in the morning. A possible explanation could be that the surface layer was probed which was elevated by turbulences. In the FS 5-7 at the lower height the newly formed ML was sampled.

The remaining NBL above the ML was not detected because of the steep and rapid transition between the lower and higher height. Within a timeframe of 1 hour the ML had incorporated the entire NBL and RL and the difference in the O_3 concentration between the higher and lower height was reduced. The data gap in between the 5th and 6th FS was due to a refuel stop.

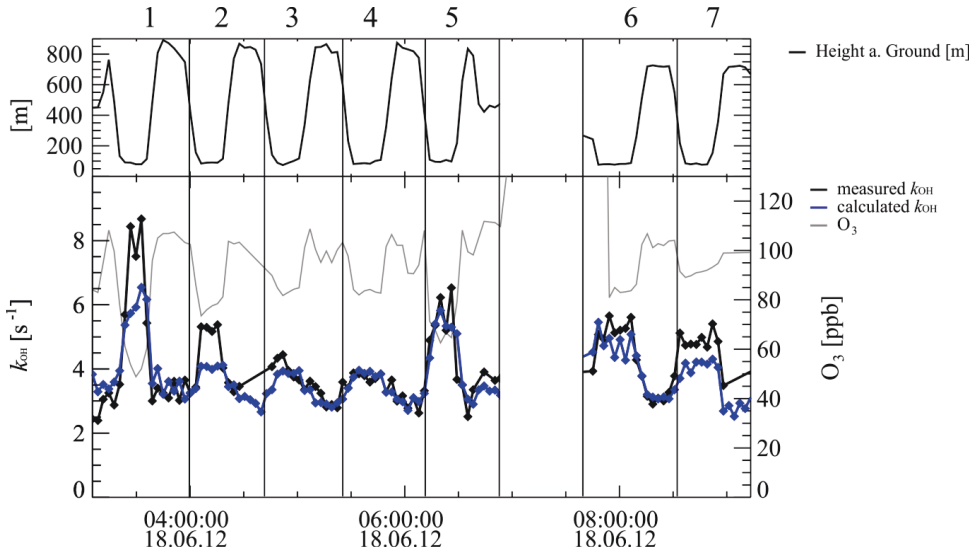

Figure 4.17: Vertical profile flight (F023/024, CL-8) on the June 18 2012 at the San Pietro Capofiume (SPC) supersite with the height above ground in the top panel of the figure. The lower panel of this shows the measured OH reactivity in black and the calculated OH reactivity in blue. The gray curve indicates the O_3 concentration. The entire flight was subdivided into 7 flight sections.

4.5.3 Measured OH reactivity

Figure 4.17 shows the measured k_{OH} time series for flight F023/024. Similar patterns of the measured OH reactivity were evident for all the vertical profile flights obtained: higher k_{OH} values at lower heights (100 m (AGL)) in the NBL and ML, and lower k_{OH} values at higher heights (800 m (AGL) and more) in the RL. Once, the ML was inter-mixed with the RL, there were no longer any significant differences between both height levels. The k_{OH}^{meas} values in the NBL ranged from 4 s^{-1} to 8 s^{-1}. In the ML the values were between 4.2 s^{-1} to 9.2 s^{-1} and in the RL between 1.7 s^{-1} and 4 s^{-1} (see Table 4.10).

Table 4.10: Measured reactivity in the nocturnal boundary layer, mixed layer and residual layer for all the vertical profile flights obtained during both campaigns (see Table 3.1/3.2).

	Nocturnal boundary layer		**Mixed layer**		**Residual layer**	
	Min [s^{-1}]	**Max [s^{-1}]**	**Min [s^{-1}]**	**Max [s^{-1}]**	**Min [s^{-1}]**	**Max [s^{-1}]**
Measured OH reactivity	**4** (F023/024)	**8** (F023/024	**4.2** (F047)	**9.2** (F027/028)	**1.7** (F040)	**4** (F013, F027/028)

These observations showed that there was a steep gradient between the NBL and the RL which indicated that there was no upward mixing from the emissions from the ground into the RL. These emissions were trapped in the stable NBL during the night evident by the higher k_{OH} values. The RL contained processed air from the previous day with a lower OH reactivity and was not affected by new primary emissions. As long as the ML was still very young in the evolvement process it is characterized by high concentrations of trace gases which were emitted from the ground and therefore a relatively high reactivity. Once the ML had incorporated more of the RL, the trace gases were diluted and the OH reactivity was lower.

4.5.4 Calculated OH reactivity and the missing reactivity

The k_{OH}^{calc} followed a similar pattern as the k_{OH}^{meas} shows higher values at lower heights in the NBL and ML compared to the RL at higher height with lower values as seen in Figure 4.18. The k_{OH}^{calc} was broken down into several classes as introduced in Chapter 4.1. For all flights it is evident that the OVOCs made the largest contribution. NO_x, AVOCs and BVOCs from primary sources showed a clear height dependency with higher contributions close to the ground and lower contributions at higher heights. The individual VOC contributions to the k_{OH}^{calc} are elaborated in further detail in Chapter 4.5.5.

The missing reactivity for flight F023/024 which is defined as the difference between k_{OH}^{meas} and k_{OH}^{calc} (Figure 4.18 and Figure 4.19) was calculated across the three different layers. In line with all other vertical profile flights larger degrees of missing reactivity were found in the NBL and ML, while the lowest missing reactivity was present in the RL.

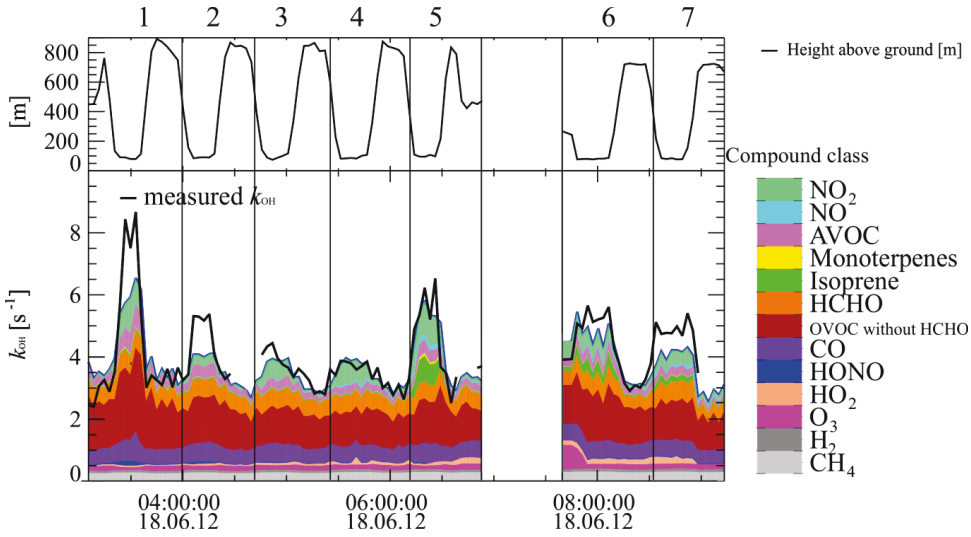

Figure 4.18: Vertical profile flight (F023/024, CL-8) on June 18 2012 at the San Pietro Capofiume (SPC) supersite with the height above ground in the top panel of the figure. The lower panel shows the measured OH reactivity in black and the single contributions of the calculated OH reactivity in color. The difference between both is the missing reactivity. The entire flight was subdivided into 7 flight sections.

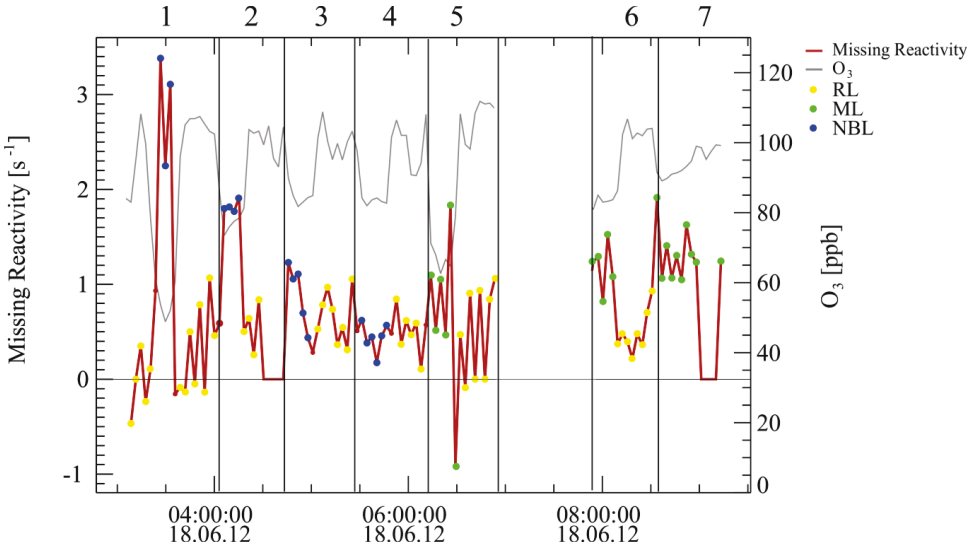

Figure 4.19: The missing reactivity for F023/024 indicated by the red line for the different layers. The gray curve is the corresponding O_3 concentration used as a base to allocate the layering. The entire flight was subdivided into 7 flight sections.

The total missing reactivity in all the vertical profile flights performed varied between - 0.5±0.73 and 2.9±0.45 s^{-1}. The errors are calculated from the sum of the random error of the

measured and calculated OH reactivity. The missing reactivity in the NBL showed the largest variation for the different flights and was within the range of 0.07±0.33 to 2.9±0.45 s^{-1} (see Table 4.11). The missing reactivity in the ML ranged between - 0.38±0.45 and 1.9±0.37 s^{-1}. The lowest missing reactivity values were measured in the RL ranging between - 0.5±0.73 and 0.6±0.78 s^{-1}.

Table 4.11: Minimum and maximum value of the missing reactivity in the nocturnal boundary layer, mixed layer and residual layer for all the vertical profile flights obtained during both campaigns (see Table 3.1/3.2) with the respective random error of the k_{OH}^{meas} and k_{OH}^{calc}.

	Nocturnal boundary layer		**Mixed layer**		**Residual layer**	
	Min [s^{-1}]	**Max [s^{-1}]**	**Min [s^{-1}]**	**Max [s^{-1}]**	**Min [s^{-1}]**	**Max [s^{-1}]**
Missing reactivity	**0.07±0.33** (F023/024)	**2.9±0.45** (F023/024)	**0.38±0.55** (F027/028)	**1.9±0.37** (F049)	**- 0.5±0.73** (F013)	**0.6±0.78** (F027/028)

To evaluate the missing reactivity the uncertainty of the measured and calculated k_{OH} was analyzed. In Figure 4.20 both the k_{OH}^{meas} and k_{OH}^{calc} were plotted with their respective random errors. There is a significant missing reactivity at the lower height of the 1st and 2nd FS in the NBL which becomes clear through the designated gap between the error bars. This missing reactivity could also be seen in the ML at the lower height in FS 7. For all other measurements the measured and calculated OH reactivity agree well within their error bars and therefore no missing reactivity can be found.

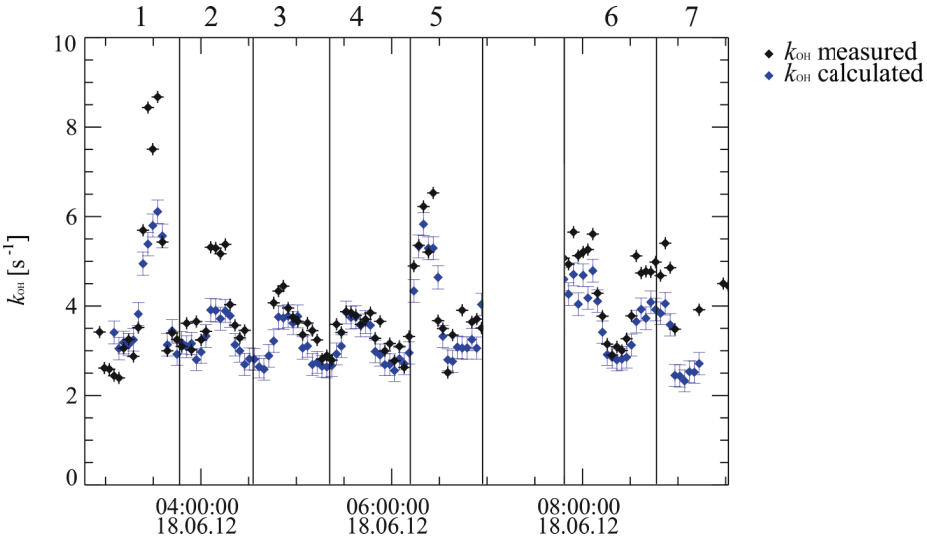

Figure 4.20: The k_{OH}^{meas} and k_{OH}^{calc} of the vertical profile flight of F023/024 with their respective calculated random error. The entire flight was subdivided into 7 flight sections.

These observations indicate that the individual contributions to the OH reactivity by the constituents were better characterized when the air was more processed and enriched in photochemical products as it was the case for the RL. In contrast, the higher missing reactivity in the NBL and ML can be explained by unmeasured trace gases. The missing source is expected to be a primary anthropogenic source, as other anthropogenic species such as toluene and NO_x show higher concentrations within the nocturnal boundary layer. It is highly unlikely that the cause was biogenic emissions such as terpenes as their emission strengths in both regions were very low. But not all the anthropogenic missing reactivity has to be an AVOC contribution as also unmeasured OVOCs can be emitted from anthropogenic sources. This is also in line with the observations for the entire campaigns showing a higher missing reactivity in the Netherlands with also a higher anthropogenic contribution.

To find unmeasured substances some chromatograms were scanned for species that have not been calibrated for. One large peak could be identified in both the Netherlands and in Italy. It had a high intensity at the mass to charge ratio of 45 and a smaller intensity at 59. This peak could be caused by the substance class of diethers which was not calibrated for in this study. Unfortunately, this peak was not identifiable and quantifiable, as the mass spectrometer was operated in the SIM mode and only specified ions were measured. The peak correlates well with the missing reactivity and was more abundant at lower heights. The substance class of ethers would be regarded as an OVOC in this study although is originates from an anthropogenic source, especially by car emissions (Porter et al., 1997). This supports the supposition that the missed substance must originate from an anthropogenic source.

4.5.5 The individual VOC contributions to the calculated OH reactivity

The contributions of the VOC species to the k_{OH}^{calc} can be sub-divided into groups, namely methane, the primarily emitted AVOCs and BVOCs, and the oxygenated VOCs. Their respective contributions are illustrated for flight F023/024 in Figure 4.21. Formaldehyde and acetaldehyde are displayed separately, as they contributed most of the single substances (see Chapter 4.3.2.1). The results show, that the individual contributions of the OVOCs exceeded the contributions of the AVOCs and BVOCs, which is in line with the observations for the entire campaign.

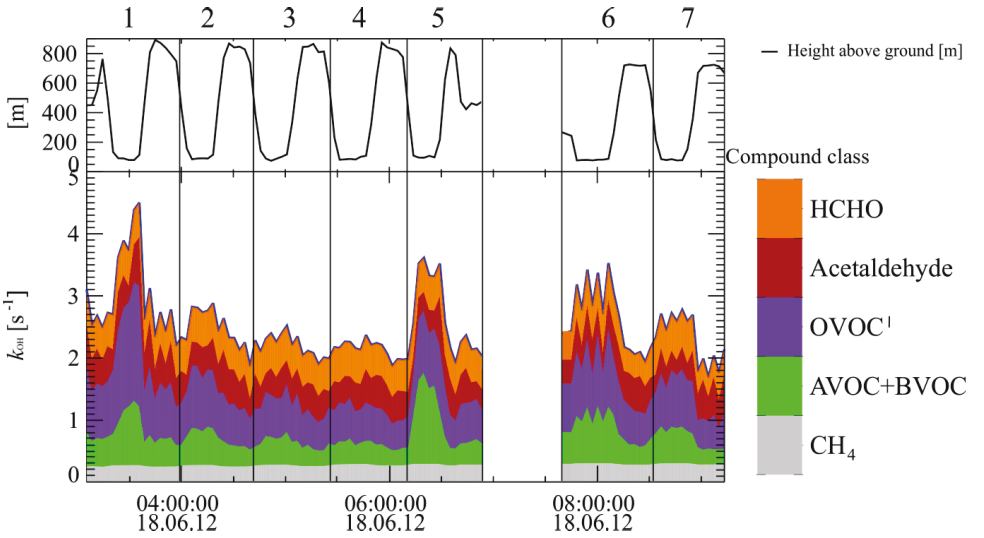

Figure 4.21: The k_{OH}(VOC) contributions, shown in the lower panel are grouped into the primarily emitted AVOCs and BOVOCs and OVOCs' (without HCHO and acetaldehyde) as well as methane. HCHO and acetaldehyde are shown separately as they constitute the largest contribution of the OVOCs. The top panel shows the flight altitude. The entire flight was subdivided into 7 flight sections.

4.5.5.1 Contributions of the primary sources to the k_{OH}^{calc}

The contributions of the primary VOCs to the k_{OH} were low, compared to the contributions of the OVOCs, reaching a maximum of 1.3 s^{-1} in the 5th FS during flight F023/024. The primary sources for k_{OH}(VOC) could be subdivided into sources with anthropogenic and biogenic origin. In addition there can also be a significant contribution of primary emitted OVOCs which is not shown here since they cannot be distinguished from the photochemically produced OVOCs.

The k_{OH} contributions of alkane, alkenes and aromatics show a height dependency: higher k_{OH}(AVOC) values at lower heights and lower k_{OH}(AVOC) values at higher heights (see Figure 4.22). Consequently, the concentrations of anthropogenic VOCs were higher closer to the ground in the NBL and ML than in the RL. When the ML was mixed combined with the RL the differences between the lowest and highest height were reduced.

The biogenic k_{OH} contributions for flight F023/024 as shown in Figure 4.23 were dominated by isoprene. This is also the case for all FS. The monoterpenes played only a subordinate role. The biogenic share was very low for the first 4 FSs until it increased after 6:00 UTC. This was caused by two factors. First, isoprene emissions are light dependent (Tingey et al., 1979) which leads to a slow increase of isoprene after sunrise. And secondly, the ground-level emissions were trapped in the surface layer and are not mixed upwards in the NBL. Only when the ML is probed for the first time did the isoprene contribution rise together with an increase of the AVOCs.

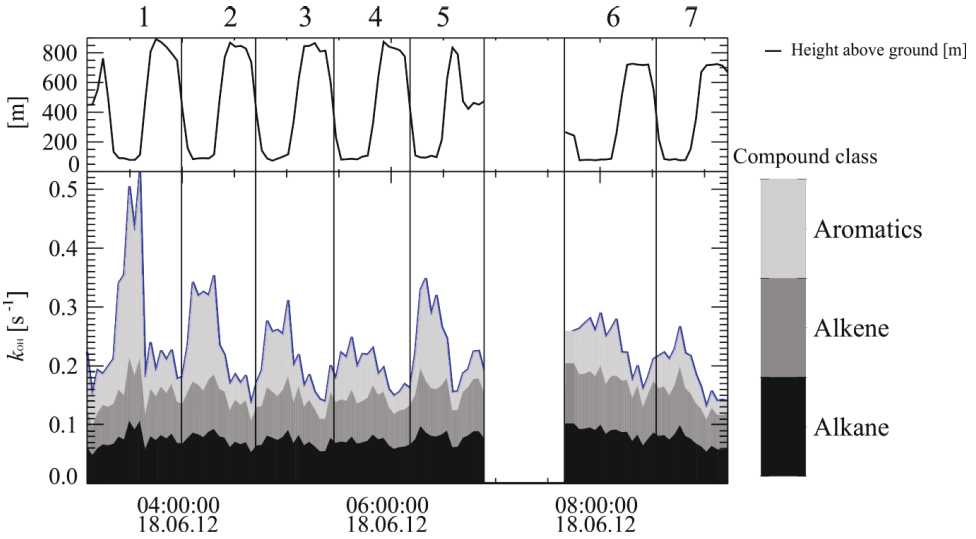

Figure 4.22: The k_{OH} contributions of the anthropogenic constituents to the k_{OH}^{calc}(AVOC) for flight F023/024 subdivided into 7 flight sections. The top panel shows flight altitude.

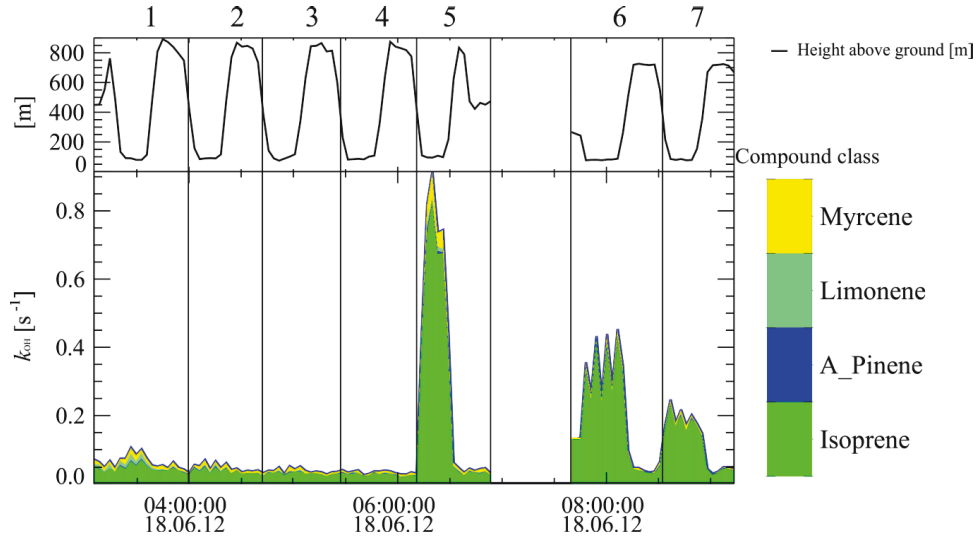

Figure 4.23: The k_{OH} contributions of the biogenic constituents to the k_{OH}^{calc}(BVOC) for flight F023/024 subdivided into 7 flight sections. The top panel shows flight altitude.

The observations showed that the concentrations of AVOCs and BVOCs were higher closer to the ground as this is closer to their source. It was also evident that the concentrations decreased towards FS 7 when the ML had evolved and mixed the NBL. The decrease could be caused by two effects, the mixing and the reaction with OH. This is elaborated in the following.

4.5.5.2 Contributions of the OVOCs to the k_{OH}^{calc}

In comparison to the primary emitted AVOCs and BVOCs, the OVOCs contribution to the k_{OH}^{calc} was larger for all profile flights. For flight F023/024 contribution of OVOCs ranged from 1.5 s^{-1} to 3.5 s^{-1} (see Figure 4.24). The k_{OH}(OVOC) height dependency, especially for FS 2-4, was not as pronounced as for k_{OH}(AVOC) and k_{OH}(BVOC). Only FS 1 and 5-7 showed a slight height dependency, with higher k_{OH}^{calc} values at the lower height level.

At the lower height of the first FS in the NBL high k_{OH}^{calc}(OVOC) values were caused by elevated alcohol concentrations, mostly dominated by methanol and ethanol (see Figure 4.24). Given FS 1 it is highly likely that these OVOCs had an anthropogenic origin, as the k_{OH}(AVOC) was also higher. Photochemical production by OH can be ruled out due to low concentrations of OH radicals this early in the day.

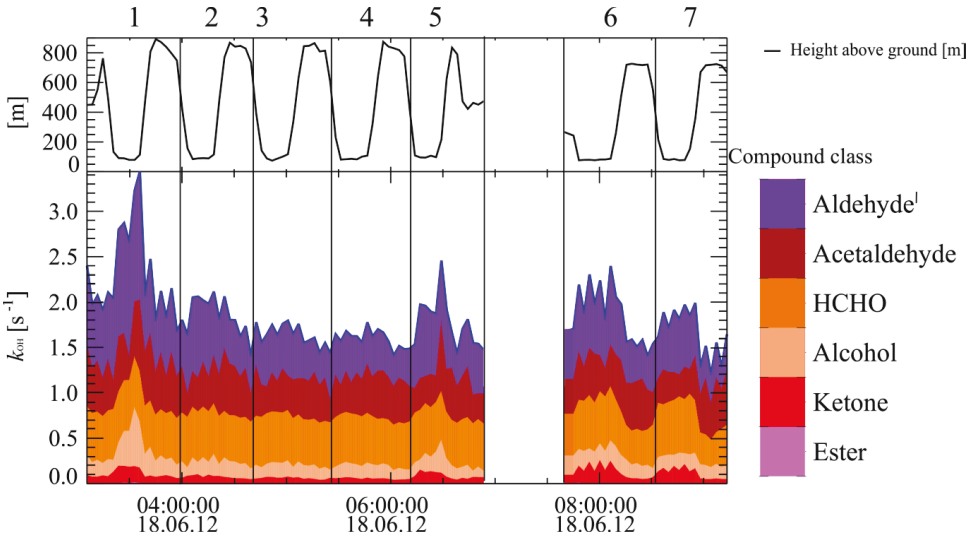

Figure 4.24: Contributions of the single OVOC classes to the k_{OH}^{calc}(OVOC) for flight F023/024 subdivided into 7 flight sections. The top panel shows flight altitude. Aldehyde^{I} is the aldehyde class without HCHO and acetaldehyde.

Also at the lower height in FS 5-7 the k_{OH}(alcohol) showed slightly higher contributions together with k_{OH}(ketone), and k_{OH}(HCHO). As for the alcohols, the increase of HCHO and ketones as MVK can originate from primary sources. Alternatively, it could be produced in the degradation process of precursors such as isoprene with the OH radical. In this case either one is very likely to be the source are as the mixed layer does contain OH radicals. To evaluate the importance of the OVOCs compared to the AVOCs and BVOCs, the ratio of k_{OH}(OVOC)/k_{OH}(VOC) including acetaldehyde and formaldehyde across the different layers was calculated. For all vertical profile flights the k_{OH}(OVOC) dominated the k_{OH}(VOC) (see Figure 4.25) with a percentage share of 44 - 76 %.

The results obtained for the different layers demonstrate that the values of the ratio were higher with a smaller variability in the NBL and the RL compared to the ML. Specifically, in the NBL the ratio showed values between 66 % and 76 % and in the RL between 72 % and 76 % for all vertical profile flights obtained in the Netherlands and Italy (see Table 4.12). In the ML the ratio of k_{OH}(OVOC)/k_{OH}(VOC) displayed the greatest variability, starting with the lowest values of 44 % when the ML is formed. With the rising of the ML, the ratio changed rapidly within a time frame of 3-4 hours to a percentage share of 75 % of OVOCs which is comparable to the value in the RL.

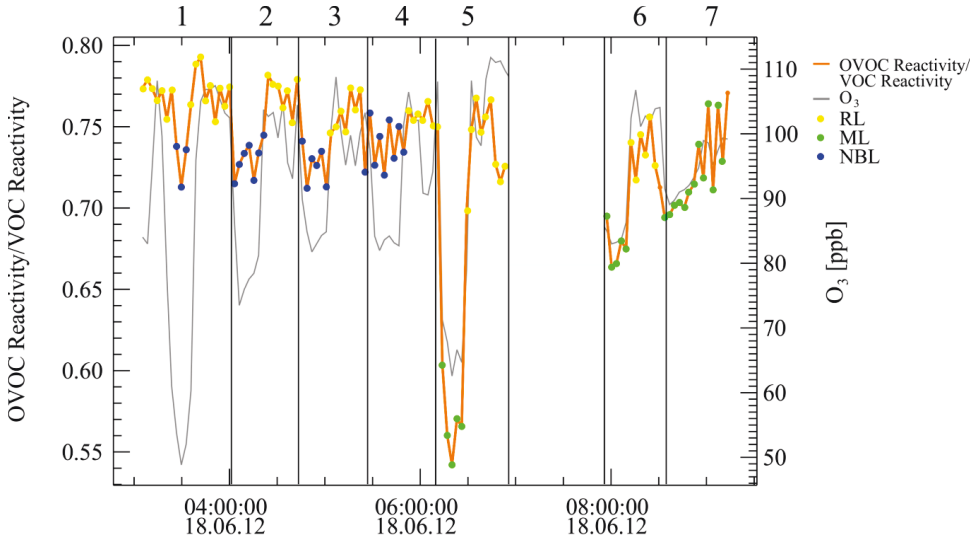

Figure 4.25: Ratio of k_{OH}(OVOC)/k_{OH}(VOC) for flight F023/024 for different layers: the NBL, RL and the evolving ML. The entire flight is subdivided into 7 flight sections.

Table 4.12: The ratio of k_{OH}(OVOC)/k_{OH}(VOC) in the NBL, ML and RL for all the obtained vertical profiles.

	Nocturnal boundary layer		**Mixed layer**		**Residual layer**	
	Min [%]	**Max [%]**	**Min [%]**	**Max [%]**	**Min [%]**	**Max [%]**
Ratio k_{OH}(OVOC)/ k_{OH}(VOC)	**66** (F049)	**76** (F023/024)	**44** (F044)	**75** (F049)	**72** (F013/023/ 024/040/ 047)	**76** (F013/047/ 049)

The similarity of the k_{OH}(OVOC)/k_{OH}(VOC) in the NBL to the RL requires further analysis. Therefore, for flight F023/024, the mean contributions for each probed layer are analyzed and depicted in Figure 4.26.

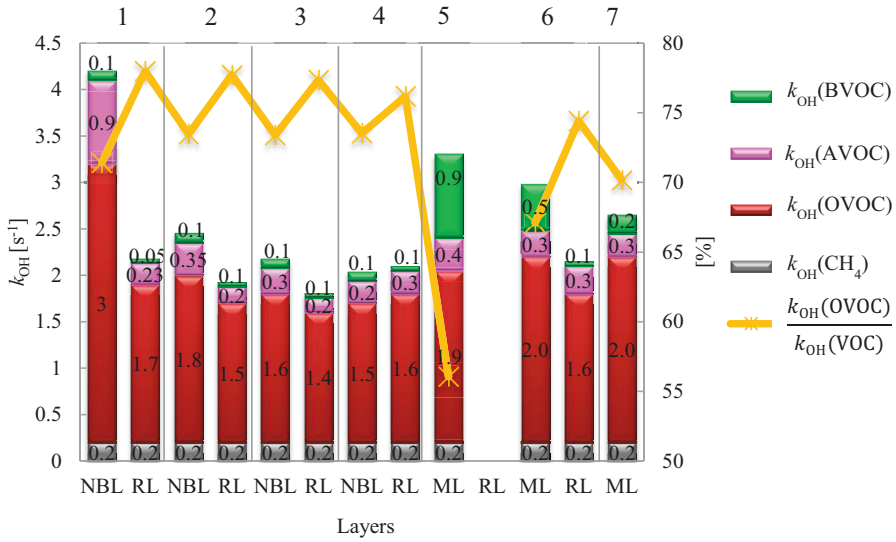

Figure 4.26: The mean k_{OH} distributions of CH_4, OVOCs, anthropogenic and biogenic VOCs for flight F023/024 shown in the bar graphs for each consecutively sampled layer in s^{-1}. The ratio of k_{OH}(OVOC)/k_{OH}(VOC) is shown in orange as percentage. The flights are subdivided into 7 flight sections.

The graph shows that in FSs 2-4 the difference between the NBL and RL was very small. In both layers k_{OH}(OVOC) was large with 1.4 - 1.8 s^{-1} while the contributions of both k_{OH}(AVOC) with 0.2 - 0.3 s^{-1} and k_{OH}(BVOC) with 0.1 s^{-1} were small. The slightly greater k_{OH}(OVOC)/k_{OH}(VOC) ratio values in the RL were caused by slightly larger k_{OH}(OVOC) contributions as well as slightly smaller contributions from the AVOCs.

The measurement in the NBL in the 1st FS appears to be the only one deviating. Here, the total k_{OH} values were higher compared to the subsequent measurements. This deviation was also reflected in differing O_3 concentrations as described in Chapter 4.5.2 and confirms the hypothesis, that parts of the surface layer have been probed. Nevertheless, the ratio of k_{OH}(OVOC)/k_{OH}(VOC) remained unchanged in subsequent measurements within the NBL.

In the RL the ratio of k_{OH}(OVOC)/k_{OH}(VOC) was almost constant for the first 5 FSs. Then it decreased by 4 % just before the RL mixes with the ML, because the contribution of k_{OH}(AVOC) increases slightly. But the overall ratio stays constant with an OVOC portion above 72 %. In contrast to the NBL is the RL completely decoupled from the ground and therefore not affected by emission and/or deposition until the point when it starts to interact with the rising ML. Then fresh emissions are mixed in and chemical production as well destruction gain in importance. This led to the reduced portion of OVOCs, which nevertheless never dropped below 72 % across all the profile flights.

When the newly formed ML was probed for the first time the k_{OH}(OVOC)/k_{OH}(VOC) relationship drastically changes within FS no. 5 (see Figure 4.26). Here, the contributions of the primary constituents of biogenic and anthropogenic sources were larger compared to the

previous FSs in the NBL. There was also a rise in the contribution of OVOCs by 0.5 s^{-1} originating from primary sources. These emissions decreased the k_{OH}(OVOC)/k_{OH}(VOC) ratio to 55 %. In the following two height FSs 6 and 7, the relative share of OVOCs in the ML was increasing again due to smaller contributions of primary sources and larger contributions of OVOCs. This fast process is illustrated in Figure A.15/A.16 for Flight F047, where the ML and the RL have been probed more often. Here, the k_{OH}(OVOC)/k_{OH} (VOC) ratio of the ML slowly approached a similar value as in the RL. This distinct pattern was observed on all morning profile flights and was caused by two processes. First, the degradation process of isoprene and AVOCs due to the increase in OH concentration produces newly formed OVOCs; and second the NBL dilutes into the ML. Due to the fast evolvement of the ML, the degradation contribution is considered minor for species with a long lifetime with OH compared to the dilution effect. Considering, the VOC with shorter lifetimes with OH as isoprene the degradation can also play a significant role. But with the current dataset it is not possible to determine the exact factor as the source strengths and the mixing velocities are known.

The analysis of the k_{OH}(OVOC)/k_{OH}(VOC) ratio has shown that the high ratio in the RL and the low ratio in the ML can be qualitatively understood, but not the high ratio in the NBL. In the following the two questions will be addressed. First, why is the ratio so stable and so high in the NBL? And second, why does this system always levels off to a ratio of above 65 % OVOC fraction?

4.5.6 Ratio of k_{OH}(OVOC)/k_{OH}(VOC) in the NBL

To identify the cause for the constant ratio between k_{OH}(OVOC) and k_{OH}(VOC) in the NBL the chemical composition has to be analyzed in detail. Under ideal conditions the NBL is characterized by concentrations of trace gases from primary emissions during the night that are trapped in a shallow surface layer (Velasco et al., 2008). Therefore, it is expected that the k_{OH}(OVOC)/k_{OH}(VOC) ratio should be lower compared to the ratio in RL which is not affected by primary emissions or photochemical production or deposition. Thus, the question arises, why the ratio of k_{OH}(OVOC)/k_{OH}(VOC) in the NBL is comparable to the RL.

Thus, the change of k_{OH}(OVOC) and k_{OH}(AVOC, BVOC) is analyzed in detail for the NBL. The change in k_{OH}(OVOC) in the NBL is affected by four different contributions, namely the emission, the production, advection and the destruction as elaborated in further detail below. OVOCs are likely emitted by primary sources; at least this is the case for the most abundant such as formaldehyde, acetaldehyde, acetone, methanol and ethanol. In this study the quantification of the fraction of OVOCs originating from primary sources is limited as there was no simultaneous measurement of OVOCs at the ground.

At nighttime there was no photochemistry taking place, so that the main OVOC production is limited to the reaction of VOCs with O_3 and NO_3. For the measured height of 100 m (AGL) this cannot be a great source as the alkene mixing ratios were very low (30-60 ppt) and the alkene lifetimes for the reaction with O_3 and NO_3 are within the range of 2.5 - 10 h calculated for an ozone concentration of 50 pbb and an estimated NO_3 concentration of 40 ppt (Platt et

al., 1984). Advection is also a factor that can lead to a change in k_{OH}(OVOC), but is also not possible to quantify with the current data set.

In the NBL the destruction term for OVOCs is limited to dry and wet deposition as the OVOCs lifetime of the reaction with NO_3 and O_3 are higher than the deposition lifetimes. However, the wet deposition can be neglected, as there was no precipitation during the vertical profile flights. The dry deposition velocity was estimated for a height of 800 m (AGL) in Table 4.13. Taking the deposition lifetimes that range between 40 and 250 h for the most abundant OVOCs into account, it becomes evident that dry deposition is not a major OVOC sink for those in the table below.

Table 4.13: Deposition velocity and deposition lifetimes of the most abundant OVOC species making the largest contributions to the k_{OH}(OVOC).

Substance	**Deposition velocity [cm s^{-1}]**	**Deposition lifetime for a PBL height of 800 m (AGL) [h]**	**Source**
HCHO	0.5 (at daytime)	44	Benning and Wahner (1998)
Acetaldehyde	0.2 (entire day)	111	Warneke et al. (2002)
Methanol	0.2 (entire day)	111	Jacob et al. (2005)
Acetone	0.09 (entire day)	246	Warneke et al. (2002)

In conclusion then the change in the k_{OH}(OVOC) is only given by the emission and advection term of the OVOCs.

The change in the primary constituents was dominated by the k_{OH}(AVOC) as there is no change in k_{OH}(BVOC) and $k_{OH}(CH_4)$ (see Figure 4.26). Comparable to the OVOCs the change in k_{OH}(AVOC) was dominated by emission, advection and destruction. There is no AVOC production term, as AVOCs are not produced.

The concentration of AVOCs is most likely increasing at night, when they are emitted at the ground and enter the shallow stable nocturnal boundary layer. Here the AVOCs are trapped instead of being mixed into the full PBL, leading to their relatively high concentrations.

Advection may lead to a change in k_{OH}(OVOC) but it has not been quantified in the course of this campaign.

The destruction of AVOC can also be disregarded, as there is no photochemistry at night. And the destruction of VOCs especially alkenes by the O_3 and NO_3 is relatively limited as discussed above. No deposition lifetimes of measured AVOCs have been reported except for PAHs with deposition lifetimes of 50 h (see Table 4.14). Lou et al. (2010) has stated a mean deposition lifetime of 24 h. Thus, the deposition of AVOCs can also be neglected.

Table 4.14: Deposition velocity and deposition lifetimes of PAH.

Substance	Deposition velocity [cm s^{-1}]	Deposition lifetime for 1000 m (AGL) [h]	Source
PAHs	0.99	50	(McVeety and Hites, 1988)

Similar to the k_{OH}(OVOC) the change in k_{OH}(AVOC) can therefore defined by emission and advection term. Therefore, the ratio of k_{OH}(OVOC)/k_{OH}(VOC) can only stay constant, when the emission strength and advection of k_{OH}(OVOC) are equal to the emission strength and advection of k_{OH}(AVOC).

This assumption is supported by the first FS in the NBL where the OH reactivity is higher but the ratio remains the same. This means that k_{OH}(AVOC) and k_{OH} (OVOC) had a similar source and they were slowly mixed up into the NBL without significant losses. But this cannot be clarified more due to missing information, the only way to determine the emission and advection term is by using a transport model.

When considering the ratio k_{OH}(OVOC)/k_{OH}(VOC), the missing reactivity which occurred predominantly in the NBL has also to be taken into account. If the missing reactivity exclusively derived from the AVOCs the k_{OH}(OVOC)/k_{OH}(VOC) ratio changes as shown in Figure 4.27.

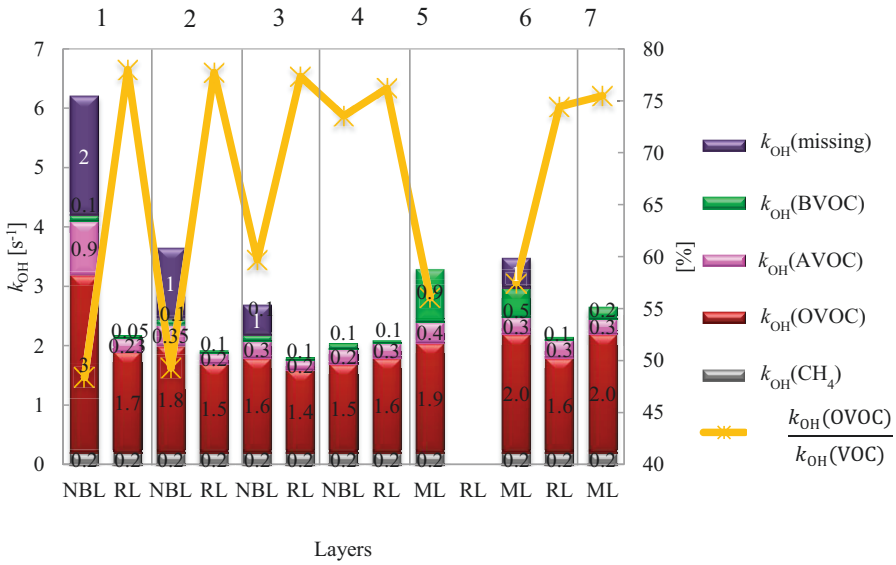

Figure 4.27: The mean k_{OH} distributions of CH_4, OVOCs, anthropogenic, biogenic VOCs including the missing reactivity for Flight F023/024 shown in the bar graphs for each consecutively sampled layer in s^{-1}. The ratio of k_{OH}(OVOC)/k_{OH}(VOC) is shown in orange in percentages. The assumption is that the entire missing reactivity originates from unmeasured AVOCs. The flight was subdivided into 7 flight sections

Here, the ratio decreases to values below 50 %, which is more in line with what would be expected from previous assumptions. But the analysis of the missing reactivity in the NBL (see Chapter 4.5.4.) shows that also a significant fraction of the missing constituents may also be OVOCs arising from anthropogenic sources. So, obviously the missing reactivity has anthropogenic sources, however it cannot be distinguished in this work if it arises from AVOCs or primary emitted OVOCs as there are no sufficient ground and eddy measurements. Thus, the chemical composition of the missing reactivity is not clear.

4.5.7 The k_{OH}(OVOC)/k_{OH}(VOC) ratio in the different layers

In all the vertical profile flights conducted during the PEGASOS campaigns the k_{OH}(OVOC)/k_{OH}(VOC) in the NBL and in the RL was higher than 65 %. Only in the early ML the ratio was below 50 %. But, after an evolvement time of 3 hours, the ratio changed to a percentage share of above 65 % also in the ML. From those findings two questions arise: why is the ratio always higher (in NBL and RL) than 65 % and how can that be explained? As this high k_{OH}(OVOC)/k_{OH}(VOC) ratio especially in the NBL was not expected.

For the analysis of the k_{OH}(OVOC)/k_{OH}(VOC) ratio measured during this campaign a model assumption has been made as shown in Figure 4.28. This assumption comprises that the entire PBL is a closed box which is always homogeneously mixed neglecting the layering during the night. The emissions of AVOCs and BVOCs are continuous and have a constant emission strength Q. The emissions of OVOCs into the system are negligible and the only source of OVOCs in the system is the reaction of primary emitted VOCs with OH. The reactions of VOCs with NO_3 and O_3 are also neglected as they are subordinate to the reaction with OH. Within this box there are no vertical gradients thus advection of AVOCs, BVOCs and OVOCs is negligible. All concentrations of AVOCs, BVOCs, OVOCs, and OH are in steady state which means that the concentrations in the system are all constant. The number of daughter product generations is limited by the deposition and photolysis lifetimes of the specific VOC and the carbon chain length of the mother substance. The reaction of the VOC and OVOCs proceeds until the formation of CO, CO_2, H_2 and H_2O.

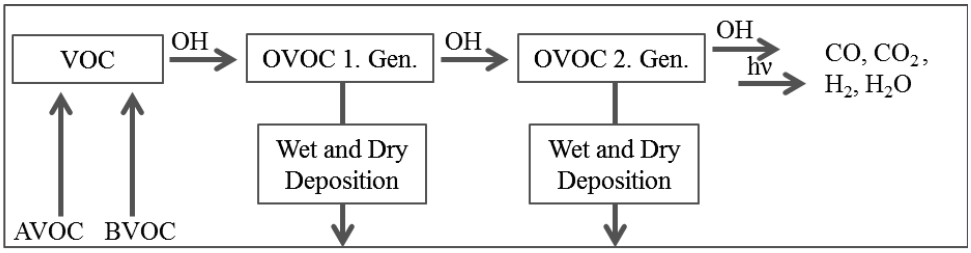

Figure 4.28: Pseudo model assumption with only AVOCs and BVOCs emitted from the ground. The source of OVOCs is the reaction with OH. The reaction proceeds until the OVOCs are deposited or CO, CO_2, H_2 and H_2O are formed. The box is well mixed with no horizontal gradients and all trace gases are in the steady state within the box.

This model assumption is applied for primary species found during the campaigns, which constitute 50 % of the reactivity of the primary emitted VOCs including 1-butene, isoprene, and toluene. The k_{OH}(OVOC)/k_{OH}(VOC) ratio is calculated for every single substance for every single generation. As not all produced OVOCs can be measured there can be a difference between the calculated and the measured ratio can be found. This is equivalent to the missing reactivity.

Within this system OH is the only reactant that determines the lifetime of all the VOCs. The primary emitted VOC A_0 reacts with OH and forms one daughter product B_1 which can react further with OH to one daughter product D_2 (see Equation 4.1). In this system substance A_0 is either an AVOC or a BVOC and as the degradation is only limited to the reaction with OH, the resulting daughter products are always OVOCs.

$$A_0 \xrightarrow[k_1]{OH} B_1 \xrightarrow[k_2]{OH} D_2 \xrightarrow[k_3]{OH} H_3 \qquad 4.1$$

When studying chemical reaction kinetics for B_1, the production and destruction term as well as the specific reaction rate constant k have to be considered. As this system is assumed to be in steady state, the rate of change of the concentration with time is approximately zero (see Equation 4.2).

$$\frac{d[B_1]}{dt} \approx 0 \qquad 4.2$$

The change of B_1 is given by

$$\frac{d[B_1]}{dt} = k_1 * [OH] * [A_0] - k_2 * [OH] * [B_1]. \qquad 4.3$$

Equation 4.3 can also be applied for D_2 and one finds for the mother substance and the two daughter generations.

$$k_1 * [OH] * [A_0] = k_2 * [OH] * [B_1] = k_3 * [OH] * [D_2] \qquad 4.4$$

In this equation the OH concentration can be cancelled. Thus, the following model approach is not dependent on the OH concentration which in reality may have diurnal and height variations. Therefore, it can be obtained

$$k_1 * [A_0] = k_2 * [B_1] = k_3 * [D_2] \qquad 4.5$$

And from that it follows that the product of the rate constant and the concentration is equal to the OH reactivity (see Equation 1.24)

$$k_{OH}(A_0) = k_{OH}(B_1) = k_{OH}(D_2). \qquad 4.6$$

So, it can be found that, the OH reactivity of the mother substance A_0 equals the OH reactivity of the daughter substance of the 1st generation (B_1) and the OH reactivity of the daughter

substance and the 2nd generation (D_2). Consequently the k_{OH}(OVOC) increases when the system proceeds to higher generations.

The k_{OH}(OVOC)/k_{OH}(VOC) ratio can be calculated as shown in Equation 4.7. For the ratio the sum of the OH reactivity of all the daughter generations (i) has to be taken into account. This can be simplified by introducing n, the number of daughter products of all generations.

$$\frac{k_{OH}(OVOC)}{k_{OH}(VOC)} = \frac{\sum k_{OH}(i)}{\sum k_{OH}(i)+k_{OH}(A_0)} = \frac{n\left(k_{OH}(A_0)\right)}{n\left(k_{OH}(A_0)\right)+\left(k_{OH}(A_0)\right)} = \frac{n}{n+1} \quad .$$

i = number of daughter generations

n = number of all daughter products 4.7

Thus, for the first generation (until B_1) the calculated k_{OH}(OVOC)/k_{OH}(VOC) ratio has a value of 50 % if only one daughter product is formed. If the system reacts further the k_{OH}(OVOC)/k_{OH}(VOC) ratio increases to 67 % in the second generation (until D_2) and 75 % in the third generation. The k_{OH}(OVOC)/k_{OH}(VOC) ratio increases even faster if not only one daughter product is formed but two as shown in Figure 4.29.

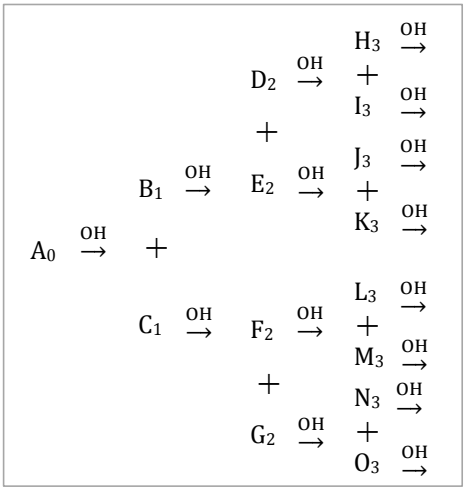

Figure 4.29: The degradation of A_0 by OH into the 3 daughter generations.

In this case also the number j of daughter products in each single generation has to be taken into account for the calculation of the k_{OH}(OVOC)/k_{OH}(VOC)ratio. This changes Equation 4.7 to

$$\frac{k_{OH}(OVOC)}{k_{OH}(VOC)} = \frac{\sum_i \sum_j k_{OH}(i,j)}{\sum_i \sum_j k_{OH}(i,j)+k_{OH}(A_0)} = \frac{n\left(k_{OH}(A_0)\right)}{n\left(k_{OH}(A_0)\right)+\left(k_{OH}(A_0)\right)} = \frac{n}{n+1} \quad .$$

i = number of daughter generations

j = number of products of one generation

n = number of all daughter products 4.8

Thus, the k_{OH}(OVOC)/k_{OH}(VOC) ratio for the first generation has a value of 67 %, 86 % in the second generation and in the third generation 93 %. This chain reaction continues and the

k_{OH}(OVOC)/k_{OH}(VOC) ratio is gradually increased, until all daughter products are transformed into CO. Although CO is degraded by the reaction with OH it is not considered here as it is not regarded as a VOC and therefore not included in the k_{OH}(OVOC)/k_{OH}(VOC) ratio.

The reaction can also be terminated if the daughter products are lost out of the system. Besides the reaction with OH the dominating loss term of the system is the deposition. The mean deposition velocity for all trace gases is estimated to 1.2 cm/s (Lou et al., 2010) which results in a mean deposition lifetime in the system with a height of 800 m (AGL) of 18.5 h. Thus, if the OVOC lifetime with OH is longer than 18.5 h this OVOC is irrelevant for the ratio. Thus, a remaining factor (y_j) has to be taken into account which accounts for the loss term (k_{loss})

$$y_j = \frac{k_{j+OH}[OH]}{k_{j+OH}[OH]+k_{loss}} \quad . \qquad 4.9$$

For all the analyzed VOCs the reaction with OH dominates the degradation by photolysis by far with the exception of HCHO. For HCHO the contribution of photolysis to the degradation process has to be considered. In this study the mean lifetime of HCHO is calculated using the mean photolysis frequencies and the mean OH concentration for the campaign (see Table 4.15). The resulting HCHO lifetime is 3 h and the fraction of the reaction with OH is 0.49. The fraction of 0.51 of the HCHO is depleted by photolysis.

Table 4.15: Mean photolysis frequencies and OH concentration for the PEGASOS campaign.

Reaction path	**Mean value of PEGASOS campaign**
J(HCHO_R)	2.4 x 10^{-5} s^{-1}
J(HCHO_M)	2.97 x 10^{-5} s^{-1}
OH	6 x 10^{6} molecules cm^{-3}

For a more realistic calculation the remaining factor (y) has to be taken into account when calculating the k_{OH}(OVOC)/k_{OH}(VOC) ratio , which leads to the following equation

$$\frac{k_{OH}(OVOC)}{k_{OH}(VOC)} = \frac{\sum_i \sum_j y_{ij} * k_{OH}(i,j)}{(\sum_i \sum_j y_{ij} * k_{OH}(i,j)) + k_{OH}(A_0)} = \frac{\sum_i \sum_j y_{ij} \; k_{OH}(A_0)}{\sum_i \sum_j y_{ij} * k_{OH}(A_0) + k_{OH}(A_0)} = \frac{\sum_i \sum_j y_{ij}}{\sum_i \sum_j y_{ij} + 1}$$

i = number of daughter generations

j = number of products of one generation

y = remaining factor 4.10

Another complexity which adds to the analysis is the branching into different reaction channels as shown in Equations 4.11 and 4.12. Only a fraction of 0.6 is reacting to B_1 and C_1 and a fraction of 0.4 to D_1. Furthermore, in this example all daughter products are further degraded by the reaction with OH.

$$A_0 + OH \xrightarrow{0.6} B_1 + C_1 \qquad k_1 \qquad 4.11$$

$$A_0 + OH \xrightarrow{0.4} D_1 \qquad k_2 \qquad 4.12$$

Considering the chemical reaction kinetics, the branching ratio has to be integrated. The resulting term for the OH reactivity of B_1, C_1 and D_1 is given in Equation 4.13. The branching factor (b_j) has to be taken into account.

$$\frac{k_{OH}(OVOC)}{k_{OH}(VOC)} = \frac{\sum_i \sum_j y_{ij} b_{ij} * k_{OH}(i,j)}{(\sum_i \sum_j y_{ij} b_{ij}\, k_{OH}(i,j)) + k_{OH}(A_0)} = \frac{\sum_i \sum_j y_{ij} b_{ij} * k_{OH}(A_0)}{\left(\sum_i \sum_j y_{ij} b_{ij} * k_{OH}(A_0)\right) + k_{OH}(A_0)} = \frac{\sum_i \sum_j y_{ij} b_{ij}}{\sum_i \sum_j y_{ij} b_{ij} + 1}$$

i = number of daughter generations
j = number of products of one generation
b = factor for the branching ratio
y = remaining factor 4.13

The $k_{OH}(OVOC)/k_{OH}(VOC)$ ratio has now a value of 62 %, which is lower than the ratio of 67% when two daughter products are produced at the same rate.

For simplification the branching factor (b_i) and the remaining factor (y_i) are summed up in the factor f_i which leads to

$$\frac{k_{OH}(OVOC)}{k_{OH}(VOC)} = \frac{\sum_i \sum_j f_{ij} * k_{OH}(i,j)}{(\sum_i \sum_j f_{ij} * k_{OH}(i,j)) * k_{OH}(A_0)} = \frac{\sum_i \sum_j f_{ij} * k_{OH}(A_0)}{(\sum_i \sum_j f_{ij} * k_{OH}(A_0)) + k_{OH}(A_0)} = \frac{\sum_i \sum_j f_{ij}}{\sum_i \sum_j f_{ij} + 1}\ .$$

i = number of daughter generations
j = number of products of one generation
$f = b_j * y_j$ 4.14

It can be concluded that the $k_{OH}(OVOC)/k_{OH}(VOC)$ ratio is dependent upon the number of possible generations, the number of daughter products, their branching ratio and the importance of photolysis reactions for formaldehyde.

All these dependencies will be taken into account in the following when applying this to a model to calculate the $k_{OH}(OVOC)/k_{OH}(VOC)$ ratio for 1-butene, isoprene and toluene. For these substances some daughter products cannot be analyzed which may lead to a gap between the theoretical $k_{OH}(OVOC)/k_{OH}(VOC)$ ratio and the effectively measured ratio. The analysis is performed in the following by applying the reaction mechanisms and the rate coefficients taken from the MCM Version 3.2.

1-Butene branches into two channels (see Figure 4.30), but products from each channel are identical. The degradation process continues until 1-butene is degraded into third daughter generation before reaching CO. In this example, the lifetimes are below 24 h, thus the deposition can be neglected, and all daughter substances can be measured.

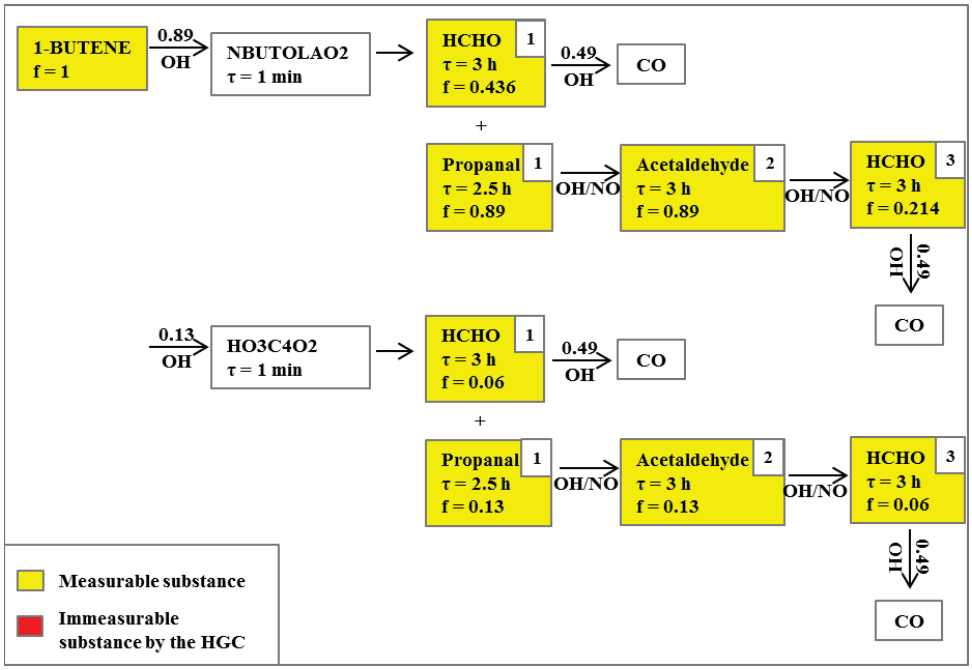

Figure 4.30: The OH degradation of 1-butene with its four generations. The denoted OH lifetimes (τ) are calculated for an OH concentration of $6x10^6$ molecules cm^{-3}. The factor *f* represents the remaining and branching factor of the k_{OH} of the mother substance. The numbers above the errors indicate that only this fraction reacts along the outlined path. All substances marked in white, are either unmeasurable with the HGC, are short-lived and thus low in concentration and make a small contribution to the OH reactivity or not included in the k_{OH}(OVOC)/k_{OH}(VOC) ratio because they are long-lived or not considered as VOCs.

The analysis of 1-butene shows that the theoretical and measurable k_{OH}(OVOC)/k_{OH}(VOC) ratio is identical as all the daughter products can be measured. Already in the second generation a ratio of above 65 % is reached (see Table 4.16).

Table 4.16: The theoretical and measurable k_{OH}(OVOC)/k_{OH}(VOC) ratio for 1-buten in the degradation with OH for the three generations. The ratios highlighted in bold numbers are above 65 %.

k_{OH}(OVOC)/k_{OH}(VOC) ratio	1. Generation	2. Generation	3. Generation
Theoretical ratio	0.60	**0.72**	**0.74**
Measurable ratio	0.60	**0.72**	**0.74**

The analysis shows different results for isoprene, as shown in Figure A.17 - A.20. Here the fourth generation of the daughter products can be reached but the fraction of unmeasured daughter products is significant, leading to a difference between the theoretical and measurable k_{OH}(OVOC)/k_{OH}(VOC) ratio (see Table 4.17). This difference is determined as the missing reactivity. Following the theoretical approach, in the second generation, this ratio

would be above 64 %. However, when considering the measured results, the 64 % ratio is only reached in the fourth generation.

Table 4.17: The theoretical and measurable k_{OH}(OVOC)/k_{OH}(VOC) ratio for isoprene in the degradation with OH for the four generations. The ratios highlighted in bold numbers are above the 65 %.

k_{OH}(OVOC)/k_{OH}(VOC) ratio	1. Generation	2. Generation	3. Generation	4. Generation
Theoretical ratio	0.55	**0.70**	**0.74**	**0.75**
Measurable ratio	0.53	0.60	0.63	0.64

For toluene the situation is completely different, as the possible measurable daughter products are limited to HCHO (see Figure A.21 - A.24 in the attachment). Some daughter products also have a lifetime with OH of 33 h (for example MALANHY (furan-2,5-dione)). However, theoretically daughter products of the fifth generation can be reached. For toluene, the difference between the theoretical and measurable k_{OH}(OVOC)/k_{OH}(VOC) ratio of all three analyzed species is the highest (see Table 4.18). The theoretical ratio is already above 70 % in the second generation, whereas the ratio does not reach a value above 24 % including the fifth generation daughter products.

Table 4.18: The theoretical and measurable k_{OH}(OVOC)/k_{OH}(VOC) ratio for toluene in the degradation with OH for the five generations. The ratios highlighted in bold numbers are above the 65 %.

k_{OH}(OVOC)/k_{OH}(VOC) ratio	1. Generation	2. Generation	3. Generation	4. Generation	5. Generation
Theoretical ratio	0.60	**0.70**	**0.73**	**0.75**	**0.75**
Measurable ratio	0.00	0.12	0.24	0.24	0.24

The analysis of the theoretical and measured k_{OH}(OVOC)/k_{OH}(VOC) ratio for all three analyzed species after the 5th generation the system had reacted to species which are either irrelevant for the ratio or are deposited. This corresponds to the measurements, where the ratio is higher than 65% for the vertical profile flights. For all three analyzed VOCs the theoretical ratio is higher than 69 % in already the second generation. However, there can be a significant difference between the theoretically derived and the measured ratio especially for isoprene and toluene. This difference is equivalent to the missing reactivity which is the highest for toluene the only measurable daughter product is HCHO. On the contrary for 1-butene all generations can be measured. Thus, the span of possible reaches k_{OH}(OVOC)/k_{OH}(VOC) ratios ranges from 24 % to 74 % if the system reacts to the last possible generation.

When applying this approach to the observations the ratio has to be weighted for the relative abundance of the reactivity in which the 3 species were observed throughout the campaigns. Throughout the entire campaigns the ratio of the OH reactivity between the three analyzed species was 1:1: 33.3 (1-butene: toluene: isoprene). Additionally, one has to take into account, that the three species only contribute around 50% to the overall reactivity. Thus, if the k_{OH}(OVOC)/k_{OH}(VOC) ratio is calculated according to their relative abundance in which they were analyzed, the value of the ratio would be 63 % under the condition that the system of

each species has reacted to its last generations. This is only relevant for very aged air masses as it would be expected in the background atmosphere. But, as the measurements were conducted above the continent with a significant amount of primary emissions it is unlikely that all species have reacted to their last generation. Also the assumption of steady state is not valid for a real atmosphere. Consequently, there have to be different sources for OVOCs that drive this ratio. As discussed in Chapter 1.2.1 the primary emitted OVOCs are also significant. Another possible source of OVOCs which has not been included in this consideration is the advection. Especially, the advection of short chained, not known substances, can function as OVOC precursors and lead to higher OVOC concentrations. These precursors could form OVOCs, far away from the primary emissions. Previous studies have suspected long lived oxidation intermediates as organic peroxides and long chained alcohols (Lewis et al., 2005), the oxidation of organic aerosol (Kwan et al., 2006) and the oxidation of unmeasured higher hydrocarbons (Olson et al., 2012) as delocalized OVOC sources.

These sources are also likely for this study; especially for formaldehyde and acetaldehyde which have lifetimes with OH of below 6 h (see Table 4.19). As there are many different oxidized VOCs that cannot be measured and yield in both is likely. And if the OH reactivity of these unmeasured long chained OVOCs is low they are completely disregarded in the simple model. They can also be advected and oxidized to short chained OVOCs far from the source. Other OVOCs as ethanol, methanol as well as acetone with longer lifetimes with OH can also be advected themselves.

Table 4.19: Lifetimes for the most abundant VOCs for a mean OH concentration of $6x10^6$ molecules cm^{-3}.

Species	**Lifetimes [h]**
Formaldehyde	5.5[a)]
Acetaldehyde	3
Methanol	51
Ethanol	14
Acetone	264

[a)] Destruction by photolysis included.

Accordingly, the overall observations of the high $k_{OH}(OVOC)/k_{OH}(VOC)$ ratio is plausible for the assumptions made and the 3 analyzed species. But this has to be analyzed further in depth especially by model calculations. Global model calculations could bring more insight into the distributions of OVOCs on a global scale, as the advection terms as well as the primary emissions are not well understood yet. Within this work this was not possible but to fully comprehend the OVOC sources and distributions model calculations are indispensable.

5. Summary and Conclusion

The analysis of the planetary boundary layer especially in the altitude range between 100 and 1000 m (AGL) is of great importance as here most of the trace gas conversion takes place. At this height VOCs are oxidized mainly by the OH radical and to a minor extent by O_3 and NO_3. To explore this altitude range was one objective of the PEGASOS study. The airship Zeppelin NT was utilized because of its unique flight performance as measuring platform. Since this part of the planetary boundary layer has only been investigated sparsely in previous research, the data presented here contributed new insights into atmospheric chemistry. The VOC measurements vertically and horizontally across different biomes in Europe from the Mediterranean in Italy to the mid-latitudes in the Netherlands showed that the concentrations of the primary emitted AVOCs and BVOCs were lower than the OVOCs, making the OVOCs important OH sinks. The comparison of the measured OH reactivity to the calculated revealed only a low missing reactivity which shows the integrity of the VOC measurements.

The focus of this work was on the VOC measurements with a fast GC-MS system (Gas Chromatography coupled with a Mass Spectrometry) on board the Zeppelin NT. The implementation of the instrument (HGC) for use on board the Zeppelin NT required reconstruction of the system in order to improve its analytical performance, to meet aviation requirements and to save weight (see Chapter 2.3). The VOC preconcentration unit was optimized to broaden the analytes spectra and enhance the measuring stability. All parameters of the GC-MS system were optimized by multiple characterization measurements in order to reduce the influence of ambient ozone, water and artifacts from the carbon bases adsorbents. The unique, interlaced instrumental setup of the preconcentration-, separation- and detection unit facilitates a 3 minute time resolution (see Chapter 2.4). The instrument was calibrated to measure 49 different substances, ranging from alkanes to oxygenated VOCs, with a mean detection limit of 5 ppt. Depending of the respective substance the instrument has a mean precision of 3 % and the accuracy varies between 10 - 25 % (see Chapter 2.5).

In 2012, two Zeppelin PEGASOS campaigns were conducted. The first campaign took place in the Netherlands, close to Rotterdam (in May 2012) and the second campaign was conducted in Italy in the area of Bologna (in June-July 2012). During both campaigns three different flight patterns were performed. Vertical profile flights were made to probe the vertical structure of the troposphere. Local transect flights were conducted to analyze different emission patterns by crossing areas with different land use, as well as over the sea (North Sea and Adrian Sea). Finally, transfer flights were flown to relocate the Zeppelin NT from Friedrichshafen, Germany, where it is stationed to the measuring sites in the Netherlands and in Italy and back. During both campaigns 43 measurement flights were performed where the HGC instrument was on board, 14 in the Netherlands and 29 in Italy. During both campaigns the instrument showed good performance with good data coverage of 82 % and 87 % (see Chapter 3.2).

Considering, all the unique data obtained in the Netherlands and in Italy VOCs showed mixing ratios with mean values below 5 ppb. Especially, low values (200 ppt) were obtained for the primary emitted VOCs, such as the anthropogenically emitted alkanes, alkenes and aromatics as well as the biogenically emitted isoprene and terpenes. Overall, higher concentrations of the anthropogenically emitted VOCs (AVOCs) were measured in the Netherlands in comparison to Italy. However, the biogenically emitted VOCs (BVOCs) reached higher values in Italy. The oxygenated VOCs (OVOCs) were the most abundant VOCs, with mean concentrations ranging from 0.7 to 4.9 ppb for both parts of the campaign. In general, methanol, ethanol, acetone and acetaldehyde made up the highest concentrations apart from formaldehyde measured by the FFL instrument. Methanol was the most abundant VOC for both parts of the campaign with a mean value of 4.9±1.9 ppb in the Netherlands and 2.5±1.8 ppb in Italy (see Chapter 3.3).

The individual contributions of the VOC together with other trace gases as NO_x and CO to the total OH reactivity were calculated and compared to the OH reactivity measured by the LIF instrument. The difference between measured total OH reactivity and calculated total OH reactivity termed 'missing reactivity' was small for both parts of the campaigns. This indicates a completeness of the VOC measurements. In the Netherlands the mean missing reactivity had a value of 1.0±1.4 s^{-1} at a mean measured OH reactivity of 6.13±1.23 s^{-1}. In Italy the mean missing reactivity was 0.1±2.2 s^{-1} at a measured total OH reactivity of 3.8±1.4 s^{-1}. It could not be assessed if the origin of the missing reactivity was from anthropogenic or biogenic sources (see Chapter 4.3). However, in the analysis of the vertical structure of the lower troposphere a significant higher missing reactivity inside the Nocturnal Boundary Layer (NBL) between 70 and 400 m above ground could be observed. Moreover, in the NBL the missing reactivity significantly correlates with higher concentrations of the anthropogenic precursors such as NO_x and AVOCs. These results indicate that the missing reactivity predominantly originated from an anthropogenic rather than biogenic emitted VOCs sources for the analyzed regions close to Rotterdam and Bologna for these specific weather conditions (see Chapter 4.5.1).

The analysis of the single contributions to the overall OH reactivity showed the importance of OVOCs as the main OH sink. The OVOCs contributed 30 % in the Netherlands and 40 % in Italy to the total OH reactivity which made them the largest contribution followed by NO_x (28 % (NL) and 18 % (IT)) and CO (9 % (NL) and 11 % (IT)). All other substance classes contributed less than 8 % (see Chapter 4.3.4). Therefore, it can be concluded that OVOCs are of great importance between the height of 100 and 1000 m which has not been investigated in depth before. Thus, OVOCs are likely to be underestimated in current models (Kwan et al., 2006; Lewis et al., 2005).

The sources of OVOCs are manifold, including primary biogenic and anthropogenic sources as well as secondary photochemical production. This made it difficult to determine the exact origin of the OVOCs in this study. In the Netherlands and in the plume of the Mannheim/Ludwigshafen region during the transfer flight to Rotterdam elevated OVOC mixing ratios were measured together with elevated mixing ratios of anthropogenic tracers. In the Mannheim/Ludwigshafen plume especially methanol and ethanol values could be observed together with toluene and xylenes (see Chapter 4.4.1). But OVOCs were also found

in significant amounts as part of the background atmosphere especially over parts of Slovenia and Austria in the transfer flight from Bologna to Graz.

For the first time, the abundance of OVOCs was assessed at different heights in the planetary boundary layer. The ratio of k_{OH}(OVOC)/k_{OH}(VOC) for the vertical profile flights was larger than 65 % in the NBL and the RL. In the fresh mixed layer this ratio fell below 50 %. However, after 3 hours the ratio increased to more than 65 % (see Chapter 4.5.2.2). A theoretical approach was applied to analyze the plausibility of the observed high ratio by calculating the expected k_{OH}(OVOC)/k_{OH}(VOC) ratio for 1-butene, isoprene and toluene for a closed system with steady state conditions. This ratio was compared to the ratio that can be measured for the same system. If all the daughter products can be measured, as it is the case for 1-butene, the maximal ratio is 74 %. In contrast, the possible measured toluene degradation products are limited only to formaldehyde. Here, the highest expected ratio that can be measured has a value of 24 %. Consequently, the high k_{OH}(OVOC)/k_{OH}(VOC) ratios as observed cannot result only from the photochemical production but a significant amount of primary emitted and advected OVOCs must also be present (see Chapter 4.5.2.4).

This study has shown that the HGC is a robust instrument for the mobile fast analysis of VOCs. The major result of this study shows that the air in the height range between 100 and 1000 m across the analyzed regions above southern and western Europe was relatively clean as it has a low OH reactivity compared to other studies as shown in Table 2.1 with low concentrations of primary emitted trace gases. But this study showed that the fraction of oxygenated VOCs was very high thus they function as the major OH sink. On the other hand aldehydes can also function as an OH source. The sources of these OVOCs are manifold but as in previous studies shown their precursors have not been understood but most probably they are long-lived oxidation products that can travel far from the point of primary emission. Therefore, the regional emitted primary trace gas is transformed into OVOC precursor that can have a global effect.

Future work could compare the results obtained for the Netherlands and Italy to those of the Zeppelin campaign that was performed in 2013 in Finland with the same set of instruments. Here, especially the analysis of the missing reactivity may be interesting as the study of Nölscher et al. (2012) reported significant amounts reaching up to a fraction of 89 % in a forest, which could not be explained. Furthermore, results on the k_{OH}(OVOC)/k_{OH}(VOC) ratio in the rural regions of Finland, with expected minor primary sources of OVOCs, could be compared to measurements across the urban regions in the Netherlands and Italy. In a next step the observations of this study should be validated using model calculations, for example by utilizing a one dimensional box model. A regional or global model, to determine the OVOC distribution as well as the OVOCs advection term would certainly offer new insights into the sources of OVOCs. Model calculations are also a research objective of the PEGASOS project in order to determine the regional and global links of atmospheric chemistry and climate change.

List of abbreviations

AGL	Above Ground Level
AMS	Aerosol Mass Spectrometer
AVOC	Anthropogenic VOC
BVOC	Biogenic VOC
CL	Cabin Layout
CO	Carbon monoxide
COD	Carbon monoxide Detector
CO_2	Carbon dioxide
GC	Gas Chromatograph
EST	University of Tartu, Estonia
FFL	Formaldehyde measurement via Fiber Laser induced fluorescence
FID	Flame Ionization Detector
FT	Focus Trap
FTH	Focus Trap Heater
FZJ	Forschungszentrum Jülich, IEK-8, Germany
FS	Flight Section
HALO	High Altitude LOng range aircraft
HCHO	Formaldehyde
HGC	HALO Gas Chromatograph
HO_2	Hydroperoxy radical
HO_x	Sum of OH and HO_2
HONO	Nitrous acid
HU	Height Unit
k_{OH}	Total OH reactivity
k_{OH}^{calc}	Calculated OH reactivity

k_{OH}^{meas}	Measured OH reactivity
k_{OH}^{miss}	Missing OH reactivity
LDA	Luftschiff Daten Aufzeichnung
LIF	Laser Induced Fluorescence
LOPAP	LOng Path Absorption Photometer for HONO measurement
MBO	2-Methyl-3-buten-2-ol
MACR	Methacrolein
ML	Mixed Layer
MS/MSD	Mass Spectrometer Detector
MVK	Methyl vinyl ketone
m/z	Mass to charge ratios
NBL	Nocturnal Boundary Layer
NO	Nitric oxide
NO_2	Nitrogen dioxide
NO_3	Nitrate radical
NO_x	Sum of NO and NO_2
O_3	Ozone
O_2	Oxygen
OH	Hydroxy Radical
PBL	Planetary Boundary Layer
PEGASOS	Pan-European-Gas-AroSOl-climate interaction Study
ppb	parts per billion volume mixing ratio
ppm	parts per million volume mixing ratio
ppt	parts per trillion volume mixing ratio
PSI	Paul Scherrer Institute, Villingen, Switzerland
RH	Relative Humidity
RL	Residual Layer
RO	Alkoxy radicals
RO_2	Peroxy radicals
SOA	Secondary Organic Aerosol

SL	Surface Layer
SPC	San Pietro Capofiume
SIM	Select Ion Monitoring
ST	Sample Trap
STH	Sample Trap Heater
UHEL	University of Helsinki, Finland
UWI	University of Wisconsin–Madison, USA
VFR	Visual Flight Rules
VOC	volatile Organic Compounds
WT	Water Trap
WTH	Water Trap Heater
ZLT	Zeppelin Luftschifftechnik, Friedrichshafen, Germany
τ_{OH}	OH lifetime

Appendix

5.1 Appendix Observations

Table A.1: Overview of the meteorology for each flight day of the north campaign (KNMI, June 2013; Wunderground, June 2013).

Date	Flight Number	Meteorology Station	Mean Temp [°C]	RH [%]	Wind speed [km/h]	Visibility [km]	Precipitation [mm]	Wind direction
17.05	006/007	Friedrichshafen	8	61	8	9.3	0	E
18.05	008/009	Mainz	14	60	11	14.8	0.4	**S**
19.05.	010	Rotterdam	15	74	10	11	0	N
21.05.	011	Rotterdam	16	86	9	7.7	0	N
22.05.	012	Rotterdam	18	81	10	7.9	0	SW
24.05.	013/014	Rotterdam	22	70	10	8.9	Fog	E
27.05.	015/016	Rotterdam	20	58	10	11.5	0	N
28.05.	017	Rotterdam	16	78	9	9	0	NW
29.05.	018	Mainz	21	43	13	14.4	0	NE

Table A.2: Overview of the meteorology for each flight day of the north campaign (Wunderground, June 2013).

Date	Flight Number	Meteorology Station	Mean Temp [°C]	RH [%]	Wind speed [km/h]	Visibility [km]	Precipitation [mm]	Wind direction
14.06.	019	Friedrichshafen	14	63	4	9.6	Fog	E/SE
15.06.	020/021	Wels	18	66	7	10.5	0	SW
16.06.	022	Gorizia	20	73	9	10	0	S
18.06.	023/024	Bologna	28	50	7	10	0	SE
20.06.	027/028	Bologna	30	46	9	10	0	SSE
21.06.	029/030	Bologna	28	49	10	10	0	W

Date	Flight Number	Meteorology Station	Mean Temp [°C]	RH [%]	Wind speed [km/h]	Visibility [km]	Precipitation [mm]	Wind direction
22.06.	031	Bologna	28	50	11	10	0	W
24.06.	032	Bologna	26	62	7	10	0	E
25.06.	033/034	Bologna	29	47	12	10	0	SW
01.07.	039	Bologna	31	41	9	10	0	W
03.07.	040	Bologna	27	46	9	10	0	W
04.07.	041	Bologna	28	45	11	10	0	W
05.07.	042/043	Bologna	28	48	12	10	0	E
07.07.	044/045	Bologna	26	57	7	10	0	E
08.07.	046	Bologna	28	40	10	10	0	W
09.07.	047	Bologna	27	42	7	10	0	W
10.07.	048	Bologna	29	38	11	10	0	W
12.07.	049	Bologna	27	44	7	10	0	SW
13.07.	050	Bologna	28	40	13	10	0	SW
16.07.	051	Bologna	24	43	8	10	0	NE
17.07.	052	Gorizia	20	51	7	10	0	E
18.07.	053	Graz	19	61	5	11.4	0	NW
19.07.	054	Wels	20	71	8	10.8	0.2	SW

Table A.3: Mean, median, standard deviation (SD), maximum and minimum of the mixing ratios of the most abundant VOC species for all flights obtained in the Netherlands.

Substance	Class	Mean [ppb]	Median [ppb]	SD [ppb]	Minimum [ppb]	Maximum [ppb]
n-Pentane	Alkane	0.124	0.098	0.126	0.009	1.017
Isopentane	Alkane	0.139	0.112	0.162	0.000	1.441
Cyclopentane	Alkane	0.041	0.031	0.035	0.007	0.287
n-Hexane	Alkane	0.047	0.039	0.049	0.009	0.550

Substance	Class	Mean [ppb]	Median [ppb]	SD [ppb]	Minimum [ppb]	Maximum [ppb]
1-Butene	Alkene	0.040	0.038	0.015	0.014	0.099
Toluene	Aromatic	0.153	0.144	0.090	0.009	0.570
m-Xylene	Aromatic	0.079	0.070	0.050	0.010	0.245
Benzene	Aromatic	0.090	0.085	0.033	0.043	0.282
Propylbenzene	Aromatic	0.011	0.010	0.006	0.002	0.034
Isoprene	Terpene	0.035	0.029	0.025	0.006	0.159
Methanol	Alcohol	4.923	4.823	1.883	0.179	12.201
Ethanol	Alcohol	1.396	1.192	0.906	0.151	7.412
1-Propanol	Alcohol	0.077	0.075	0.052	0.000	0.322
Acetaldehyde	Aldehyde	1.060	1.001	0.442	0.230	2.224
Propanal	Aldehyde	0.594	0.498	0.318	0.222	1.642
Butanal	Aldehyde	0.102	0.073	0.078	0.003	0.428
Pentanal	Aldehyde	0.157	0.134	0.054	0.081	0.307
Hexanal	Aldehyde	0.189	0.183	0.069	0.091	0.488
Methacrolein	Aldehyde	0.085	0.066	0.055	0.012	0.217
Benzaldehyde	Aldehyde	0.190	0.173	0.123	0.040	0.739
Acetone	Ketone	2.241	1.807	0.958	1.134	5.027
Butanone	Ketone	0.661	0.655	0.381	0.188	2.066
Methyl vinyl ketone	Ketone	0.262	0.187	0.215	0.048	0.987
Methyl acetate	Ester	0.110	0.084	0.076	0.011	0.407
n-Pentane	Alkane	0.043	0.034	0.039	0.000	0.373
Isopentane	Alkane	0.080	0.061	0.074	0.002	0.790
Cyclopentane	Alkane	0.021	0.017	0.018	0.000	0.138

Table A.4: Mean, median, standard deviation (SD), maximum and minimum of the mixing ratios of the most abundant VOC species for all flights obtained in Italy.

Substance	Class	Mean [ppb]	Median [ppb]	SD [ppb]	Minimum [ppb]	Maximum [ppb]
n-Hexane	Alkane	0.025	0.021	0.018	0.000	0.180
1-Butene	Alkene	0.018	0.015	0.015	0.000	0.156
Toluene	Aromatic	0.116	0.100	0.092	0.000	1.074
m-Xylene	Aromatic	0.035	0.025	0.030	0.001	0.283
Benzene	Aromatic	0.042	0.039	0.028	0.000	0.219
Propylbenzene	Aromatic	0.010	0.007	0.012	0.000	0.181
Isoprene	Terpene	0.130	0.045	0.203	0.000	2.066
Methanol	Alcohol	2.478	1.951	1.807	0.021	11.443
Ethanol	Alcohol	0.690	0.526	0.710	0.001	8.020
1-Propanol	Alcohol	0.036	0.025	0.037	0.000	0.349
Acetaldehyde	Aldehyde	1.364	1.158	0.925	0.012	5.966
Propanal	Aldehyde	0.341	0.298	0.176	0.022	1.417
Butanal	Aldehyde	0.068	0.048	0.065	0.000	0.573
Pentanal	Aldehyde	0.103	0.091	0.065	0.000	0.794
Hexanal	Aldehyde	0.108	0.083	0.080	0.007	0.639
Methacrolein	Aldehyde	0.053	0.041	0.030	0.010	0.343
Benzaldehyde	Aldehyde	0.170	0.116	0.292	0.000	6.010
Acetone	Ketone	1.597	1.300	0.796	0.457	4.546
Butanone	Ketone	0.324	0.274	0.222	0.055	2.231
Methyl vinyl ketone	Ketone	0.191	0.135	0.162	0.012	1.241
Methyl acetate	Ester	0.135	0.118	0.090	0.006	0.529
Ethyl acetate	Ester	0.129	0.103	0.109	0.000	1.267

5.2 Appendix Discussion

Table A.5: The OH rate constants for the measured VOCs and the measured inorganic substances used to calculate the OH reactivity.

Compound	***k*(T)** **[cm^3 molecule^{-1} s^{-1}]**	***k*(298K)** **[cm^3 molecule^{-1} s^{-1}]**	**Literature**
Mesitylene	[a]	5.67E-11	Calvert et al. (2000)
2,3-Dimethyl-2-pentene	[a]	1.03E-10	Atkinson et al. (1997)
2;3-Dimethybutane	1.66E-17*T^2*EXP(407/T)	5.78E-12	Atkinson and Arey (2003)
Acetaldehyde	4.7E-12*EXP(345/T)	1.50E-11	Calvert et al. (2000)
Acetone	{8.8E-12*EXP(-1320/T) + 1.7E-14*EXP(423/T)}	1.75E-13	Jenkin et al. (1997), Saunders et al. (2003)
α-Pinene	1.2E-11*EXP(440/T)	5.25E-11	Jenkin et al. (1997), Saunders et al. (2003)
Benzaldehyde	5.9E-12*EXP(225/T)	1.26E-11	
Benzene	2.3E-12*EXP(-190/T)	1.22E-12	
1-Butene	6.6E-12*EXP(465/T)	3.14E-11	Jenkin et al. (1997), Saunders et al. (2003)
Butanal	6.0E-12*EXP(410/T)	2.38E-11	Jenkin et al. (1997), Saunders et al. (2003)
Butanone	1.5E-12*EXP(-90/T)	1.11E-12	Jenkin et al. (1997), Saunders et al. (2003)
cis-Pentene	[a]	6.54E-11	Jenkin et al. (1997), Saunders et al. (2003)
Cyclohexane	2.88E-17*T^2*EXP(309/T)	7.21E-12	Jenkin et al. (1997), Saunders et al. (2003)
Cyclohexanone	[a]	5.40E-12	Jenkin et al. (1997), Saunders et al. (2003)
Cyclohexene	[a]	6.77E-11	Atkinson et al. (1997)
Cyclopentane	2.73E-17*T^2*EXP(214/T)	4.97E-12	Atkinson and Arey (2003)
Cyclopentene	[a]	6.70E-11	Atkinson and Gawad (1985)
Ethanol	3*10^(-12)*EXP(20/T)	3.21E-12	Jenkin et al. (1997), Saunders et al. (2003)
Ethylacetate	6.92E-19*T^2*EXP(986/T)	1.68E-12	Jenkin et al. (1997), Saunders et al. (2003)
Ethylbenzene	[a]	7.00E-12	Jenkin et al. (1997), Saunders et al. (2003)
Hexanal	[a]	3.00E-11	D'Anna et al. (2001)
Indane	[a]	1.90E-11	Jenkin et al. (1997), Saunders et al. (2003)
Isopentane	[a]	3.60E-12	Atkinson and Arey (2003)
Isoprene	2.7E-11*EXP(390/T)	9.99E-11	Jenkin et al. (1997), Saunders et al. (2003)
Isopropylbenzene	[a]	6.30E-12	Jenkin et al. (1997), Saunders et al. (2003)
Limonene	4.28E-11*EXP(401/T)	1.64E-10	Jenkin et al. (1997), Saunders et al. (2003)

Compound	k(T) [cm^3 $molecule^{-1}$ s^{-1}]	k(298K) [cm^3 $molecule^{-1}$ s^{-1}]	Literature
m-Xylene	a)	2.31E-11	Jenkin et al. (2003), Bloss et al. (2005)
p-Xylene	a)	1.43E-11	Jenkin et al. (2003), Bloss et al. (2005)
Methacrolein	8.0E-12*EXP(380/T)	2.86E-11	Jenkin et al. (1997), Saunders et al. (2003)
Methanol	2.85E-12*EXP(-345/T)	8.95E-13	Jenkin et al. (1997), Saunders et al. (2003)
Methyl acetate	8.54E-19*T^2*EXP(455/T)	3.49E-13	Jenkin et al. (1997), Saunders et al. (2003)
Methyl vinyl ketone	2.6E-12*EXP(610/T)	2.014E-11	Jenkin et al. (1997), Saunders et al. (2003)
Myrcene	9.19E-12*EXP(1071/T)	3.34E-10	Hites and Turner (2009)
n-Butane	9.8E-12*EXP(-425/T)	2.35E-12	Jenkin et al. (1997), Saunders et al. (2003)
n-Heptane	1.59E-17*T^2*EXP(478/T)	7.02E-12	Jenkin et al. (1997), Saunders et al. (2003)
n-Hexane	1.53E-17*T^2*EXP(414/T)	5.45E-12	Jenkin et al. (1997), Saunders et al. (2003)
n-Nonane	2.51E-17*T^2*EXP(447/T)	9.99E-12	Jenkin et al. (1997), Saunders et al. (2003)
n-Octane	2.76E-17*T^2*EXP(378/T)	8.71E-12	Jenkin et al. (1997), Saunders et al. (2003)
n-Pentane	2.44E-17*T^2*EXP(183/T)	4.00E-12	Jenkin et al. (1997), Saunders et al. (2003)
o-Xylene	a)	1.36E-11	Jenkin et al. (2003), Bloss et al. (2005)
1-Pentene	a)	3.14E-11	Atkinson et al. (1997)
Pentanal	6.34E-12*EXP(448/T)	2.85E-11	Jenkin et al. (2003), Bloss et al. (2005)
1-Propanol	4.6E-12*EXP(70/T)	5.82E-12	Jenkin et al. (1997), Saunders et al. (2003)
2-Propanol	2.6E-12*EXP(200/T)	5.09E-12	Jenkin et al. (1997), Saunders et al. (2003)
Propanal	4.9E-12*EXP(405/T)	1.91E-11	Jenkin et al. (1997), Saunders et al. (2003)
Propylbenzene	a)	5.80E-12	Calvert et al. (2002)
Styrene	a)	5.80E-11	Calvert et al. (2002)
Toluene	1.8E-12*EXP(340/T)	5.63E-12	Jenkin et al. (2003), Bloss et al. (2005)
trans-Pentene	a)	6.69E-11	Jenkin et al. (1997), Saunders et al. (2003)
Formaldehyde	5.4E-12*EXP(135/T)	8.49E-12	Atkinson et al. (2006)
Methane	1.85E-12*EXP(-1690/T)	6.37E-15	Atkinson et al. (2006)
Ammonia	3.5E-12*EXP(-925/T)	1.60E-13	Atkinson et al. (2004)
Carbonmonoxide	1.44E-13 (1 + [M]/4.2E19)	1.44E-13	Atkinson et al. (2006)
Nitrous Acid	2.5E-12*EXP(260/T)	5.98E-12	Atkinson et al. (2004)
Nitrogen monoxide	7.4E-31 (T/300)-2.4 [M]	1.47E-11	Atkinson et al. (2004)

Compound	***k*(T)** **[cm^3 molecule^{-1} s^{-1}]**	***k*(298K)** **[cm^3 molecule^{-1} s^{-1}]**	**Literature**
Nitrogen dioxide	3.3E-30 (T/300)-3.0 [M]	6.57E-11	Atkinson et al. (2004)
Ozone	1.70E-12*EXP(-940/T)	7.25E-14	Atkinson et al. (2004)
Hydrogen	7.7E-12*EXP(-2100/T)	6.70E-15	Atkinson et al. (2004)

[a)] No temperature dependency reported.

Table A.6: Mean, median, standard deviation, minimum and maximum values of the $k_{\mathrm{OH}}^{\mathrm{calc}}$ for the data obtained in the Netherlands.

	Mean **[s^{-1}]**	**Median** **[s^{-1}]**	**SD** **[s^{-1}]**	**Min** **[s^{-1}]**	**Max** **[s^{-1}]**
k_{OH}(VOC)	**2.79**	**2.77**	**0.80**	**1.68**	**4.27**
k_{OH} (CH_4)	0.25	0.25	0.01	0.23	0.27
k_{OH} (BVOC)	0.19	0.12	0.19	1.23	2.80
k_{OH} (AVOC)	0.46	0.40	0.26	0.04	0.57
k_{OH} (OVOC)	1.90	1.91	0.46	0.18	1.00
k_{OH} (inorg)	**2.54**	**2.36**	**1.21**	**1.05**	**4.84**
k_{OH}(H_2)	0.07	0.07	0.01	0.07	0.08
k_{OH} (O_3)	0.09	0.09	0.02	0.06	0.13
k_{OH} (HO_2)	0.01	0.01	0.01	0.00	0.04
k_{OH} (HONO)	0.04	0.02	0.03	0.01	0.11
k_{OH} (CO)	0.58	0.55	0.11	0.49	0.80
k_{OH} (NO)	0.48	0.41	0.40	0.07	1.14
k_{OH} (NO_2)	1.27	1.21	0.79	0.28	2.87

Table A.7: Mean, median, standard deviation, minimum and maximum values of the k_{OH}^{calc} for the data obtained in Italy.

	Mean [s^{-1}]	Median [s^{-1}]	SD [s^{-1}]	Min [s^{-1}]	Max [s^{-1}]
k_{OH}(VOC)	**2.69**	**2.40**	**1.19**	**1.53**	**4.63**
k_{OH} (CH_4)	0.26	0.26	0.01	0.24	0.29
k_{OH} (BVOC)	0.32	0.13	0.54	0.02	1.29
k_{OH} (AVOC)	0.36	0.23	0.47	0.08	1.06
k_{OH} (OVOC)	1.75	1.67	0.64	1.06	2.57
k_{OH} (inorg)	**1.62**	**1.08**	**2.15**	**0.69**	**3.05**
k_{OH}(H_2)	0.08	0.08	0.01	0.07	0.09
k_{OH} (O_3)	0.12	0.10	0.07	0.08	0.17
k_{OH} (HO_2)	0.05	0.04	0.05	0.00	0.15
k_{OH} (HONO)	0.02	0.02	0.02	0.01	0.04
k_{OH} (CO)	0.54	0.44	1.03	0.35	0.61
k_{OH} (NO)	0.24	0.05	1.73	0.00	0.48
k_{OH} (NO_2)	0.57	0.31	2.83	0.06	1.58

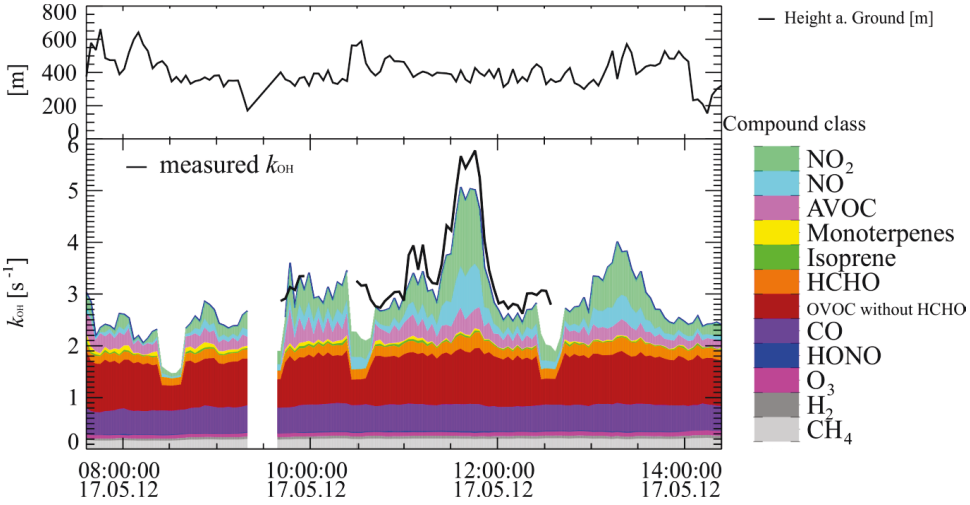

Figure A.1: North transfer flight (F006/007, CL-8) from Friedrichshafen to Mainz-Finthen with a refuel stop in Malmsheim at 9:30 UTC. The upper part of this figure shows the height above ground in meters. The lower part of this figure shows the measured OH reactivity in black and the single contributions of the calculated OH reactivity in color. The difference between both is the missing reactivity. During the three sections at 8:30, 10:30 and 12:30 the HGC instrument was calibrated inflight.

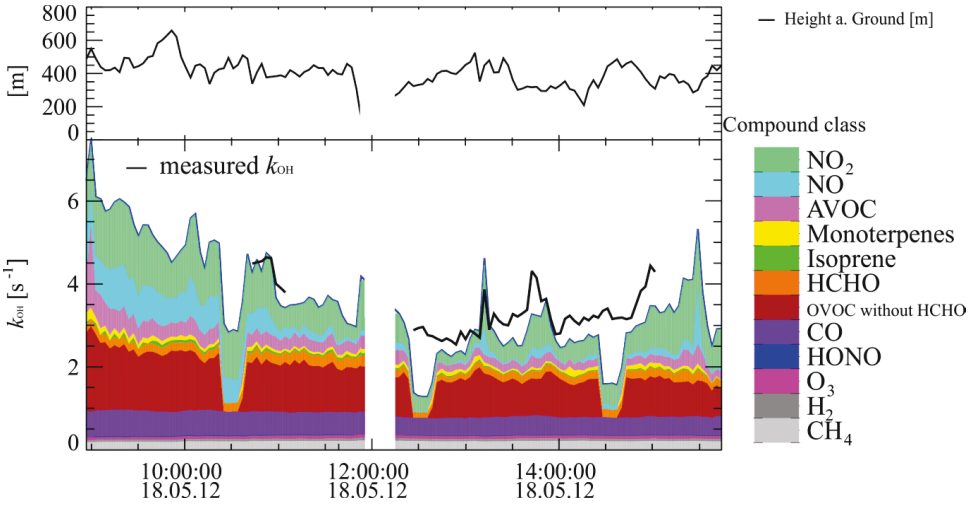

Figure A.2: North transfer flight (F008/009, CL-8) from Mainz-Finthen to Rotterdam with a refuel stop in Bonn at 12:00 UTC. The upper part of this figure shows the height above ground in meters. The lower part of this figure shows the measured OH reactivity in black and the single contributions of the calculated OH reactivity in color. The difference between both is the missing reactivity. During the three sections at 10:30, 12:30 and 14:30 the HGC instrument was calibrated inflight.

Table A.8: Median, standard deviation, minimum and maximum values of the k_{OH}^{calc} for the data obtained in first flight leg of the north transfer from Friedrichshafen to Mainz-Finthen.

	Median [s^{-1}]	**SD [s^{-1}]**	**Min [s^{-1}]**	**Max [s^{-1}]**
k_{OH}^{meas}	3.1	0.9	2.6	5.8
k_{OH}^{calc}	2.8	0.6	1.9	5.1
k_{OH}^{miss}	0.3	0.3	-0.5	1.0

Table A.9: Median, median, standard deviation, minimum and maximum values of the k_{OH}^{calc} for the data obtained in second flight leg of the north transfer from Mainz-Finthen to Rotterdam.

	Median [s^{-1}]	**SD [s^{-1}]**	**Min [s^{-1}]**	**Max [s^{-1}]**
k_{OH}^{meas}	3.2	0.6	2.5	4.6
k_{OH}^{calc}	2.8	1.1	2.1	6.8
k_{OH}^{miss}	0.4	0.3	-0.6	1.0

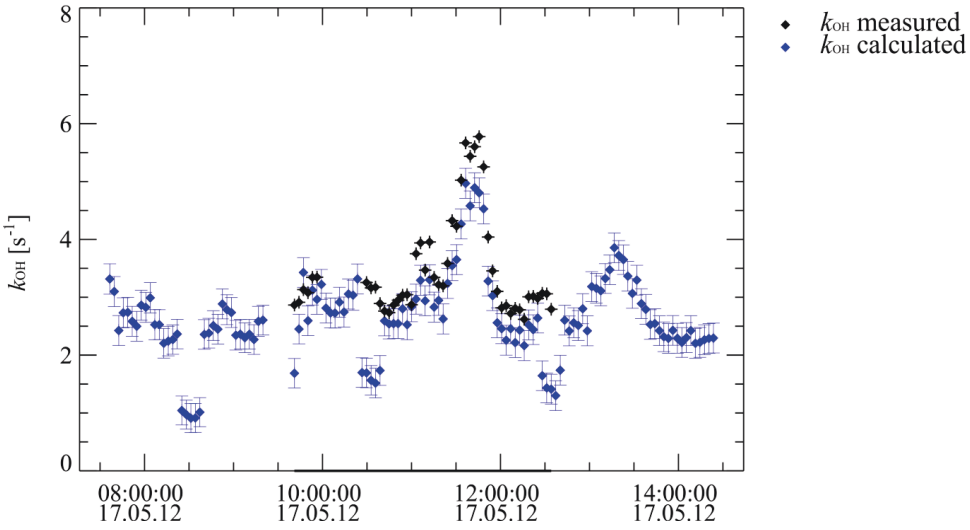

Figure A.3: The k_{OH}^{meas} and k_{OH}^{calc} of the first flight leg of the north transfer flight (F006/007) from Friedrichshafen to Mainz-Finthen with their respective random error.

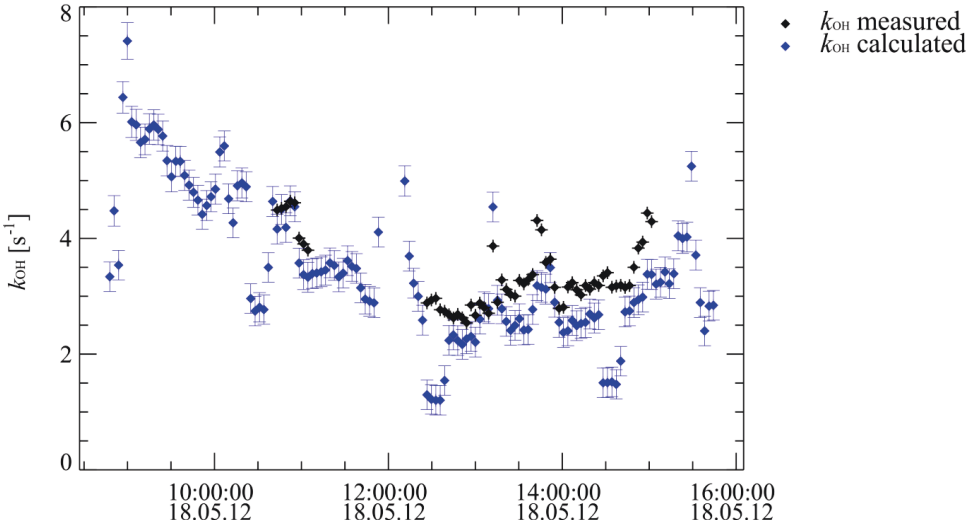

Figure A.4: The k_{OH}^{meas} and k_{OH}^{calc} of the second flight leg of the north transfer flight (F008/009) from Mainz-Finthen to Rotterdam with their respective random error.

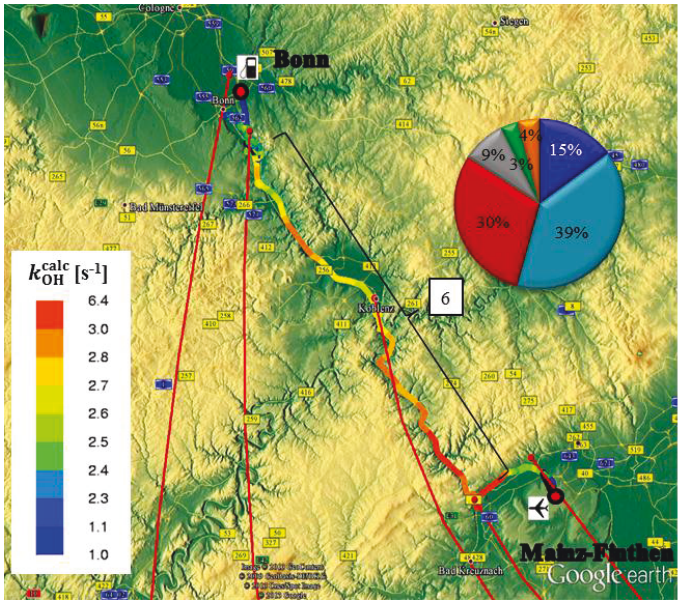

Figure A.5: Transfer flight from Mainz-Finthen to the refuel stop in Bonn (F008) color coded by the total k_{OH}^{calc}. The red lines show the 12 h back trajectories for 400 m (AGL). The pie chart resemble the partitioning of k_{OH}^{calc}. The section in dark blue show the k_{OH}(others), which is the sum of k_{OH}(CO), k_{OH}(HO_2), k_{OH}(HONO), k_{OH}(O_3) and k_{OH}(H_2), light blue k_{OH}(NO_x), red k_{OH}(OVOC), gray k_{OH}(AVOC), green k_{OH}(BVOC) and orange k_{OH}(CH_4).

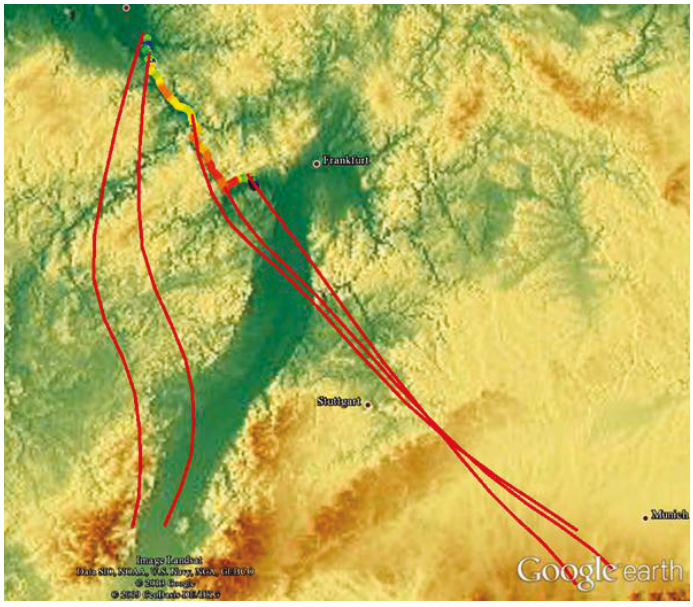

Figure A.6: Back trajectories from Mainz-Finthen to the refuel stop in Bonn (F008).

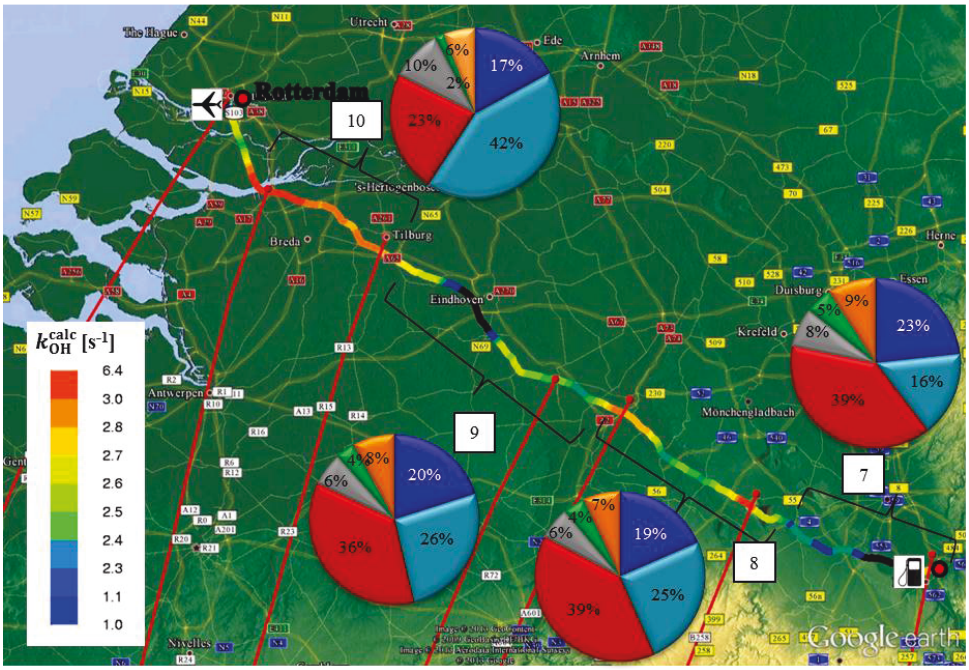

Figure A.7: Transfer flight (F009) from the refuel stop in Bonn to Rotterdam color coded by the total k_{OH}^{calc}. This flight track is divided into four sections. The red lines show the 12 h back trajectories for 400 m (AGL). The pie charts resemble the partitioning of k_{OH}^{calc}. Sections in dark blue show the k_{OH}(others), which is the sum of k_{OH}(CO), k_{OH}(HO_2), k_{OH}(HONO), k_{OH}(O_3) and k_{OH}(H_2), light blue k_{OH}(NO_x), red k_{OH}(OVOC), gray k_{OH}(AVOC), green k_{OH}(BVOC) and orange k_{OH}(CH_4).

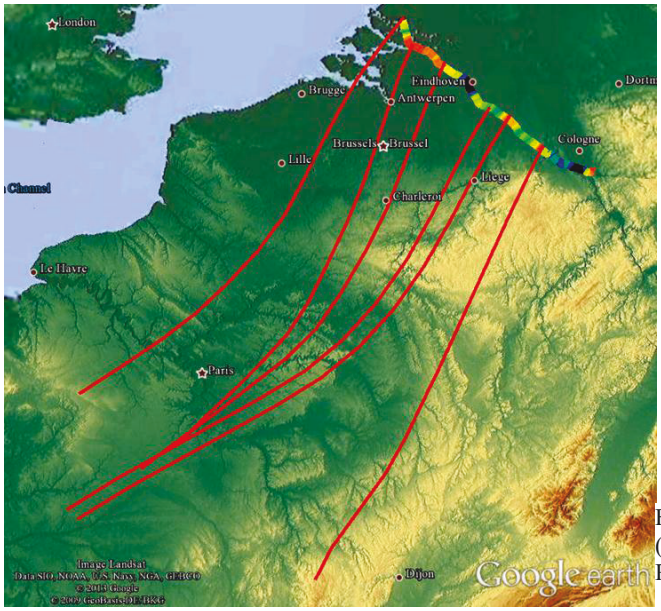

Figure A.8: Back trajectories for (F009) from the refuel stop in Bonn to Rotterdam.

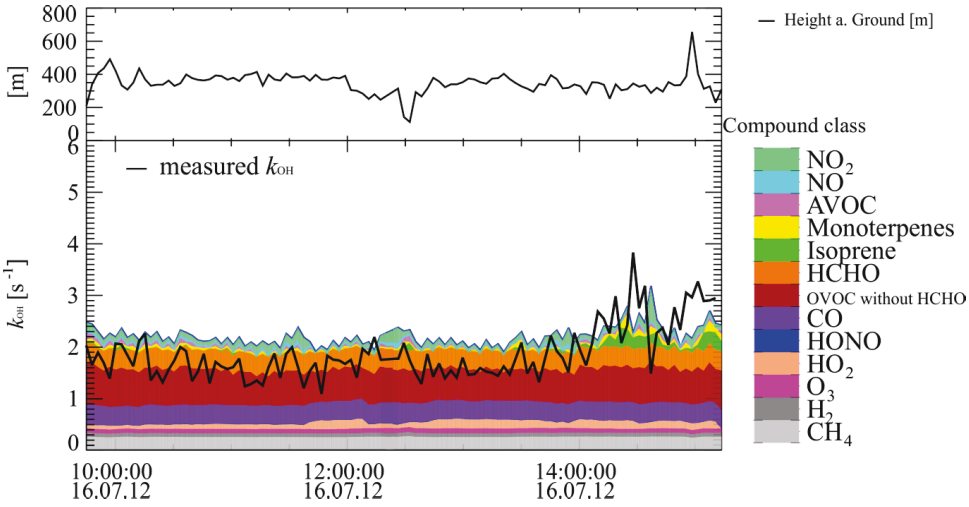

Figure A.9: South transfer flight (F051, CL-8) from Bologna to Gorizia. The upper part of this figure shows the height above ground in meters. The lower part of this figure shows the measured OH reactivity in black and the single contributions of the calculated OH reactivity in color. The difference between both is the missing reactivity.

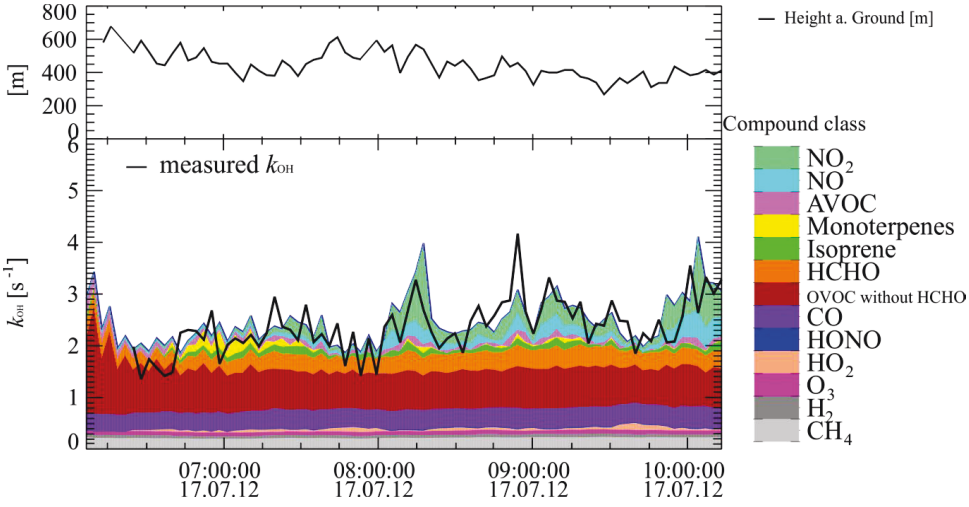

Figure A.10: South transfer flight (F052, CL-8) from Gorizia to Graz. The upper part of this figure shows the height above ground in meters. The lower part of this figure shows the measured OH reactivity in black and the single contributions of the calculated OH reactivity in color. The difference between both is the missing reactivity.

Table A.6: Median, standard deviation, minimum and maximum values of the k_{OH}^{calc} for the data obtained in first flight leg of the south transfer from Bologna to Gorizia.

	Median [s^{-1}]	**SD** [s^{-1}]	**Min** [s^{-1}]	**Max** [s^{-1}]
k_{OH}^{meas}	1.8	0.5	1.1	3.8
k_{OH}^{calc}	2.3	0.2	1.9	3.2
k_{OH}^{miss}	-0.4	0.5	-1.7	1.6

Table A.7: Median, standard deviation, minimum and maximum values of the k_{OH}^{calc} for the data obtained in second flight leg of the south transfer from Gorizia to Graz.

	Median [s^{-1}]	**SD** [s^{-1}]	**Min** [s^{-1}]	**Max** [s^{-1}]
k_{OH}^{meas}	2.4	0.5	1.4	4.2
k_{OH}^{calc}	2.4	0.5	1.9	4.1
k_{OH}^{miss}	-0.03	0.4	-1.4	1.1

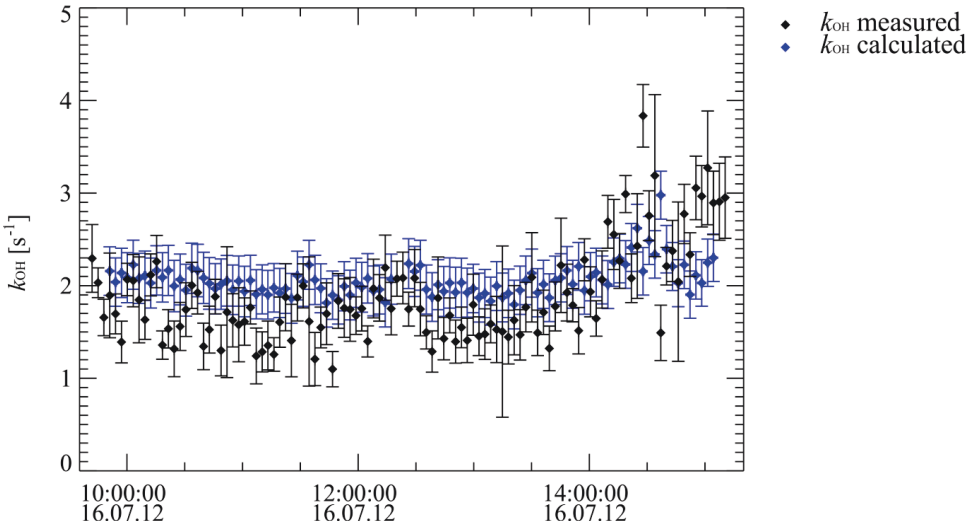

Figure A.11: The k_{OH}^{meas} and k_{OH}^{calc} of the first flight leg of the south transfer flight (F051, CL-8) from Bologna to Gorizia with their respective random error.

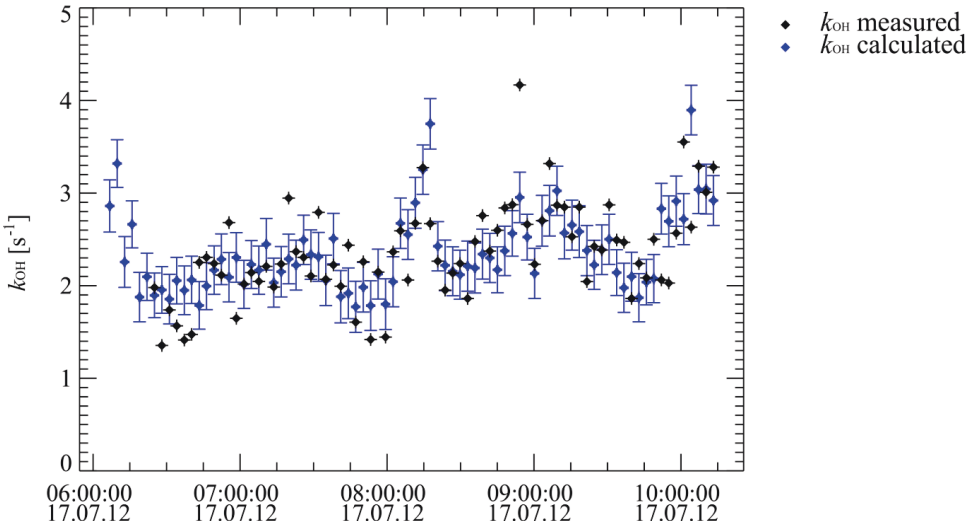

Figure A.12: The k_{OH}^{meas} and k_{OH}^{calc} of the second flight leg of the south transfer flight (F052, CL-8) from Gorizia to Graz with their respective random error.

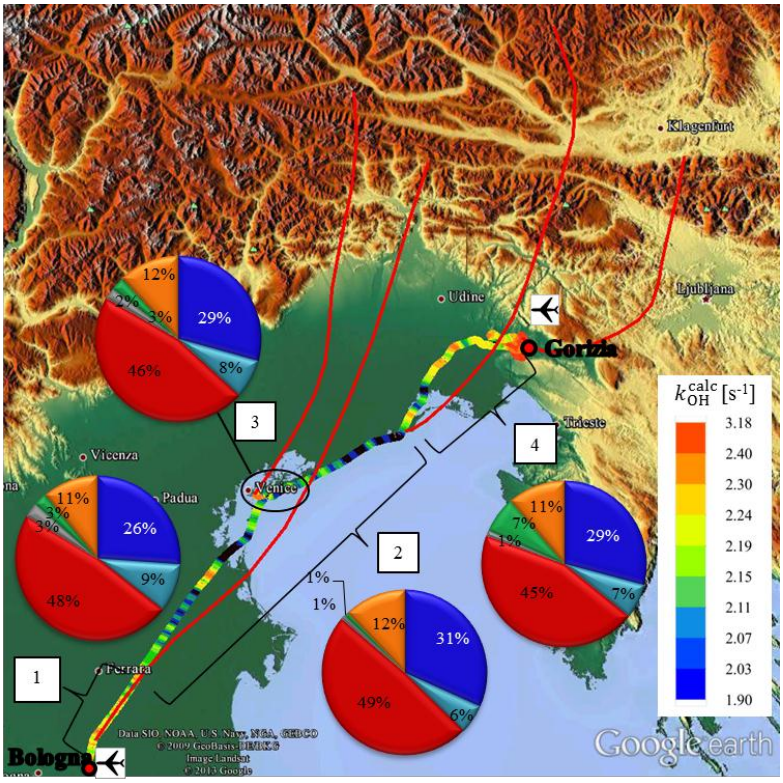

Figure A.13: First flight leg of the south transfer flight (F009 – CL 8) from Bologna and Gorizia color coded by the total k_{OH}^{calc}. This flight track is divided into four sections. The red lines show the 12 h back trajectories for 400 m (AGL). The pie charts resemble the partitioning of k_{OH}^{calc}. Sections in dark blue show the k_{OH}(others), which is the sum of k_{OH}(CO), k_{OH}(HO_2), k_{OH}(HONO), k_{OH}(O_3) and k_{OH}(H_2), light blue k_{OH}(NO_x), red k_{OH}(OVOC), gray k_{OH}(AVOC), green k_{OH}(BVOC) and orange k_{OH}(CH_4).

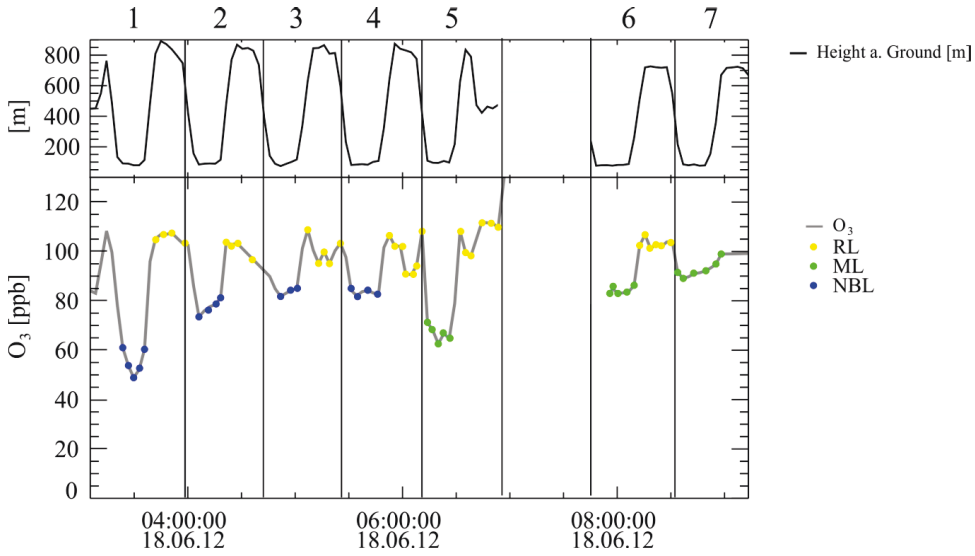

Figure A.14: The ozone concentration for flight F023/024with the allocation to the three layers: the NBL, RL and the evolving ML subdivided into 7 flight sections. In the top panel of the figure the height above ground is displayed.

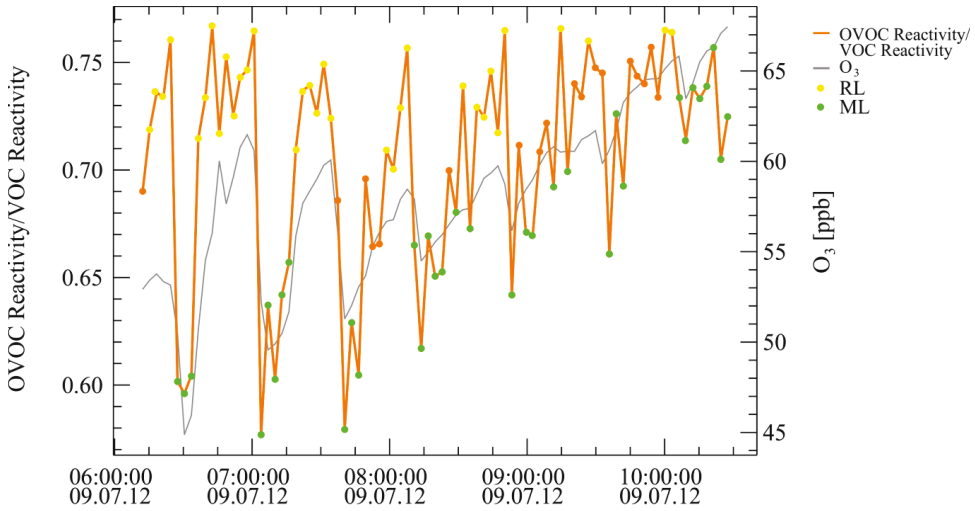

Figure A.15: The ratio of k_{OH}(OVOC)/k_{OH}(VOC) of flight F047 for the mixed layer and residual layer.

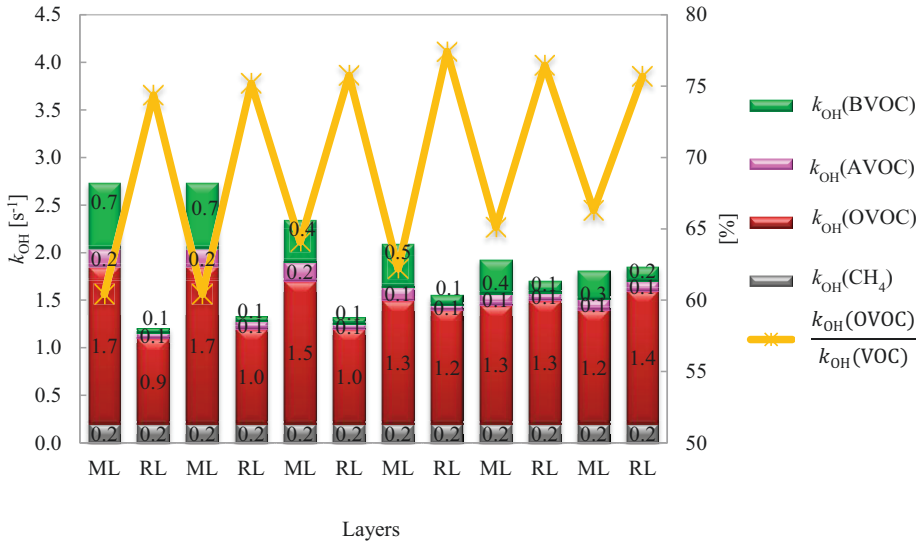

Figure A.16: The mean k_{OH} distributions of CH_4, OVOCs, anthropogenic and biogenic VOCs for Flight F047shown in the bar graphs for each consecutively sampled layer in s^{-1}. The ratio of k_{OH}(OVOC)/k_{OH}(VOC) from is shown in blue in % on the right y-axis.

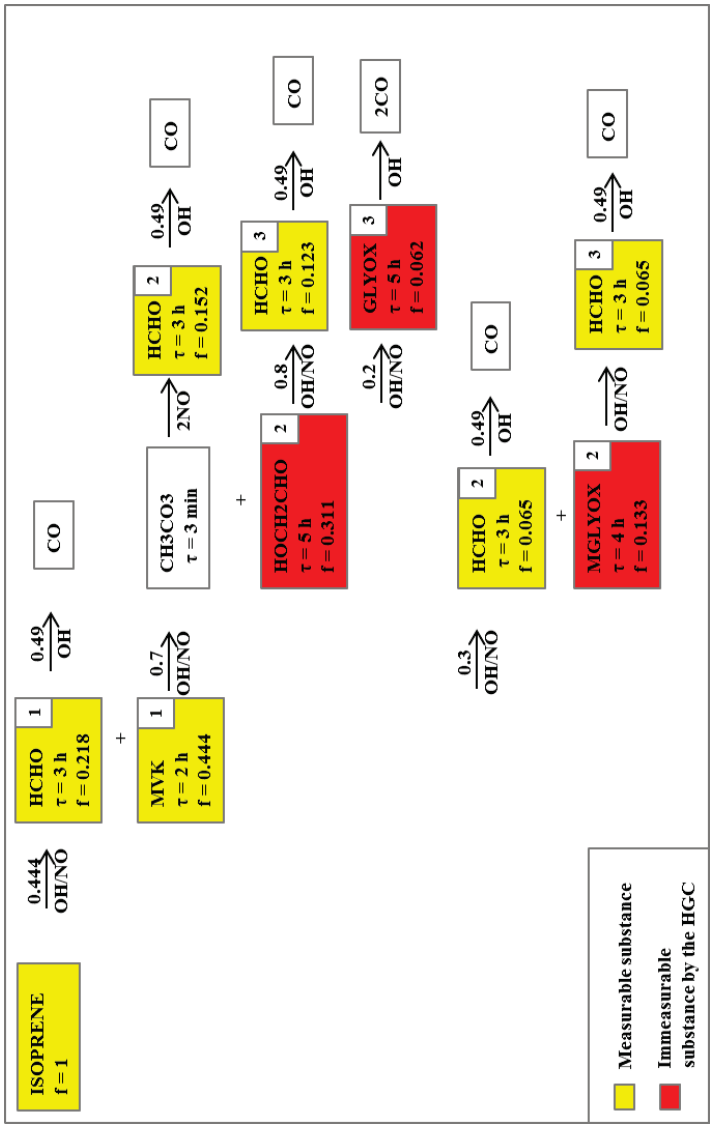

Figure A.17: The OH degradation of isoprene marked in yellow with its four generations. The denoted OH lifetimes (τ) are calculated for an OH concentration of $6x10^6$ molecules cm^{-3}. The factor *f* represents the remaining and branching factor of the k_{OH} of the mother substance. The numbers above the errors indicate that only this fraction reacts along the outlined path. All substances marked in white, are either unmeasurable with the HGC, are short-lived and thus low in concentration and make a small contribution to the OH reactivity or not included in the $k_{OH}(OVOC)/k_{OH}(VOC)$ ratio because they are long-lived or not considered as VOCs. The abbreviation HOCH2CHO is taken from the MCM v 3.2 and represents glycolaldehyde.

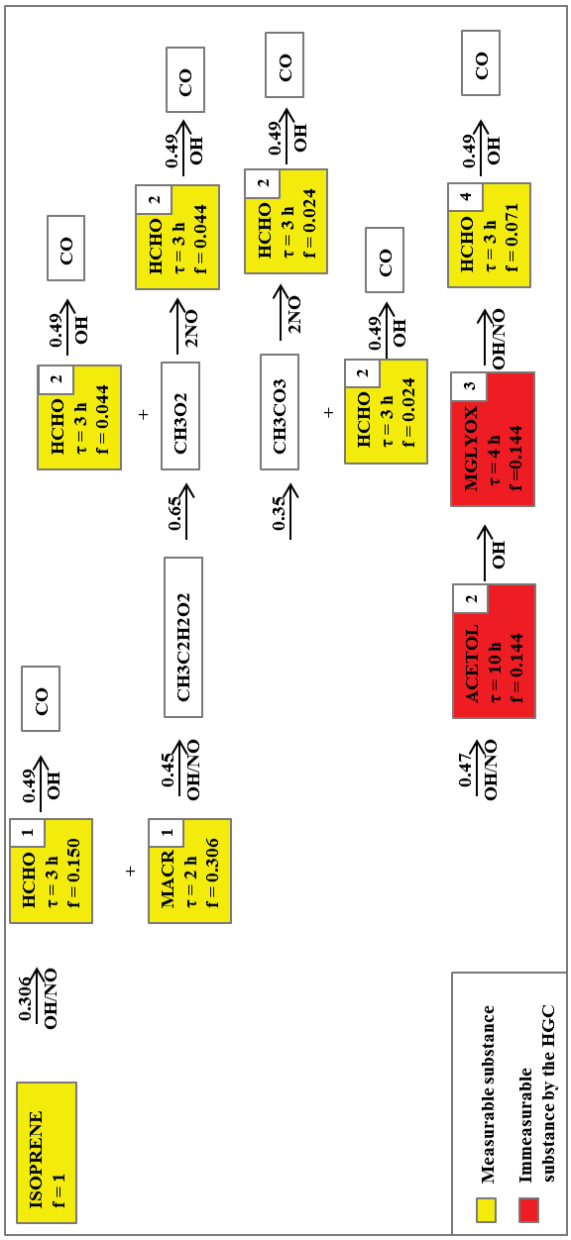

Figure A.18: The OH degradation of isoprene marked in yellow with its five generations. The denoted OH lifetimes (τ) are calculated for an OH concentration of $6x10^6$ molecules cm^{-3}. The factor *f* represents the remaining and branching factor of the k_{OH} of the mother substance. The numbers above the errors indicate that only this fraction reacts along the outlined path. All substances marked in white, are either unmeasurable with the HGC, are short-lived and thus low in concentration and make a small contribution to the OH reactivity or not included in the k_{OH}(OVOC)/k_{OH}(VOC) ratio because they are long-lived or not considered as VOCs.

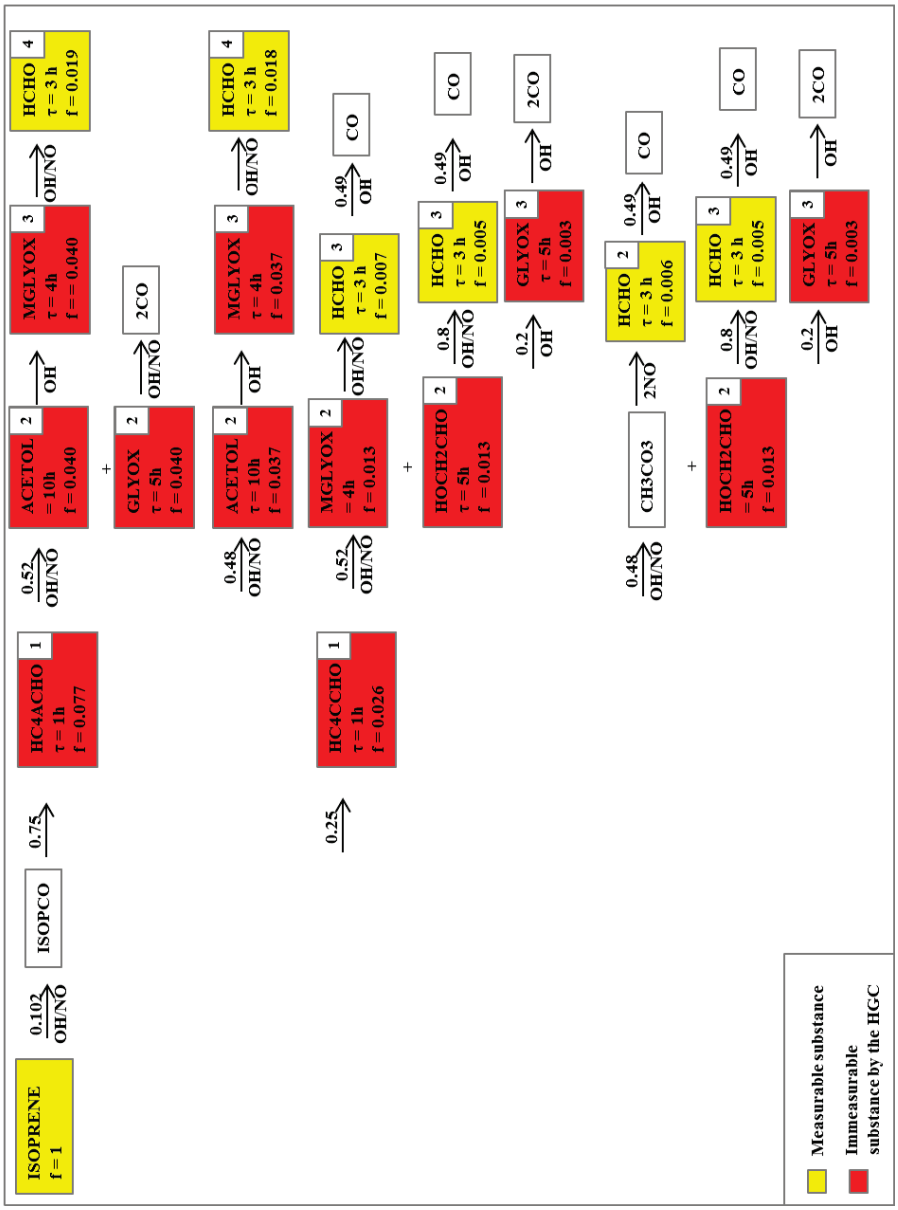

Figure A.19: The OH degradation of isoprene marked in yellow with its four generations. The denoted OH lifetimes (τ) are calculated for an OH concentration of $6x10^6$ molecules cm^{-3}. The factor *f* represents the remaining and branching factor of the k_{OH} of the mother substance. The numbers above the errors indicate that only this fraction reacts along the outlined path. All substances marked in white, are either unmeasurable with the HGC, are short-lived and thus low in concentration and make a small contribution to the OH reactivity or not included in the k_{OH}(OVOC)/k_{OH}(VOC) ratio because they are long-lived or not considered as VOCs. The abbreviation HC4ACHO is taken from the MCM v 3.2 and represents (2E)-4-hydroxy-3-methyl-2-butenal and HOCH2CHO abbreviates glycolaldehyde.

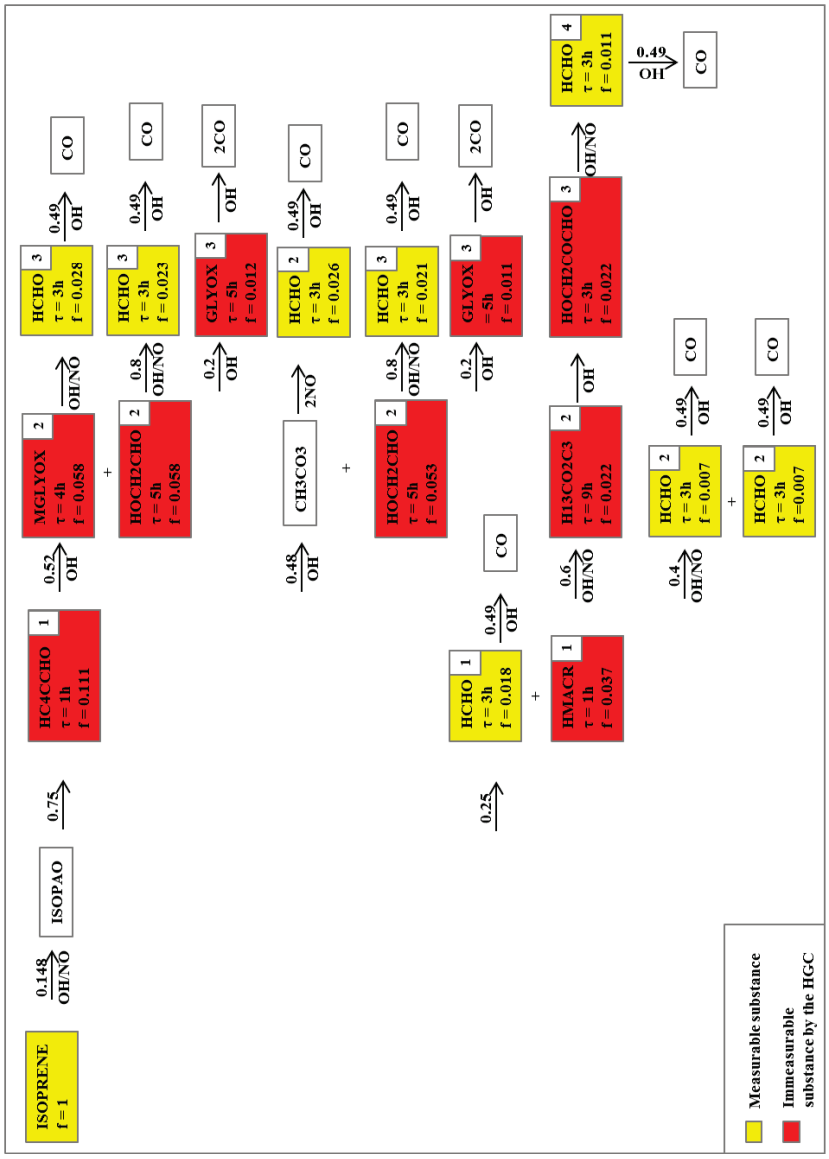

Figure A.20: The OH degradation of isoprene marked in yellow with its five generations. The denoted OH lifetimes (τ) are calculated for an OH concentration of $6x10^6$ molecules cm^{-3}. The factor *f* represents the remaining and branching factor of the k_{OH} of the mother substance. The numbers above the errors indicate that only this fraction reacts along the outlined path. All substances marked in white, are either unmeasurable with the HGC, are short-lived and thus low in concentration and make a small contribution to the OH reactivity or not included in the k_{OH}(OVOC)/k_{OH}(VOC) ratio because they are long-lived or not considered as VOCs. The abbreviation HC4ACHO is taken from the MCM v 3.2 and represents (2E)-4-hydroxy-3-methyl-2-butenal, HOCH2CHO abbreviates glycolaldehyde, HMAR abbreviates 2-(hydroxymethyl)prop-2-enal, H13CO2C3 abbreviates dihydroxyacetone and HOCH2COCHO abbreviates 3-Hydroxy-2-oxopropanal.

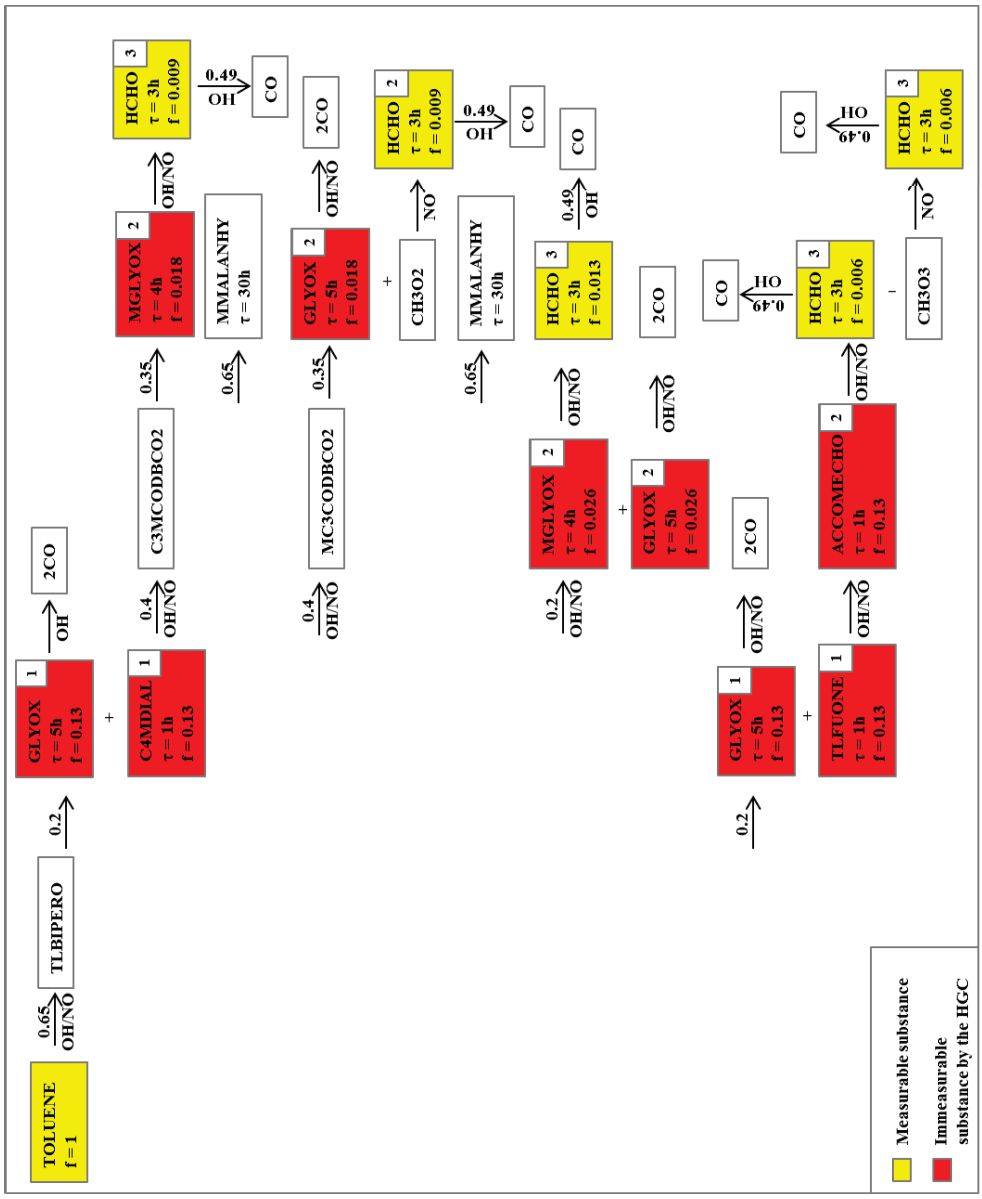

Figure A.21: The OH degradation of toluene marked in yellow with its four generations. The denoted OH lifetimes (τ) are calculated for an OH concentration of $6x10^6$ molecules cm^{-3}. The factor *f* represents the remaining and branching factor of the k_{OH} of the mother substance. The numbers above the errors indicate that only this fraction reacts along the outlined path. All substances marked in white, are either unmeasurable with the HGC, are short-lived and thus low in concentration and make a small contribution to the OH reactivity or not included in the k_{OH}(OVOC)/k_{OH}(VOC) ratio because they are long-lived or not considered as VOCs. The abbreviation C4MDIAL is taken from the MCM v 3.2 and represents 2-methyl-2-butenedial, TLFUONE abbreviates 2-penten-4-olide, ACCOMECHO abbreviates acetyl-3-oxopropanoate and MMALANHY abbreviates 2,5-furandione.

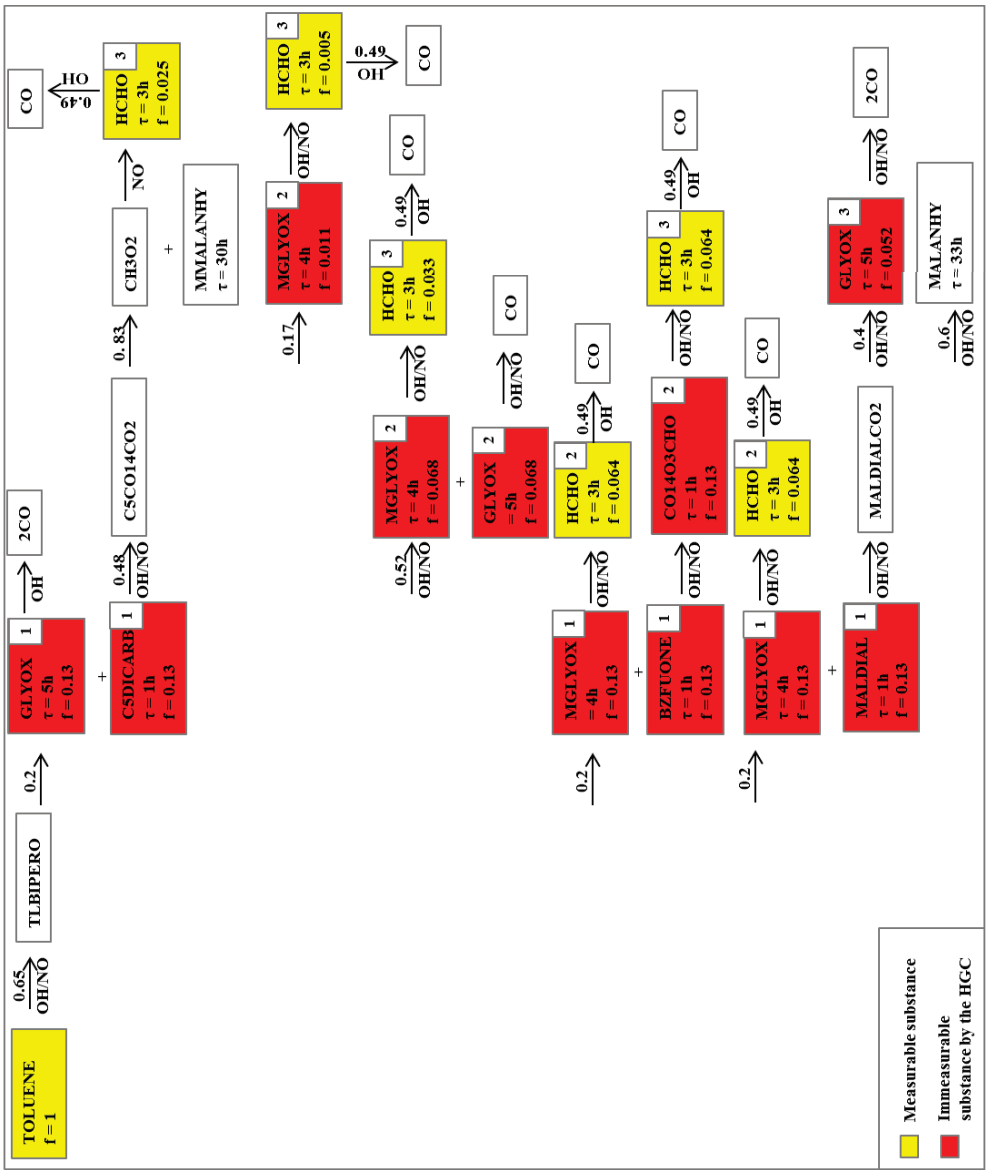

Figure A.22: The OH degradation of toluene marked in yellow with its four generations. The denoted OH lifetimes (τ) are calculated for an OH concentration of $6x10^6$ molecules cm^{-3}. The factor f represents the remaining and branching factor of the k_{OH} of the mother substance. The numbers above the errors indicate that only this fraction reacts along the outlined path. All substances marked in white, are either unmeasurable with the HGC, are short-lived and thus low in concentration and make a small contribution to the OH reactivity or not included in the k_{OH}(OVOC)/k_{OH}(VOC) ratio because they are long-lived or not considered as VOCs. The abbreviation C5DICARB is taken from the MCM v 3.2 and represents 4-oxopent-2-enal, BZFUONE abbreviates 2-butenolide, MALDIAL abbreviates 2-butenedial, MMALANHY abbreviates 3-methyl-2,5-furandione and MALANHY abbreviates 2,5-furandione.

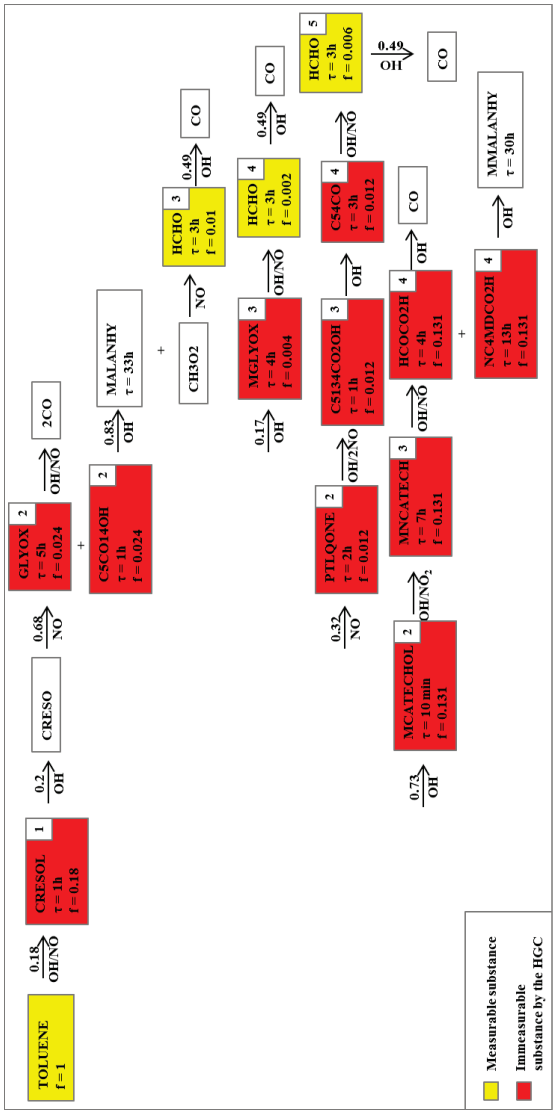

Figure A.23: The OH degradation of toluene marked in yellow with its five generations. The denoted OH lifetimes are calculated for an OH concentration of 6×10^6 molecules cm^{-3}. The factor *f* represents the remaining and branching factor of the k_{OH} of the mother substance. The numbers above the errors indicate that only this fraction reacts along the outlined path. All substances marked in white, are either unmeasurable with the HGC, are short-lived and thus low in concentration and make a small contribution to the OH reactivity or not included in the $k_{OH}(OVOC)/k_{OH}(VOC)$ ratio because they are long-lived or not considered as VOCs. The abbreviation MCATECHOL is taken from the MCM v 3.2 and represents 3-methylcatechol, C5CO14OH abbreviates 4-oxo-2-pentenoic acid, PTLQONE abbreviates p-toluquinone, MNCATECH abbreviates 3-methyl-6-nitro-1,2-benzenediol, MALANHY abbreviates 2,5-furandione, C5134CO2OH abbreviates 2-hydroxy-3,4-dioxopentanal, HCOCO2H abbreviates glyoxylate, C54CO abbreviates 2,3,4-trioxopentanal and MMALANHY abbreviates 3-methyl-2,5-furandione.

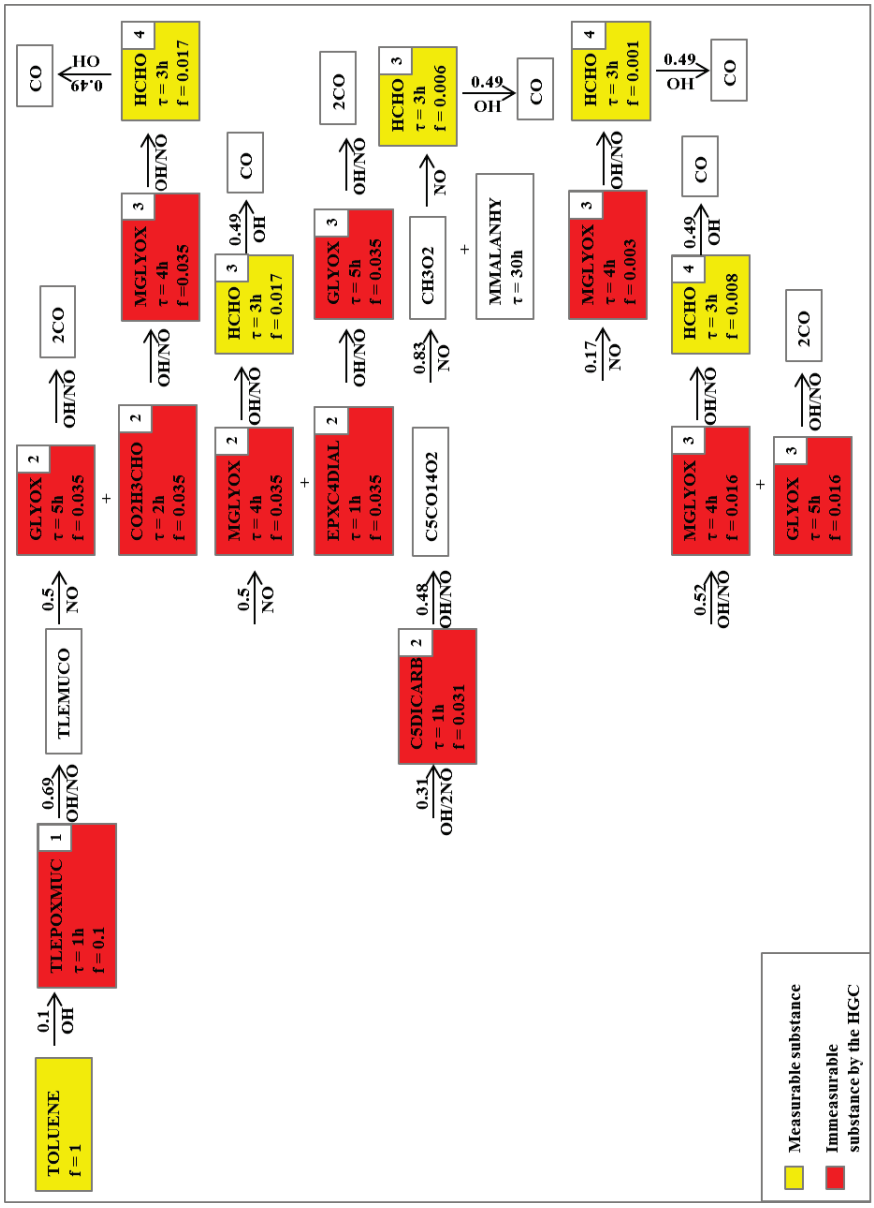

Figure A.24: The OH degradation of toluene marked in yellow with its five generations. The denoted OH lifetimes are calculated for an OH concentration of $6x10^6$ molecules cm^{-3}. The factor *f* represents the remaining and branching factor of the k_{OH} of the mother substance. The numbers above the errors indicate that only this fraction reacts along the outlined path. All substances marked in white, are either unmeasurable with the HGC, are short-lived and thus low in concentration and make a small contribution to the OH reactivity or not included in the k_{OH}(OVOC)/k_{OH}(VOC) ratio because they are long-lived or not considered as VOCs. The abbreviation C5DICARB is taken from the MCM v 3.2 and represents 4-oxopent-2-enal, CO2H3CHO abbreviates 2-hydroxy-3-oxobutanal, EPXC4DIAL abbreviates oxirane-2,3-dicarbaldehyde and MMALANHY abbreviates 3-methyl-2,5-furandione.

Bibliography

Acker, K., Kezele, N., Klasinc, L., Möller, D., Pehnec, G., Šorgo, G., Wieprecht, W., Žužul, S., 2008. Atmospheric H2O2 measurement and modeling campaign during summer 2004 in Zagreb, Croatia. Atmospheric Environment 42, 2530-2542.

Almbauer, R.A., Oettl, D., Bacher, M., Sturm, P.J., 2000. Simulation of the air quality during a field study for the city of Graz. Atmospheric Environment 34, 4581-4594.

Altshuller, A.P., 1993. Production of aldehydes as primary emissions and from secondary atmospheric reactions of alkenes and alkanes during the night and early morning hours. Atmospheric Environment. Part A. General Topics 27, 21-32.

Altshuller, A.P., Lefohn, A.S., 1996. Background Ozone in the Planetary Boundary Layer Over the United States. Journal of the Air & Waste Management Association 46, 134-141.

Ammann, C., Spirig, C., Neftel, A., Steinbacher, M., Komenda, M., Schaub, A., 2004. Application of PTR-MS for measurements of biogenic VOC in a deciduous forest. International Journal of Mass Spectrometry 239, 87-101.

Andreae, M., Artaxo, P., Fischer, H., Freitas, S., Grégoire, J.M., Hansel, A., Hoor, P., Kormann, R., Krejci, R., Lange, L., 2001. Transport of biomass burning smoke to the upper troposphere by deep convection in the equatorial region. Geophys Res Lett 28, 951-954.

Apel, E.C., Brauers, T., Koppmann, R., Bandowe, B., Bossmeyer, J., Holzke, C., Tillmann, R., Wahner, A., Wegener, R., Brunner, A., 2008. Intercomparison of oxygenated volatile organic compound measurements at the SAPHIR atmosphere simulation chamber. Journal of Geophysical Research: Atmospheres (1984–2012) 113.

Apel, E.C., Hills, A., Lueb, R., Zindel, S., Eisele, S., Riemer, D., 2003. A fast-GC/MS system to measure C2 to C4 carbonyls and methanol aboard aircraft. Journal of Geophysical Research: Atmospheres (1984–2012) 108.

Apel, E.C., Riemer, D.D., Hills, A., Baugh, W., Orlando, J., Faloona, I., Tan, D., Brune, W., Lamb, B., Westberg, H., Carroll, M.A., Thornberry, T., Geron, C.D., 2002. Measurement and interpretation of isoprene fluxes and isoprene, methacrolein, and methyl vinyl ketone mixing ratios at the PROPHET site during the 1998 Intensive. Journal of Geophysical Research: Atmospheres 107, ACH 7-1-ACH 7-15.

Arnold, F., Knop, G., Ziereis, H., 1986. Acetone measurements in the upper troposphere and lower stratosphere - Implications for hydroxyl radical abundances.

Atkinson, R., 2000. Atmospheric chemistry of VOCs and NOx. Atmospheric Environment 34, 2063-2101.

Atkinson, R., Arey, J., 2003. Atmospheric degradation of volatile organic compounds. Chemical Reviews 103, 4605-4638.

Atkinson, R., Baulch, D., Cox, R., Crowley, J., Hampson, R., Hynes, R., Jenkin, M., Rossi, M., Troe, J., 2004. Evaluated kinetic and photochemical data for atmospheric chemistry: Volume I-gas phase reactions of O x, HO x, NO x and SO x species. Atmos Chem Phys 4, 1461-1738.

Atkinson, R., Baulch, D., Cox, R., Crowley, J., Hampson, R., Hynes, R., Jenkin, M., Rossi, M., Troe, J., Subcommittee, I., 2006. Evaluated kinetic and photochemical data for atmospheric chemistry: Volume II–gas phase reactions of organic species. Atmos Chem Phys 6, 3625-4055.

Atkinson, R., Baulch, D., Cox, R., Hampson Jr, R., Kerr, J., Rossi, M., Troe, J., 1997. Evaluated kinetic and photochemical data for atmospheric chemistry: supplement VI. IUPAC subcommittee on gas kinetic data evaluation for atmospheric chemistry. Journal of Physical and Chemical Reference Data 26, 1329.

Atkinson, R.S., Gawad, N.A., 1985. Intramolecular reactions of N-nitrenes: oxidation of 3-amino-2-(2.4-dimethoxyphenylpropyl) quinazolin-4 (3H)-one. Journal of the Chemical Society, Perkin Transactions 1, 341-344.

Beljaars, A.C.M., Holtslag, A.A.M., 1991. Flux Parameterization over Land Surfaces for Atmospheric Models. Journal of Applied Meteorology 30, 327-341.

Benning, L., Wahner, A., 1998. Measurements of atmospheric formaldehyde (HCHO) and acetaldehyde (CH_3CHO) during POPCORN 1994 using 2.4-DNPH coated silica cartridges, Atmospheric Measurements during POPCORN—Characterisation of the Photochemistry over a Rural Area. Springer, pp. 105-117.

Betz, W.R., Mapoldo, S.G., Wachob, G.D., Firth, M.C., 1989. Characterization of Carbon Molecular Sieves and Activated Charcoal for Use in Airborne Contaminant Sampling. American Industrial Hygiene Association Journal 50, 181-187.

Bizjak, M., Turšič, J., Lešnjak, M., Cegnar, T., 1999. Aerosol black carbon and ozone measurements at Mt. Krvavec EMEP/GAW station, Slovenia. Atmospheric Environment 33, 2783-2787.

Bloss, C., Wagner, V., Jenkin, M., Volkamer, R., Bloss, W., Lee, J., Heard, D., Wirtz, K., Martin-Reviejo, M., Rea, G., 2005. Development of a detailed chemical mechanism (MCMv3. 1) for the atmospheric oxidation of aromatic hydrocarbons. Atmos Chem Phys 5, 641-664.

Bošnir, J., Puntarić, D., Škes, I., Klarić, M., Šimić, S., Zorić, I., Galić, R., 2003. Toxic metals in freshwater fish from the Zagreb area as indicators of environmental pollution. Collegium antropologicum 27, 31-39.

Bottenheim, J.W., Shepherd, M.F., 1995. C2 C6 hydrocarbon measurements at four rural locations across Canada. Atmospheric Environment 29, 647-664.

Bouwman, A.F., Lee, D. S., Asman, W. A. H., Dentener, F. J., Van Der Hoek, K. W., Olivier, J. G. J. , 1997. A global high-resolution emission inventory for ammonia. Global Biogeochem Cy 11, 561-587.

Calvert, J.G., Atkinson, R., Becker, K.H., Kamens, R.M., Seinfeld, J.H., Wallington, T.J., Yarwood, G., 2002. The mechanisms of atmospheric oxidation of aromatic hydrocarbons. Oxford University Press New York.

Calvert, J.G., Atkinson, R., Kerr, J., Madronich, S., Moortgat, G., Wallington, T.J., Yarwood, G., 2000. The mechanisms of atmospheric oxidation of the alkenes. Oxford University Press New York.

Carlier, P., Hannachi, H., Mouvier, G., 1986. The chemistry of carbonyl compounds in the atmosphere - A review. Atmospheric Environment (1967) 20, 2079-2099.

Cavanagh, L.A., Schadt, C.F., Robinson, E., 1969. Atmospheric hydrocarbon and carbon monoxide measurements at Point Barrow, Alaska. Environ Sci Technol 3, 251-257.

Chatani, S., Shimo, N., Matsunaga, S., Kajii, Y., Kato, S., Nakashima, Y., Miyazaki, K., Ishii, K., Ueno, H., 2009. Sensitivity analyses of OH missing sinks over Tokyo metropolitan area in the summer of 2007. Atmos. Chem. Phys 9, 8975-8986.

Ciccioli, P., Brancaleoni, E., Cecinato, A., di Palo, C., Brachetti, A., Liberti, A., 1986. Gas chromatographic evaluation of the organic components present in the atmosphere at trace levels with the aid of carbopack b for pre-concentration of the sample. Journal of Chromatography A 351, 433-449.

Crutzen, P.J., Andreae, M.O., 1990. Biomass burning in the tropics: Impact on atmospheric chemistry and biogeochemical cycles. Science 250, 1669-1678.

D'Anna, B., Andresen, Ø., Gefen, Z., Nielsen, C.J., 2001. Kinetic study of OH and NO_3 radical reactions with 14 aliphatic aldehydes. Physical Chemistry Chemical Physics 3, 3057-3063.

de Gouw, J., Warneke, C., 2007. Measurements of volatile organic compounds in the earth's atmosphere using proton-transfer-reaction mass spectrometry. Mass Spectrometry Reviews 26, 223-257.

Dewulf, J., Van Langenhove, H., Everaert, M., Vanthournout, H., 1998. Volatile organic compounds in the Scheldt estuary along the trajectory Antwerp–Vlissingen: concentration profiles, modelling and estimation of emissions into the atmosphere. Water Research 32, 2941-2950.

Di Carlo, P., Brune, W.H., Martinez, M., Harder, H., Lesher, R., Ren, X., Thornberry, T., Carroll, M.A., Young, V., Shepson, P.B., Riemer, D., Apel, E., Campbell, C., 2004. Missing OH Reactivity in a Forest: Evidence for Unknown Reactive Biogenic VOCs. Science 304, 722-725.

Donoso, L., Romero, R., Rondón, A., Fernandez, E., Oyola, P., Sanhueza, E., 1996. Natural and anthropogenic C2 to C6 hydrocarbons in the central-eastern Venezuelan atmosphere during the rainy season. J Atmos Chem 25, 201-214.

Edwards, P., Evans, M., Furneaux, K., Hopkins, J., Ingham, T., Jones, C., Lee, J., Lewis, A., Moller, S., Stone, D., 2013. OH reactivity in a South East Asian Tropical rainforest during the Oxidant and Particle Photochemical Processes (OP3) project. Atmos Chem Phys 13, 5233-5278.

Ehhalt, D.H., 1999. Photooxidation of trace gases in the troposphere. Physical Chemistry Chemical Physics 1, 5401-5408.

European Environment Agency, E., June 2013. in: (EEA), T.E.E.A. (Ed.), Copenhagen Denmark p. http://www.eea.europa.eu/.

Finlayson-Pitts, B.J., Pitts Jr, J.N., 1999. Chemistry of the upper and lower atmosphere: theory, experiments, and applications. Access Online via Elsevier.

Fleming, J., Albus, H., Neidhart, B., Wegscheider, W., 1997. Glossary of analytical terms (VII). Accred Qual Assur 2, 51-52.

Friedli, H.R., Atlas, E., Stroud, V.R., Giovanni, L., Campos, T., Radke, L.F., 2001. Volatile organic trace gases emitted from North American wildfires. Global Biogeochem Cy 15, 435-452.

Gabele, P.A., 1990. Characterization of Emissions from a Variable Gasoline/Methanol Fueled Car. Journal of the Air & Waste Management Association 40, 296-304.

Galbally, I.E., Kirstine, W., 2002. The Production of Methanol by Flowering Plants and the Global Cycle of Methanol. J Atmos Chem 43, 195-229.

George, C., 2001. High-speed analysis of volatile organic compounds in environmental samples using small-diameter capillary columns and purge-and-trap GC-MS systems. LC GC North America 19, 578-588.

Gleick, P.H., 1996. Water resources. Oxford University Press, New York.

Glueckauf, E., 1951. The composition of atmospheric air. Compendium of Meteorology, 3-10.

Goldan, P.D., Kuster, W.C., Fehsenfeld, F.C., Montzka, S.A., 1993. The observation of a C5 alcohol emission in a North American pine forest. Geophys Res Lett 20, 1039-1042.

Goldan, P.D., Kuster, W.C., Fehsenfeld, F.C., Montzka, S.A., 1995. Hydrocarbon measurements in the southeastern United States: The Rural Oxidants in the Southern Environment (ROSE) Program 1990. Journal of Geophysical Research: Atmospheres 100, 25945-25963.

Goldstein, A., Daube, B., Munger, J., Wofsy, S., 1995. Automated in-situ monitoring of atmospheric non-methane hydrocarbon concentrations and gradients. J Atmos Chem 21, 43-59.

Goldstein, A.H., Galbally, I.E., 2007. Known and Unexplored Organic Constituents in the Earth's Atmosphere. Environ Sci Technol 41, 1514-1521.

Grabmer, W., Graus, M., Lindinger, C., Wisthaler, A., Rappenglück, B., Steinbrecher, R., Hansel, A., 2004. Disjunct eddy covariance measurements of monoterpene fluxes from a Norway spruce forest using PTR-MS. International Journal of Mass Spectrometry 239, 111-115.

Grabmer, W., Kreuzwieser, J., Wisthaler, A., Cojocariu, C., Graus, M., Rennenberg, H., Steigner, D., Steinbrecher, R., Hansel, A., 2006. VOC emissions from Norway spruce (Picea

abies) twigs in the field - Results of a dynamic enclosure study. Atmospheric Environment 40, 128-137.

Graedel, T.E., Crutzen, P.J., 1993. Atmospheric change: an earth system perspective. WH Freeman and Co.

Grant, A., Witham, C., Simmonds, P., Manning, A., O'Doherty, S., 2010. A 15 year record of high-frequency, in situ measurements of hydrogen at Mace Head, Ireland. Atmos. Chem. Phys 10, 1203-1214.

Greenberg, J., Guenther, A., Harley, P., Otter, L., Veenendaal, E., Hewitt, C., James, A., Owen, S., 2003. Eddy flux and leaf-level measurements of biogenic VOC emissions from mopane woodland of Botswana. Journal of Geophysical Research: Atmospheres (1984–2012) 108.

Greenberg, J.P., Helmig, D., Zimmerman, P.R., 1996. Seasonal measurements of nonmethane hydrocarbons and carbon monoxide at the Mauna Loa Observatory during the Mauna Loa Observatory Photochemistry Experiment 2. Journal of Geophysical Research: Atmospheres (1984–2012) 101, 14581-14598.

Grob, R.L., Barry, E.F., 2004. Modern practice of gas chromatography. Wiley. com.

Guenther, A., Hewitt, C.N., Erickson, D., Fall, R., Geron, C., Graedel, T.E., Harley, P., Klinger, L., Lerdau, M., McKay, W.A., Pierce, T., Scholes, B., Steinbrecher, R., Tallamraju, R., Taylor, J., Zimmerman, P., 1995. A global model of natural volatile organic compound emissions. Journal of Geophysical Research: Atmospheres 100, 8873-8892.

Guenther, A., Karl, T., Harley, P., Wiedinmyer, C., Palmer, P., Geron, C., 2006. Estimates of global terrestrial isoprene emissions using MEGAN (Model of Emissions of Gases and Aerosols from Nature). Atmos Chem Phys 6, 3181-3210.

Guicherit, R., Schulting, F.L., 1985. The occurrence of organic chemicals in the atmosphere of The Netherlands. Science of The Total Environment 43, 193-219.

Haagen-Smit, A.J., 1952. Chemistry and physiology of Los Angeles smog. Industrial & Engineering Chemistry 44, 1342-1346.

Hansen, A.D.A., Rosen, H., Novakov, T., 1984. The aethalometer — An instrument for the real-time measurement of optical absorption by aerosol particles. Science of The Total Environment 36, 191-196.

Häseler, R., Brauers, T., Holland, F., Wahner, A., 2009. Development and application of a new mobile LOPAP instrument for the measurement of HONO altitude profiles in the planetary boundary layer. Atmospheric Measurement Technique Discussions 2, 2027-2054.

Hayward, S., Tani, A., Owen, S.M., Hewitt, C.N., 2004. Online analysis of volatile organic compound emissions from Sitka spruce (Picea sitchensis). Tree Physiology 24, 721-728.

Heikes, B.G., Chang, W., Pilson, M.E.Q., Swift, E., Singh, H.B., Guenther, A., Jacob, D.J., Field, B.D., Fall, R., Riemer, D., 2002. Atmospheric methanol budget and ocean implication. Global Biogeochem Cy 16, 1133.

Hellén, H., Kuronen, P., Hakola, H., 2012. Heated stainless steel tube for ozone removal in the ambient air measurements of mono- and sesquiterpenes. Atmospheric Environment 57, 35-40.

Helmig, D., 1999. Air analysis by gas chromatography. Journal of Chromatography A 843, 129-146.

Helmig, D., Greenberg, J.P., 1994. Automated in situ gas chromatographic-mass spectrometric analysis of ppt level volatile organic trace gases using multistage solid-adsorbent trapping. Journal of Chromatography A 677, 123-132.

Helmig, D., Vierling, L., 1995. Water-Adsorption Capacity of the Solid Adsorbents Tenax-Ta, Tenax-Gr, Carbotrap, Carbotrap-C, Carbosieve-Siii, and Carboxen-569 and Water Management-Techniques for the Atmospheric Sampling of Volatile Organic Trace Gases. Anal Chem 67, 4380-4386.

Hites, R.A., Turner, A.M., 2009. Rate constants for the gas-phase β-myrcene+ OH and isoprene+ OH reactions as a function of temperature. International Journal of Chemical Kinetics 41, 407-413.

Hofzumahaus, A., Holland, F., 2006. Zeppelin NT, a new Platform for Atmospheric Studies in the Planetary Boundary Layer.

Hofzumahaus, A., Holland, F., Wahner, A., 2006. Vorbereitung eines Zeppelin NT für die Nutzung als Flugplattform für atmosphärische Messungen in der Planetarischen Grenzschicht.

Hofzumahaus, A., Rohrer, F., Lu, K., Bohn, B., Brauers, T., Chang, C.C., Fuchs, H., Holland, F., Kita, K., Kondo, Y., 2009a. Amplified trace gas removal in the troposphere. Science 324, 1702-1704.

Hofzumahaus, A., Wahner, A., Bohn, B., Borchardt, J., Brauers, T., Broch, S., Buchholz, A., Buers, H.J., Del-Maso, M., Große-Brauchmann, P., Häseler, R., Holland, F., Janson, S., Kiendler-Scharr, A., Klemp, D., Mentel, T.F., Müsgen, P., Oebel, A., Raak, D., Rohrer, F., Spindler, C., Tillmann, R., Wegener, R., Wenk, A.-K., Heue, K.-P., Platt, U., Koppmann, R., Heuser, H.-P., Hösen, E., Wintel, J., Knieling, P., Krebsbach, M., Elbern, H., Goris, N., Nieradzik, L., 2009b. Zeppelin-gestützte Untersuchungen der regionalen Photochemie und Luftqualität über verschieden genutzten Landflächen.

Holland, F., Hofzumahaus, A., Schäfer, R., Kraus, A., Pätz, H.W., 2003. Measurements of OH and HO_2 radical concentrations and photolysis frequencies during BERLIOZ. J Geophys Res-Atmos 108.

Holzinger, R., Warneke, C., Hansel, A., Jordan, A., Lindinger, W., Scharffe, D.H., Schade, G., Crutzen, P.J., 1999. Biomass burning as a source of formaldehyde, acetaldehyde, methanol, acetone, acetonitrile, and hydrogen cyanide. Geophys Res Lett 26, 1161-1164.

Hottle, J.R., Huisman, A.J., Digangi, J.P., Kammrath, A., Galloway, M.M., Coens, K.L., Keutsch, F.N., 2009. A Laser Induced Fluorescence-Based Instrument for In-Situ Measurements of Atmospheric Formaldehyde. Environ Sci Technol 43, 790-795.

Hübschmann, H.J., 1996. Handuch der GC/MS-Grundlagen und Anwendungen. VCH Verlagsgesellschaft, Weinheim.

Hulskotte, J.H.J., Denier van der Gon, H.A.C., 2010. Fuel consumption and associated emissions from seagoing ships at berth derived from an on-board survey. Atmospheric Environment 44, 1229-1236.

Ibrahim, O., Shaiganfar, R., Sinreich, R., Stein, T., Platt, U., Wagner, T., 2010. Car MAX-DOAS measurements around entire cities: quantification of NO x emissions from the cities of Mannheim and Ludwigshafen (Germany). Atmos Meas Tech 3, 709-721.

Ingham, T., Goddard, A., Whalley, L.K., Furneaux, K.L., Edwards, P.M., Seal, C.P., Self, D.E., Johnson, G.P., Read, K.A., Lee, J.D., Heard, D.E., 2009. A flow-tube based laser-induced fluorescence instrument to measure OH reactivity in the troposphere. Atmos. Meas. Tech. Discuss. 2, 621-657.

IPCC, 2007. Climate Change 2007:Synthesis Report, Tech. rep, Intergovenmental Panel on Climate Chage, 2007.

IUPAC, February 2013. http://www.iupac-kinetic.ch.cam.ac.uk/, in: Centre for Atmospheric Science, C.U., UK (Ed.). IUPAC Subcommittee for Gas Kinetic Data Evaluation.

Jacob, D., 1999. Introduction to atmospheric chemistry. Princeton University Press.

Jacob, D.J., Field, B.D., Li, Q., Blake, D.R., De Gouw, J., Warneke, C., Hansel, A., Wisthaler, A., Singh, H.B., Guenther, A., 2005. Global budget of methanol: Constraints from atmospheric observations. Journal of Geophysical Research: Atmospheres (1984–2012) 110.

Jenkin, M., Saunders, S., Wagner, V., Pilling, M., 2003. Protocol for the development of the Master Chemical Mechanism, MCM v3 (Part B): tropospheric degradation of aromatic volatile organic compounds. Atmos Chem Phys 3, 181-193.

Jenkin, M.E., Saunders, S.M., Pilling, M.J., 1997. The tropospheric degradation of volatile organic compounds: A protocol for mechanism development. Atmospheric Environment 31, 81-104.

Johnson, A.M., 2011. The Development and Deployment of FOTOS: A Fast Observation of Trace Organic System.

Junninen, H., Ehn, M., Petaja, T., Luosujarvi, L., Kotiaho, T., Kostiainen, R., Rohner, U., Gonin, M., Fuhrer, K., Kulmala, M., Worsnop, D.R., 2010. A high-resolution mass spectrometer to measure atmospheric ion composition. Atmos Meas Tech 3, 1039-1053.

Jüttner, F., 1988. Quantitative analysis of monoterpenes and volatile organic pollution products (VOC) in forest air of the Southern Black Forest. Chemosphere 17, 309-317.

Kanakidou, M., Seinfeld, J.H., Pandis, S.N., Barnes, I., Dentener, F.J., Facchini, M.C., Dingenen, R.V., Ervens, B., Nenes, A.N.C.J.S.E., Nielsen, C.J., 2005. Organic aerosol and global climate modelling: a review. Atmos Chem Phys 5, 1053-1123.

Kansal, A., 2009. Sources and reactivity of NMHCs and VOCs in the atmosphere: A review. Journal of hazardous materials 166, 17-26.

Karl, T., Guenther, A., Lindinger, C., Jordan, A., Fall, R., Lindinger, W., 2001. Eddy covariance measurements of oxygenated volatile organic compound fluxes from crop

harvesting using a redesigned proton-transfer-reaction mass spectrometer. Journal of Geophysical Research: Atmospheres (1984–2012) 106, 24157-24167.

Karl, T., Guenther, A., Spirig, C., Hansel, A., Fall, R., 2003. Seasonal variation of biogenic VOC emissions above a mixed hardwood forest in northern Michigan. Geophys Res Lett 30.

Kelsey, R.G., 1996. Anaerobic induced ethanol synthesis in the stems of greenhouse-grown conifer seedlings. Trees 10, 183-188.

Kesselmeier, J., Bode, K., Hofmann, U., Müller, H., Schäfer, L., Wolf, A., Ciccioli, P., Brancaleoni, E., Cecinato, A., Frattoni, M., 1997. Emission of short chained organic acids, aldehydes and monoterpenes from Quercus ilex L. and Pinus pinea L. in relation to physiological activities, carbon budget and emission algorithms. Atmospheric Environment 31, 119-133.

Keuken, M., Roemer, M., van den Elshout, S., 2009. Trend analysis of urban NO2 concentrations and the importance of direct NO2 emissions versus ozone/NOx equilibrium. Atmospheric Environment 43, 4780-4783.

Keuken, M., Zandveld, P., van den Elshout, S., Janssen, N.A.H., Hoek, G., 2011. Air quality and health impact of PM10 and EC in the city of Rotterdam, the Netherlands in 1985–2008. Atmospheric Environment 45, 5294-5301.

Kitson, F.G., Larsen, B.S., McEwen, C.N., 1996. Gas Chromatographie and Mass Spectrometry a Practical Guide.

KNMI, June 2013. http://www.knmi.nl/climatology/daily_data/index.cgi, in: ´ (Ed.). The Royal Netherlands Meteorological Institute, De Bilt, Netherlands

Konrad, S., 2000. Untersuchungen zur Radikalchemie in der Abluftfahne von Berlin - ein Beitrag zum Feldexperiment BERLIOZ.

Koppmann, R., 2008. Volatile organic compounds in the atmosphere. Wiley. com.

Koppmann, R., Bauer, R., Johnen, F., Plass, C., Rudolph, J., 1992. The distribution of light nonmethane hydrocarbons over the mid-Atlantic: Results of the Polarstern cruise ANT VII/1. J Atmos Chem 15, 215-234.

Koppmann, R., Johnen, F., Khedim, A., Rudolph, J., Wedel, A., Wiards, B., 1995. The influence of ozone on light nonmethane hydrocarbons during cryogenic preconcentration. Journal of Geophysical Research: Atmospheres (1984–2012) 100, 11383-11391.

Korytár, P., Janssen, H.-G., Matisová, E., Brinkman, U.A.T., 2002. Practical fast gas chromatography: methods, instrumentation and applications. TrAC Trends in Analytical Chemistry 21, 558-572.

Kovacs, T.A., Brune, W.H., 2001. Total OH Loss Rate Measurement. J Atmos Chem 39, 105-122.

Kuhn, U., Andreae, M., Ammann, C., Araujo, A.d., Brancaleoni, E., Ciccioli, P., Dindorf, T., Frattoni, M., Gatti, L., Ganzeveld, L., 2007. Isoprene and monoterpene fluxes from Central Amazonian rainforest inferred from tower-based and airborne measurements, and implications on the atmospheric chemistry and the local carbon budget. Atmos Chem Phys 7, 2855-2879.

Kwan, A.J., Crounse, J.D., Clarke, A.D., Shinozuka, Y., Anderson, B.E., Crawford, J.H., Avery, M.A., McNaughton, C.S., Brune, W.H., Singh, H.B., 2006. On the flux of oxygenated volatile organic compounds from organic aerosol oxidation. Geophys Res Lett 33.

Lamanna, M.S., Goldstein, A.H., 1999. In situ measurements of C2-C10 volatile organic compounds above a Sierra Nevada ponderosa pine plantation. Journal of Geophysical Research: Atmospheres 104, 21247-21262.

Leclercq, P., Cramers, C.A., 1985. Optimum performance of capillary GC columns as a function of tube diameter and film thickness under various operating conditions. Computer program for calculation of H-ū curves and minimum analysis times. Journal of High Resolution Chromatography 8, 764-771.

Leibrock, E., Slemr, J., 1997. Method for measurement of volatile oxygenated hydrocarbons in ambient air. Atmospheric Environment 31, 3329-3339.

Levy, H., 1972. Photochemistry of the lower troposphere. Planetary and Space Science 20, 919-935.

Lewis, A., Hopkins, J., Carpenter, L., Stanton, J., Read, K., Pilling, M., 2005. Sources and sinks of acetone, methanol, and acetaldehyde in North Atlantic marine air. Atmos. Chem. Phys 5, 1963-1974.

Li, P., Perreau, K.A., Covington, E., Song, C.H., Carmichael, G.R., Grassian, V.H., 2001. Heterogeneous reactions of volatile organic compounds on oxide particles of the most abundant crustal elements: Surface reactions of acetaldehyde, acetone, and propionaldehyde on SiO2, Al2O3, Fe2O3, TiO2, and CaO. Journal of Geophysical Research: Atmospheres 106, 5517-5529.

Lindinger, W., Hansel, A., Jordan, A., 1998. On-line monitoring of volatile organic compounds at pptv levels by means of proton-transfer-reaction mass spectrometry (PTR-MS) medical applications, food control and environmental research. International Journal of Mass Spectrometry and Ion Processes 173, 191-241.

Lloyd, A.C., 1979. Tropospheric chemistry of aldehydes. In chemical kinetics data needs for modeling the lower troposphere. National Bureau of Standards Special Publication 557, 27-48.

Lou, S., Holland, F., Rohrer, F., Lu, K., Bohn, B., Brauers, T., Chang, C.C., Fuchs, H., Haseler, R., Kita, K., Kondo, Y., Li, X., Shao, M., Zeng, L., Wahner, A., Zhang, Y., Wang, W., Hofzumahaus, A., 2010. Atmospheric OH reactivities in the Pearl River Delta - China in summer 2006: measurement and model results. Atmos Chem Phys 10, 11243-11260.

Mao, J., Ren, X., Brune, W.H., Olson, J.R., Crawford, J.H., Fried, A., Huey, L.G., Cohen, R.C., Heikes, B., Singh, H.B., Blake, D.R., Sachse, G.W., Diskin, G.S., Hall, S.R., Shetter, R.E., 2009. Airborne measurement of OH reactivity during INTEX-B. Atmos Chem Phys 9, 163-173.

Mao, J., Ren, X., Chen, S., Brune, W.H., Chen, Z., Martinez, M., Harder, H., Lefer, B., Rappenglück, B., Flynn, J., Leuchner, M., 2010. Atmospheric oxidation capacity in the summer of Houston 2006: Comparison with summer measurements in other metropolitan studies. Atmospheric Environment 44, 4107-4115.

McIlveen, R., 1992. Fundamentals of weather and climate. Routledge.

McNair, H.M., Miller, J.M., 2009. Basic Gas Chromatography.

McVeety, B.D., Hites, R.A., 1988. Atmospheric deposition of polycyclic aromatic hydrocarbons to water surfaces: A mass balance approach. Atmospheric Environment (1967) 22, 511-536.

Mirme, S., Mirme, A., 2011. The mathematical principles and design of the NAIS - a spectrometer for the measurement of cluster ion and nanometer aerosol size distributions. Atmospheric Measurement Techniques Discussions 4, 7405-7434.

Mohler, O., Reiner, T., Arnold, F., 1993. A novel aircraft-based tandem mass spectrometer for atmospheric ion and trace gas measurements. Rev Sci Instrum 64, 1199-1207.

Montzka, S.A., Trainer, M., Goldan, P.D., Kuster, W.C., Fehsenfeld, F.C., 1993. Isoprene and its oxidation products, methyl vinyl ketone and methacrolein, in the rural troposphere. Journal of Geophysical Research: Atmospheres 98, 1101-1111.

Nguyen, H.T.-H., Takenaka, N., Bandow, H., Maeda, Y., de Oliva, S.T., Botelho, M.M.f., Tavares, T.M., 2001. Atmospheric alcohols and aldehydes concentrations measured in Osaka, Japan and in Sao Paulo, Brazil. Atmospheric Environment 35, 3075-3083.

Nölscher, A., Williams, J., Sinha, V., Custer, T., Song, W., Johnson, A., Axinte, R., Bozem, H., Fischer, H., Pouvesle, N., 2012. Summertime total OH reactivity measurements from boreal forest during HUMPPA-COPEC 2010. Atmos. Chem. Phys 12, 8257-8270.

Olson, J., Crawford, J., Brune, W., Mao, J., Ren, X., Fried, A., Anderson, B., Apel, E., Beaver, M., Blake, D., 2012. An analysis of fast photochemistry over high northern latitudes during spring and summer using in-situ observations from ARCTAS and TOPSE. Atmos Chem Phys 12, 6799-6825.

Palmer, P.I., Jacob, D.J., Jones, D., Heald, C.L., Yantosca, R.M., Logan, J.A., Sachse, G., Streets, D.G., 2003. Inverting for emissions of carbon monoxide from Asia using aircraft observations over the western Pacific. Journal of Geophysical Research: Atmospheres (1984–2012) 108.

Pandis, S.N., 2010. Description of Work PEGASOS, European Comission, Framework Programme 7 (FP7-ENV-2010.1.1.2-1).

Plass-Dülmer, C., Brauers, T., Rudolph, J., 1998. POPCORN: A field study of photochemistry in north-eastern Germany. J Atmos Chem 31, 5-31.

Platt, U.F., Winer, A.M., Biermann, H.W., Atkinson, R., Pitts, J.N., 1984. Measurement of nitrate radical concentrations in continental air. Environ Sci Technol 18, 365-369.

Porter, E., Wenger, J., Treacy, J., Sidebottom, H., Mellouki, A., Téton, S., LeBras, G., 1997. Kinetic Studies on the Reactions of Hydroxyl Radicals with Diethers and Hydroxyethers. The Journal of Physical Chemistry A 101, 5770-5775.

Prinn, R.G., Huang, J., Weiss, R.F., Cunnold, D.M., Fraser, P.J., Simmonds, P.G., McCulloch, A., Harth, C., Salameh, P., O'Doherty, S., 2001. Evidence for substantial variations of atmospheric hydroxyl radicals in the past two decades. Science 292, 1882-1888.

Ren, X., Harder, H., Martinez, M., Lesher, R.L., Oliger, A., Simpas, J.B., Brune, W.H., Schwab, J.J., Demerjian, K.L., He, Y., 2003. OH and HO_2 Chemistry in the urban atmosphere of New York City. Atmospheric Environment 37, 3639-3651.

Ren, X.R., Brune, W.H., Mao, J.Q., Mitchell, M.J., Lesher, R.L., Simpas, J.B., Metcalf, A.R., Schwab, J.J., Cai, C.X., Li, Y.Q., Demerjian, K.L., Felton, H.D., Boynton, G., Adams, A., Perry, J., He, Y., Zhou, X.L., Hou, J., 2006a. Behavior of OH and HO_2 in the winter atmosphere in New York city. Atmospheric Environment 40, S252-S263.

Ren, X.R., Brune, W.H., Oliger, A., Metcalf, A.R., Simpas, J.B., Shirley, T., Schwab, J.J., Bai, C.H., Roychowdhury, U., Li, Y.Q., Cai, C.X., Demerjian, K.L., He, Y., Zhou, X.L., Gao, H.L., Hou, J., 2006b. OH, HO_2, and OH reactivity during the PMTACS-NY Whiteface Mountain 2002 campaign: Observations and model comparison. J Geophys Res-Atmos 111.

Riemer, D., Pos, W., Milne, P., Farmer, C., Zika, R., Apel, E., Olszyna, K., Kliendienst, T., Lonneman, W., Bertman, S., Shepson, P., Starn, T., 1998. Observations of nonmethane hydrocarbons and oxygenated volatile organic compounds at a rural site in the southeastern United States. Journal of Geophysical Research: Atmospheres 103, 28111-28128.

Rolph, G.D., 2013. http://www.ready.noaa.gov Real-time Environmental Applications and Display sYstem (READY) Website, in: NOAA Air Resources Laboratory, C.P., MD. (Ed.).

Rubach, F., 2013. Aerolsol processes in the Planetary Boundary Layer: High resolution Aerolsol Mass Spectrometer on a Zepplin NT Airship.

Rudich, Y., Talukdar, R., Burkholder, J.B., Ravishankara, A.R., 1995. Reaction of Methylbutenol with the OH Radical: Mechanism and Atmospheric Implications. The Journal of Physical Chemistry 99, 12188-12194.

Rudolph, J., Johnen, F., Khedim, A., 1986. Problems connected with the analysis of halocarbons and hydrocarbons in the non-urban atmosphere. International journal of environmental analytical chemistry 27, 97-122.

Sadanaga, Y., Yoshino, A., Watanabe, K., Yoshioka, A., Wakazono, Y., Kanaya, Y., Kajii, Y., 2004. Development of a measurement system of OH reactivity in the atmosphere by using a laser-induced pump and probe technique. Rev Sci Instrum 75, 2648.

Saunders, S., Jenkin, M., Derwent, R., Pilling, M., 2003. Protocol for the development of the Master Chemical Mechanism, MCM v3 (Part A): tropospheric degradation of non-aromatic volatile organic compounds. Atmos Chem Phys 3, 161-180.

Schade, G.W., Goldstein, A.H., 2001. Fluxes of oxygenated volatile organic compounds from a ponderosa pine plantation. Journal of Geophysical Research: Atmospheres (1984–2012) 106, 3111-3123.

Seinfeld, J.H., Pandis, S.N., 2006. Atmospheric chemistry and physics: from air pollution to climate change. John Wiley & Sons.

Shirley, T., Brune, W., Ren, X., Mao, J., Lesher, R., Cardenas, B., Volkamer, R., Molina, L., Molina, M.J., Lamb, B., 2006. Atmospheric oxidation in the Mexico City metropolitan area (MCMA) during April 2003. Atmos Chem Phys 6, 2753-2765.

Singh, H., Chen, Y., Staudt, A., Jacob, D., Blake, D., Heikes, B., Snow, J., 2001. Evidence from the Pacific troposphere for large global sources of oxygenated organic compounds. Nature 410, 1078-1081.

Singh, H., Chen, Y., Tabazadeh, A., Fukui, Y., Bey, I., Yantosca, R., Jacob, D., Arnold, F., Wohlfrom, K., Atlas, E., Flocke, F., Blake, D., Blake, N., Heikes, B., Snow, J., Talbot, R., Gregory, G., Sachse, G., Vay, S., Kondo, Y., 2000. Distribution and fate of selected oxygenated organic species in the troposphere and lower stratosphere over the Atlantic. Journal of Geophysical Research: Atmospheres 105, 3795-3805.

Singh, H., Salas, L., Chatfield, R., Czech, E., Fried, A., Walega, J., Evans, M., Field, B., Jacob, D., Blake, D., 2004a. Analysis of the atmospheric distribution, sources, and sinks of oxygenated volatile organic chemicals based on measurements over the Pacific during TRACE-P. Journal of Geophysical Research: Atmospheres (1984–2012) 109.

Singh, H.B., Hanst, P.L., 1981. Peroxyacetyl nitrate (PAN) in the unpolluted atmosphere: An important reservoir for nitrogen oxides. Geophys Res Lett 8, 941-944.

Singh, H.B., Kanakidou, M., Crutzen, P.J., Jacob, D.J., 1995. High concentrations and photochemical fate of oxygenated hydrocarbons in the global troposphere. Nature 378, 50-54.

Singh, H.B., O'hara, D., Herlth, D., Sachse, W., Blake, D., Bradshaw, J.D., Kanakidou, M., Crutzen, P.J., 1994. Acetone in the atmosphere: Distribution, sources, and sinks. Journal of Geophysical Research: Atmospheres (1984–2012) 99, 1805-1819.

Singh, H.B., Salas, L.J., Chatfield, R.B., Czech, E., Fried, A., Walega, J., Evans, M.J., Field, B.D., Jacob, D.J., Blake, D., 2004b. Analysis of the atmospheric distribution, sources, and sinks of oxygenated volatile organic chemicals based on measurements over the Pacific during TRACE-P. Journal of Geophysical Research: Atmospheres (1984–2012) 109.

Singh, H.B., Zimmerman, P.B., 1992. Atmospheric distribution and sources of nonmethane hydrocarbons. Gaseous pollutants: Characterization and cycling, p. 177-235. 1, 177-235.

Sinha, V., Williams, J., Crowley, J., Lelieveld, J., 2008. The Comparative Reactivity Method–a new tool to measure total OH Reactivity in ambient air. Atmos Chem Phys 8, 2213-2227.

Snider, J.R., Dawson, G.A., 1985. Tropospheric light alcohols, carbonyls, and acetonitrile: Concentrations in the southwestern United States and Henry's Law data. Journal of Geophysical Research: Atmospheres 90, 3797-3805.

Stull, R., 1988. An Introduction to Boundary Layer Meeteorology, Atmospheric Science Library. Springer.

Tingey, D.T., Manning, M., Grothaus, L.C., Burns, W.F., 1979. The Influence of Light and Temperature on Isoprene Emission Rates from Live Oak. Physiologia Plantarum 47, 112-118.

Vairavamurthy, A., Roberts, J.M., Newman, L., 1992. Methods for determination of low molecular weight carbonyl compounds in the atmosphere: A review. Atmospheric Environment. Part A. General Topics 26, 1965-1993.

Van Der Eerden, L., De Vries, W., Van Dobben, H., 1998. Effects of ammonia deposition on forests in the Netherlands. Atmospheric Environment 32, 525-532.

van Deursen, M.M., Beens, J., Janssen, H.G., Leclercq, P.A., Cramers, C.A., 2000. Evaluation of time-of-flight mass spectrometric detection for fast gas chromatography. Journal of Chromatography A 878, 205-213.

van Ierland, E., Graveland, C., Huiberts, R., 2000. An environmental economic analysis of the new rail link to European main port Rotterdam. Transportation Research Part D: Transport and Environment 5, 197-209.

Velasco, E., Márquez, C., Bueno, E., Bernabé, R., Sánchez, A., Fentanes, O., Wöhrnschimmel, H., Cárdenas, B., Kamilla, A., Wakamatsu, S., 2008. Vertical distribution of ozone and VOCs in the low boundary layer of Mexico City. Atmos Chem Phys 8, 3061-3079.

Wang, J.-L., Chen, S.-W., Chew, C., 1999. Automated gas chromatography with cryogenic/sorbent trap for the measurement of volatile organic compounds in the atmosphere. Journal of Chromatography A 863, 183-193.

Warneke, C., Luxembourg, S.L., de Gouw, J.A., Rinne, H.J.I., Guenther, A.B., Fall, R., 2002. Disjunct eddy covariance measurements of oxygenated volatile organic compounds fluxes from an alfalfa field before and after cutting. Journal of Geophysical Research: Atmospheres 107, ACH 6-1-ACH 6-10.

Wiedinmyer, C., Guenther, A., Harley, P., Hewitt, N., Geron, C., Artaxo, P., Steinbrecher, R., Rasmussen, R., 2004. Global organic emissions from vegetation, Emissions of atmospheric trace compounds. Springer, pp. 115-170.

Williams, R.L., Lipari, F., Potter, R.A., 1990. Formaldehyde, Melhanol and Hydrocarbon Emissions from Methanol-fueled Cars. Journal of the Air & Waste Management Association 40, 747-756.

Wisthaler, A., Hansel, A., Dickerson, R.R., Crutzen, P.J., 2002. Organic trace gas measurements by PTR-MS during INDOEX 1999. Journal of Geophysical Research: Atmospheres 107, 8024.

Wisthaler, A., Jensen, N., Winterhalter, R., Lindinger, W., Hjorth, J., 2001. Measurements of acetone and other gas phase product yields from the OH-initiated oxidation of terpenes by proton-transfer-reaction mass spectrometry (PTR-MS). Atmospheric Environment 35, 6181-6191.

Wittrock, F., Richter, A., Oetjen, H., Burrows, J.P., Kanakidou, M., Myriokefalitakis, S., Volkamer, R., Beirle, S., Platt, U., Wagner, T., 2006. Simultaneous global observations of glyoxal and formaldehyde from space. Geophys Res Lett 33, L16804.

Woolfenden, E., 1997. Monitoring VOCs in Air Using Sorbent Tubes Followed by Thermal Desorption-Capillary GC Analysis: Summary of Data and Practical Guidelines. Journal of the Air & Waste Management Association 47, 20-36.

Wunderground, June 2013. http://www.wunderground.com/. Weather Underground, Inc. The Weather Channel Media Solutions Group; San Francisco.

Yokouchi, Y., 1994. Seasonal and diurnal variation of isoprene and its reaction products in a semi-rural area. Atmospheric Environment 28, 2651-2658.

Yoshino, A., Sadanaga, Y., Watanabe, K., Kato, S., Miyakawa, Y., Matsumoto, J., Kajii, Y., 2006. Measurement of total OH reactivity by laser-induced pump and probe technique - comprehensive observations in the urban atmosphere of Tokyo. Atmospheric Environment 40, 7869-7881.

Zappoli, S., Andracchio, A., Fuzzi, S., Facchini, M.C., Gelencsér, A., Kiss, G., Krivácsy, Z., Molnár, Á., Mészáros, E., Hansson, H.C., Rosman, K., Zebühr, Y., 1999. Inorganic, organic and macromolecular components of fine aerosol in different areas of Europe in relation to their water solubility. Atmospheric Environment 33, 2733-2743.

Zimmerman, P.R., Greenberg, J.P., Westberg, C.E., 1988. Measurements of atmospheric hydrocarbons and biogenic emission fluxes in the Amazon boundary layer. Journal of Geophysical Research: Atmospheres (1984–2012) 93, 1407-1416.

Acknowledgements

Nun möchte ich mich von ganzem Herzen bei all denjenigen bedanken, die mich während meiner Promotion unterstützt haben und ohne die diese Arbeit nicht möglich gewesen wäre.

Ein besonders großer Dank gilt *PD Dr. Andreas Hofzumahaus* für die Betreuung meiner Arbeit und die Übernahme des Referats. Vielen Dank für die vielen Diskussionen und Anmerkungen, die maßgeblich zum Gelingen dieser Arbeit beigetragen haben.
Prof. Dr. Andreas Wahner möchte ich für die Übernahme des Koreferats danken aber auch für die Möglichkeit, die hier dargestellte Arbeit am IEK-8 durchzuführen sowie für die freundliche Unterstützung während der Arbeit.
Ich danke *Prof. Dr. Gerd Meyer* für die Übernahme des Prüfungsvorsitzes während meiner Disputation. Außerdem möchte ich *Dr. Heike Klesper* für die Übernahme des Beisitzes danken.
Dr. Robert Wegener danke ich für die Betreuung und die Möglichkeit dies interessante Thema zu bearbeiten. Ganz besonders danke ich ihm für die hilfreiche Unterstützung bei vielen IDL- und Inventor-Fragen.
Ein ganz besonderer Dank gilt *PD Dr. Thomas Mentel* für die ausgezeichnete Unterstützung vor allem in der letzten Phase dieser Arbeit. Vielen Dank für die vielen Gespräche, die auch über die Wissenschaft hinausgingen.
Ich danke *Dr. Franz Rohrer* für die vielen überaus wertvollen wissenschaftlichen Diskussionen und Anregungen, die zum Gelingen dieser Arbeit beigetragen haben. *Dr. Franz Rohrer* und *Dr. Lu Keding* gilt auch mein Dank für die Bereitstellung der NO_x-, CO- und O_3-Daten.
Ich möchte *Bernhard Rose* und *Wolfgang Waltke,* Mitarbeiter der Firma Gerstel, danken, ohne deren umfassende Hilfe, die Bedienung und der Umbau des HGCs nur schwer möglich gewesen wären.
Ich danke *Ann-Katrin Wenk* für die Einführung in das Arbeiten mit dem HGC. Besonders ihre vielen Hinweise zur Bedienung waren sehr hilfreich.

Ich danke *Knut Dahlhoff* wie auch den Mitarbeitern von ZAT für die tatkräftige Unterstützung beim Umbau des HGCs. *Harry Beck* danke ich für die außerordentliche Hilfe beim Umbau des HGCs, ohne die dies nicht möglich gewesen wäre. Ebenso danke ich den gesamten Mitarbeitern der Mechanischen Werkstatt des Instituts für die Unterstützung. Ich möchte *Dr. Frank Holland* für die Hilfe bei der Erstellung der Dokumentation danken sowie für seine Unterstützung bei IDL-Fragen. *Mathias Bachner* danke ich für die Hilfe bei Elektronikfragen.
Ein großer Dank gilt den *Mitarbeiten von ZLT*, besonders *Artur Brauchle* und *René Frank,* die

maßgeblich am Zertifizierungsprozess des HGCs beteiligt waren. Ich bedanke mich auch für die sehr gute Kooperation mit den *Piloten*, *Prüfern* und der *Ground Crew* während den Zeppelinmesskampagnen.
Ein besonderer Dank gilt *Dominik Raak* für die ``Elektronik-Erste-Hilfe´´ auf den Kampagnen. *Dr. Ralf Tillmann* danke ich für die außerordentliche Unterstützung während den Messkampagnen. Ich danke *Florian Rubach* für die Hilfe beim Umbau des HGC, der Erstellung der Dokumentation wie aber auch auf den Kampagnen.
Dr. Hendrik Fuchs und der gesamten *LIF Gruppe* danke ich für die Bereitstellung sowohl der k_{OH}- als auch der OH- und HO_2-Daten. Ich danke *Dr. Frank Keutsch, Dr. Glenn Wolfe* und *Jennifer Kaiser*, die mir die HCHO-Daten zur Verfügung stellten. *Dr. Li Xin* und *Rolf Häseler* danke ich für die HONO-Daten. *Dr. Birger Bohn* und *Insa Lohse* danke ich für die Bereitstellung der Photolysefrequenzen.
Joachim Borchardt danke ich herzlich für die freundliche und immer positive Büroatmosphäre während der letzten 3 Jahre. Ich danke *Helga London* und *Michael Decker* für die tatkräftige Unterstützung bei IT-Fragen und den vielen wertvollen Gesprächen. *Gabi Nork, Brigitte Berger* und *Franziska Kaspereit* möchte ich für ihre umfassende Unterstützung bei administrativen Fragen danken. Ich danke *Christian Ehlers* für die vielen Hinweise zum Promotionsverfahren an der Universität zu Köln.

Ich danke *allen Mitarbeitern des IEK-8s*, die meine Zeit am Institut unvergesslich gemacht haben, sodass ich mich immer sehr gerne zurück erinnern werde.

Für die finanzielle Unterstützung danke ich der *Deutschen Forschungsgemeinschaft* für die Finanzierung meiner Stelle im Rahmen des HALO Projektes (WE-4384/2-2) und der *Europäischen Kommission* für die Finanzierung des PEGASOS Projektes (Framework Program 7 (FP7-ENV-2010-265148)).

Besonders für die intensiven Freundschaften während meiner Zeit in Jülich danke ich *Martin Kaminski, Dr. Sebastian Broch* und *Sebastian Gomm.* Ihr habt mich maßgeblich während dieser Zeit inspiriert und unterstützt! Ich hoffe, dass diese Freundschaften die Zeit in Jülich überdauern werden. Dir *Sebastian B.* danke ich ganz besonders für deine Unterstützung vor allem in der letzten Phase mit deiner unglaublichen Geduld und den unzähligen Korrekturen. Der *BSG Donnerstag Volleyball Gruppe* danke ich für die offene Integration in die Gruppe, besonders aber danke ich *Ursula Funk-Kath* für ihre freundliche Art. *Inga Riemann*, *Tanya Penwill* und *Sascha Weber* danke ich besonders für die Freundschaften über die letzten Jahre, ihr habt mich durch diese Zeit getragen. Ich danke der gesamten *Maastrichter Crew* für die vielen unvergesslichen Stunden.

Ein ganz besonderer großer Dank gilt *meinen Eltern*, ihr habt mir dies alles ermöglicht und mich gerade auch in der letzten Phase durch viele Mut machende Gespräche sehr unterstützt.

Mein größter Dank gilt *Stephan* für die letzten Jahre, die außerordentlich turbulent aber auch wunderschön waren. Von ganzem Herzen danke ich dir für deine grandiose Unterstützung während der gesamten Arbeit, besonders aber in der letzten Phase. Ich freue mich auf die vielen neuen Abenteuer, die wir zusammen erleben werden.

Erklärung

Ich versichere, dass ich die von mir vorgelegte Dissertation selbstständig angefertigt, die benutzten Quellen und Hilfsmittel vollständig angegeben und die Stellen der Arbeit – einschließlich Tabellen, Karten und Abbildungen-, die anderen Werken im Wortlauft oder dem Sinn nach entnommen sind, in jedem Einzelfall als Entlehnung kenntlich gemacht habe; dass diese Dissertation noch keiner anderen Fakultät oder Universität zur Prüfung vorgelegen hat; dass sie - abgesehen von unten angegebenen Teilpublikationen - noch nicht veröffentlicht worden ist sowie, dass ich eine solche Veröffentlichung vor Abschluss des Promotionsverfahrens nicht vornehmen werde.

Die Bestimmungen dieser Promotionsordnung sind mir bekannt. Die von mir vorgelegte Dissertation ist von PD Dr. Andreas Hofzumahaus betreut worden.

Es liegen keine Teilpublikationen vor.

Ich versichere, dass ich alle Angaben wahrheitsgemäß nach besten Wissen und Gewissen gemacht habe und verpflichte mich, jedmögliche, die obigen Angaben betreffenden Veränderungen, dem Dekanat unverzüglich mitzuteilen.

Köln, _____

Band / Volume 193
Full-waveform inversion of crosshole GPR data for hydrogeological applications
A. Klotzsche (2013), X, 164 pp
ISBN: 978-3-89336-915-7

Band / Volume 194
Long Term Stability and Permeability of Mixed Ion Conducting Membranes under Oxyfuel Conditions
X. Li (2013), III, 143 pp
ISBN: 978-3-89336-916-4

Band / Volume 195
Innovative Beschichtungs- und Charakterisierungsmethoden für die nasschemische Herstellung von asymmetrischen Gastrennmembranen auf Basis von SiO_2
J. Hoffmann (2013), V, 152 pp
ISBN: 978-3-89336-917-1

Band / Volume 196
Aerosol processes in the Planetary Boundary Layer: High resolution Aerosol Mass Spectrometry on a Zeppelin NT Airship
F. Rubach (2013), iii, 141 pp
ISBN: 978-3-89336-918-8

Band / Volume 197
Institute of Energy and Climate Research IEK-6: Nuclear Waste Management - Report 2011 / 2012 Material Science for Nuclear Waste Management
M. Klinkenberg, S. Neumeier, D. Bosbach (Eds.) (2013), 195 pp
ISBN: 978-3-89336-980-1

Band / Volume 198
Material migration in tokamak plasmas with a three-dimensional boundary
R. Laengner (2013), vi, 140, XVII pp
ISBN: 978-3-89336-924-9

Band / Volume 199
Improved characterization of river-aquifer interactions through data assimilation with the Ensemble Kalman Filter
W. Kurtz (2013), xxv, 125 pp
ISBN: 978-3-89336-925-6

Band / Volume 200
Innovative SANEX process for trivalent actinides separation from PUREX raffinate
A. Sypula (2013), 220 pp
ISBN: 978-3-89336-927-0

Band / Volume 201
Transport and deposition of functionalized multi-walled carbon nanotubes in porous media
D. Kasel (2013), 103 pp
ISBN: 978-3-89336-929-4

Band / Volume 202
Full-waveform inversion of surface ground penetrating radar data and coupled hydrogeophysical inversion for soil hydraulic property estimation
S. Busch (2013), 112 pp
ISBN: 978-3-89336-930-0

Band / Volume 203
Politikszenarien für den Klimaschutz VI – Treibhausgas-Emissionsszenarien bis zum Jahr 2030
Advances in Systems Analysis 5
P. Hansen, S. Gores und F. Chr. Matthes (Hrsg.)
(2013), XX, 257 pp
ISBN: 978-3-89336-932-4

Band / Volume 204
Effect of Composition, Microstructure and Component Thickness on the Oxidation Behaviour of Laves Phase Strengthened Interconnect Steel for Solid Oxide Fuel Cells (SOFC)
C. Asensio Jimenez (2014), 210 pp
ISBN: 978-3-89336-935-5

Band / Volume 205
Airborne VOC measurements on board the Zeppelin NT during the PEGASOS campaigns in 2012 deploying the improved Fast-GC-MSD System
J. Jäger (2014), VIII, 182 pp
ISBN: 978-3-89336-936-2

Energie & Umwelt / Energy & Environment
Band / Volume 205
ISBN 978-3-89336-936-2

JÜLICH
FORSCHUNGSZENTRUM